DYNAMIC MODELING AND CONTROL

OF A 50 MW_e

OTEC POWER PLANT

by

GREGORY ALLEN THOMAS

S.B., Massachusetts Institute of Technology
(1979)

SUBMITTED IN PARTIAL FULFILLMENT
OF THE REQUIREMENTS FOR THE
DEGREE OF

MASTER OF SCIENCE IN
MECHANICAL ENGINEERING

at the

Massachusetts Institute of Technology

September 1980

© Massachusetts Institute of Technology

Signature redacted

Signature of Author...
Department of Mechanical Engineering
August 22, 1980

Signature redacted

Certified by..
David N. Wormley
Thesis Supervisor

Signature redacted

Accepted by...
Warren M. Rohsenow
Chairman, Department Committee

ARCHIVES
MASSACHUSETTS INSTITUTE
OF TECHNOLOGY

SEP 24 1980

DYNAMIC MODELING AND CONTROL

OF A 50 MW_e

OTEC POWER PLANT

by

GREGORY ALLEN THOMAS

Submitted to the Department of Mechanical Engineering on August 22, 1980, in partial fulfillment of the requirements for the degree of Master of Science.

ABSTRACT

A research effort was conducted to model the slow speed dynamics of a 50 MW_e Ocean Thermal Energy Conversion (OTEC) power plant in order to design an effective control system for the plant when it is interfaced with a large on-shore power grid by either direct AC or a DC rectifier/inverter transmission system. The OTEC plant processes are modeled using mass, momentum, and energy balances along with corresponding constituitive relationships for each component. Several simplifying assumptions are made to reduce the complexity and to increase the "workability" of the model. The result is a reduced order, physically based, dynamic model of the OTEC power plant which is subsequently linearized about an operating steady state.

The results from the study show that the OTEC plant can be adequately controlled by a turbine-generator speed governor using a bypass valve to divert vapor flow from the turbine when operating at reduced loads. Improved system performance is achieved using a multi-state variable feedback control system designed by linear-quadratic regulator theory. DC power load regulation is used to control the power plant when operating at full capacity.

The study also shows that severe wave action can have a substantial effect on the performance of the warm water pumping system and the power plant in general. A pumping power surge controller is designed to minimize these effects.

Thesis Supervisor: David N. Wormley
Title: Professor of Mechanical Engineering

ACKNOWLEDGEMENTS

I wish to give many thanks to Professor David N. Wormley, who provided insights and guidance throughout the life of the project.

My gratitude goes to Professor Mike O' Callaghan, who was extremely helpful during the early stages of the project.

I also wish to thank a colleague, José Sotelo, who was always of tremendous assistance and a valuable source of inspiration to me.

My special heartfelt thanks to Leslie Regan, for working so diligently on such short notice to type this thesis.

But most of all, my deepest gratitude and love goes to Susan, whose never ending supply of love and support made it all possible.

Funding for this research was provided by the United States Department of Energy, Contract #EX-76-A-01-2295, issued to the M.I.T. Energy Laboratory and the Department of Mechanical Engineering.

TABLE OF CONTENTS

		Page
TITLE PAGE		1
ABSTRACT		2
ACKNOWLEDGEMENTS		3
TABLE OF CONTENTS		4
NOMENCLATURE		7
LIST OF FIGURES		12
LIST OF TABLES		17
CHAPTER I - INTRODUCTION		18
	1.1 General Description of the OTEC System	18
	1.2 Scope of Effort	23
CHAPTER II - MODEL DEVELOPMENT		27
	2.1 Description of System Model	27
	2.1.1 Basic Modeling Criteria	28
	2.2 Evaporator Model	29
	2.2.1 Seawater Side Analysis	30
	2.2.2 Vapor Side Analysis	37
	2.2.3 Further Evaporator Analysis	40
	2.3 Condenser Model	45
	2.4 Turbine-Generator Model	49
	2.5 Cold Water System Model	55
	2.6 Warm Water System Model	61
	2.7 Ammonia Vapor Transport Model	65
	2.8 Generator AC Load Model	68
	2.9 Generator DC Load Model	71
	2.10 Seawater Pump Motor Model	73
	2.11 System Model Development from Component Models	74
	2.12 Linearization and Normalization of Model	75
	2.13 Steady State System Model	78

Page

CHAPTER III - OPEN LOOP DYNAMIC ANALYSIS 83

3.1 Open Loop Time Constant Analysis 83

3.2 Open Loop Model Dynamic Simulations 90

3.2.1 Turbine-Generator Torque Load Disturbance 91
3.2.2 Warm Seawater Temperature Disturbance 91
3.2.3 Cold Water System Pump Torque Disturbance 91
3.2.4 Bypass Valve Opening Disturbance .. 95
3.2.5 Cold Water Pump Motor Frequency Disturbance 97
3.2.6 Wave Disturbances 97

3.3 Open Loop Model Steady State Validation .. 105

3.4 Open Loop Dynamic Analysis Conclusions ... 109

3.4.1 Subsystem Interactive Transient Response 110
3.4.2 Effects of Disturbances 110
3.4.3 Effects of Control Mechanisms 112

CHAPTER IV - PARAMETRIC SENSITIVITY ANALYSIS 114

4.1 100% Load Level Sensitivities 115

4.2 Bypass Valve Sensitivities 116

CHAPTER V - CONTROL SYSTEM DEVELOPMENT 122

5.1 Turbine-Generator Overspeed Protection ... 124

5.2 OTEC Plant Control - AC Power Grid 126

5.3 OTEC Plant Control - DC Power Transmission 145

5.3.1 Basic Speed Governor Control 147
5.3.2 State Variable Feedback Control ... 172
5.3.3 DC Load Control 196

5.4 Pump Motor Controls 201

CHAPTER VI - DISCUSSION 209

6.1 OTEC Plant Start Up Considerations 209

6.2 Set Point Control Considerations 212

6.3 OTEC Baseload Power System Considerations. 214

Page

CHAPTER VII - CONCLUSIONS.................................. 216

LIST OF REFERENCES... 223

APPENDIX I - EVAPORATOR ANALYSIS........................... 225

APPENDIX II - TURBINE FLOW ANALYSIS........................ 231

APPENDIX III- SEAWATER SYSTEM ANALYSIS..................... 234

APPENDIX IV - NONLINEAR SYSTEM EQUATIONS................... 239

APPENDIX V - PHYSICAL TIME CONSTANT ESTIMATION............. 242

APPENDIX VI - GOVERNOR FEEDBACK GAIN DESIGN................ 248

APPENDIX VII- OTEC PLANT PARAMETERS........................ 251

APPENDIX VIII- STEADY STATE MODEL COMPUTER OUTPUT.......... 257

NOMENCLATURE

I. Analysis Nomenclature

1) Basic Symbols

T	temperature
p	pressure
$\dot{m}$	mass flow rate
ρ	density
τ	torque
ω	angular velocity
$\underline{\bar{X}}$	vapor quality
F	volume flow rate
P	power
V	volume
J	rotational inertia
L	length
I	Fluid inertance
s	Laplace operator
x	synchronous reactance
δ	power angle
U	overall heat transfer coefficient
AX	cross-sectional area
r	radius
H	dynamic fluid head
K	vapor flow coefficient
μ	fluid viscosity
z	pump efficiency
g_c	local gravitational constant
ID	inner diameter
OD	outside diameter

R	modeling resistance
h	enthalpy
y	number of cold water systems/cold pipe
E	voltage
i	current
K^*	open loop governor sensitivity
δ^*	governor droop
λ_i	ith eigenvalue
$\underline{N}_i$	ith eigenvector
$H(s)$	linear transfer function
ε	heat transfer lumping coefficient
v	velocity
m	mass
N	number of
$\underline{x}$	vector of states
$\underline{u}$	vector of input disturbances
$\underline{y}$	vector of outputs
c_p	specific heat
AS	surface area
ξ	damping ratio
ω_n	natural frequency

2) Subscripts

L	load
f	friction
t	heat exchanger tubes
T	terminal
m	motor
e	electric
DC	direct current
#	station number

s synchronous frequency

F fluid

v vapor

i inside

o outside

ev evaporator

cd condenser

wp warm water pump

cp cold water pump

tg turbine-generator

pi cold water pipe

bp bypass valve

w water

ℓ liquid

ss steady state

ℓv liquid to vapor

$v\ell$ vapor to liquid

∞ infinite bus

G generator

3) Special Symbols

L_{eq} equivalent flow length

h_{fg} heat of vaporization

A_{tg} turbine blade exit area

r_{tg} turbine blade mid-radius

α,β turbine blade mid-radius exit angles

u_{tg} turbine blade mid-radius velocity

w_d pump design speed

AS_i tube outside surface area/unit length

AS_o tube outside surface area

h_i tube inside heat transfer coefficient

AS_o' - tube outside surface area/unit length

L_{eff} - effective length of heat exchanger tubes

II. Computer Nomenclature

1) First Digits

HD - pump head

EFF - efficiency

ANG - power angle

T - temperature

P - pressure

MD - mass flow rate

RHO - density

TAU - torque

N - angular velocity

X - vapor quality

VD - volume flow rate

POW - power

E - voltage

2) Next Digits

a) flow path in Figure 1

b) device to which variable applies

WP - warm water pump

EV - evaporator

TG - turbine-generator

CP - cold water pump

CD - condenser

PI - cold water pipe

BP - bypass valve

L - load

INF - infinite bus

E - electric

c) last two digits

SS - steady state

MX - maximum

LIST OF FIGURES

FIGURE NUMBER	TITLE	PAGE
1	Detailed OTEC Power Cycle Schematic..........	19
2	Schematic of the Simplified Evaporator.......	31
3	Seawater Side Heat Transfer Process Schematic..................................	32
4	Schematic of the Evaporator Model............	41
5	Information Flow Diagram of the Evaporator System....................................	44
6	Schematic of the Simplified Condenser........	46
7	Schematic of the Condenser Model.............	48
8	Information Flow Diagram of the Condenser System....................................	50
9	Schematic of the Turbine-Generator Model.....	51
10	Information Flow Diagram of the Turbine-Generator System..........................	54
11	Schematic of the Cold Water System Model.....	57
12	Information Flow Diagram of the Cold Water System....................................	60
13	Schematic of the Warm Water System Model.....	62
14	Information Flow Diagram of the Warm Water System....................................	64
15	Schematic of the Vapor Transport System Model.....................................	67
16	Generator-Infinite Bus Circuit Model.........	70
17	Circuit Diagram of HVDC Transmission System..	70
18	Simplified Pump Motor Circuit Model..........	70
19	Schematic of the OTEC System Model...........	76
20	Vapor Flow Dynamics Load Sensitivity.........	87
21	Thermal Dynamics Load Sensitivity............	88
22	Turbine Dynamics Load Sensitivity............	89
23	Turbine-Generator Load Disturbance (Open Loop)....................................	92

FIGURE NUMBER	TITLE	PAGE
24	Warm Seawater Temperature Disturbance (Open Loop)	93
25	Cold Water Pump Torque Disturbance (Open Loop)	94
26	Bypass Valve Opening Disturbance (Open Loop)	96
27	Cold Water Pump Frequency Disturbance (Open Loop)	98
28	Cold Water Pump Frequency Disturbance (Open Loop)	99
29	Warm Water System Wave Disturbance (Open Loop)	101
30	Warm Water System Wave Disturbance (Open Loop)	102
31	Warm Water System Disturbance (Open Loop)	103
32	Cold Water System Wave Disturbance (Open Loop)	104
33	Warm Water System Wave Disturbance (Open Loop)	106
34	Warm Water System Wave Disturbance (Open Loop)	107
35	Warm Water System Wave Disturbance (Open Loop)	108
36	Power Output Sensitivity to the Bypass Valve	118
37	Turbine Vapor Flow Sensitivity to the Bypass Valve	119
38	Turbine-Generator Speed Sensitivity to the Bypass Valve	120
39	Governor Model Schematic	123
40	5% Governor Droop Characteristics	123
41	Turbine-Generator Load Drop-Uncontrolled	125
42	Turbine-Generator Load Drop-Overspeed Controller	127
43	AC Bus Frequency Disturbance (Open Loop)	128
44	AC Bus Frequency Disturbance-Initial Governor Control	130

FIGURE NUMBER	TITLE	PAGE
45	AC Bus Frequency Disturbance-Initial Governor Control	131
46	AC Bus Frequency Disturbance-Initial Governor Control	132
47	Open Loop Governor Sensitivity (power criterion)	134
48	Governor Gain for 5% Droop (AC Bus)	135
49	AC Bus Frequency Disturbance-Compensated Governor Control	136
50	AC Bus Frequency Disturbance-Compensated Governor Control	137
51	AC Bus Frequency Disturbance-Compensated Governor Control	138
52	AC Bus Frequency Disturbance-Compensated Governor Control	139
53	AC Bus Frequency Disturbance-Compensated Governor Control	140
54	AC Bus Frequency Disturbance-Compensated Governor Control	141
55	AC Bus Frequency Disturbance-Compensated Governor Control	142
56	AC Bus Frequency Disturbance-Compensated Governor Control	143
57	AC Bus Frequency Disturbance-Compensated Governor Control	144
58	DC Load Demand Disturbance (Open Loop)	146
59	Open Loop Governor Sensitivity (turbine speed criterion)	148
60	DC Load Demand Disturbance-1% Droop Governor	149
61	DC Load Demand Disturbance-1% Droop Governor	150
62	DC Load Demand Disturbance-1% Droop Governor	151
63	DC Load Demand Disturbance-3% Droop Governor	152
64	DC Load Demand Disturbance-3% Droop Governor	153
65	DC Load Demand Disturbance-3% Droop Governor	154
66	DC Load Demand Disturbance-5% Droop Governor	155

FIGURE NUMBER	TITLE	PAGE
67	DC Load Demand Disturbance-5% Droop Governor	156
68	DC Load Demand Disturbance-5% Droop Governor	157
69	Governor Gain for 3% Droop (DC Load)	159
70	DC Load Demand Disturbance-3% Droop Governor	161
71	DC Load Demand Disturbance-3% Droop Governor	162
72	Actuator Dynamics Model	163
73	DC Load Demand Disturbance-3% Droop Governor (Lag)	165
74	DC Load Demand Disturbance-3% Droop Governor (Lag)	166
75	DC Load Demand Disturbance-3% Droop Governor (Lag)	167
76	Warm Seawater Temperature Disturbance-3% Droop Governor (Lag)	168
77	Warm Seawater Temperature Disturbance-3% Droop Governor (Lag)	169
78	Warm Seawater Temperature Disturbance-3% Droop Governor (Lag)	170
79	Warm Seawater Temperature Disturbance-3% Droop Governor (Lag)	171
80	DC Load Demand Disturbance-L-Q Controller	176
81	DC Load Demand Disturbance-L-Q Controller	177
82	DC Load Demand Disturbance-L-Q Controller	178
83	DC Load Demand Disturbance-L-Q Controller	179
84	DC Load Demand Disturbance-L-Q Controller (Lag)	180
85	DC Load Demand Disturbance-L-Q Controller (Lag)	181
86	DC Load Demand Disturbance-L-Q Controller (Lag)	182
87	DC Load Demand Disturbance-Actuator Compensated L-Q Controller	184

FIGURE NUMBER	TITLE	PAGE
88	DC Load Demand Disturbance-Actuator Compensated L-Q Controller	186
89	DC Load Demand Disturbance-Actuator Compensated L-Q Controller	187
90	DC Load Demand Disturbance-Actuator Compensated L-Q Controller	188
91	DC Load Demand Disturbance-Actuator Compensated L-Q Controller	189
92	DC Load Demand Disturbance-Actuator Compensated L-Q Controller	190
93	Warm Seawater Temperature Disturbance-Actuator Compensated L-Q Controller	191
94	Warm Seawater Temperature Disturbance-Actuator Compensated L-Q Controller	192
95	Warm Seawater Temperature Disturbance-Actuator Compensated L-Q Controller	193
96	Warm Seawater Temperature Disturbance-Actuator Compensated L-Q Controller	194
97	DC Load Control Schematic	163
98	Bypass Valve Opening Disturbance-DC Load Controller	198
99	Bypass Valve Opening Disturbance-DC Load Controller	199
100	Bypass Valve Opening Disturbance-DC Load Controller	200
101	Wave Disturbance Attenuation of Cold Water System	202
102	Wave Disturbance Attenuation of Warm Water System	203
103	Open Loop Block Diagram of Warm Water System	205
104	Power Fluctuation Feedback Control System	205
105	Warm Water System Wave Disturbance-Power Controller	207
106	Turbine Flow Velocity Vector Analysis	232
107	Vapor Flow System Schematic	244
108	Cold Water Flow System Circuit Analogy	244

LIST OF TABLES

TABLE NUMBER	TITLE	PAGE
1	Westinghouse-Carmichael System Design Specifications	20
2	OTEC Model State Variables	79
3	OTEC Model Input Variables	79
4	OTEC Model Output Variables	80
5	Model System Description Numbers	81
6	OTEC Plant Time Constants (100% Load)	85
7	OTEC Plant Time Constant Sensitivity to Load	86
8	Steady State Comparison of Dynamic and Steady State Models	109
9	Full Load Sensitivities	115
10	Bypass Valve Sensitivities	117
11	Turbine Flow Rate Sensitivity	121
12	Turbine-Generator Speed Dynamics for 3% Droop	160

I. INTRODUCTION

1.1 General Description of the OTEC System

The Ocean Thermal Energy Conversion (OTEC) power plant is a closed Rankine cycle heat engine operating on the thermal gradient between the warm seawater at the surface of the ocean and the cold seawater in the ocean depths. Because of the low temperatures and pressures involved in the process, ammonia or refrigerant 12 is used as the working fluid for the cycle. The thermodyanmic cycle begins when heat is transferred to a pressurized liquid in a heat exchanger using the warm surface seawater (~80°F) as a heat source, causing the liquid to vaporize. The vapor is then expanded through a turbine to produce power. Heat is removed from the low pressure vapor exiting the turbine in another heat exchanger using the cold ocean floor seawater (~40°F) as a heat sink, resulting in condensation of the vapor. The low pressure liquid condensate is repressurized by a feedpump and returned to the evaporator to complete the cycle. A schematic diagram of the overall power cycle is shown in Figure 1. The liquid ammonia drain tank and recirculation pump are used to collect the unevaporated excess ammonia from the evaporator. This excess is necessary in normal operation to insure that none of the evaporator heat transfer area is exposed.

Many different OTEC power system designs exist which are based upon this simple concept. The design upon which the modeling

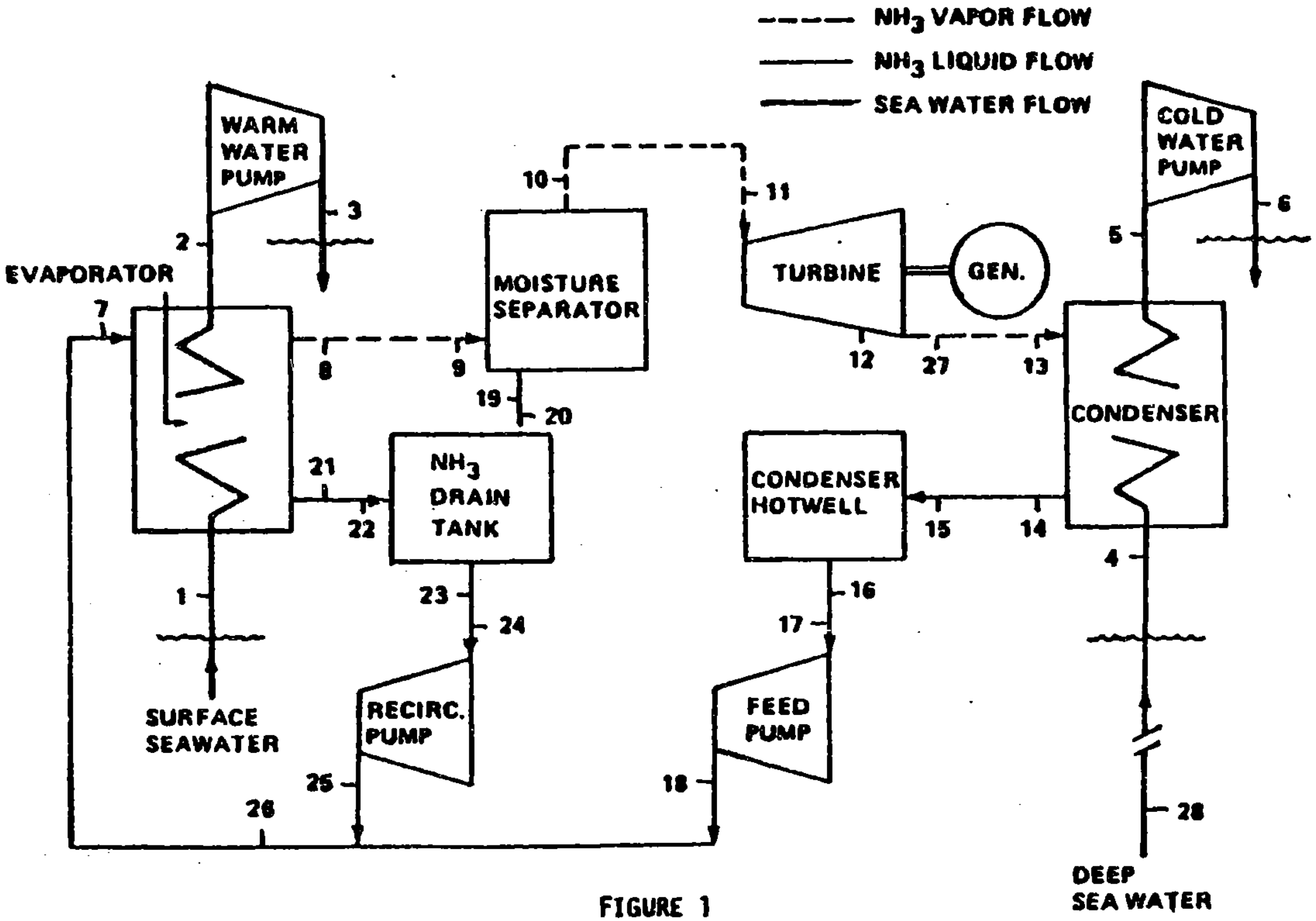

FIGURE 1

DETAILED OTEC POWER CYCLE SCHEMATIC

and subsequent analysis of this research effort is based is the proposed Westinghouse 50 MWe OTEC power module[1] in conjunction with the state of the art OTEC power plant analysis of Carmichael.[2] Some of the principle design features of this state of the art design are presented in Table 1.

TABLE 1: WESTINGHOUSE-CARMICHAEL SYSTEM DESIGN SPECIFICATIONS

Component	Design Specifications
Gross Power	67.4 Mw
Net Power	50.0 Mw
Heat Exchangers	Thin film tube and shell-horizontal tube
Turbine	Single stage-axial double flow
Baseload Power Plant	8-50 MW power modules
Cold Water Pipe	Length-3280 feet Diameter-100 ft
Working Fluid	Ammonia
Design ΔT	40°F
Seawater Pumps	Single stage-axial flow - 55 RPM
Turbine Control	Bypass valve

Many other OTEC power plant designs have been developed which operate from this closed loop cycle. Most differ in the design of the heat exchangers. Lockheed[3] proposes plate type cross-flow heat exchangers in which water flows horizontally through tubes while vertically flowing ammonia condenses or evaporates. Johns Hopkins[4] proposes a folded tube, shell-less concept for the heat exchangers in which liquid ammonia is evaporated by successive passes through the heat exchanger tubes. Other OTEC concepts include vertical falling film shell and tube heat exchanger designs. Practically all of the OTEC designs use ammonia as the working fluid. Turbine designs vary from single-stage, single flow concepts to turbines using multiple stages and double flow arrangements. Turbine control for most proposed OTEC designs consist of either inlet control valves or turbine vapor flow bypass valves, or both.

Much attention has been given to the steady state optimization of the OTEC power plant parameters and components in order to maximize power output while minimizing capital and operating costs. Very little attention has been given to the operational dynamic performance of the plant in order to analyze the transient interactions within the system in response to ocean environment and load disturbances. However, it is this dynamic performance which is of importance to the stability and control of the OTEC power plant when it is ultimately placed into operation.

This work focuses on the dynamic interactions between the mechanical, thermal, and fluid subsystems of the OTEC power plant, normally referred to as the slow speed dynamics of the system. Electrical transients, in most cases, are assumed to be an order of magnitude faster than these dynamics and are neglected. The principle objective of this work is to construct a reduced order, physically based, lumped parameter dynamic model which will identify the important dynamics of the OTEC power plant. This model is then used to analyze the sensitivity and transient behavior of the plant in response to system input disturbances. Finally, a control system is developed based on the dynamic model which will maintain the OTEC plant at a desired operating level while causing it to exhibit satisfactory transient stability and response.

The control strategy for the OTEC power plant is somewhat different than that of a conventional power plant. Because the evaporation rate in the heat exchanger is principally controlled by the seawater and ammonia vapor thermodyanmic state under normal operating conditions, the liquid ammonia subsystem is essentially decoupled from the vapor ammonia power loop. Thus, the plant power output cannot be quickly adjusted by varying the liquid ammonia feed rate into the evaporator. Because of the power required to maintain the large flow rates of seawater in the heat exchangers, these auxillary requirements cannot be neglected as they are in a conventional power plant. The large vapor flow rate and the low turbine pressure ratio preclude the use of turbine inlet control valves. Westinghouse[5] has shown that these would reduce the maximum output of the plant by as much as 4%. A bypass valve between the evaporator and condenser which would divert flow from the turbine is proposed as a principle means of controlling the plant output.

Because there is no "fuel" cost for the OTEC power plant, economics require that it be operated at maximum power output for a large percentage of the operational lifetime of the plant. This severely reduces the ability of the plant to response to outside disturbances. This load requirement also introduces the goal of maximizing the power output for a given set of environmental conditions by optimizing the plant operating conditions, i.e., set point control. Disturbances attributed to the ocean environment, that is, wave and seawater temperature fluctuations, must be taken into account by the control system.

The baseload power plant consisting of 8 separate 50 MW power modules sits on an isolated platform in the ocean, thus introducing the necessity of underwater power transmission to shore. Two types of power transmission are proposed: AC transmission for plants located within 50 kilometers of the shoreline; and an AC/DC rectifier/inverter transmission system for units located farther out. Both transmission systems possess certain dynamic characteristics which must be addressed. Because of its location, the OTEC baseload unit also experiences synchronization problems and loss of on-shore load requires that new stability and safety precautions be taken.

1.2 Scope of Effort

A reduced order, physically based, lumped parameter dynamic model of the OTEC power plant is developed using mass, energy, and momentum balances for each separate subsystem. This effort has been undertaken in conjunction with corresponding efforts by Sotelo[6] and Macedo[7]. In order to reduce the number of independent states and the complexity of the model, several simplifying assumptions are made for each component and subsequently justified. The resulting predominantly nonlinear constitutive relations and differential state equations for each subsystem are combined by input-output causal relationships to form a complete system model. This nonlinear system model is linearized about an operating point, resulting in a set of coupled first order linear time invariant state perturbation equations of the form:

$$\Delta\dot{\underline{x}} = \underline{\bar{A}}\,\Delta\underline{x} + \underline{\bar{B}}\,\Delta\underline{y} \tag{1}$$

$$\Delta\underline{y} = \underline{\bar{C}}\,\Delta x + \underline{\bar{D}}\,\Delta\underline{u} \tag{2}$$

where $\Delta\underline{x}$ - vector of state perturbations
$\Delta\underline{y}$ - vector of output perturbations
$\Delta\underline{u}$ - vector of input disturbance perturbations
$\underline{\bar{A}},\underline{\bar{B}},\underline{\bar{C}},\underline{\bar{D}}$ - constant coefficient matrices

The justification for proceeding with the analysis in this form is twofold: a) linear time invariant state perturbation equations greatly simplify the analysis of the dynamics and sensitivities of the system and b) they allow the powerful techniques of both modern and classical control theory to be used while designing the control system for the OTEC plant. The major drawback of linearized perturbation analysis is that the results are only valid for "small" variations from the steady state operating level.

The next step in the analysis is the coding of a computer model which evaluates the steady state operating level of the OTEC power plant given certain environmental and system conditions and which then generates the linearized state equations of the plant model. This effort is followed by the determination of system time constants from the model and open loop transient response simulations of the model to various disturbances. This analysis allows the assessment of which states of the system are the most important, and which input disturbances have the most effect on the system. Sensitivity studies are performed to show how changes in certain conditions of the plant affect steady state conditions elsewhere in the plant.

Effort has also been directed to design a control system which satisfies the OTEC plant operating requirements as set forth previously. More specifically, controllers are designed to regulate the turbine-generator speed in an effort to match the system power to the load and to regulate the power of the seawater pumps. A linear-quadratic state variable feedback controller is designed using a simplified reduced order model in an effort to obtain even better system regulation. The control system is designed for units using AC and DC transmission systems and is verified for different steady state operating levels.

The final section of this analysis effort deals qualitatively with special problems of the OTEC power plant-specifically, start up of the system and subsequent interface with the on-shore power grid; maximization at full load or set point control; and, finally, the special problems associated with the baseload power system of 8 operating 50 MW modules.

The model development in this research effort, although based on the Westinghouse OTEC design concept, can be applied to other closed cycle OTEC designs using different heat exchanger configurations provided the following three criteria are met:

1) the evaporation rate must not be very sensitive to the ammonia liquid influx rate into the evaporator

2) the seawater flow in the heat exchangers must be directly coupled to the pumping systems

3) the heat exchangers must be basically a shell and tube design

Because the turbine is a single stage, double-flow design, the analysis would require modification if any alternate design concept is used. The seawater pump analysis is only valid for axial flow centrifugal pumps. The vapor transport system model is valid for design concepts consisting of the identical flow paths.

II. MODEL DEVELOPMENT

2.1 Description of System Model

The OTEC power plant consists principally of the ammonia closed cycle power loop and the seawater pumping systems. The warm water system pumps warm surface seawater through the evaporator tubes which vaporizes the pressurized liquid ammonia entering the evaporator. The ammonia vapor flows out of the evaporator shell and through a liquid separator, which removes any entrained liquid from the vapor. The vapor then flows to the turbine and through it, resulting in the production of mechanical power. The reduced pressure vapor exiting the turbine enters the condenser and is condensed by the cold seawater circulating through the condenser tubes. The liquid ammonia condensate exits the condenser and is repressurized and combined with the excess liquid efflux from the evaporator to complete the cycle. The cold water system pumps the cold seawater from the ocean depths up through a large cold water pipe, through the condenser, and discharges it back into the ocean. The vapor flow through the turbine is modulated by a bypass valve which diverts flow from the evaporator directly to the condenser in order to control the power output of the turbine-generator. The generator is connected to a large on-shore power grid via either direct AC or a DC rectifier/inverter transmission system. The large seawater pumps are powered by AC synchronous motors operating from a variable frequency controller.

The OTEC power plant can be segregated into several principal subsystems or components. This simplifies the modeling process by allowing each principal component to be modeled separately. Mathematical models are developed for each of the following OTEC components: a) the evaporator, b) the condenser, c) the turbine-generator, d) the cold water system, e) the warm water system, f) the vapor transport system, g) the seawater pump motors, and h) the generator load. These separate component models are combined according to the configuration and physical process coupling of the OTEC plant design. A schematic diagram of the complete system model is shown in Figure 19.

2.1.1 Basic Modeling Criteria

Before the modeling process can commence, certain basic criteria must be established in order to lay the initial groundwork for further model development. The first and most important consideration is that the model be physically based, that is, it is derived from actual physical parameters of the OTEC power plant. Thus, the model is developed according to the basic physical principles governing the actual processes in each component of the system. A second criteria is that, since the model is to be used for computer simulations of transient behavior and as a tool in control development, it is desirable that the dynamics of the system model be represented by coupled ordinary differential state equations, necessitating a lumped parameter modeling approach. This approach is used for the heat exchanger heat transfer processes, even though they might be more accurately modeled as distributed parameter systems. A distributed parameter modeling approach results in transcendental functions which do not easily lend themselves to computer simulations. A third basic assumption is that whenever duplicate mechanical devices, such as pumps, perform the same function for a given systen they are assumed to operate identically both dynamically and statically and are represented by a single device.

2.2 Evaporator Model

The evaporator for the OTEC power system is a shell and tube heat exchanger consisting of a large number of horizontal tubes housed in a large cylindrical shell. The evaporization system works as follows: high pressure liquid ammonia enters at the top of the evaporator and is collected in storage trays. The storage trays distribute the liquid ammonia evenly over the rows of horizontal tubes below where it forms a thin film surrounding the tubes. Warm surface seawater is pumped through the tubes which raises the liquid film to its saturation temperature and, as a result, nucleate boiling and evaporation occurs releasing ammonia vapor into the evaporator shell. The unvaporized excess liquid ammonia leaves the evaporator at the bottom and is refluxed back into the liquid feed system. The ammonia vapor leaves the evaporator through a liquid separator which removes any entrained liquid from the vapor before it enters the turbine.

Before the heat exchanger evaporization process can be modeled, certain basic simplifying assumptions must be made. First, a one-dimensional model is assumed, that is, the state and properties of a given cross-sectional area may be represented by constant quantities. Secondly, axial heat transfer by conduction along the length of the heat exchanger is neglected. Thirdly, the heat exchanger model is derived using mass and energy conservation for each component which is considered to be important. Lastly, because of the complexity of the heat transfer process when each heat exchanger tube is examined independently, the evaporator is modeled as a single tube heat exchanger of equivalent heat transfer area. Figure 2 is a schematic diagram of the idealized evaporator process.

2.2.1 Seawater Side Analysis

The heat transfer process on the seawater side of the evaporator using the basic modeling assumptions becomes a purely convective process shown in Figure 3.

Conservation of mass for the seawater side, assuming constant fluid density, leads to the identity

$$\dot{m}_{win} = \dot{m}_{wout} \qquad (3)$$

where $\dot{m}_{win}$ - water mass flow rate in
$\dot{m}_{wout}$ - water mass flow rate out

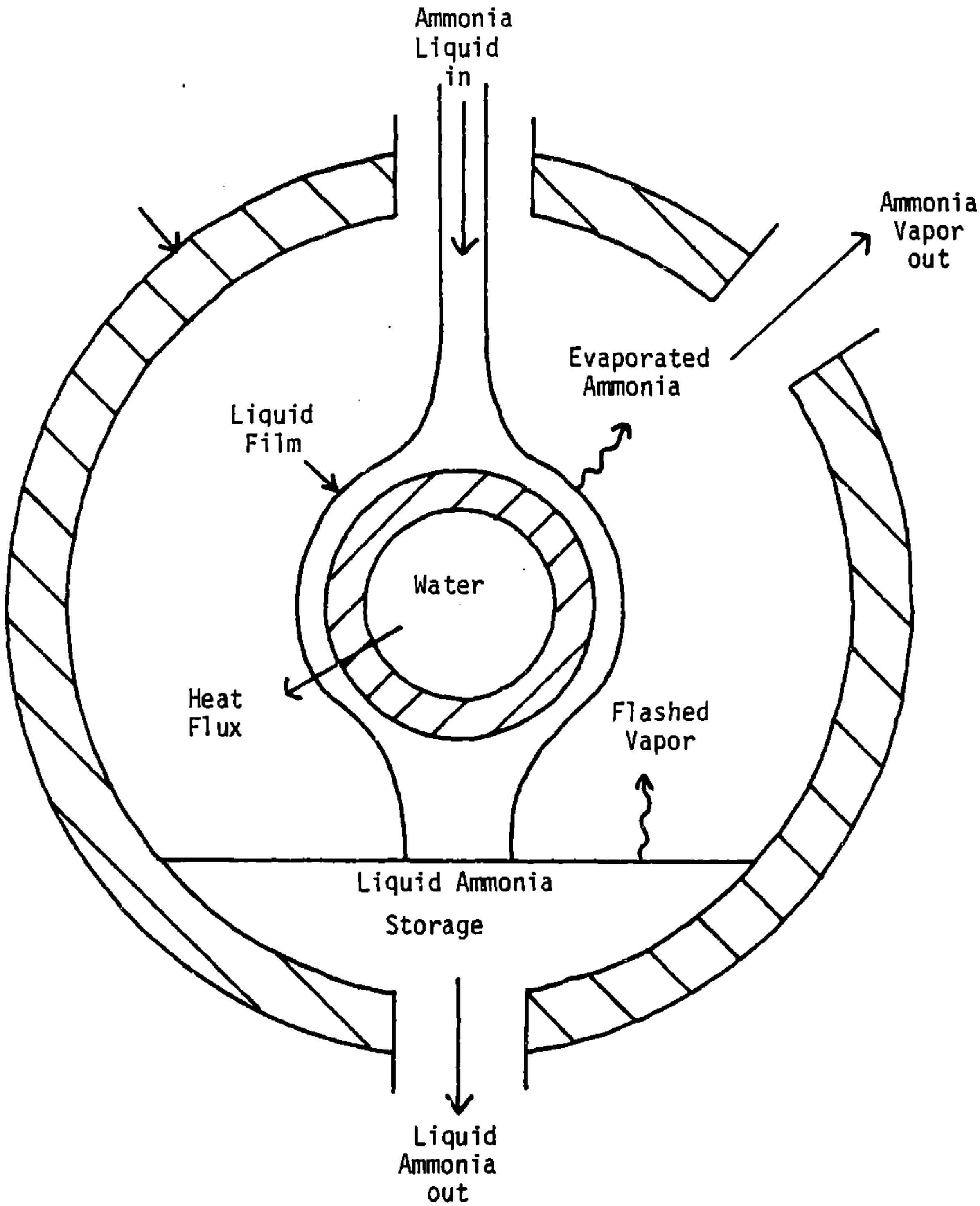

FIGURE 2: SCHEMATIC OF THE SIMPLIFIED EVAPORATOR

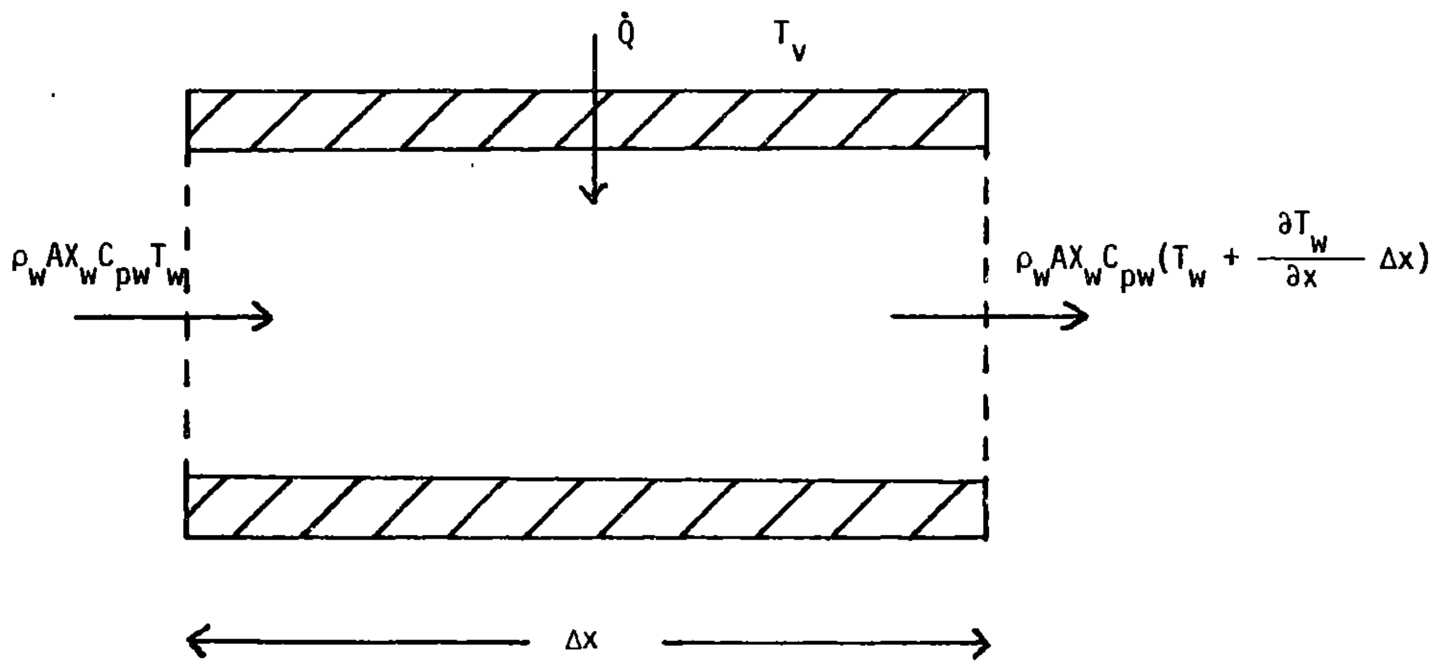

FIGURE 3: SEAWATER SIDE HEAT TRANSFER PROCESS SCHEMATIC

Conservation of energy for the water side results in

$$\rho_w \, AX_w \, C_{pw} \, \frac{\partial T_w}{\partial t} + \rho_w \, AX_w \, C_{pw} \, v_w \, \frac{\partial T_w}{\partial t} = \dot{Q} \qquad (4)$$

where
- ρ_w - water density
- AX_w - cross sectional flow area
- C_{pw} - water specific heat
- T_w - water temperature
- v_w - water velocity
- $\dot{Q}$ - heat flux into water

and for fully developed flow the heat transfer rate is represented by

$$\dot{Q} = h_i AS_i (T_t - T_w) \qquad (5)$$

where
- h_i - tube inside heat transfer coefficient
- AS_i - tube inside surface area/unit length
- T_t - tube temperature

resulting in

$$\rho_w \, AX_w \, C_{pw} \, \frac{\partial T_w}{\partial t} + \rho_w \, AX_w \, C_{pw} \, v_w \, \frac{\partial T_w}{\partial t} = h_i AS_i (T_t - T_w) \qquad (6)$$

At this point, a further simplifying assumption is made. Profos[8], in his analysis of heat exchanger dynamics, defined the percolation time constant as

$$T_p = \frac{\rho_t \, AX_t \, C_{pt} L_t}{\rho_w \, AX_w \, C_{pw} v_w} \qquad (7)$$

where T_p - percolation time constant

ρ_t - tube density

AX_t - tube cross-sectional area

C_{pt} - tube specific heat

This time constant essentially defines the time required for a change in water temperature to be reflected in the tube wall temperature. For the evaporator, evaluation of this time constant gives $T_p \approx 0.6$ seconds. Since this time constant is sufficiently small, it allows the water and tube heat capacities to be lumped together in the dynamic sense. This is accomplished by defining a new effective heat capacity/unit length based on the specific heat of water

$$(\rho AX)_{eff}\, C_{pw} = (\rho_w\, A_w + \rho_t AX_t \frac{C_{pt}}{C_{pw}}) C_{pw} \tag{8}$$

Both specific heats are assumed to be constant.

Rewriting Equation (6) to include the lumped tube and water masses

$$(\rho AX)_{eff}\, C_{pw} \frac{\partial T_w}{\partial t} + \rho_w\, AX_w\, C_{pw} v_w \frac{\partial T_w}{\partial x} = UAS_o'(T_v - T_w) \quad (\text{r}$$

where AS_o' - tube outside surface area / unit length

U - overall heat transfer coefficient

T_v - vapor temperature

The overall heat transfer coefficient, U, is now used in place of the inside heat transfer coefficient to reflect the lumping of the tube and water masses, and the vapor temperature replaces the tube wall temperature.

Equation (9) is a distributed parameter partial differential equation involving differentials of both space and time. In order to reduce it to an ordinary differential equation involving only differentials of time, simplifying assumptions are made. For a given differential length of the evaporator tube, the water temperature in that volume can be represented by a single value, the so-called "stirred tank" modeling approach. Using this assumption, Equation (9) is integrated along a differential length ΔL to obtain

$$(\rho AX)_{eff}\, C_{pw} \Delta L \, \frac{dT_w}{dt} + \rho_w\, AX_w\, C_{pw} v_w (T_{wout} - T_{win}) = UAS_o' \Delta L (T_v - T_w) \quad (10)$$

where ΔL - differential tube length

T_{out} - water temperature at outlet

T_{win} - water temperature at inlet

where T_w represents the lumped water temperature of the differential volume and is some function of both the inlet and outlet water temperatures of that lump.

$$T_w = \psi T_{wout} + (1 - \psi) T_{win} \tag{11}$$

Masada[9] showed that unless ψ=1 ($T_w = T_{wout}$), dynamic responses obtained by Equation (11) result which conflict with actual physical phenomena. Therefore, Equation (10) can be rewritten as

$$(\rho AX)_{eff}\, C_{pw} \Delta L \frac{dT_{wout}}{dt} + \rho_w\, AX_w C_{pw} v_w (T_{wout} - T_{win}) = UAS_o' \Delta L (T_v - T_{wout}) \tag{12}$$

Before continuing, it is necessary to determine how many "lumps" are necessary to adequately represent the thermal process dynamics of the water-tube portion of the evaporator. Masada[10] showed that for disturbances on the vapor side and for fluid flow rate disturbances to this process, a one lump approximation for the entire heat exchanger is valid for the frequency range of interest. For inlet temperature disturbances, a one lump approximation is only valid at very low frequency variations. However, for the OTEC system, inlet seawater temperatures vary slowly, on the order of minutes to hours, thus making the one lump approximation a valid representation of the heat exchanger process. Equation (12) can now be written as a one lump approximation representing the water-tube thermal process for the entire evaporator.

$$(\rho AX)_{eff}\, C_{pw} L_{ev} \frac{dT_{wout}}{dt} + \rho_w\, AX_w C_{pw} v_w (T_{wout} - T_{win}) = UAS_o (T_v - T_{wout}) \tag{13}$$

where L_{ev} - length of evaporator tubes

2.2.2 Vapor Side Analysis

Analysis of the vapor side of the evaporator requires that liquid mass, vapor mass, and energy be conserved. The liquid mass balance is (neglecting any effects of the liquid storage tray)

$$\frac{dm_\ell}{dt} = \Sigma\dot{m}_{\ell in} - \Sigma\dot{m}_{\ell out} - \Sigma\dot{m}_{\ell v} + \Sigma\dot{m}_{v\ell} \quad (14)$$

where
m_ℓ - liquid mass in volume
$\dot{m}_{\ell in}$ - liquid mass influx to volume
$\dot{m}_{\ell out}$ - liquid mass efflux from volume
$\dot{m}_{\ell v}$ - liquid mass vaporized
$\dot{m}_{v\ell}$ - vapor mass condensed

Vapor mass conservation requires that

$$\frac{dm_v}{dt} = \Sigma\dot{m}_{\ell v} - \Sigma\dot{m}_{v\ell} - \Sigma\dot{m}_{vout} \quad (15)$$

where
m_v - vapor mass in volume
$\dot{m}_{vout}$ - vapor mass efflux from volume

If the assumption is made that the liquid and vapor in the evaporator are always in saturated equilibrium and further neglect the heat capacity of the liquid shell, the energy balance on the vapor side is written as:

$$\frac{dE_{cv}}{dt} = \dot{Q}_{net} + \Sigma\dot{m}_{\ell}\, h_{\ell in} + \Sigma\dot{m}_{\ell}\, h_{\ell out} - \Sigma\dot{m}_{v} h_{vout} \quad (16)$$

where
- E_{cv} - total energy in volume
- $\dot{Q}_{net}$ - energy transfer into volume
- h_{ℓ} - enthalpy of liquid
- h_{v} - enthalpy of vapor

In order to reduce the complexity of this equation, the following simplifying assumptions are made:

1) neglect the mass of the liquid film

2) neglect the heat capacity of the liquid storage in the evaporator shell

3) constant volume in the evaporator shell-the liquid storage level does not change

4) constant heat of vaporization-2% variation maximum

5) effects because of variations in liquid enthalpy flux are negligible-this effect is included in the steady state model but as long as the recycle ratio ($\dot{m}_{\ell in}/\dot{m}_{\ell out}$) remains fairly constant, there is no effect in the process dynamics

6) neglect flashing of liquid storage in evaporator shell

7) neglect heat loss to environment-insulation and small temperature gradient with the outside environment make this negligible

8) ammonia vapor quality, x = 1.0

9) neglect liquid ammonia entrained in vapor

(10) the ammonia internal energy equals the enthalpy (u=h) - variations in internal energy equal variations in enthalpy, that is, $\Delta h = \Delta u + \Delta PV$, where ΔPV is negligible

(11) neglect the heat capacity of the ammonia vapor; ≈ 2% of total dynamic variation

(12) boiling dynamics are very fast compared to the other heat transfer dynamics

Since $m_v = \rho_v V_{ev}$ and the evaporator volume is constant (assumption 3), Equation (15) can be re-written as

$$V_{ev} \frac{d\rho_v}{dt} = \Sigma\dot{m}_{\ell v} - \Sigma\dot{m}_{vout} - \Sigma\dot{m}_{v\ell} \tag{15a}$$

where V_{ev} - evaporator void volume

ρ_v - vapor density

Under the assumption that the ammonia vapor is saturated equilibrium, the vapor pressure is no longer independent of its temperature, i.e., $P_v = f(T_v)$. Also, referring to the ideal gas law

$$P_v = \rho_v R T_v \tag{17}$$

where P_v - vapor pressure

R - ideal gas constant

T_v - vapor temperature

the vapor density is also a function of the vapor temperature at saturation, or $\rho_v = f(T_v)$. This leads to the conclusion that Equations (15) and (16) are not independent of one another, and, therefore, can be combined in the analysis.

Under the above assumptions, Equations (14) and (16) are rewritten in the following simplified form. (See Appendix I)

$$V_{ev} \frac{d\rho_v}{dt} = \frac{UAS_o(T_{wout}-T_v)}{h_{fg}} - \dot{m}_{vout} \qquad (18)$$

where $\quad h_{fg}$ - heat of vaporization

$$\dot{m}_{\ell out} = \dot{m}_{\ell in} - \dot{m}_{\ell v} \qquad (19)$$

2.2.3 Further Evaporator Analysis

Figure 4 is a schematic diagram of the simplified heat transfer process. The assumption of a constant overall heat transfer coefficient is made to further simplify the evaporator analysis. While this is not true dynamically in the physical process, it can be shown that for perturbations of the lumped parameter model, it is a valid assumption. The heat transfer coefficient inside the tube, h_i, is very sensitive to the fluid velocity. McAdams,[11] among others, has determined this sensitivity to be

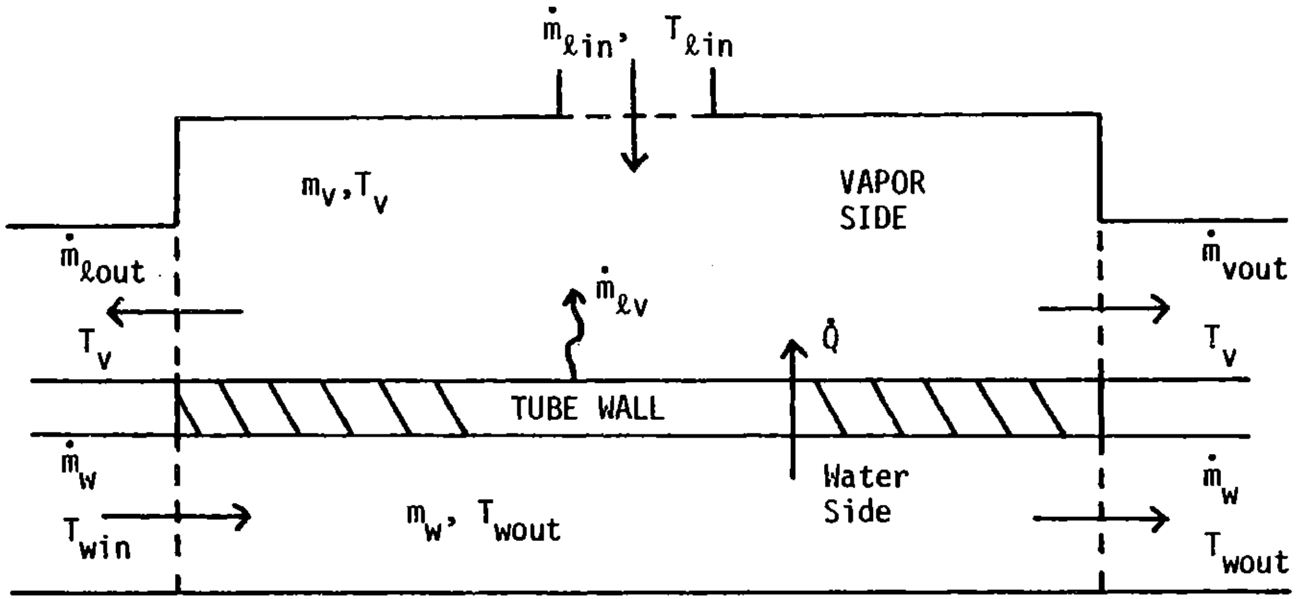

FIGURE 4: SCHEMATIC OF THE EVAPORATOR MODEL

$$h_i = K\, v_w^{0.8} \tag{20}$$

where K is a constant. The actual heat transfer rate perturbation as a result of a fluid flow disturbance is approximately 15% greater when compared to the heat transfer rate of a constant overall heat transfer coefficient. However, because of the lumped approximation of the fluid temperature in the model, a disturbance in the fluid flow produces an approximately 15% greater heat transfer rate than physically occurs, since the water temperature actually varies from the inlet to the outlet temperature. These two modeling errors have opposite and cancelling effects as a result of fluid velocity disturbances. The "lumping" error is much less pronounced during vapor side and water inlet temperature disturbances. Thus, the assumption of a constant heat transfer coefficient is reasonably accurate. A heat transfer lumping coefficient was introduced into the analyais[12] to correct the error between the heat transfer for the "lumped" temperature model and the heat transfer for the distributed temperature of the actual process.

$$UAS_o(\varepsilon\, T_{wout} - T_v) \tag{21}$$

However, accurate results are obtained using a lumping coefficient equal to unity for the linearized perturbation model.

The two dynamic state equations for the vaporator are written in the following form:

$$\frac{dT_{wout}}{dt} = Z_1(T_{win} - T_{wout}) - Z_2(T_{wout} - T_v) \tag{22}$$

$$\frac{d\rho_v}{dt} = Z_3(T_{wout} - T_v) - Z_4\, \dot{m}_{vout} \tag{23}$$

where $$Z_1 = \frac{\rho_w A X_w v_w}{(\rho A X)_{eff} L_{ev}} \qquad Z_2 = \frac{UAS_o}{(\rho A X)_{eff} c_{pw} L_{ev}}$$

$$Z_3 = \frac{UAS_o}{V_{ev} h_{fg}} \qquad Z_4 = \frac{1}{V_{ev}}$$

The two independent physical states in the evaporator are the water outlet temperature, T_{wout}, and the ammonia vapor density, ρ_v. An input-output information flow diagram for the evaporator is given in Figure 5.

One interesting feature of the evaporator model as developed from these simplifying assumptions is that the liquid ammonia side of the OTEC system is completely decoupled from the vapor power loop. This means that the output of the plant is controlled by the thermodynamic state of the seawater and ammonia vapor in the heat exchangers, provided burnout does not occur; i.e., provided the influx of liquid ammonia remains sufficient to wet all of the heat transfer surface.

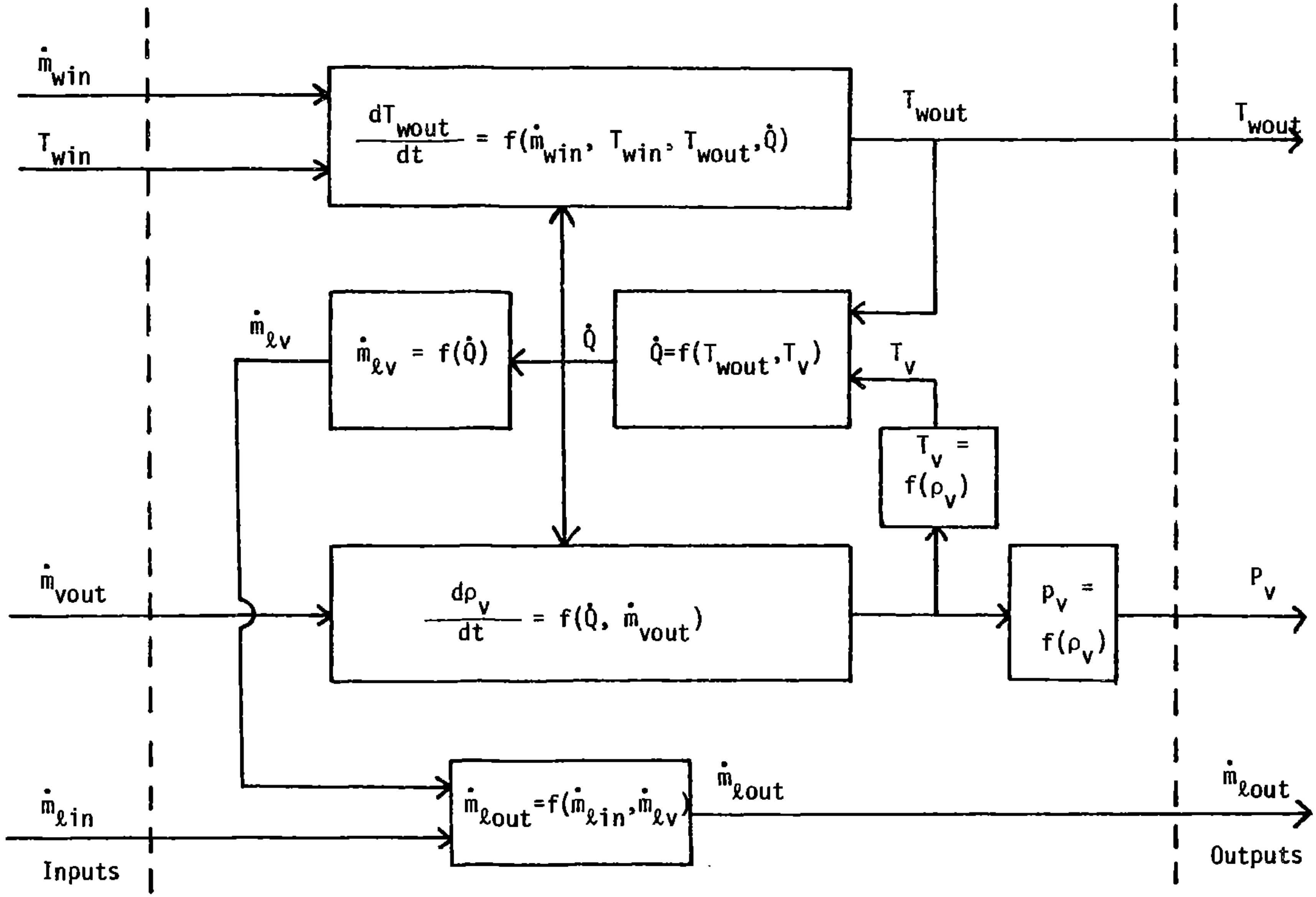

FIGURE 5: INFORMATION FLOW DIAGRAM OF THE EVAPORATOR SYSTEM

2.3 Condenser Model

The condenser for the OTEC power plant is almost identical to the evaporator in terms of heat exchanger design. The reduced pressure vapor from the turbine exit enters the condenser shell and is condensed in a thin film around the condenser tubes by heat transfer to the cold ocean floor seawater which is pumped through the tubes. This liquid condensate leaves the condenser at the bottom and is recycled to the liquid ammonia feed system. Figure 6 is a diagram of simplified condenser system.

The same basic modeling assumptions used for the evaporator are invoked for the condenser: a) a one-dimensional model, b) neglect axial conduction, c) mass and energy conservation, and d) a single tube approximation. The analysis for the water side is identical except for the direction of net heat transfer. The vapor side analysis is very similar except for two minor exceptions:

1) the ammonia vapor entering the condenser is at constant quality, $x = x_{ss}$

2) there is no liquid entrainment in the vapor

These assumptions modify the mass and energy balances in the condenser to include the following terms

$$\dot{m}_{vin} = x_{ss}\,\dot{m}_{in} \tag{24}$$

$$\dot{m}_{\ell in} = (1 - X_{ss})\dot{m}_{in} \tag{25}$$

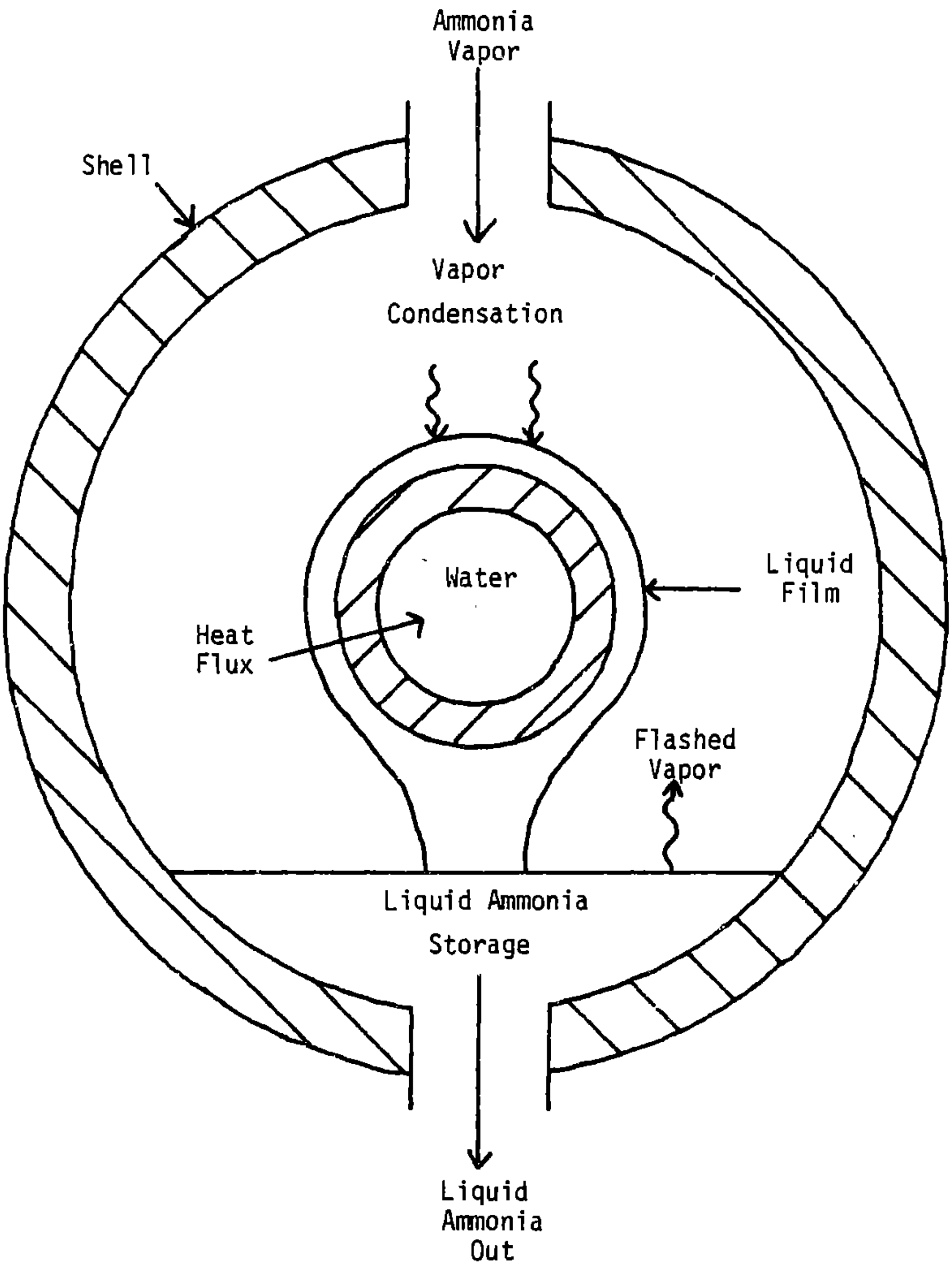

FIGURE 6: SCHEMATIC OF THE SIMPLIFIED CONDENSER

where x_{ss} - steady state vapor quality

$\dot{m}_{in}$ - total mass flow rate into volume

Figure 7 is a schematic diagram of the simplified condenser heat transfer process.

Using an analysis for the condenser analogous to that of Appendix I for the evaporator, the following condenser state equations are derived:

$$\frac{dT_{wout}}{dt} = Z_5(T_{win} - T_{wout}) + Z_6(T_v - T_{wout}) \tag{26}$$

$$\frac{d\rho_v}{dt} = Z_7\,\dot{m}_{vin} - Z_8(T_v - T_{wout}) \tag{27}$$

where
$$Z_5 = \frac{\rho_w AX_w c_{pw} v_w}{(\rho AX)_{eff} c_{pw} L_{cd}} \qquad Z_6 = \frac{UAS_o}{(\rho AX)_{eff} c_{pw} L_{cd}}$$

$$Z_7 = \frac{X_{ss}}{V_{cd}} \qquad Z_8 = \frac{UAS_o}{V_{cd} h_{fg}}$$

V_{cd} - condenser void volume

L_{cd} - length of condenser tubes

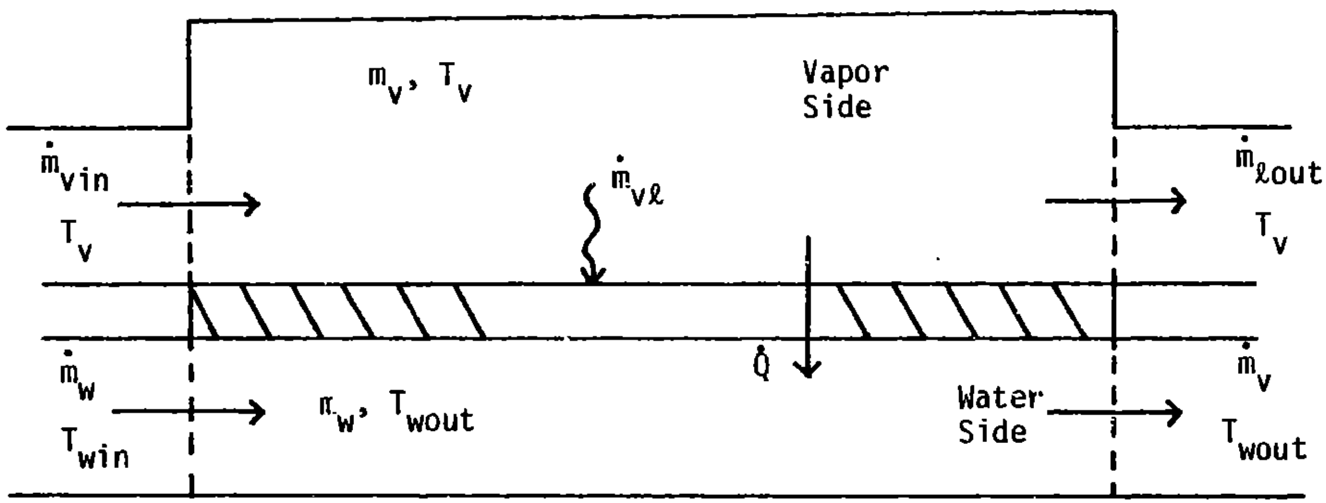

FIGURE 7: SCHEMATIC OF THE CONDENSER MODEL

The two independent physical states in the condenser are the water outlet temperatures, T_{wout}, and the ammonia vapor density, ρ_v. Figure 8 is an input-output information flow diagram for the condenser.

2.4 Turbine-Generator Model

The turbine for the OTEC power plant is a double axial flow, low pressure ratio, high flow prime mover. It is designed for a gross power output of 68 MW at an angular velocity of 1800 RPM. Because of the low pressure ratio, the turbine is of single stage design and uses no reheats. The turbine is connected directly to the generator by a rigid shaft.

Figure 9 is a schematic diagram of the turbine-generator system. Conservation of angular momentum for the system yields the following dynamic equation.

$$J_{tg} \frac{dw_{tg}}{dt} = \tau_{tg} - \tau_L - \tau_f \tag{28}$$

where
- J_{tg} - turbine-generator rotational inertia
- w_{tg} - turbine-generator angular velocity
- τ_{tg} - turbine-generator input torque
- τ_L - turbine-generator torque load
- τ_f - turbine-generator friction torque

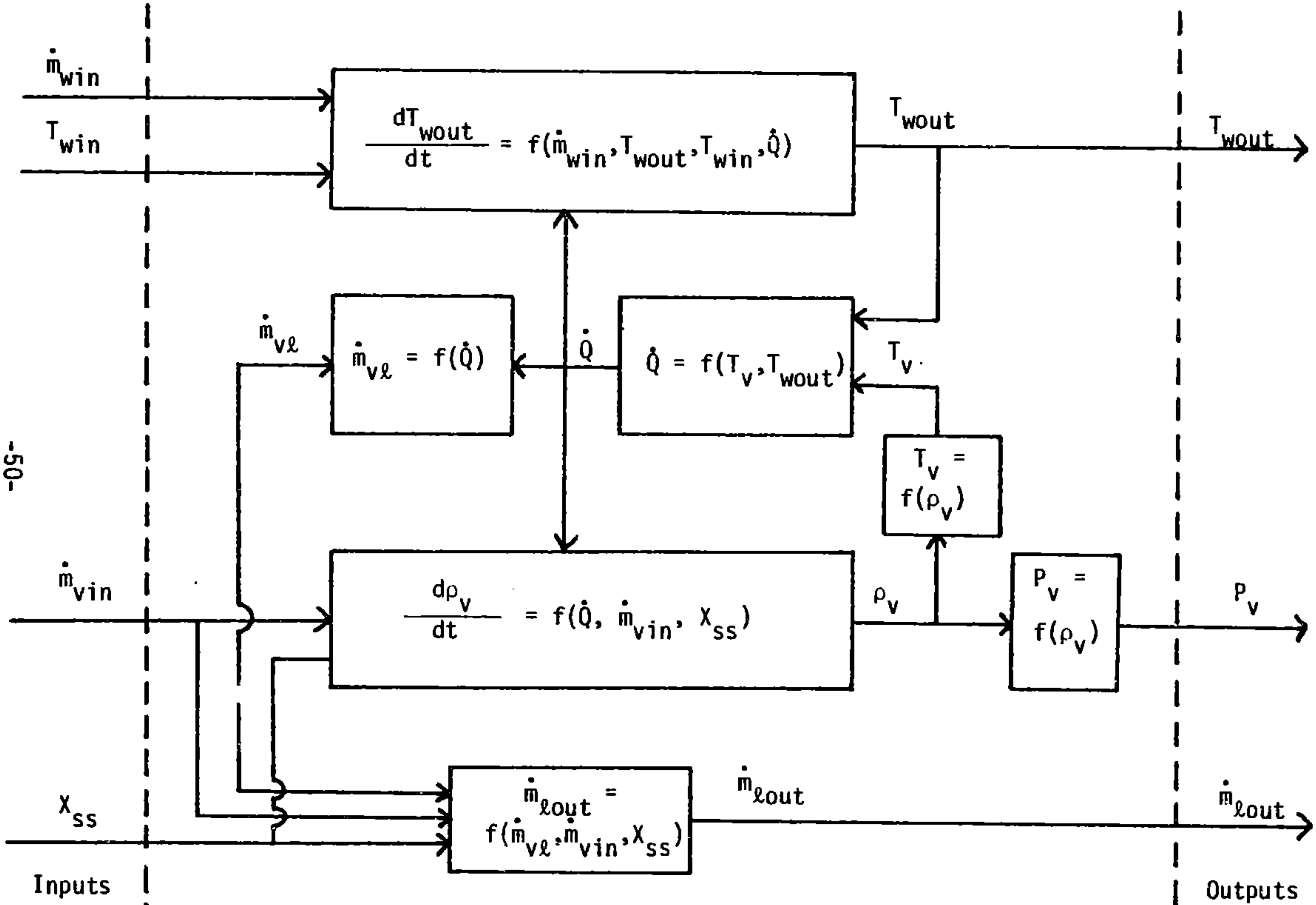

FIGURE 8: INFORMATION FLOW DIAGRAM OF THE CONDENSER SYSTEM

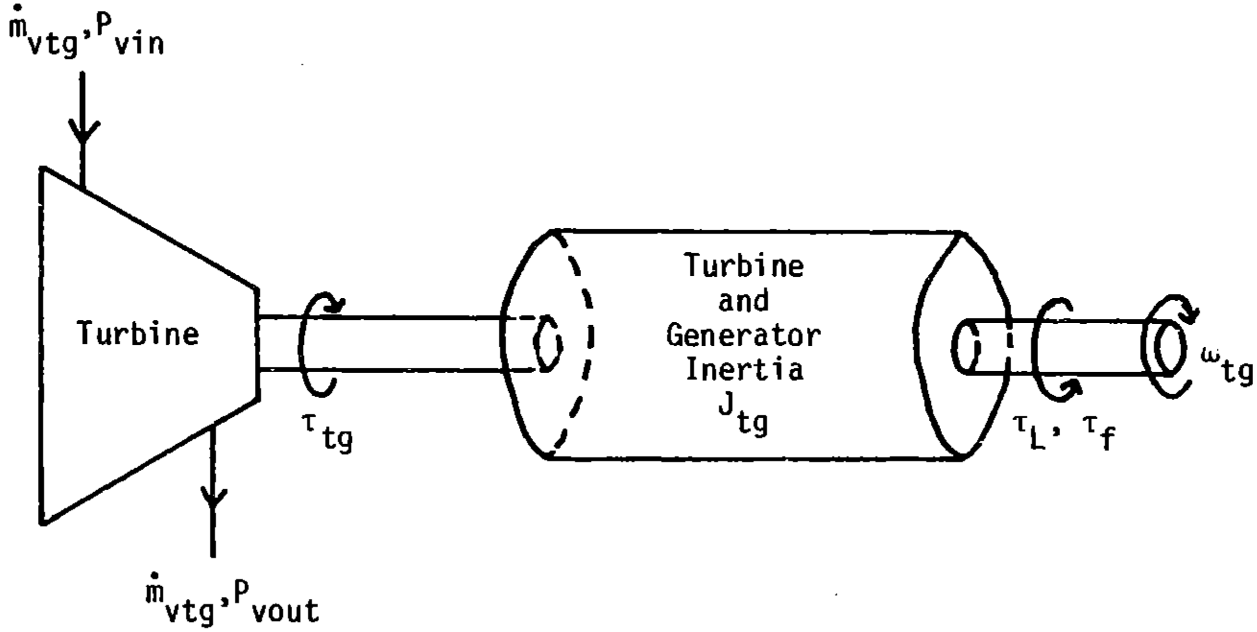

FIGURE 9: SCHEMATIC OF THE TURBINE-GENERATOR MODEL

Because the turbine and generator are coupled by a rigid shaft, their rotational inertias are combined. The load torque, τ_L, is a result of the electrical load on the generator. The friction torque, τ_f, is supplied by the mechanical losses in the turbine-generator system. The mechanical input torque, τ_{tg}, is generated by the expansion of the ammonia vapor in the turbine.

The power produced in the turbine by vapor expansion is represented by Euler's equation:

$$P_{tg} = \dot{m}_{vtg}(h_{vin}-h_{vout}) \tag{29}$$

where P_{tg} - turbine-generator power

$\dot{m}_{vtg}$ - turbine vapor mass flow rate

Performing a simple fluid flow analysis on the turbine blades, the turbine torque generated by the ammonia flow is derived. (See Appendix II)

$$\tau_{tg} = B_1 \frac{\dot{m}_{vtg}^{2}}{\rho_v} + B_2 \dot{m}_{vtg}\omega_{tg} \tag{30}$$

where r_{tg} - turbine blade mid-radius

A_{tg} - turbine blade exit area

α_1, α_2 - turbine blade mid-radius exit angles

$$B_1 = \frac{r_{tg}}{2A_{tg}} (\tan\alpha_1 + \tan\beta_2)$$

$$B_2 = - \frac{1}{r_{tg}^{\ 2}}$$

This turbine-generator torque is modified for the double flow turbine and the vapor density is assumed to be evaluated at the turbine exit conditions.

The following simplifying assumptions are made:

1) the turbine exit conditions are identical to those in the condenser (i.e., negligible pressure drop between the turbine outlet and the condenser)

2) the vapor entering the turbine is in saturated equilibrium at $x = 1.0$

3) the vapor leaving the turbine is in saturated equilibrium at $x = x_{ss}$

4) neglect any vapor storage effects in the turbine-steam bowl time constant ≈ 0.1 sec is negligible

5) the mechanical torque loss, τ_f, is a function of the generator torque load, that is,

$$\tau_f = a\tau_L \tag{31}$$

where $a << 1$

6) The power supplied by the turbine is equal to the generated electrical power-the generator efficiency is 100%.

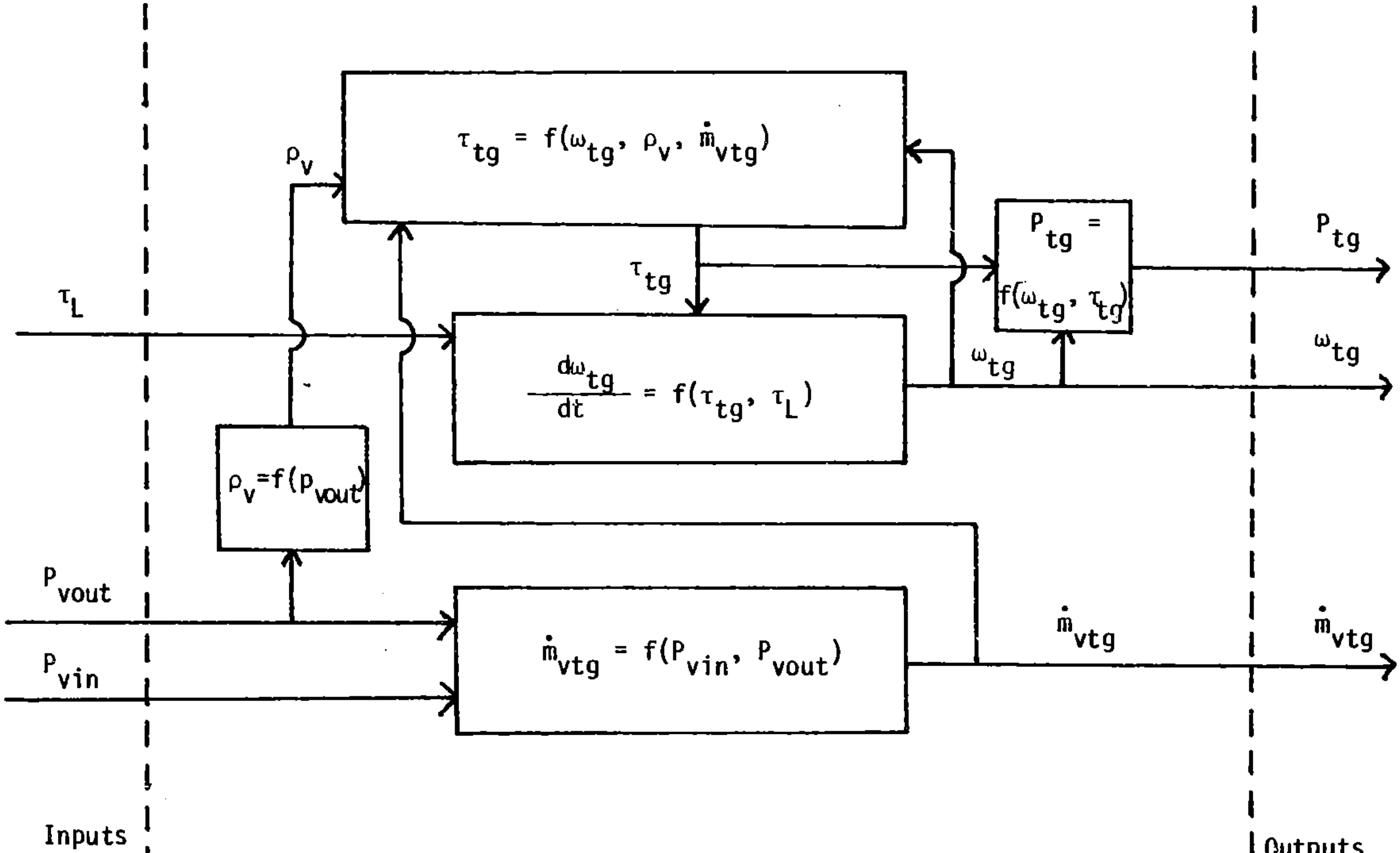

FIGURE 10: INFORMATION FLOW DIAGRAM OF THE TURBINE-GENERATOR SYSTEM

The vapor mass flow rate through the turbine is given by Stodola's ellipse law[13]

$$\dot{m}_{vtg} = K_{tg}\sqrt{1 - \left(\frac{P_{vout}}{P_{vin}}\right)^2} \tag{32}$$

where K_{tg} is a function of the flow path and can be evaluated at the steady state design conditions of the turbine.

The independent physical state for the turbine-generator is the shaft speed, ω_{tg}. An input-output information flow diagram for the turbine-generator system is shown in Figure 10.

2.5 Cold Water System Model

The cold water system of the OTEC power plant brings cold ocean floor seawater from 3280 feet below the surface up through a 100 foot diameter pipe, through the condenser, and discharges it about 200 feet below sealevel. This task is accomplished by two 55 rpm, 5800 HP pumps operating at the condenser discharge. These pumps must overcome both the frictional flow losses in the system and the fluid head resulting from the density gradient between the cold, dense seawater in the cold water pipe and the warmer, less dense seawater in the surrounding ocean. The baseload OTEC power system has eight separate condenser pumping stations operating from one cold pipe. All pumping stations are assumed to operate simulataneously and identically both in the steady state and during a transient. The seawater from the cold pipe enters a manifold from which it is drawn into each condenser. There is no free surface in the manifold and, therefore, no capacitance effects. The following modeling assumptions are made:

1) slug flow in both the cold pipe and the condenser system

2) fluid inertia effects in the condenser system are an order of magnitude less than those in the cold pipe and are neglected

3) fluid entrance and exit losses are neglected-less than 7% of the total losses

4) constant fluid density in the cold water system

A schematic diagram of the cold water system is shown in Figure 11. The system is modeled by means of a momentum balance for the fluid in the cold pipe and an energy balance for the cold water pumps. The momentum balance for the cold pipe yields

$$H_1 - H_2 - \Delta H_{fpi} = y\ I_{pi} \frac{dF_{wcp}}{dt} \tag{33}$$

where

$H_{\#}$ - total dynamic head at station

ΔH_{fpi} - friction head losses in cold water pipe

y - no. of 50MW modules/cold pipe

I_{pi} - fluid inertance of cold pipe

F_{wcp} - water flow rate through condenser

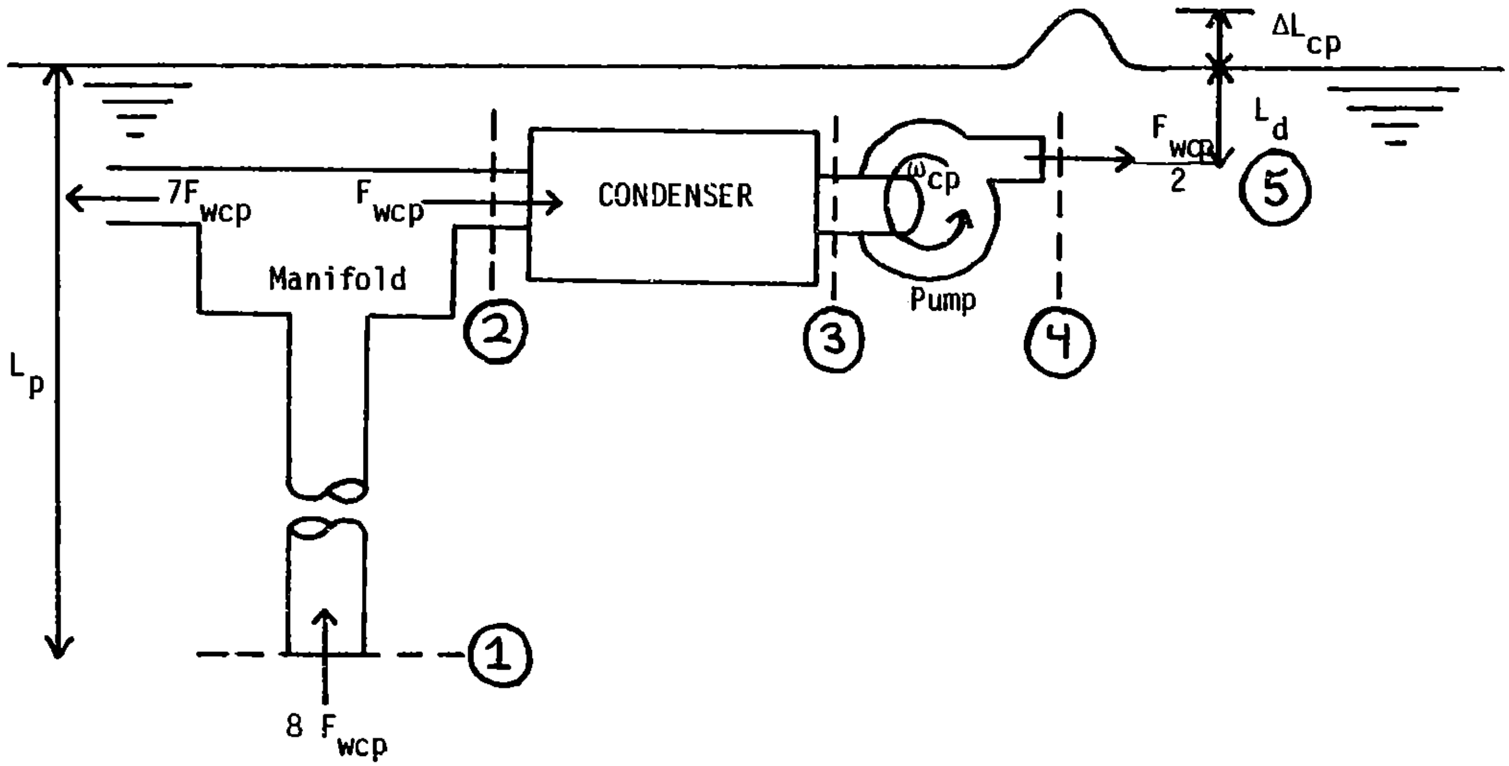

FIGURE 11: SCHEMATIC OF THE COLD WATER SYSTEM MODEL

The total dynamic head, H, is given by

$$H = P_w + \rho_w z + \frac{1}{2} \rho_w v_w^2 / g_c \tag{34}$$

where P_w - water pressure

z - relative height

g_c - local gravitational constant

Frictional head losses are determined by a turbulent flow momentum loss analysis

$$\Delta H_f = 4f \left[\frac{L_{ea}}{ID}\right] \frac{\rho_w}{2g_c} v_w^2 \tag{35}$$

where the friction factor, f, is given by

$$f = .046/Re^{0.2} \tag{36}$$

a function of the Reynold's number

$$Re = \frac{\rho_w v_w ID}{\mu_w} \tag{37}$$

where μ_w - fluid viscosity

ID - flow passage inner diameter

L_{eq} - equivalent flow length

The dynamic head at the top of the cold pipe is evaluated by beginning at the pump discharge and evaluating the change in head through the pump and condenser systems. (See Appendix III)

An energy balance for a single cold water pump reveals the following:

$$P_{supplied} = \frac{\Delta H_{cp} F_{wcp}}{2\eta_{cp}} + \frac{d}{dt}\left(\frac{1}{2} J_{cp}\omega_{cp}^2\right) \tag{38}$$

where
- $P_{supplied}$ - power supplied to pump
- ΔH_{cp} - head produced by pump
- η_{cp} - pump efficiency
- J_{cp} - pump rotational inertia
- ω_{cp} - pump angular velocity

The first term on the right hand side of Equation (38) is the power delivered from the pump to the fluid while the second term represents the change in energy stored by the rotating pump. The head increase for a pump is a function of both the pump speed and the flow through the pump (obtained from pump design data)

$$\Delta H_{cp} = A\left(\frac{\omega_{cp}}{\omega_d}\right)^2 + B\left(\frac{\omega_{cp}}{\omega_d}\right)\frac{F_{wcp}}{2} + \frac{CF_{wcp}^2}{4} \tag{39}$$

where ω_d - design speed of pump

$$\eta_{cp} = [D + E\,\frac{F_{wcp}}{2} + F\,\frac{F_{wcp}^2}{4}]/100 \tag{40}$$

The coefficients in Equations (39) and (40) are evaluated by fitting data from the pump performance curves.[14]

The rotational inertia, J_{cp}, is the sum of the inertia of the pump blades and shaft and also of the fluid in the pump. An empirical approximation is used which states that the fluid mass in the pump increases the rotational inertia of the pump by 50%.

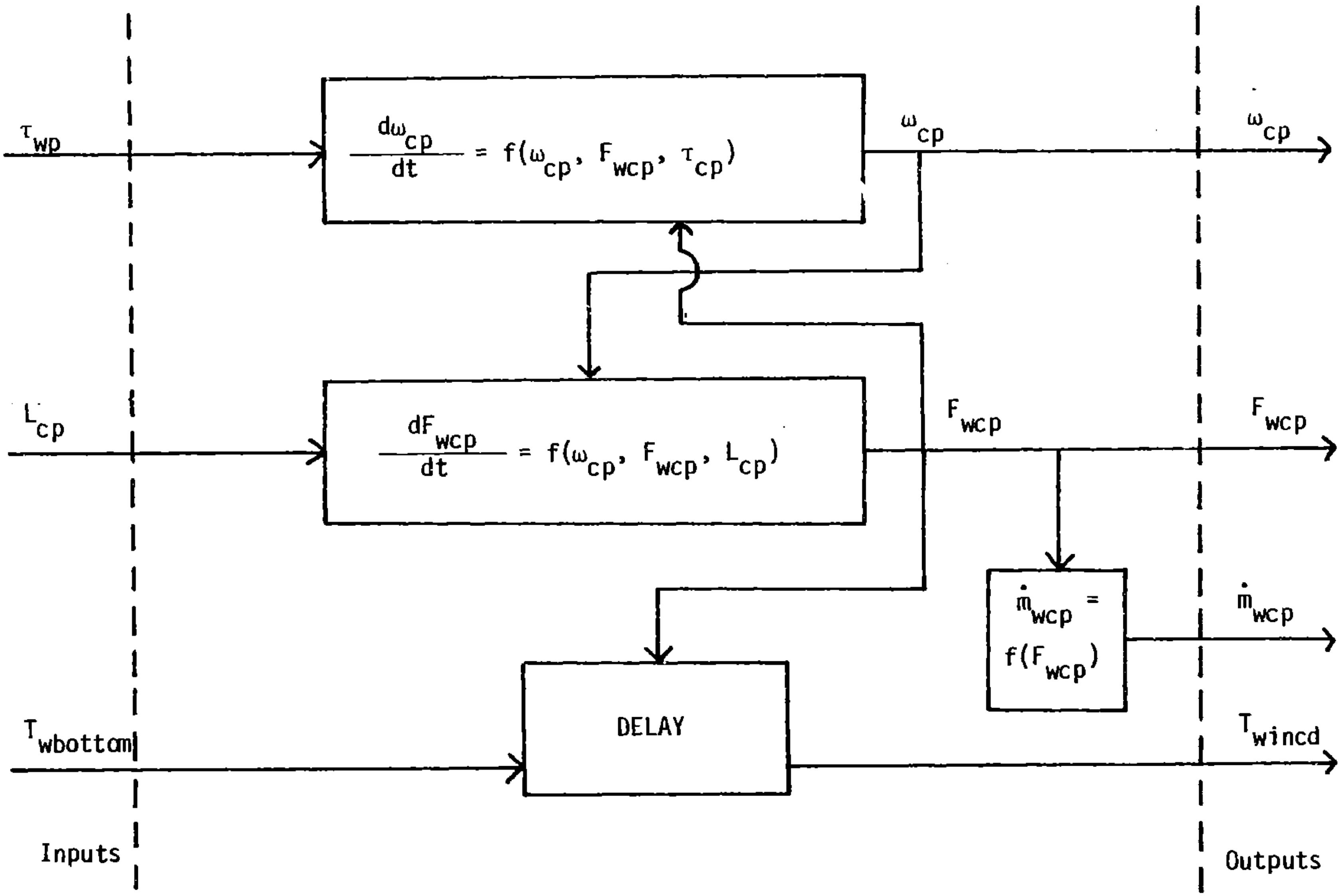

FIGURE 12: INFORMATION FLOW DIAGRAM OF THE COLD WATER SYSTEM

The two independent physical states of the cold water system are the water flow rate, F_{wcp}, and the pump shaft speed, ω_{cp}. Figure 12 is an input-output information flow diagram for the cold water system.

2.6 Warm Water System Model

The warm water system for the OTEC power plant circulates warm seawater from the surface of the ocean through the evaporator tubes and discharges it approximately 200 feet below the surface. Two 55 rpm, 4110 HP pumps operating at the evaporator discharge are used to circulate the water, overcoming the frictional losses principally in the evaporator tubes. The modeling assumptions are analogous to those of the cold water system.

1) slug flow throughout the system
2) fluid inertia effects are neglected in the system
3) fluid entrance and exit losses are neglected
4) constant fluid density inside the warm water system
5) depth at the water inlet is the same as the depth at the outlet

A schematic diagram of the system is shown in Figure 13.

Because of the assumption of negligible fluid inertia, the seawater flow is no longer an independent state; rather, it is a function of the pump speed. Therefore, we need only to define an energy balance of the pump in order to model the system.

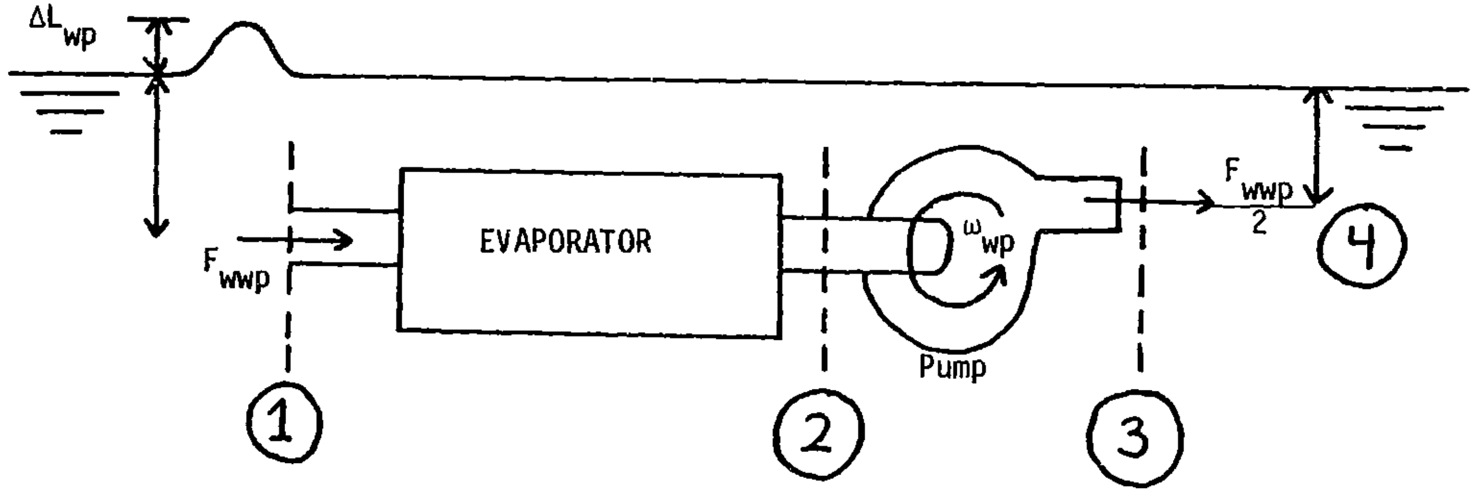

FIGURE 13: SCHEMATIC OF THE WARM WATER SYSTEM MODEL

$$P_{supplied} = \frac{\Delta H_{wp} F_{wwp}}{2\ \eta_{wp}} + \rho_{wwp} F_{wwp} \Delta L_{wp} + \frac{d}{dt} \left(\frac{1}{2} J_{wp} \omega_{wp}^{2}\right) \qquad (41)$$

where ΔL_{wp} = wave height above normal sealevel at evaporator inlet

The first term on the right in Equation (41) is again the power delivered by the pump to the fluid, and the third term is the change in stored rotational energy. The additional term in the equation is the power delivered to the pump because of wave action by the change in head of the fluid between the inlet and discharge. The pump head, ΔH_{wp}, and the pump efficiency, η_{wp}, are evaluated as before.

In order to determine the seawater flow, F_{wwp}, as a function of the pump speed, ω_{wp}, it is necessary to equate the frictional losses in the system to the pump head and evaluate the steady state operating point. (See Appendix III) This results in a relationship of the form

$$F_{wwp} = C_{wp} \omega_{wp} \qquad (42)$$

where C_{wp} is a constant of proportionality. The pump rotational inertia, J_{wp}, is once again increased by 50% in order to compensate for the fluid mass in the pump.

The independent physical state of the warm water system is the pump shaft speed, ω_{wp}. Figure 14 is an input-output infor-

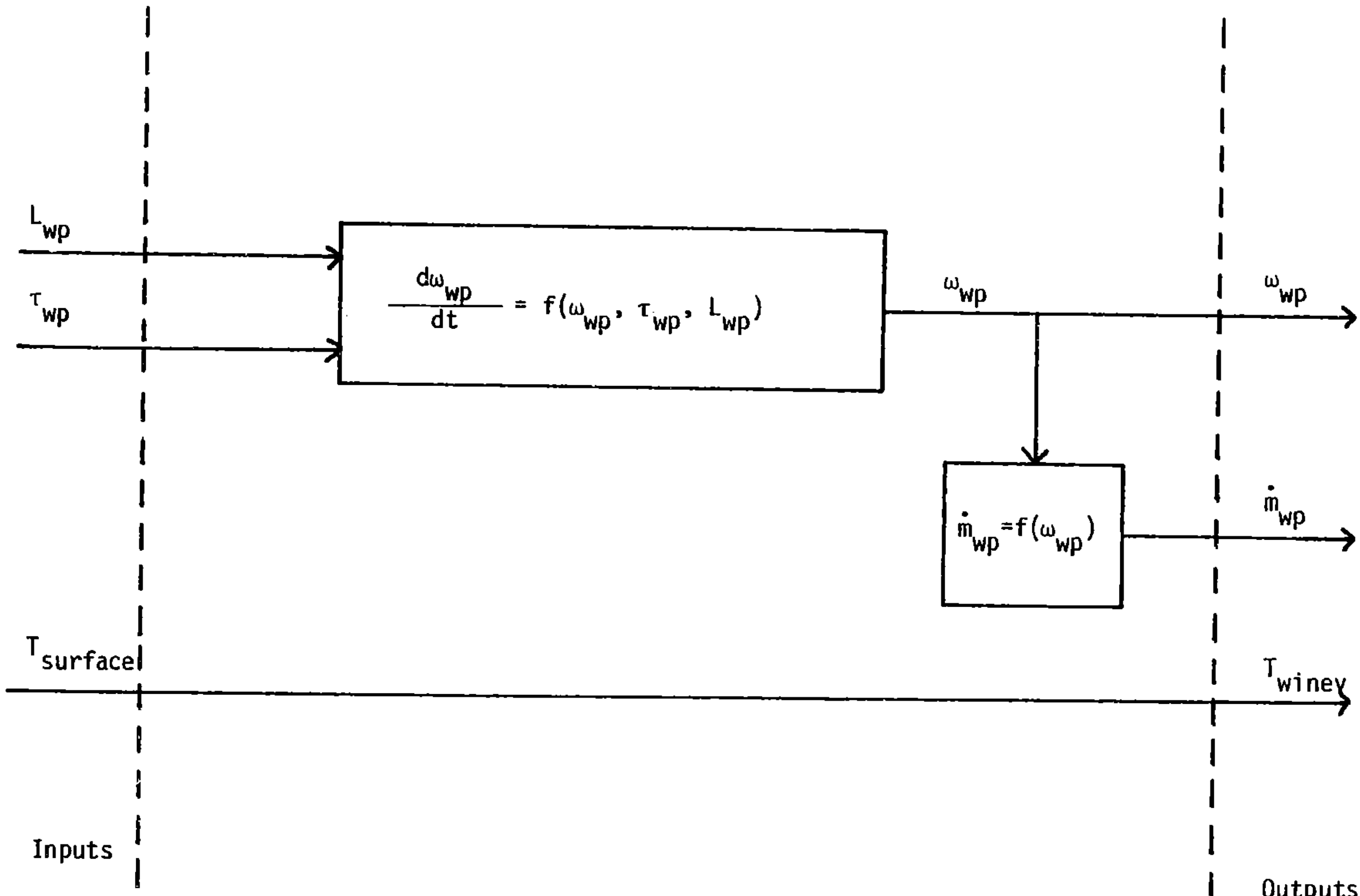

FIGURE 14: INFORMATION FLOW DIAGRAM OF THE WARM WATER SYSTEM

mation flow diagram for the warm water system.

2.7 Ammonia Vapor Transport Model

The primary ammonia vapor loop for the OTEC power plant consists of pipes which transport the ammonia vapor from the evaporator to the turbine and from the turbine to the condenser. There is also a vapor line directly from the evaporator to the condenser which is used to bypass vapor flow from the turbine. The vapor flow in this line is modulated by a valve. The primary vapor transport system is composed of very large diameter pipes in order to minimize the frictional pressure losses for the extremely large vapor flow rates in the system. There are no turbine flow control valves in the primary loop since the losses associated with these would reduce the maximum power output of the plant by as much as 4%.

The simplifying assumptions for the vapor transport model are:

1) the ammonia vapor is always in saturated equilibrium
2) neglect any liquid ammonia entrained in the vapor
3) neglect any saturated liquid ammonia in the vapor
4) the entrance and exit states of the bypass valve are identical to the corresponding states of the turbine
5) neglect fluid inertia and capacitance effects in the vapor system

Figure 15 is a schematic diagram of the vapor transport system.

The constituitive relation giving the vapor mass flow rate as a function of the pressure difference between any two points in the vapor transport system is identical to the turbine flow relation

$$\dot{m}_v = K\sqrt{1 - \left(\frac{P_{vout}}{P_{vin}}\right)^2} \tag{43}$$

where K is a function of the flow geometry and can be evaluated for each flow path by the steady state pressure losses of the OTEC plant. The bypass valve is also represented in the same manner.

$$\dot{m}_{vbp} = K_{bp}\sqrt{1 - \left(\frac{P_{v3}}{P_{v2a}}\right)^2}. \tag{44}$$

where $\dot{m}_{vbp}$ - vapor mass flow rate through the bypass valve
K_{bp} - bypass valve flow constant

However, K_{bp} is not a constant but is proportional to the bypass valve opening area. Using assumption 4, the ratio of the vapor mass flow through the bypass valve to the vapor mass flow through the turbine is determined.

$$\frac{\dot{m}_{vbp}}{\dot{m}_{vtg}} = \frac{K_{bp}}{K_{tg}} \tag{45}$$

Applying the conservation of mass at junction 2, it is obvious that

$$\dot{m}_{vtg} = \dot{m}_v - \dot{m}_{vbp} \tag{45a}$$

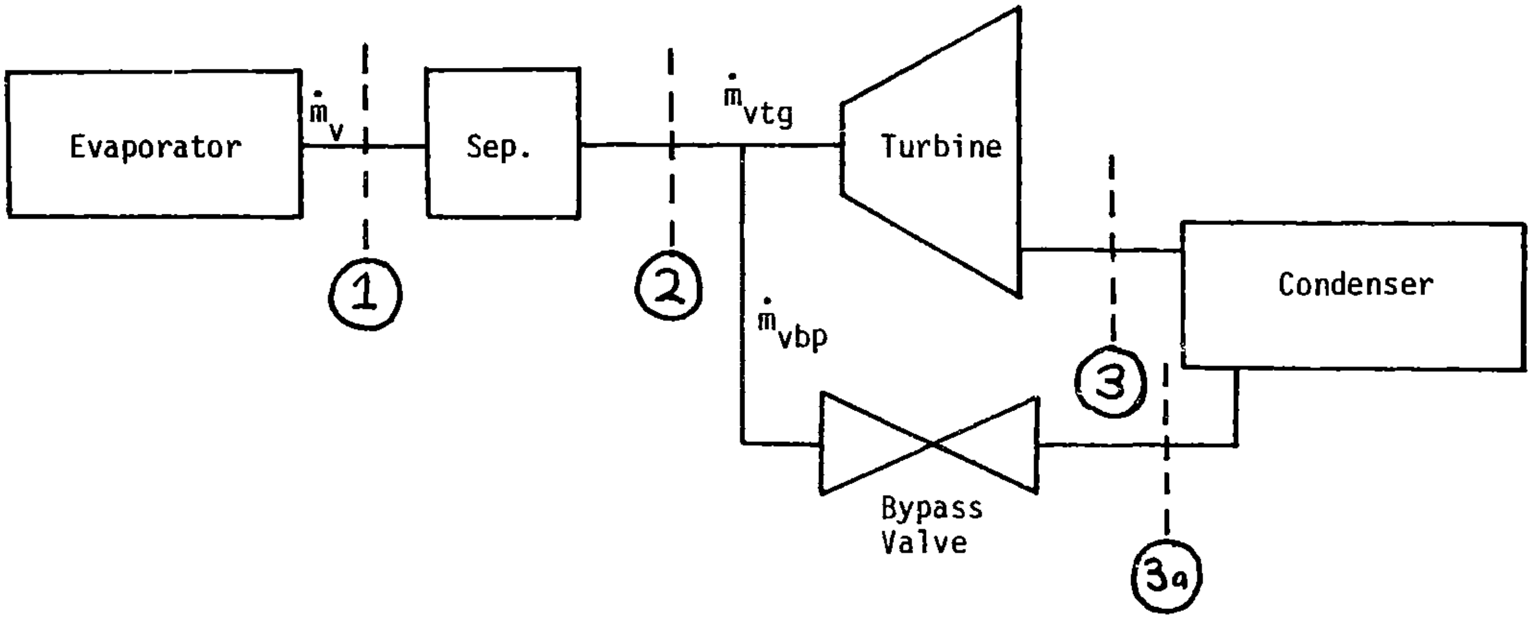

FIGURE 15: SCHEMATIC OF THE VAPOR TRANSPORT SYSTEM MODEL

Combining Equations (44) and (45), the turbine vapor mass flow as a function of the total vapor mass flow and the bypass valve opening is shown to be:

$$\dot{m}_{vtg} = \dot{m}_v / (1 + \frac{K_{bp}}{K_{tg}}) \tag{46}$$

The ammonia vapor transport system has no independent states, that is, the total vapor flow through the OTEC plant is completely determined by the vapor states in the heat exchangers and by the bypass valve opening. It is interesting to point out that the bypass valve has no direct control over the vapor flow through the turbine; it is solely determined by the pressure drop across the turbine. The bypass valve controls the turbine vapor flow indirectly by altering the pressure difference between the evaporator and the condenser. The bypass valve acts to alter the total flow area between the evaporator and condenser which changes the total vapor flow rate and, therefore, the pressure ratio at the turbine. The turbine vapor mass flow is a highly nonlinear function of the bypass valve opening as shown in Equation (16). This is an important factor in controller design.

2.8 Generator AC Load Model

OTEC baseload power systems located within 50 kilometers of the shoreline are directly connected to the onshore AC power grid via underwater AC power cables. Thus, the electric generator is modeled as a synchronous machine directly connected to an infinite bus which is characterized by a constant voltage and frequency. The bus is also assumed to have the capacity to utilize all of the power generated by the turbine-generator. The simplified circuit model is shown in Figure 16.

The power output of a synchronous generator when connected to an infinite bus is given by[15]

$$P_e = \frac{E_G E_\infty}{x_G} \sin \delta_G \tag{47}$$

where P_e - electric power produced by generator
E_G - generator field voltage
E_∞ - infinite bus voltage
x_G - generator synchronous reactance
δG - generator power angle

The generator power angle, δ_G, is defined as

$$\frac{d}{dt} (\delta_G) = 2\, \omega_{tg} - \omega_\infty \tag{48}$$

where ω_∞ - infinite bus frequency

The factor of 2 is necessary because the generator has six electrical poles and operates at an angular speed of 1800 rpm. The generator is kept in synchronization with the infinite bus by the power angle, which operates essentially as an integral control on the turbine-generator speed through the power load. The torque load on the turbine-generator is given by

$$\tau_L = 2\, P_e/\omega_\infty \tag{49}$$

or

$$\tau_L = 2\, \frac{E_G E_\infty}{\omega_\infty x_G} \tag{50}$$

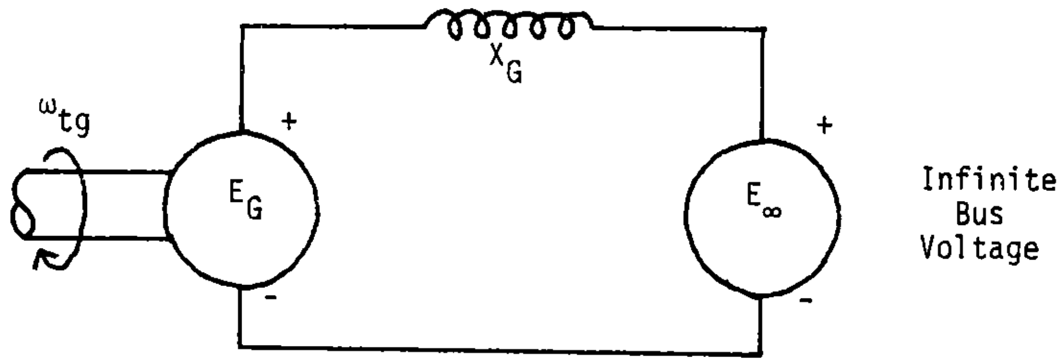

FIGURE 16: GENERATOR-INFINITE BUS CIRCUIT MODEL

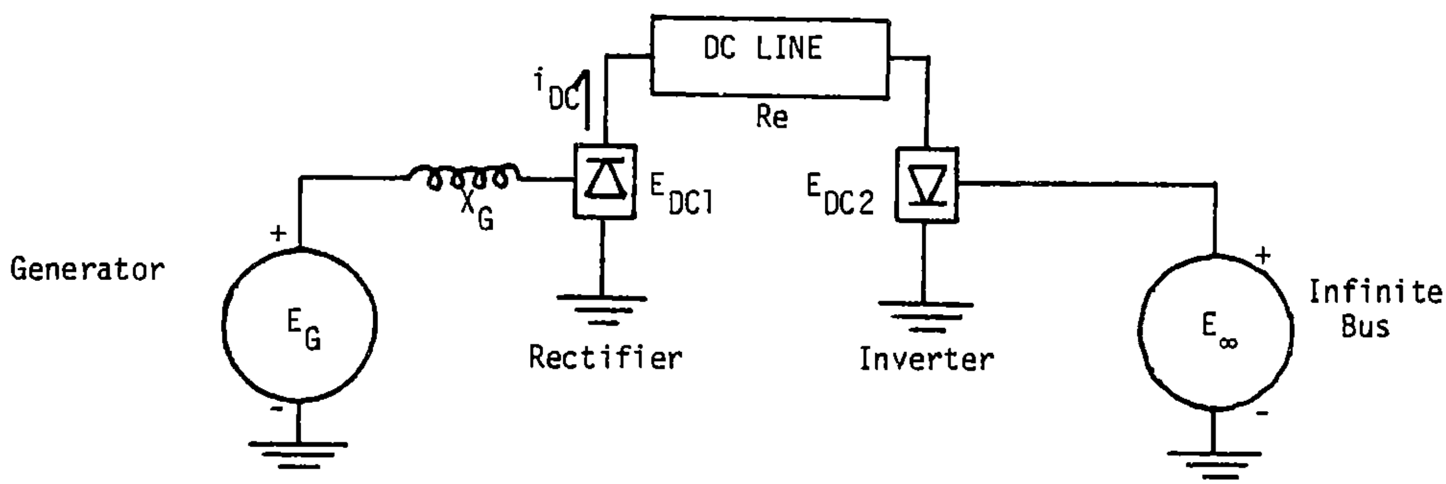

FIGURE 17: CIRCUIT DIAGRAM OF HVDC TRANSMISSION SYSTEM

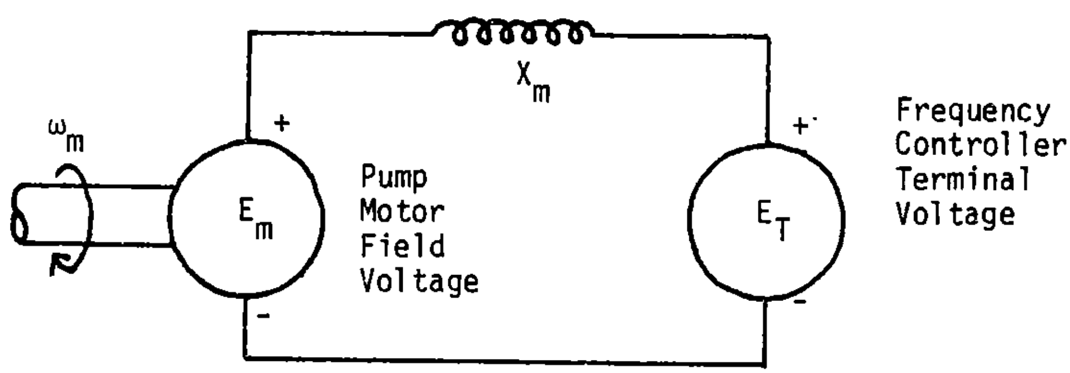

FIGURE 18: SIMPLIFIED PUMP MOTOR CIRCUIT MODEL

The AC generator load model contains one independent state, the generator power angle, δ_G.

2.9 Generator DC Load Model[16]

When the baseload OTEC power platform is located further than 50 kilometers from the shoreline, it becomes necessary to transmit the power through an underwater high voltage direct current (HVDC) transmission system. This is necessary because the corona losses and the capacitance effects of underwater alternating current transmission become economically prohibitive at these distances. The proposed solid state HVDC transmission system for the OTEC plant rectifies the AC voltage at the OTEC generator bus for underwater transmission and then inverts the DC voltage to an AC voltage at the on-shore AC power grid. A simplified circuit model of the HVDC transmission system is shown in Figure 17.

The AC/DC voltage conversion/inversion process is accomplished by the sequential operation of arrays of semi-conductor devices known as thyristers. The DC voltage at the terminals of the transmission system is regulated in two ways: a) by changing the firing angle of the thyrister valves and, b) by adjusting the tap changers on the AC transformers. Thyrister firing angle control of the DC terminal voltage requires 1-10 milliseconds; transformer tap changer control, 5-6 seconds. Thus, thyrister firing angle control is employed for fast voltage regulation while the transformer tap changer is used to maintain an acceptable AC power factor at the sending and receiving ends. The DC current through the transmission line is given by Ohm's law

$$i_{DC} = \frac{E_{DC1} - E_{DC2}}{Re} \tag{51}$$

where i_{DC} - DC current through transmission line

$E_{DC\#}$ - DC transmission line terminal voltages

Re - transmission line resistance

while the power transmitted at the sending and receiving ends of the DC system is given by

$$P_{e1} = E_{DC1} i_{DC} \tag{52}$$

$$P_{e2} = E_{DC2} i_{DC} \tag{53}$$

The regulation of HVDC rectifier/inverter transmission systems is accomplished in two basic modes; a) maintenance of prescribed DC terminal voltages, or b) regulation of the desired DC line current. Two other modes of control, involving a coordination of these two basic modes, are power control and frequency control. In the power control mode of operation, the power transmitted by the HVDC system is maintained at the desired demand level regardless of disturbances in the AC systems at the sending or receving end. The frequency controlled mode of operation is concerned with regulating the AC frequency at the sending or receiving end of the transmission system by modifying the power transmitted through the DC line. In either mode, the speed of response of the HVDC system to disturbances is limited by the dynamic response of the transmission line, which, in most cases, is on the order of 10-100 milliseconds.

The HVDC transmission system for the baseload OTEC power plant operates principally in the power controlled mode. Because of its rapid response time, the HVDC link is modeled as a power load on the turbine generator.

$$P_L = P_{DC} \tag{54}$$

where
P_L - power load on generator
P_{DC} - DC transmission line power load demand

$$\tau_L = P_L/\omega_{tg} \tag{55}$$

2.10 Seawater Pump Motor Model

Each of the seawater pumps on both the warm and cold water systems is powered by a synchronous AC motor directly connected to the pump shaft. The speed of the motors is regulated by a solid state DC rectifier/inverter system operating in the frequency controlled mode. Since in the normal mode of operation the power supply for the pump motors (either the AC power grid or the OTEC plant) is much larger than the required pumping power, the frequency of the pump motor variable frequency controller is modeled as a constant infinite bus frequency. A simplified circuit model is shown in Figure 18. If the motor terminal voltage is maintained constant by the frequency controller, the power supplied to each pump motor is given by

$$P_e = \frac{E_m E_T}{x_m} \sin \delta_m \tag{56}$$

where E_m - pump motor field voltage
E_T - pump motor terminal voltage
x_m - pump motor synchronous reactance
δ_m - pump motor power angle

The pump motor power angle is given by

$$\frac{d}{dt}(\delta_m) = \omega_m - \omega_s \tag{57}$$

where ω_s - pump motor frequency set point

The torque supplied to each pump motor is given by

$$\tau_m = \frac{E_m E_T}{\omega_s x_m} \sin \delta_m \tag{58}$$

where τ_m - torque supplied by pump motor

The pump models for each water pumping system contain one independent state, the pump motor power angle, δ_m.

2.11 System Model Development from Component Models

Each of the component models is combined by input-output causal relationships in order to obtain the full OTEC power system model. This results in a set of coupled nonlinear first order state equations of the form

$$\dot{\underline{x}} = f(\underline{x}, \underline{u}; t) \tag{59}$$

$$\underline{y} = g(\underline{x}, \underline{u}; t) \tag{60}$$

describing the dynamics of the OTEC power plant. Figure 19 is an information flow diagram showing inputs, outputs, states, and signal flows for the completed system model. The nonlinear system equations are presented in Appendix IV.

2.12 Linearization and Normalization of Model

Any state, disturbance, or output of the OTEC plant dynamic model can be represented by its steady state component plus a perturbation from the steady state. This is represented in vector form as

$$\begin{aligned} \underline{x} &= \underline{x}_{ss} + \Delta\underline{x} \\ \underline{u} &= \underline{u}_{ss} + \Delta\underline{u} \\ \underline{y} &= \underline{y}_{ss} + \Delta\underline{y} \end{aligned} \tag{61}$$

where $(\ )_{ss}$ - steady state component

$\Delta(\ )$ - perturbation

In order to obtain a linearized perturbation model of the OTEC plant, a Taylor series expansion is performed on the set of coupled first order nonlinear equations representing the system model. Neglecting all higher order terms and evaluating all derivatives at the steady state

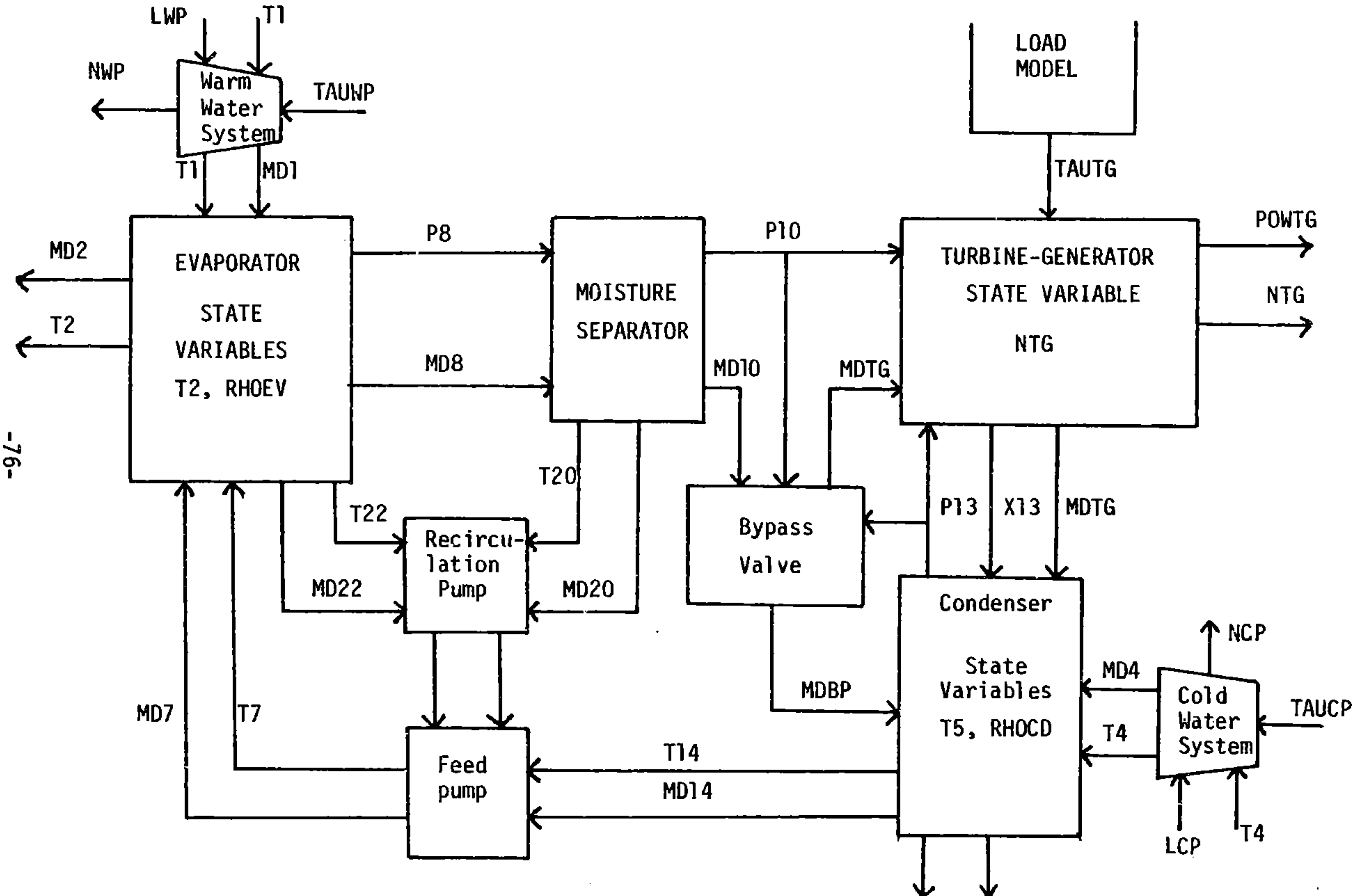

FIGURE 19: SCHEMATIC OF THE OTEC SYSTEM MODEL

$$\Delta\dot{\underline{x}} = \frac{\partial \underline{f}}{\partial \underline{x}}\bigg|_{ss} \Delta\underline{x} + \frac{\partial \underline{f}}{\partial \underline{u}}\bigg|_{ss} \Delta\underline{u} \tag{62}$$

$$\Delta\underline{y} = \frac{\partial \underline{g}}{\partial \underline{x}}\bigg|_{ss} \Delta\underline{x} + \frac{\partial \underline{g}}{\partial \underline{u}}\bigg|_{ss} \Delta\underline{u} \tag{63}$$

This results in a linear, time invariant, state perturbation model, valid for small deviations from the steady state, of the form

$$\Delta\dot{\underline{x}} = \underline{\bar{A}}\ \Delta\underline{x} + \underline{\bar{B}}\ \Delta\underline{u} \tag{64}$$

$$\Delta\underline{y} = \underline{\bar{C}}\ \Delta\underline{x} + \underline{\bar{D}}\ \Delta\underline{u} \tag{65}$$

where $\underline{\bar{A}}$, $\underline{\bar{B}}$, $\underline{\bar{C}}$, and $\underline{\bar{D}}$ are constant coefficient matrices.

To help simplify the analysis, the linearized equations are non-dimensionalized and certain important non-dimensional parameters are identified for each system component. Each of the state, input disturbance, and output perturbations is normalized with respect to its own steady state component.

$$\Delta x = \frac{x - x_{ss}}{x_{ss}}$$

$$\Delta u = \frac{u - u_{ss}}{u_{ss}} \tag{66}$$

$$\Delta y = \frac{y - y_{ss}}{y_{ss}}$$

Four exceptions to this steady state normalization are:

1) all temperature perturbations in the evaporator system are normalized with respect to the evaporator seawater outlet temperature

2) all temperature perturbations in the condenser system are normalized with respect to the condenser seawater outlet temperature

3) the bypass valve flow coefficient, ΔK_{bp}, is normalized with respect to the turbine flow coefficient, K_{tg}

4) the wave disturbances, ΔL_{cp} and ΔL_{wp}, are normalized with respect to 1 foot

As a result, all state, input disturbance, and output perturbations are in terms of a percent variation from the steady state norm. The constant coefficient matrices of the full load model are listed in Appendix VIII.

The normalized states, input disturbances, and outputs of the linearized plant model are listed in Tables 2, 3 and 4.

2.13 Steady State System Model

A computer program was developed to evaluate both the steady state conditions and the constant coefficient perturbation matrices for the OTEC plant model. The inputs to the program are:

1) Steady state power load
2) Steady state bypass valve opening coefficient
3) Steady state condenser vapor temperature
4) Steady state warm seawater temperature
5) Steady state cold seawater temperature

TABLE 2: OTEC MODEL STATE VARIABLES

STATE	DESCRIPTION
ΔT2	Evaporator seawater outlet temperature
ΔRHOEV	Evaporator ammonia vapor density
ΔTS	Condenser seawater outlet temperature
ΔRHOCD	Condenser ammonia vapor density
ΔNTG	Turbine-generator speed
ΔNCP	Cold water pump speed
ΔMDCP	Cold water system seawater mass flow rate
ΔNWP	Warm water pump speed
ΔANGTG	Turbine-generator power angle
ΔANGCP	Cold water pump power angle
ΔANGWP	Warm water pump power angle

TABLE 3: OTEC MODEL INPUT VARIABLES

INPUT	DESCRIPTION
ΔT1	Evaporator seawater inlet temperature
ΔTAUL	Turbine-generator torque load
ΔTAUCP	Cold water pump motor torque
ΔTAUWP	Warm water pump motor torque
ΔT4	Condenser seawater inlet temperature
ΔKBP	Bypass valve flow coefficient
ΔMD7	Evaporator ammonia liquid influx
ΔLCP	Cold water system wave height
ΔLWP	Warm water system wave height
ΔPOWL	Turbine-generator DC power demand load
ΔNINF	Power grid (infinite bus) frequency
ΔNSCP	Cold water pump frequency setpoint
ΔNSWP	Warm water pump frequency setpoint
ΔEINF	Power grid (infinite bus) voltage
ΔEPM	Pump motor field voltage

TABLE 4: OTEC MODEL OUTPUT VARIABLES

OUTPUT	DESCRIPTION
ΔPOWTG	Turbine-generator power output
ΔMD10	Total ammonia vapor mass flow rate
ΔPEV	Evaporator ammonia vapor pressure
ΔPCD	Condenser ammonia vapor pressure
ΔMDWP	Warm water system seawater mass flow rate
ΔMDTG	Turbine ammonia vapor mass flow rate
ΔMD21	Evaporator ammonia liquid efflux
ΔMD14	Condenser ammonia liquid efflux
ΔTEV	Evaporator ammonia vapor temperature
ΔTCD	Condenser ammonia vapor temperature
ΔPOWE	Generator electric power output
ΔPOWCP	Cold water pump power input
ΔPOWWP	Warm water pump power input

6) System description number

The program evaluates the steady state variables of the OTEC plant by allowing all time derivatives of the nonlinear system model to go to zero and solving the resulting set of coupled nonlinear algebraic equations.

$$\dot{\underline{x}} = \underline{f}(\underline{x}_{ss}, \underline{u}_{ss}) = 0 \tag{67}$$

$$\underline{y} = \underline{g}(\underline{x}_{ss}, \underline{u}_{ss})$$

The "lumped" heat exchanger temperatures are replaced by an equivalent log-mean heat transfer temperature difference for the steady state analysis.

The system description number determines the type of model. These are listed in Table 5.

TABLE 5: MODEL SYSTEM DESCRIPTION NUMBERS

SDN	MODEL DESCRIPTION	ORDER
1	Generator torque load, pump motors omitted	8
2	AC bus load, pump motors omitted	9
-2	Generator torque load, AC bus unsynchronized, p.m. omitted	9
3	AC bus load, pump motors included	11
-3	Generator torque load, AC bus unsynchronized, p.m. included	11
4	DC power demand load, pump motors coupled to OTEC plant	10
-4	DC power demand load, pump motors coupled to outside source	10

The order of the system is equal to the number of independent states in the dynamic model.

For SDN = -2,-3, the generator power angle, δ_G, is normalized with respect to 1 radian. The steady state model for zero power load can only be evaluated for SDN = 1. The turbine-generator torque load perturbation for zero power load is normalized with respect to the full load torque.

The program prints a listing of the coefficient matrices, steady state values, and some important parameters, along with the states, inputs, and outputs of the dynamic model. A copy of the output is listed in Appendix VIII.

The parameters of the OTEC plant are listed in the Parameter subroutine. These parameters can be modified to adjust the model for design changes in the Westinghouse concept or to adapt the model to other OTEC plant design concepts which meet the requirements discussed in Section 1.2.

III. OPEN LOOP DYNAMIC ANALYSIS

Much information about the OTEC plant dynamic behavior is determined by examining the open loop, or uncontrolled, behavior of the OTEC model. The open loop eigenvalues and eigenvectors provide a measure of the speed of response of the different subsystem modes of the plant, that is, which transients decay quickly and which take an appreciable time to return to a steady state. The eigenvalues-eigenvectors also provide information about which subsystems are strongly "coupled", that is, those components which are strongly interactive, and which are not. Dynamic simulations of the open loop OTEC model in response to input disturbances give insight into how effective certain control mechanisms are and how certain environmental disturbances affect the system. The open loop state equations and transfer functions are useful in the eventual control system analysis and design.

3.1 Open Loop Time Constant Analysis

The eigenvalues and eigenvectors of a linear time invariant state determined system represent the transient response of that system. The eigenvalues, λ_i, are indicative of the time response of the system while the eigenvectors, $\underline{N}_i$, show how strongly the transient response of each state is coupled to a particular eigenvalue. In equation form, the transient response of a given system is

$$\underline{\bar{x}} = \underline{\bar{N}}e^{\underline{\bar{\lambda}}_D t} \tag{69}$$

where

$$\underline{\bar{\lambda}}_D = \text{diag}[\lambda_1, \lambda_2, \ldots \lambda_n]$$

$$\underline{\bar{N}} = \begin{bmatrix} \underline{N}_1^T \\ \underline{N}_2^T \\ \vdots \\ \underline{N}_n^T \end{bmatrix}$$

The associated time constants of the system, τ_i, are functions of the eigenvalues, λ_i. The coupled system time constants for each component as determined by the eigenvalue-eigenvector analysis are compared to the estimated physical time constants for each separate component in Table 6. (See Appendix V for time constant estimation)

This comparison clearly demonstrates that the evaporator-condenser system is strongly coupled. The turbine-generator is dependent upon the vapor flow and is strongly influenced by the vapor flow dynamics even though its principle time constant remains unchanged. The warm and cold water system dynamics are entirely independent from the remainder of the open loop OTEC plant. The water pumping systems only affect the open loop plant by changes in the seawater flow rate. Thus, for constant seawater flow rates, the main power loop and seawater flow systems of the OTEC plant are decoupled in the open loop.

TABLE 6: OTEC PLANT TIME CONSTANTS (100% LOAD)

Component	Estimated Physical Time Constant		System "Coupled" Time Constant
Evaporator	Thermal	- 3.3 sec.	5.56 sec.
	Vapor Flow	- 3.3 sec.	0.64 sec.
Condenser	Thermal	- 3.9 sec.	7.2 sec.
	Vapor Flow	- 3.3 sec.	0.77 sec.
Turbine-Generator	14.1 sec.		14.1 sec.
Warm Water System	0.23 sec.		0.23 sec.
Cold Water System	Pump	- 0.14 sec.	0.14 sec.
	Flow	- 17.9 sec.	26.6 sec.

The dynamics of the open loop OTEC plant are dependent on the steady state level at which the plant is operating. The time constants of the OTEC model were evaluated at different steady state power levels while maintaining constant seawater flow rates. These results are presented in Table 7.

TABLE 7: OTEC PLANT TIME CONSTANT SENSITIVITY TO LOAD

LOAD	TURBINE (sec)	THERMAL (sec)		VAPOR FLOW (sec)		BYPASS VALVE COEFF. (lbm/hr)
100%	14.1	7.19	5.56	0.77	0.64	0
80%	14.9	7.16	5.33	0.77	0.60	4.15×10^6
60%	15.9	7.14	5.05	0.77	0.55	9.16×10^6
40%	17.4	7.12	4.74	0.77	0.49	15.57×10^6
20%	19.8	7.11	4.38	0.77	0.40	24.75×10^6
10%	21.7	7.10	4.20	0.77	0.35	31.47×10^6
0%	24.6	7.10	4.00	0.77	0.29	41.50×10^6

Figures 20 and 21 show the effect of the increased total vapor flow in the system on the thermal and vapor flow dynamics. In each case, while one of the time constants remains essentially constant, the other decreases; the thermal time constant, from 5.56 seconds to 4.00 seconds - the vapor flow time constant, from 0.64 seconds to 0.29 seconds. This increase in the speed of response is the result of the greater heat exchanger ΔT's and the larger vapor flow rates which reduce the thermal and vapor "holdup/thruput" ratios, respectively. Figure 22 shows the result of reduced vapor flow through the turbine on the turbine-generator dynamics. The reduced vapor flow decreases the turbine velocity droop and slows down the response time.

The addition of the synchronous pump motors in the seawater pumping systems alters the open loop eigenvalues of that system.

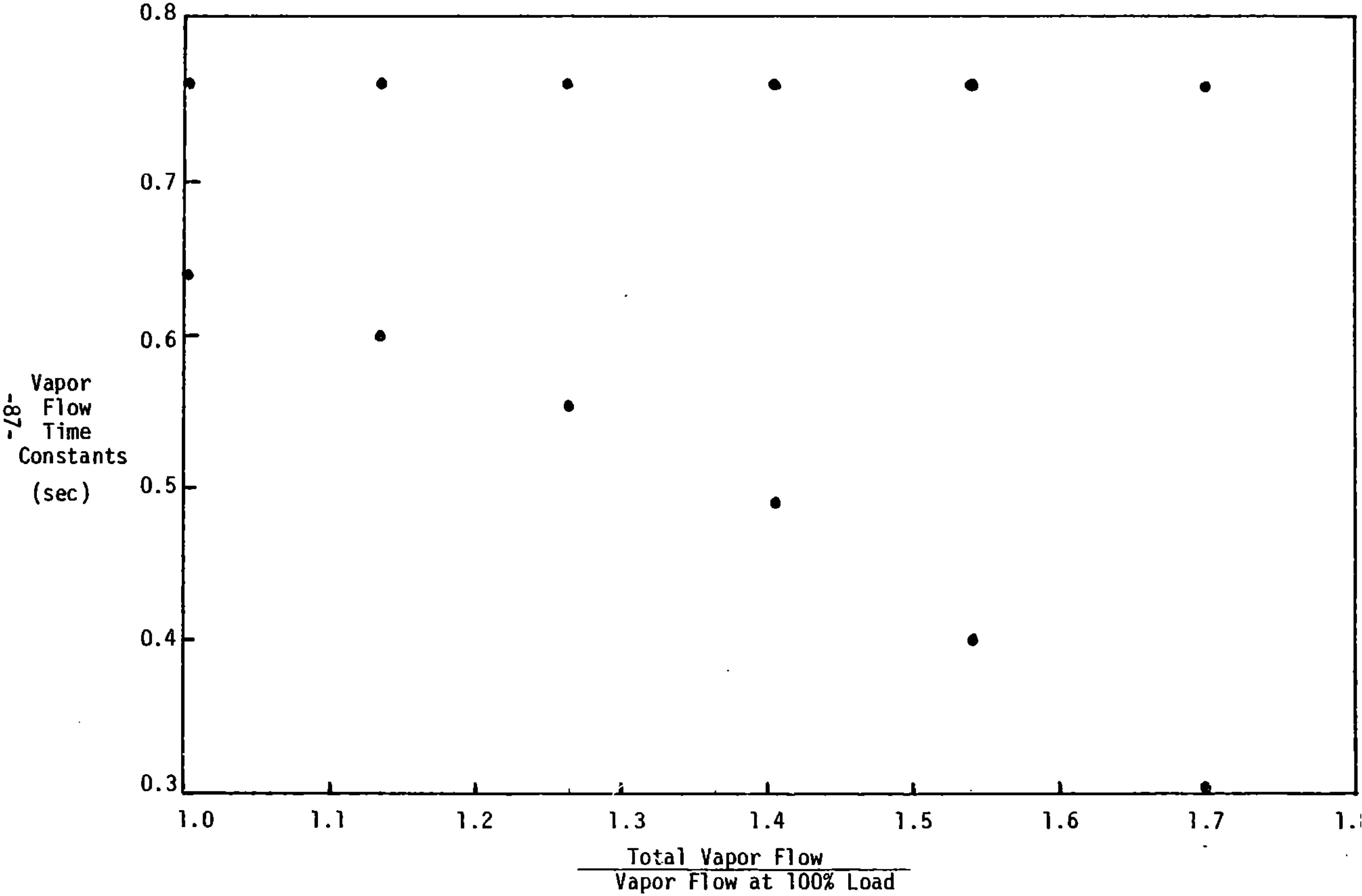

FIGURE 20: VAPOR FLOW DYNAMICS LOAD SENSITIVITY

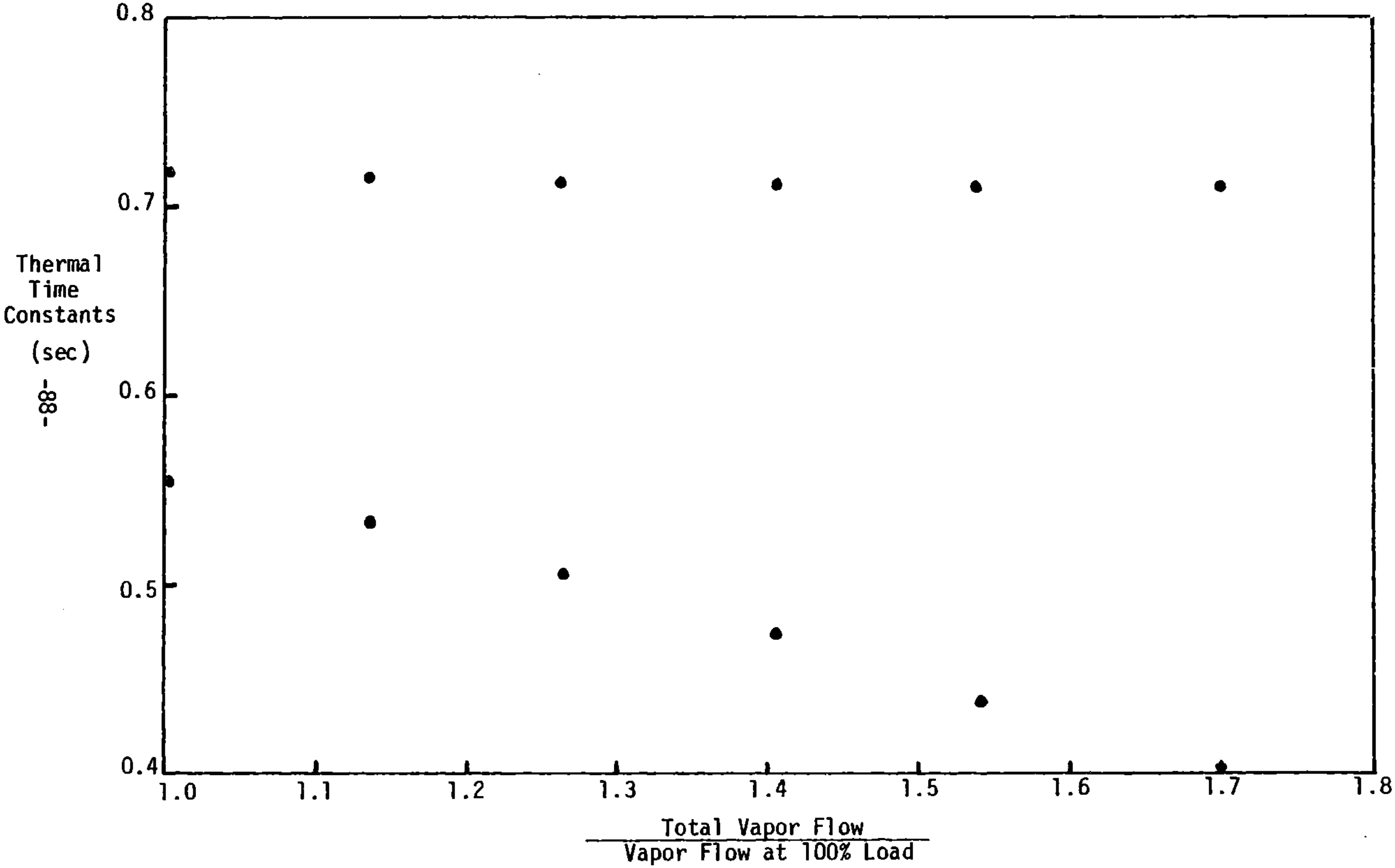

FIGURE 21: THERMAL DYNAMICS LOAD SENSITIVITY

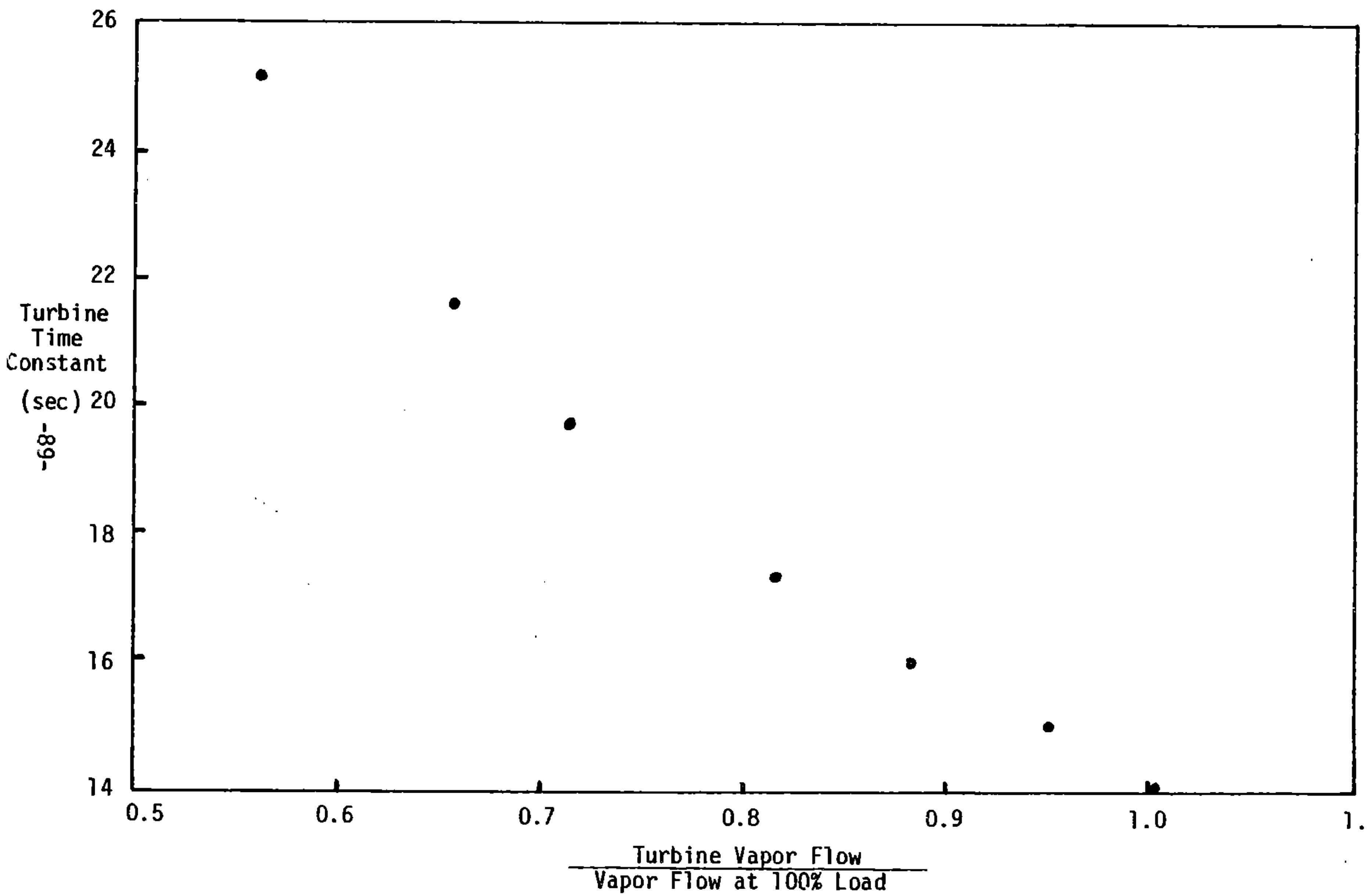

FIGURE 22: TURBINE DYNAMICS LOAD SENSITIVITY

The new pumping dynamics have the following characteristics:

Cold Seawater Pump: $\xi = 0.65$

$\omega_n = 6.09$ rad/sec

Warm Seawater Pump: $\xi = 0.42$

$\omega_n = 6.31$ rad/sec

The response of the pumping systems is now characteristic of a second order underdamped system. The open loop dynamics of the turbine-generator are also altered when the generator is connected directly to the AC power grid.

Turbine-Generator: $\xi = 0.005$

$\omega_n = 7.44$ rad/sec

This is indicative of a highly underdamped oscillatory turbine-generator synchronous response.

3.2 Open Loop Model Dynamic Simulations

Several dynamic simulations of the model at 100% power load were run to demonstrate how the OTEC power plant and its components behave in response to input disturbances. The turbine-generator load is maintained at a constant level unless otherwise indicated. The results are presented in this section.

3.2.1 Turbine-Generator Torque Load Disturbance

Figure 23 is a simulation of the turbine-generator response to a 10% step increase in the generator-torque load. The turbine-generator speed decreases approximately 10% and reaches the steady state in about 60 seconds following the disturbance as predicted by the time constant analysis. All other system variables remain constant.

3.2.2 Warm Seawater Temperature Disturbance

Figure 24 is a simulation of the OTEC plant model response to a 0.2% step increase in the warm seawater temperature (~1°F). The evaporator seawater outlet temperature increases by less than 0.2% in approximately 20 seconds. The increase in the seawater temperature results in greater vapor production which causes the vapor pressure to rise, lagging slightly behind the seawater temperature. The evaporator equilibrates at a new saturated temperature and pressure in approximately 30 seconds. The condenser vapor pressure increases slightly because of the increased vapor flow in the system, reaching equilibrium in 40-45 seconds. The turbine-generator speed initially remains constant but begins to increase as the vapor flow in the system rises, increasing about 3% in 60-70 seconds.

3.2.3 Cold Water System Pump Torque Disturbance

Figure 25 is a simulation of the OTEC plant model in

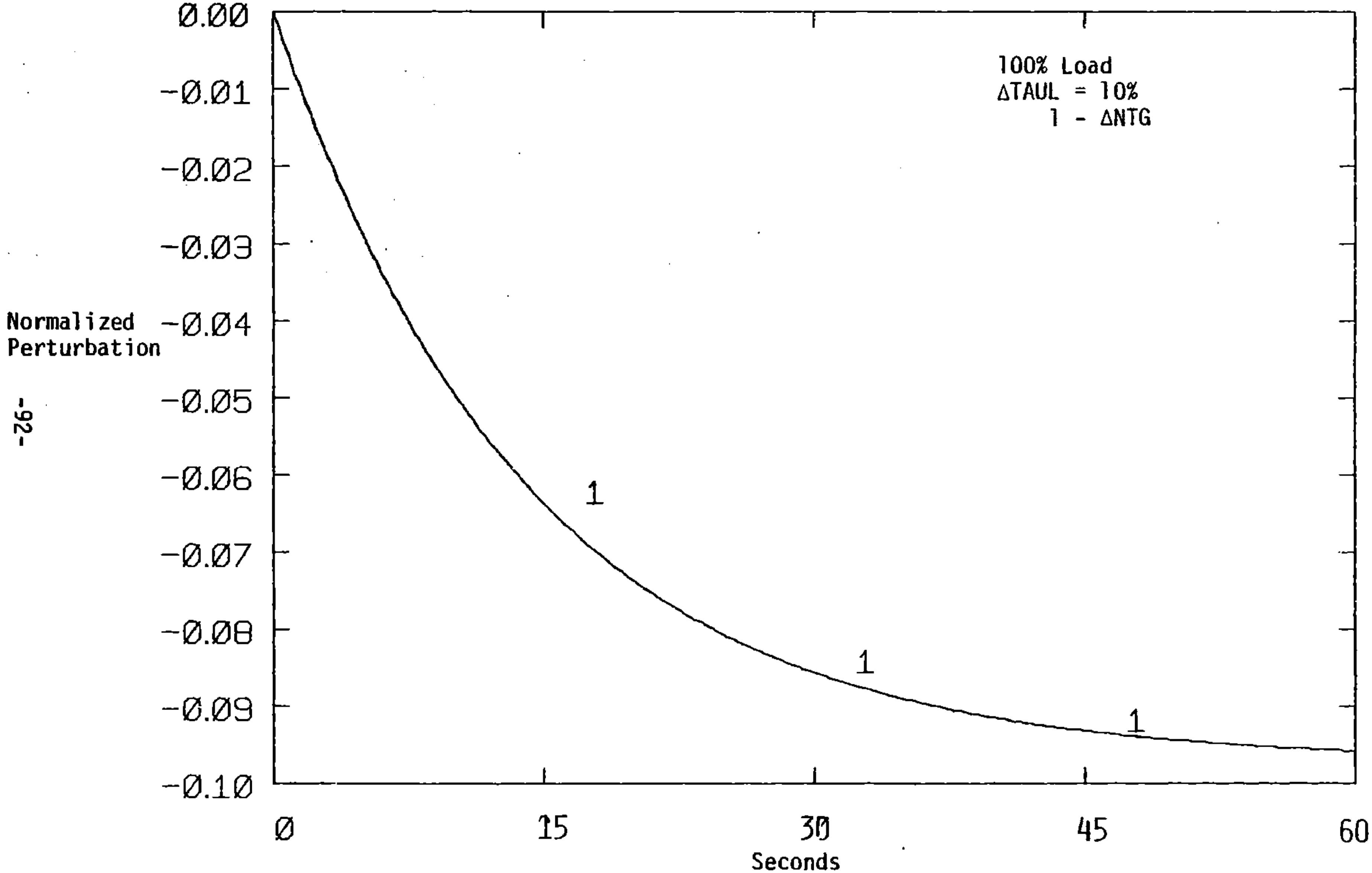

FIGURE 23: TURBINE-GENERATOR LOAD DISTURBANCE (Open Loop)

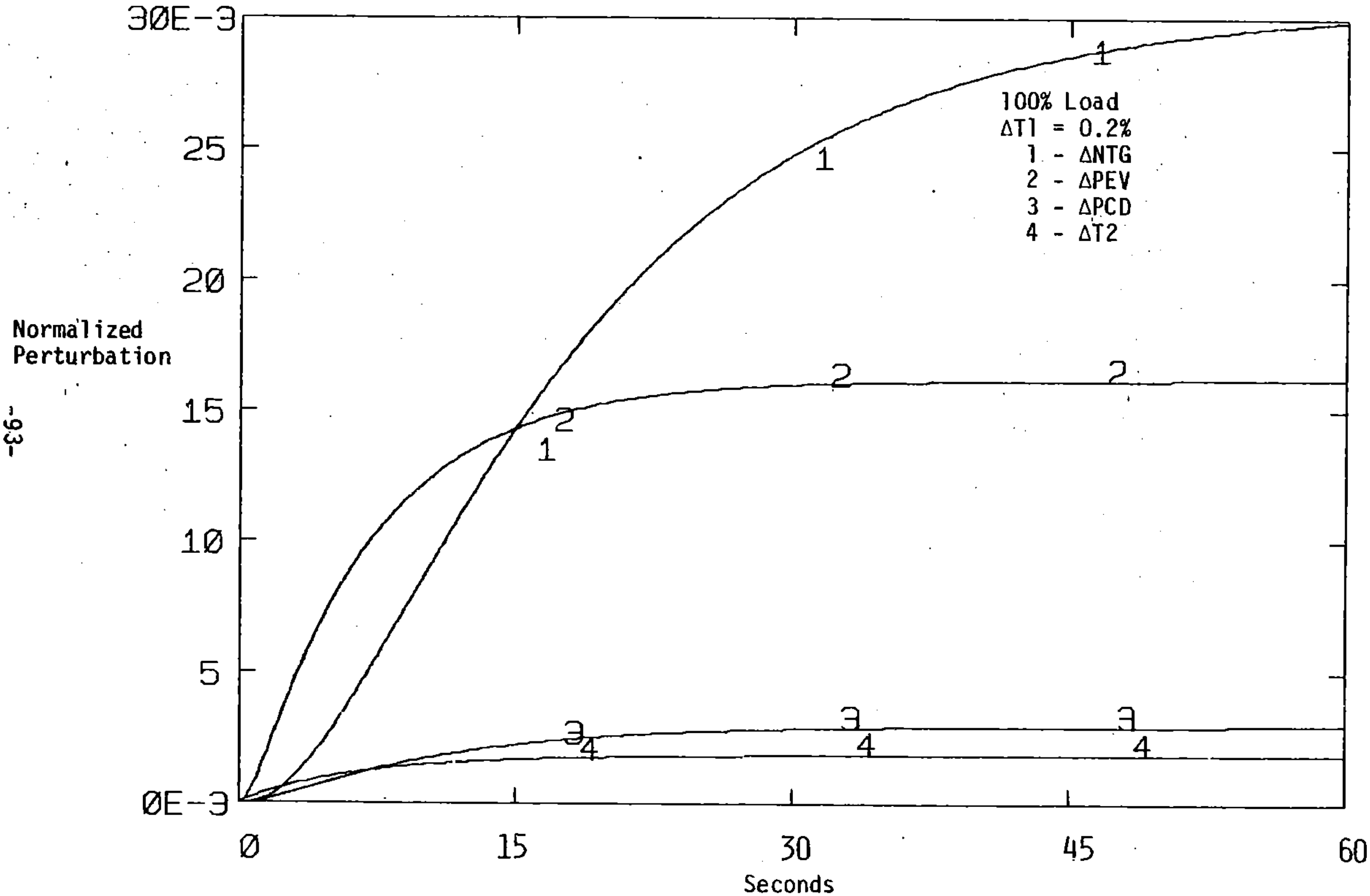

FIGURE 24: WARM SEAWATER TEMPERATURE DISTURBANCE (Open Loop)

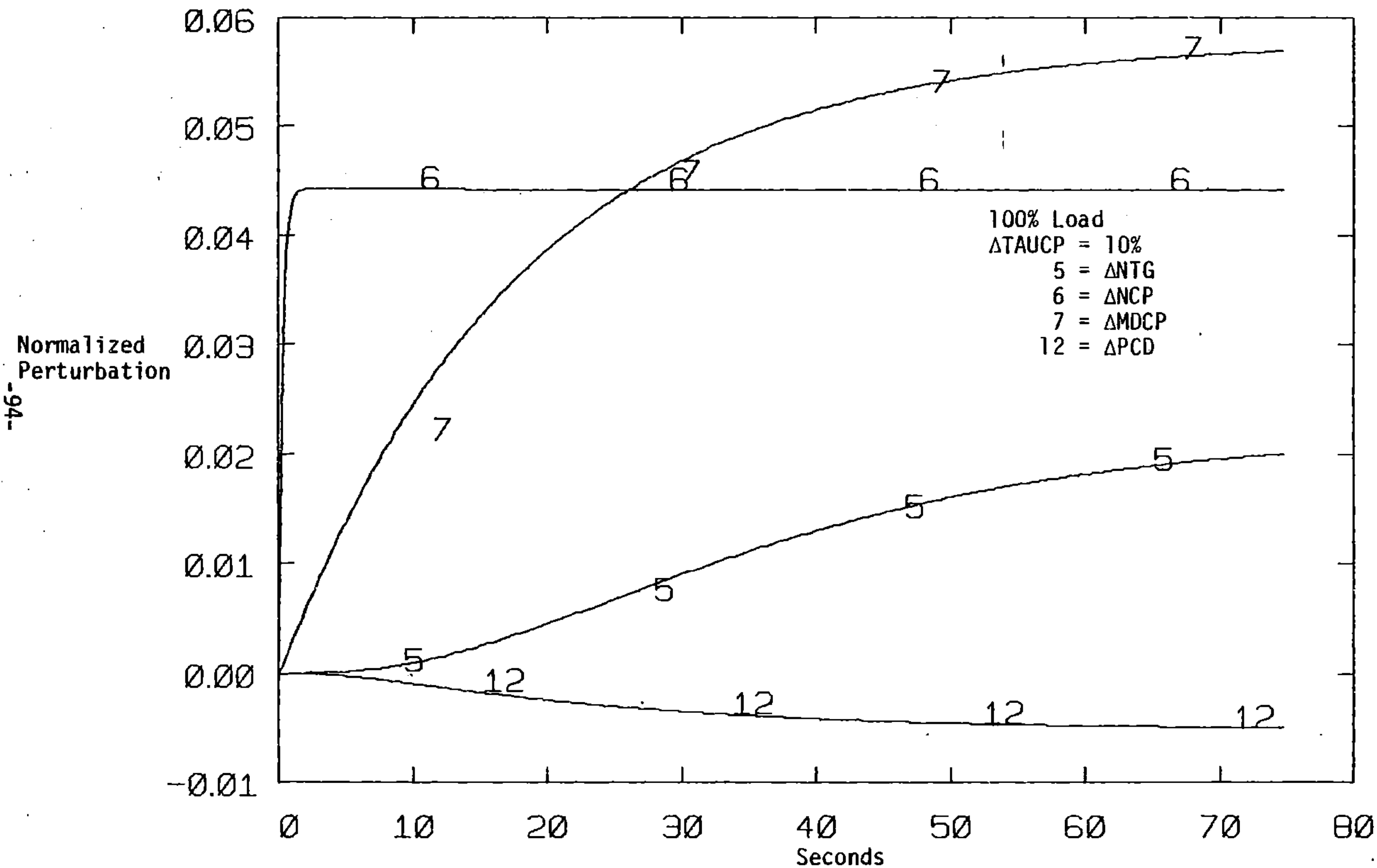

FIGURE 25: COLD WATER PUMP TORQUE DISTURBANCE (Open Loop)

response to a 10% step increase in the input torque of the cold water system pumps. The pump speed increases by 4 1/2% very rapidly (2 seconds). The seawater flow rate in the condenser rises much more slowly because of the large fluid inertia in the cold pipe, reaching a final steady state level of + 6% in 70-80 seconds. Because of the increased seawater flow, the condenser operates more efficiently and the condenser vapor saturation temperature and pressure decreases. The decrease in the condenser vapor pressure induces a larger vapor flow rate in the system which causes the turbine-generator speed to increase to a steady state level of +2% following a 5-10 second initial lag. Since the heat exchangers equilibrate more quickly than the seawater flow transient, the system dynamics are essentially governed by the slow water flow response in the condenser.

3.2.4 Bypass Valve Opening Disturbance

Figure 26 shows the response of the OTEC plant model to a 10% step increase in the bypass valve opening. The total vapor flow in the system increases by 10% instantaneously as a result of the increased flow area. This causes a rapid depressurization of the evaporator and condenser, respectively, which in turn reduces the total vapor flow and the turbine vapor flow rate. This transient occurs in approximately 2-3 seconds after which the heat exchangers require 20-30 seconds to reach thermal equilibrium at

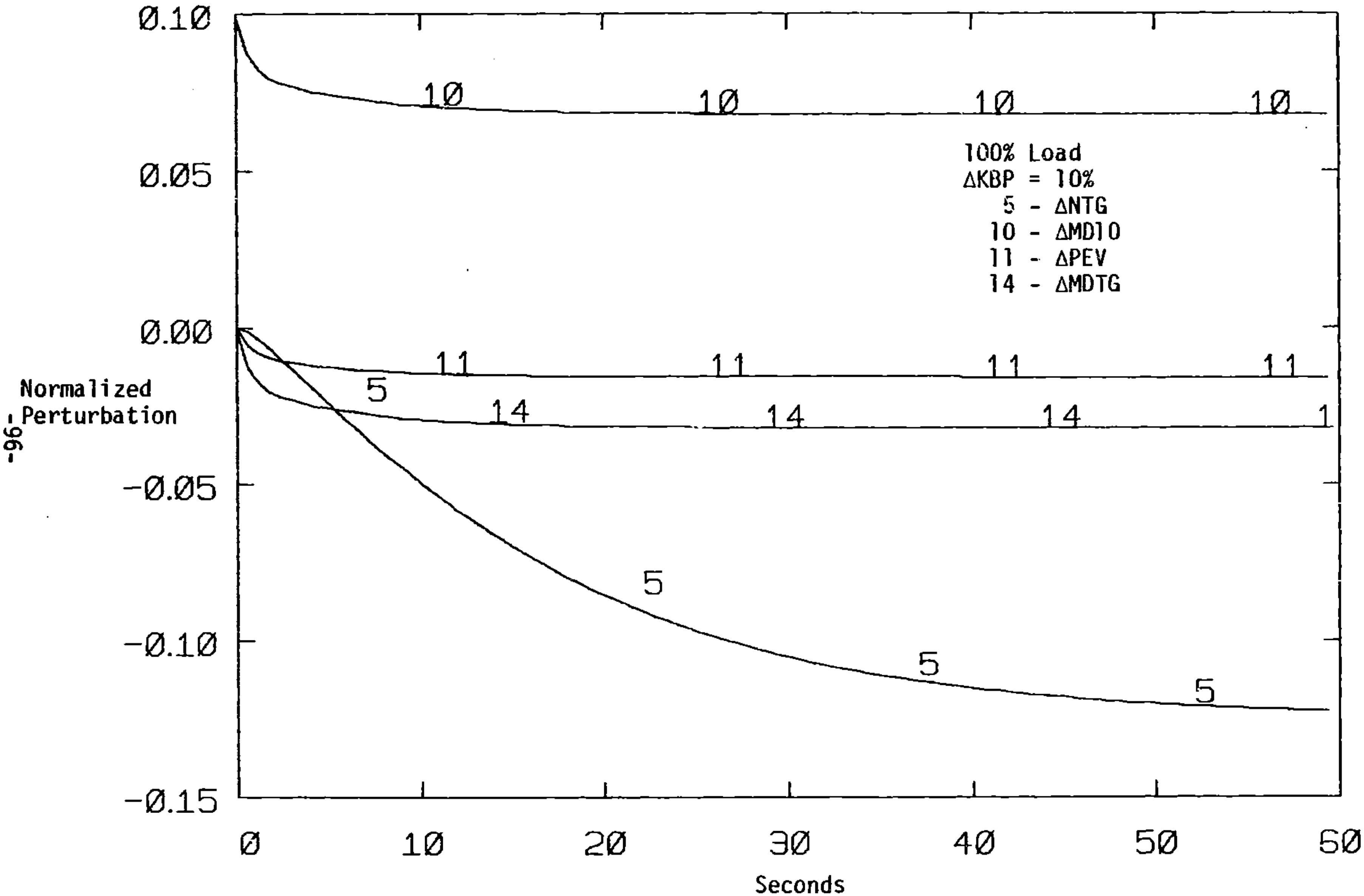

FIGURE 26: BYPASS VALVE OPENING DISTURBANCE (Open Loop)

the new saturation temperatures and pressures. The turbine-generator speed decreases following a negligible lag because of the rapidly decreasing turbine vapor flow, falling a total of 12 1/2% in 60-70 seconds.

3.2.5 Cold Water Pump Motor Frequency Disturbance

The synchronous pump motor model was added to the cold water system and the OTEC system response to a 5% step increase in the pump motor frequency set point was simulated. The results are shown in Figure 27 and 28. Initially, the pump speed increases by . ' in about 1 second while the pumping power increases by 20%, both with a slight overshoot. As the seawater flow rate through the condenser slowly increases, the pump head and therefore the pumping power decline until it reaches a steady state of +17% in approximately 70 seconds. The remainder of the OTEC system behaves very similar to the previous cold water system transient.

3.2.6 Wave Disturbances

Wave disturbances on the seawater pumping systems are modeled as sinusoidally varying waves of given period and amplitude. Although the actual disturbance is more realistically a stochastic process involving a range of wave frequencies and amplitudes, it is felt that this type of simplistic wave model gives a reasonable approximation of the worst wave behavior in any given sea state. The effects of two sea states are investigated = Sea State 2 and

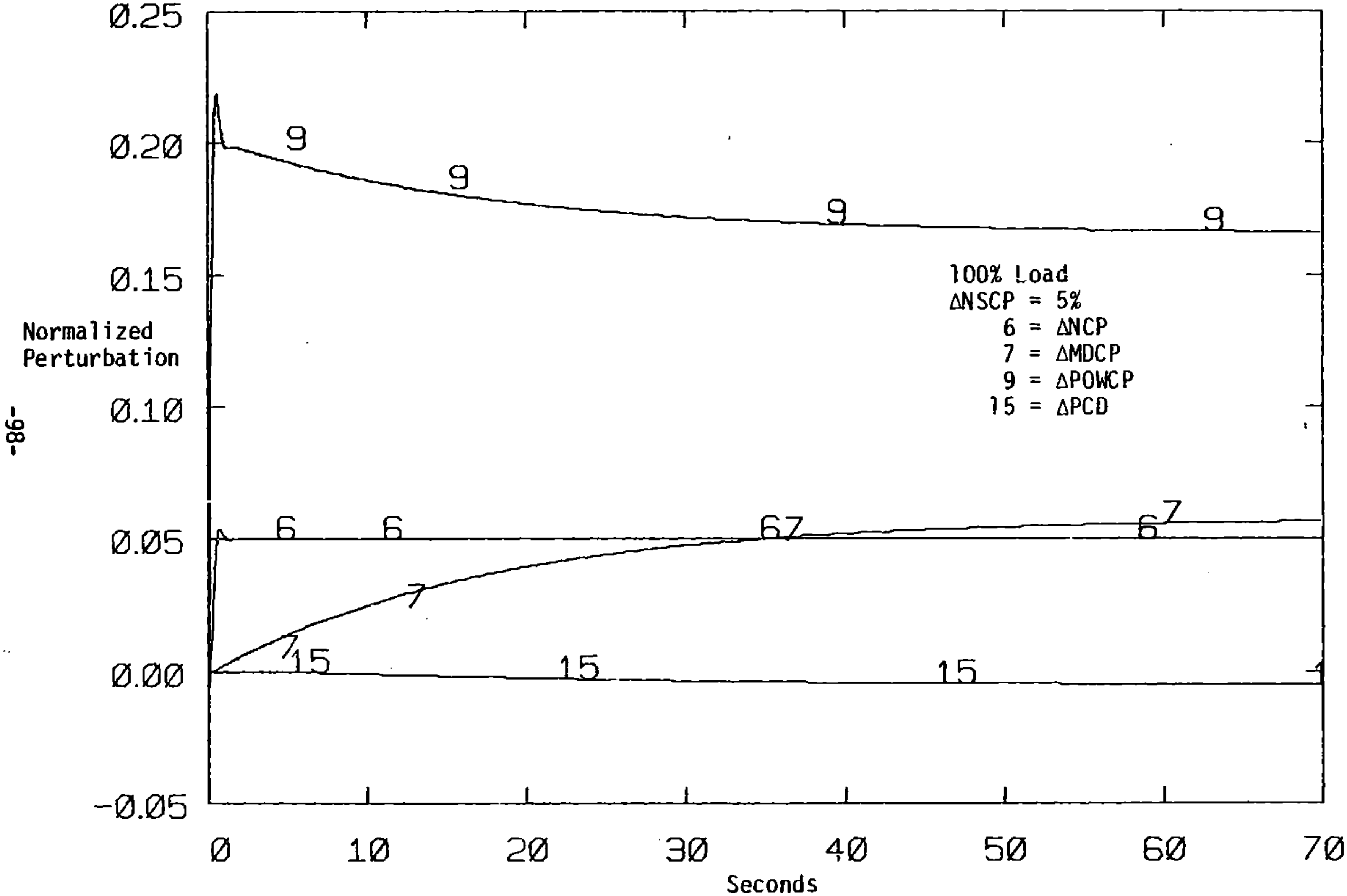

FIGURE 27: COLD WATER PUMP FREQUENCY DISTURBANCE (Open Loop)

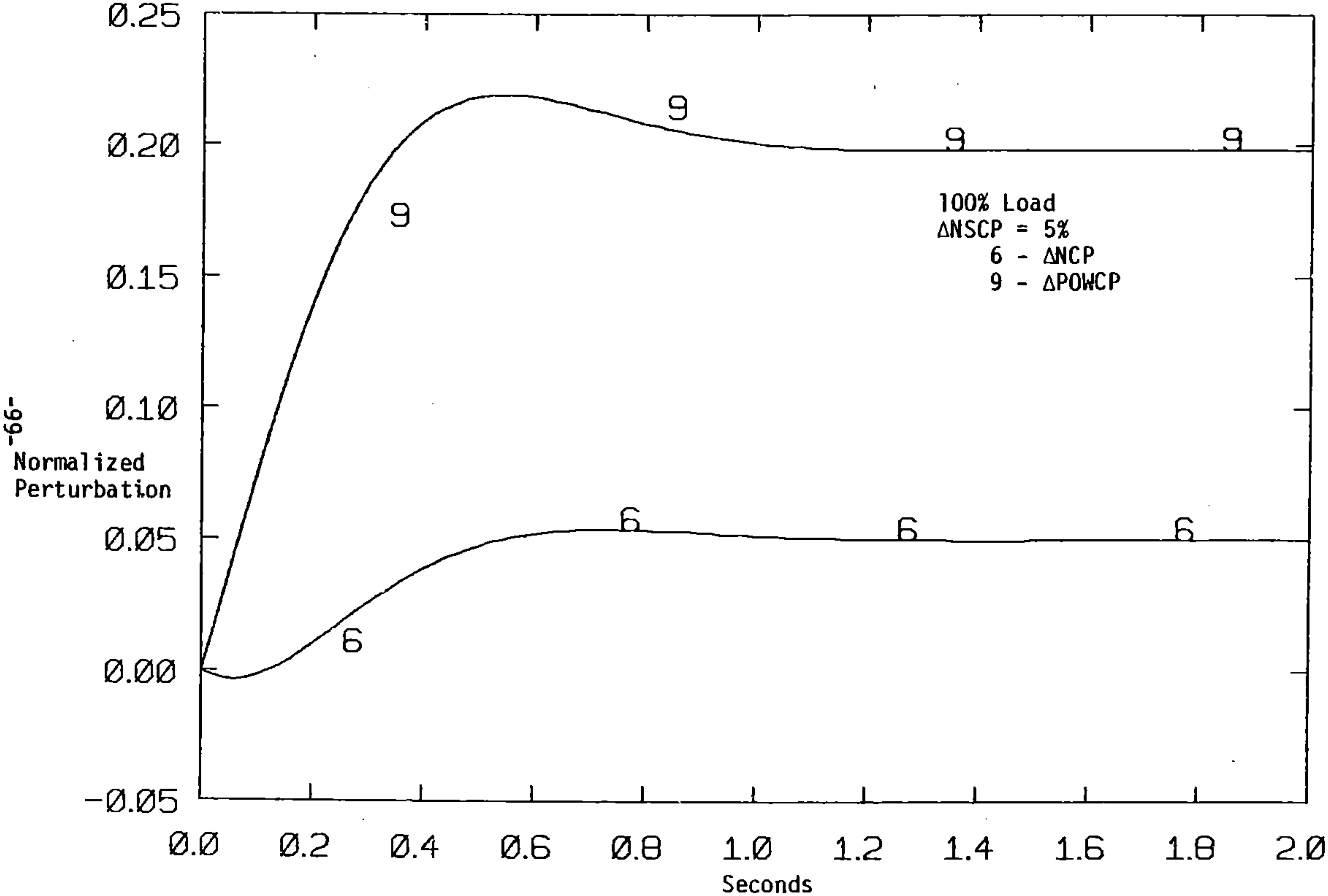

FIGURE 28: COLD WATER PUMP FREQUENCY DISTURBANCE (Open Loop)

Sea State 6. Sea State 2 is the normal operating sea state for the OTEC plant and is characterized by winds of 5-8 knots and waves with a significant wave amplitude of 2 feet and a period of 2 seconds. Sea State 6 is the maximum operating sea state for the OTEC plant characterized by winds of 22-27 knots and waves with a significant wave amplitude of 12 feet and a period of 10 seconds.[17]

Figure 29 is a simulation of the OTEC plant response when the warm water system is subjected to Sea State 2. The power supplied to the pumps is held constant. The variation in seawater flow rate is approximately 5%. However, because of the thermal lags in the evaporator, the overall system experiences negligible effects during this sea state. Figures 30 and 31 are a simulation of the OTEC plant response when the warm water system is subjected to the Sea State 6. Here, the variation in seawater flow is about 30%. Because of the low frequency of the wave disturbance, the thermal and other lags in the system are not able to "filter out" this disturbance quite as well. The effects on the OTEC plant are noticeable = 1.6% variation in turbine-generator power output, 0.5% variation in vapor mass flow rate, and approximately 0.2% variation in the turbine-generator speed. By contrast, when the cold water system is subjected to Sea State 6 (Figure 32), the variation in the seawater flow is a maximum of 3% while the pump speed varies less than 1%. This is a result of the large fluid inertia in the cold water pipe which tends to resist any changes in the

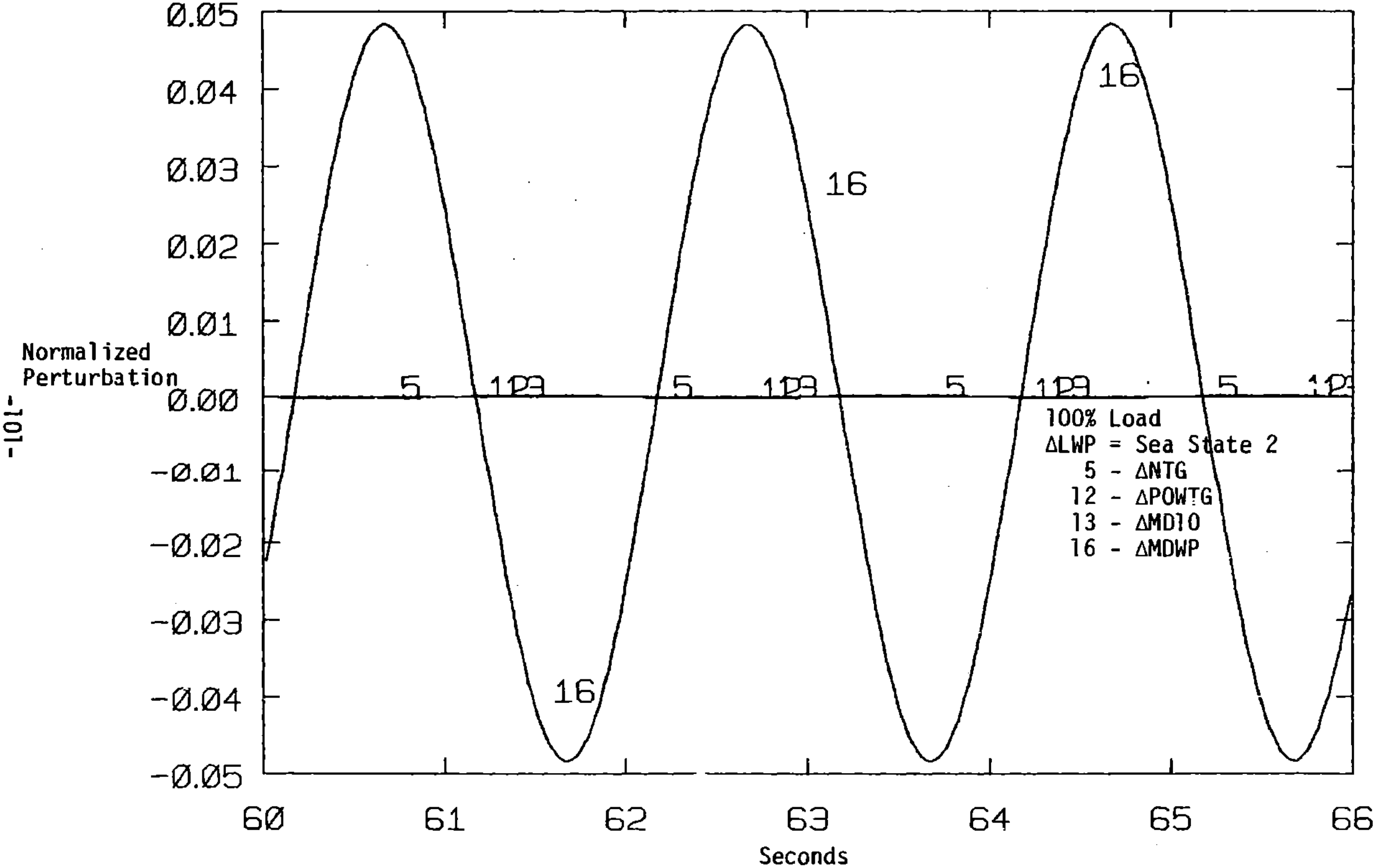

FIGURE 29: WARM WATER SYSTEM WAVE DISTURBANCE (Open Loop)

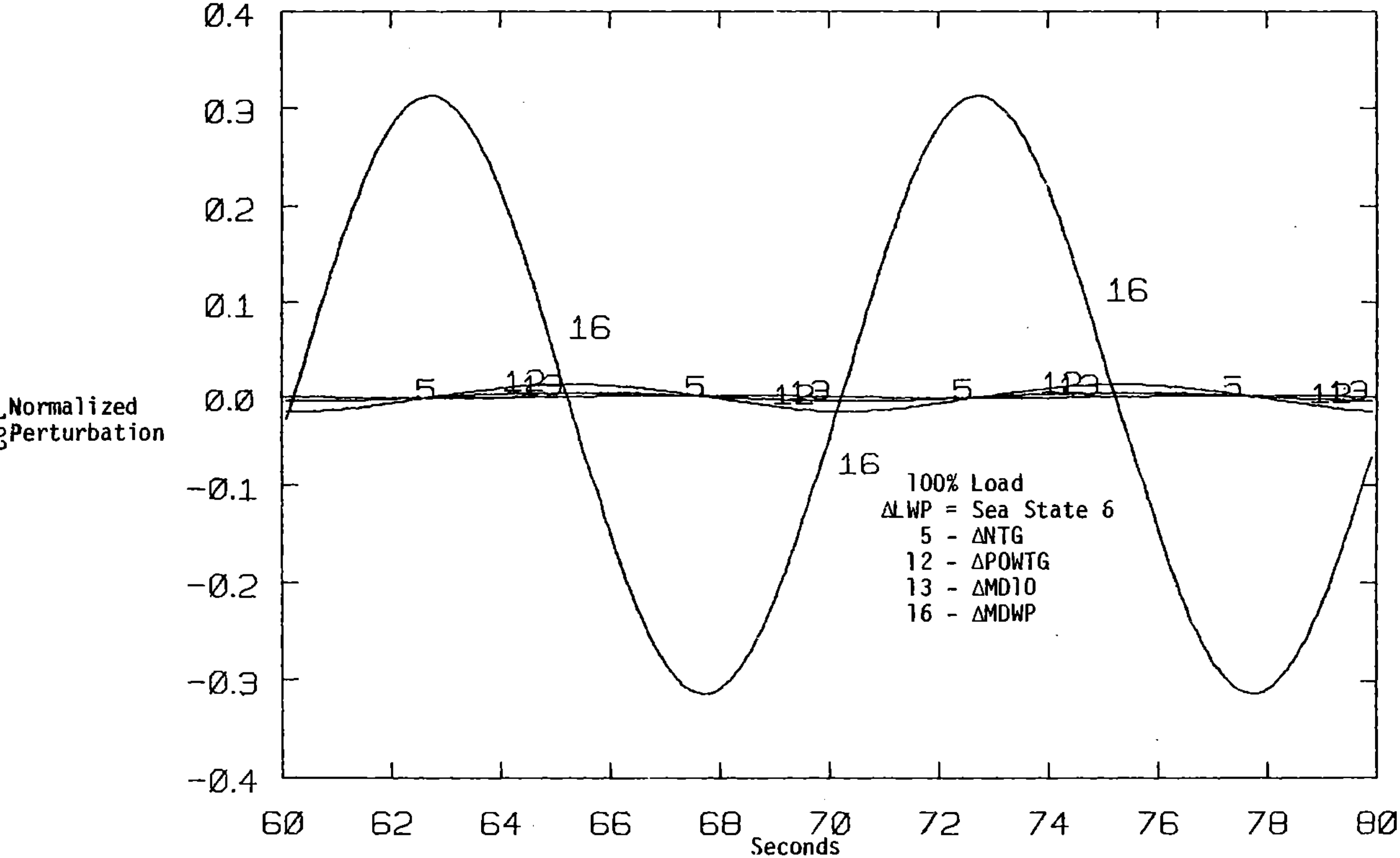

FIGURE 30: WARM WATER SYSTEM WAVE DISTURBANCE (Open Loop)

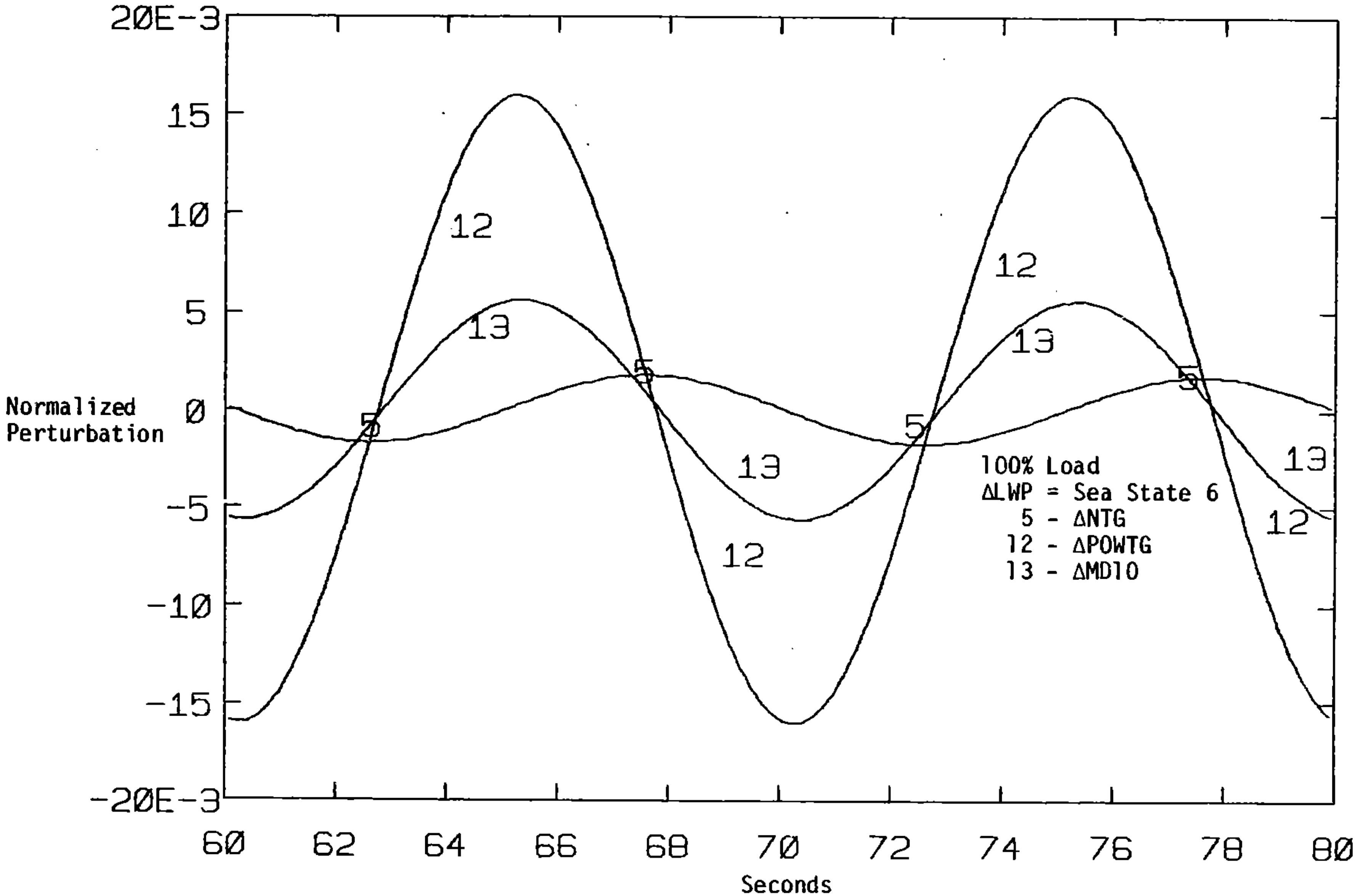

FIGURE 31: WARM WATER SYSTEM DISTURBANCE (Open Loop)

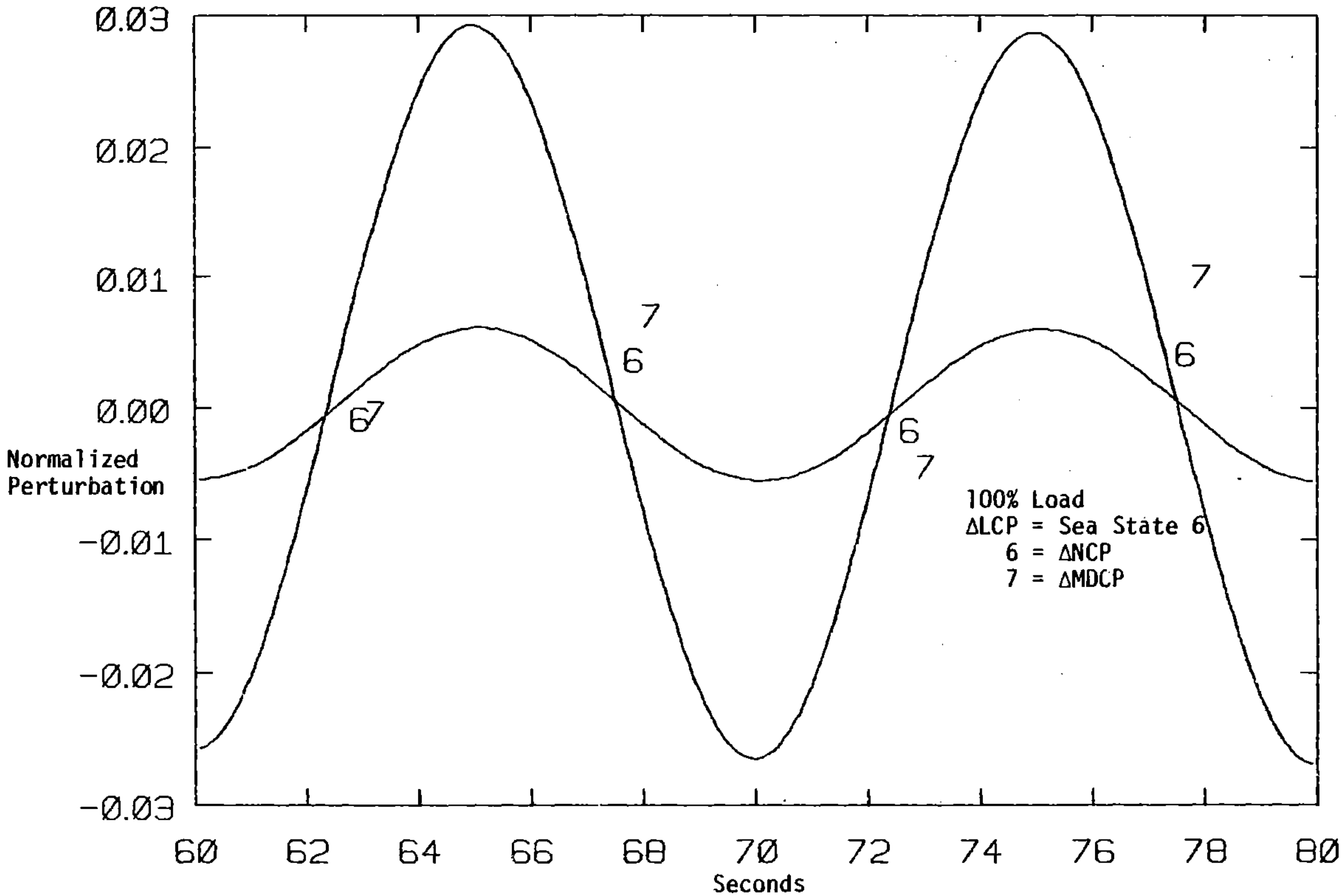

FIGURE 32: COLD WATER SYSTEM WAVE DISTURBANCE (Open Loop)

seawater flow rate and "filters out" the wave disturbance.

When the frequency controlled synchronous pump motors are included into the system model, the results for the warm water system are somewhat different. The system was subjected to three different wave types:

a) Figure 33 Wave amplitude - 1 foot
Wave period - 1 second

b) Figure 34 Wave amplitude - 5 feet
Wave period - 5 seconds

c) Figure 35 Sea State 6

The results show that the synchronous motor serves to keep the seawater flow rate variation under 5% in each case. However, this is at the expense of increasingly large power fluctuations to the pump motors, beginning at 10% in the first case, progressing to a 45% variation in the second case, and reaching a maximum of 100% in Sea State 6.

3.3 Open Loop Model Steady State Validation

In order to validate the steady state accuracy of the linear dynamic open loop OTEC model, the 100% power level model is subjected to a bypass valve opening disturbance corresponding to the bypass valve opening of the 80% load steady state model evaluated by the computer program. The final steady state variables of the dynamic simulation are compared to the corresponding

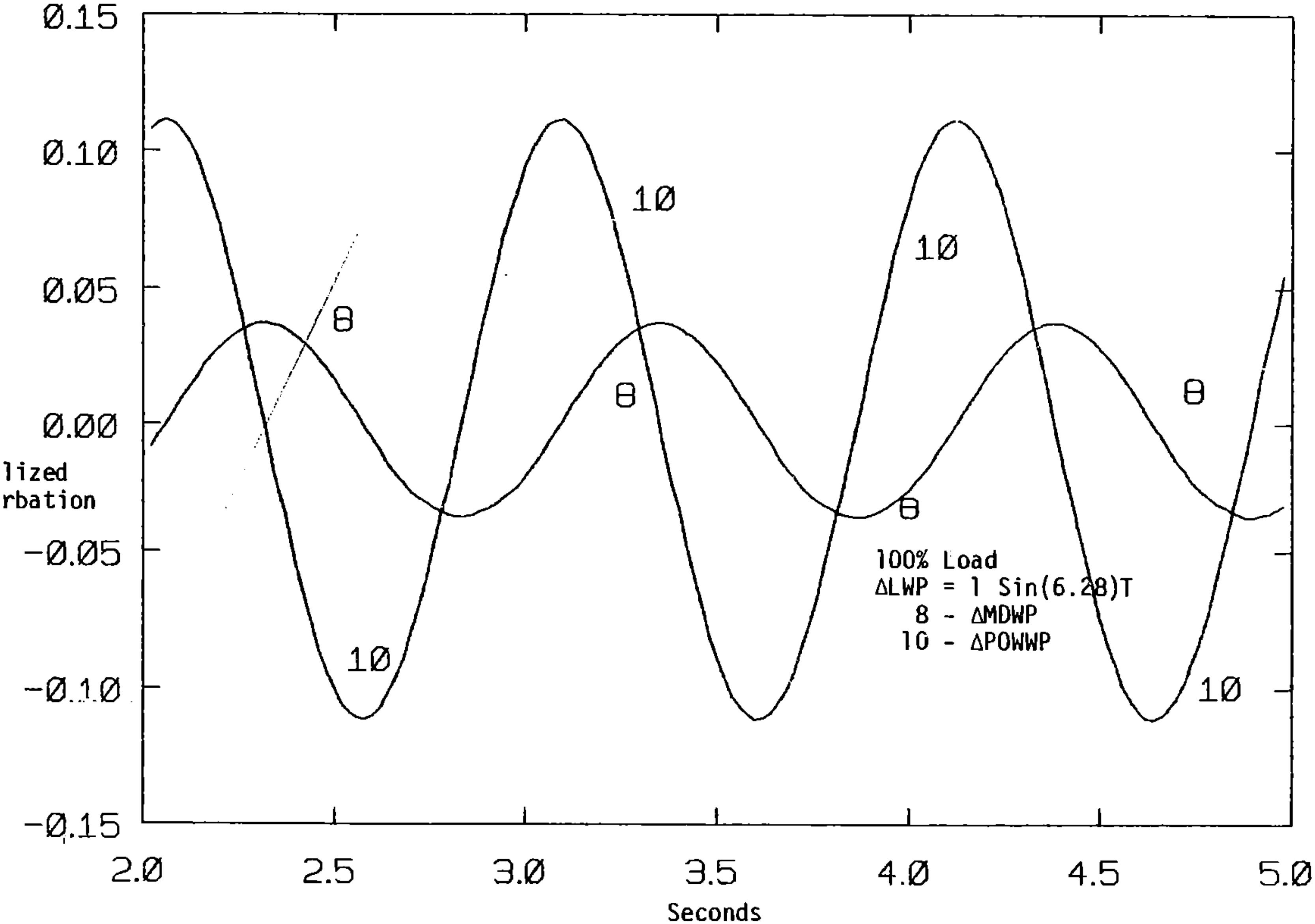

FIGURE 33: WARM WATER SYSTEM WAVE DISTURBANCE (Open Loop)

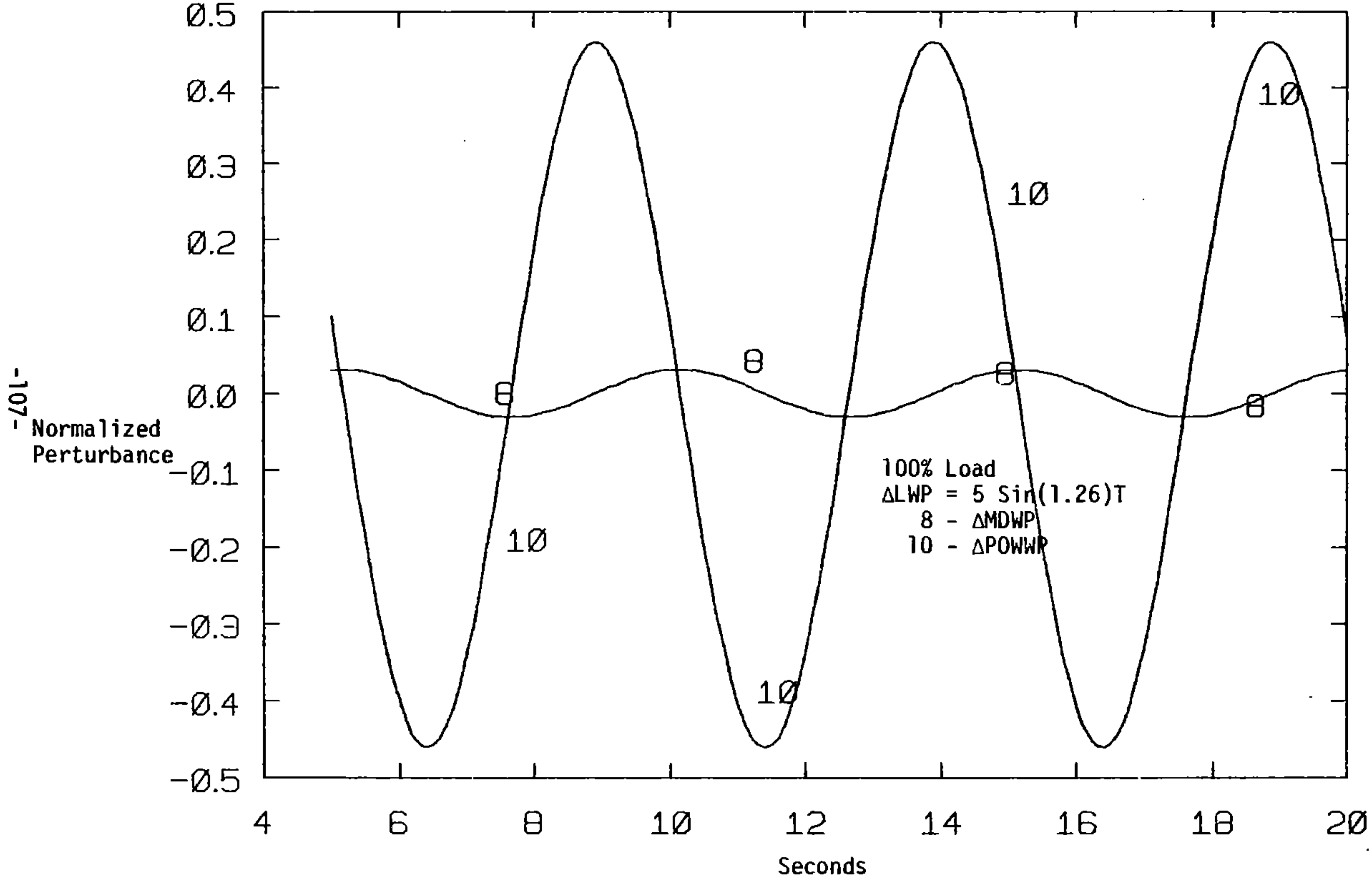

FIGURE 34: WARM WATER SYSTEM WAVE DISTURBANCE (Open Loop)

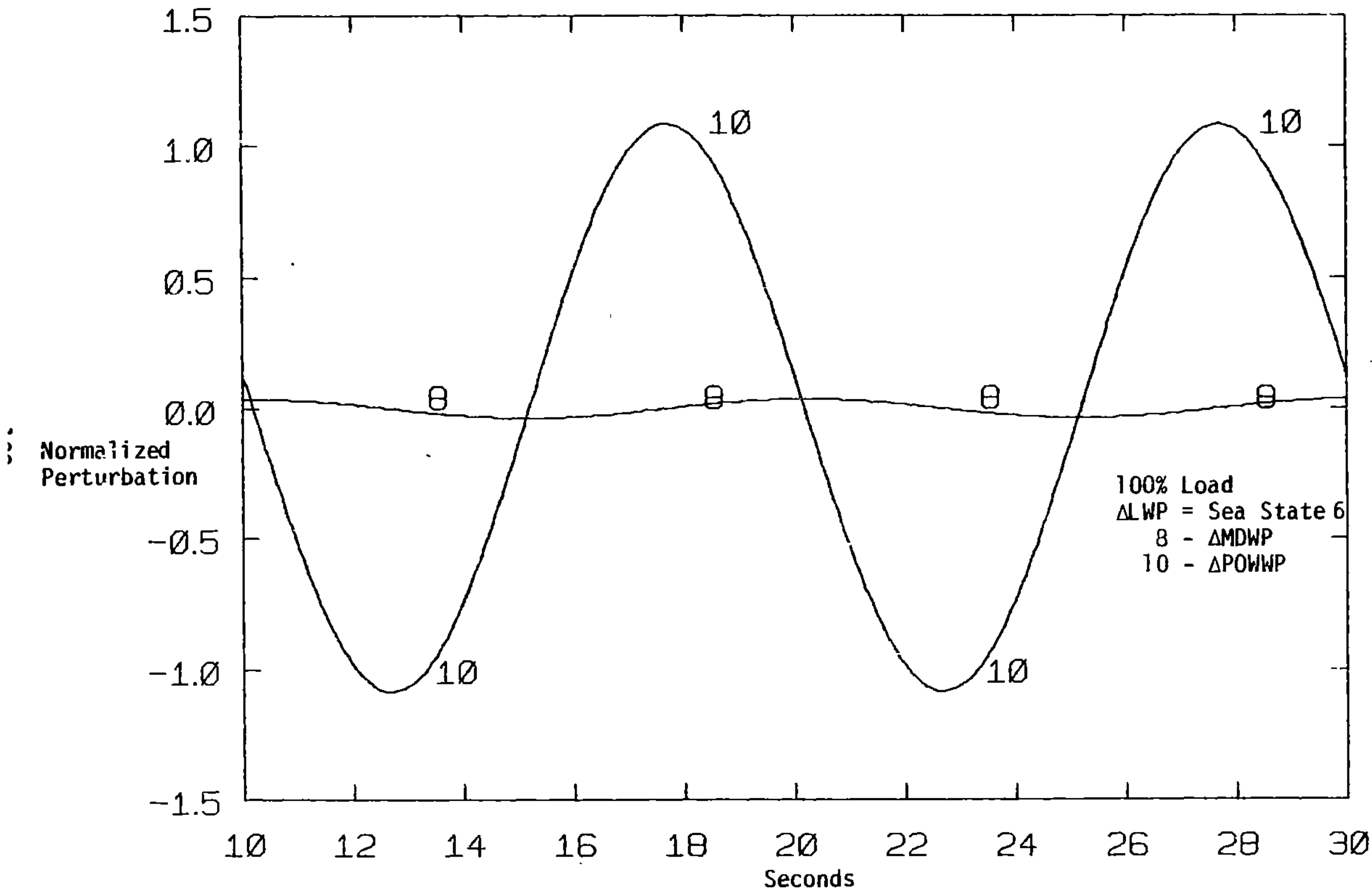

FIGURE 35: WARM WATER SYSTEM WAVE DISTURBANCE (Open Loop)

variables of the steady state model in Table 8.

TABLE 8: STEADY STATE COMPARISON OF DYNAMIC AND STEADY STATE MODELS

VARIABLE	NONLINEAR STEADY STATE MODEL	LINEAR DYNAMIC MODEL	% ERROR
POWTGSS	53.93 MW	51.13 MW	-4.2%
TCDSS	51.685°F	52.013°F	+0.6%
TEVSS	68.330°F	68.037°F	-0.4%
T2SS	73.587°F	73.584°F	0%
T5SS	46.319°F	46.336°F	+0.03%
MDTGSS	14.29×10^{6} lbm/hr	14.18×10^{6} lbm/hr	-0.8%

The OTEC linear dynamic model shows generally good agreement with the steady state nonlinear model, the largest error being 4.2% for the turbine-generator output power.

3.4 Open Loop Dynamic Analysis Conclusions

Some conclusions can be drawn about the OTEC power plant based on the previous open loop analysis of the dynamic model. These are divided into three categories:

1) Subsystem interactive transient response, 2) Effects of disturbances, and 3) Effects of control mechanisms. Each category is examined in the following sections.

3.4.1 Subsystem Interactive Transient Response

The main power loop of the OTEC plant, consisting of heat exchangers, turbine-generator, and vapor system, has essentially three separate transient effects. The fastest of these is the vapor flow rate transient which requires 2-3 seconds to fully respond to disturbances in the ammonia vapor path, whether they are changes in the heat exchanger pressure or in the bypass valve opening. The heat exchangers require 20-30 seconds to reach thermal equilibrium following a change in the saturation state of the ammonia vapor or changes in the seawater flow rate or seawater inlet temperature on the fluid side. The open loop turbine-generator requires from 60-80 seconds to reach steady state in response to a disturbance. For a load disturbance, the response time is approximately 60 seconds. However, since the turbine-generator speed is also dependent upon the vapor flow rate through the turbine, its response time is affected by transients in the vapor flow system. For a bypass valve opening disturbance, the vapor flow transient is fast and the turbine-generator responds with no appreciable lag. However, when the disturbance must propagate through the thermal and even the water system lags, the vapor flow rate transient is controlled by these slow processes and the turbine-generator response is very sluggish.

3.4.2 Effects of Disturbances

The effects of a change in the seawater temperature propagate very slowly throughout the OTEC plant and result primarily in reduced power output. However, wave disturbances to the warm water system do have some effects on plant operation. The 1.6% turbine-generator power variation resulting from the warm seawater flow fluctuations during Sea State 6 using pumps supplied with constant power probably will not cause any adverse affects as long as the OTEC power plant is coupled to a large power grid which can accept these minor power fluctuations. Since the frequency is also low (~0.1 Hz), the disturbance should not pose any control problems. A possible adverse effect may result from the large seawater flow surges (~30%) which could cause undue pump fatigue and related problems.

Other, more serious, problems are encountered when the motor frequency controlled synchronous pumping systems are used. The seawater flow fluctuations remain essentially constant (~5%) and, therefore, the resulting turbine-generator power variations are negligible. However, the pumping power surges are not negligible, rising as high as 100% during Sea State 6. This variation in pumping power in nearly 10% of the total OTEC power module output. If the OTEC pump system is connected directly to a large AC power grid, these power surges might not be too objectionable. If, on the other hand, the pumping system were supplied directly from the OTEC generator, a power fluctuation of this magnitude could be unacceptable and could aggravate stability and control problems.

In addition, the stress cycling in the pump could result in mechanical fatigue problems.

3.4.3 Effects of Control Mechanisms

There are essentially three mechanisms which are used to control the OTEC plant: a) the warm water pump, b) the cold water pump, and c) the bypass valve. There are two types of disturbances which must be compensated for: rapid, unexpected changes in the power load and gradual changes to the OTEC environment. The first type of disturbance requires a control mechanism which is fast acting. Changes in the seawater flow of the cold and warm water systems are shown to have a slow effect on the turbine-generator, having to contend with the thermal lags in the heat exchangers. The cold water system is further hampered by the sluggish cold pipe flow response. Changing the seawater flows requires large power surges to the pumps, which, if directly supplied from the OTEC generator, are shown to cause instabilities in the closed loop.[18] Thus, the seawater pumps are more practically used as a mechanism to maximize the power output in response to the second type of disturbance. [See Section 6.2] The bypass valve, however, directly influencing the vapor flow rate, has a quick effect on the turbine-generator, qualifying it as an effective closed loop control mechanism.

One final result is obtained from the steady state nonlinear model. The bypass valve opening which results in zero gross power from the turbine-generator is

$$K_{bp} = 4.15 \times 10^7 \text{ lbm/hr} \tag{70}$$

which corresponds to $\Delta K_{bp} = 2$. This result is obtained for constant seawater flow rates in the heat exchangers. Referring to Equation (46), the fully open bypass valve diverts 2/3 of the total vapor flow from the turbine at zero gross power output.

IV. PARAMETRIC SENSITIVITY ANALYSIS

Linearized dynamic models are a valuable tool in analyzing the steady state sensitivity of a system to various variable parameters. Dynamic transfer functions of the form

$$\frac{y_i}{u_i} = \frac{a_o + a_1 s + a_2 s^2 + \dots a_n s^m}{b_o + b_1 s + b_2 s^2 + \dots b_n s^n} \tag{71}$$

where $a_{1,n}$ $b_{1,n}$ - constants

s - Laplace operator

relating a given system input to a given system output are easily obtained from the state equations of the linearized dynamic model. By allowing all the time derivatives of the transfer function to approacn zero ($s \rightarrow 0$), a steady state sensitivity relationship between the input and output results.

$$\left(\frac{y_i}{u_i}\right)_{ss} = \frac{a_o}{b_o} \qquad (72$$

The examination of these steady state sensitivities provides valuable information as to how certain OTEC plant variable parameters affect others.

Two sets of sensitivities are studied in this section. The first is OTEC system sensitivities at 100% power level which are useful for the steady state optimization problem, that is, maximization of the output of the power plant. The second set is the system sensitivities to the bypass valve at varying power levels, a valuable tool in the design of a control system.

It must be emphasized that these sensitivities, derived from a simplified dynamic model, are not of sufficient accuracy for use in a rigorous steady state optimization analysis. They are useful for an initial rough estimation of the steady state behavior of the OTEC power plant. A detailed steady state model is required for this type of analysis and is beyond the scope of this work.

4.1 100% Load Level Sensitivities

The most important sensitivities of the OTEC plant at full load are those associated with the seawater pumping systems. Table 9 contains a listing of these.

TABLE 9: FULL LOAD SENSITIVITIES

SENSITIVITY	NORMALIZED	UNITS
ΔPOWTG/ΔMDWP	0.17	0.12 MW/%
ΔPOWTG/ΔMDCP	0.38	0.25 MW/%
ΔPOWCP/ΔMDCP	2.7	0.21 MW/%
ΔPOWWP/ΔMDWP	3.3	0.16 MW/%
ΔMD10/ΔMDWP	6.6×10^{-2}	1.0×10^{4} (lbm/hr)/%
ΔMD10/ΔMDCP	7.2×10^{-2}	1.1×10^{4} (lbm/hr)/%
ΔTEV/ΔMDWP	9.1×10^{-3}	0.049 °F/%
ΔTCD/ΔMDCP	9.2×10^{-3}	0.047 °F/%
ΔMDCP/ΔNCP	1.2	1.7×10^{7} (lbm/hr)/%
ΔMDWP/ΔNWP	1.0	1.4×10^{7} (lbm/hr)/%
ΔPOWTG/ΔMDTG	4.1	0.28 MW/%

Some important OTEC plant characteristics are apparent from this analysis. First, a change in condenser seawater flow has approximately twice the effect on the turbine-generator power output as a comparable change in the evaporator flow. This is the direct result of changes in vapor density in the system. As the condenser becomes more effective because of increased seawater flow, the average ammonia vapor temperature is decreased and the vapor becomes less dense, resulting in a higher vapor velocity in the turbine for a given mass flow rate. Conversely, the evaporator becomes more effective as a result of an increased seawater flow and the vapor temperature and density increases, reducing the vapor velocity in the turbine. Another interesting observation is that increases in the turbine-generator power output because of increased seawater flow rates are almost identically offset by increases in the pumping power of both the warm and cold water systems. Thus it appears that the system is optimized with respect to net power output at this load level.

4.2 Bypass Valve Sensitivities

It is necessary to evaluate the sensitivity variation of the bypass valve at different nominal openings in order to design an effective turbine-generator controller. The most important system variables affected by the bypass valve are the turbine-generator power output, the turbine vapor flow rate, and the turbine-generator speed. These sensitivities are analyzed and presented in Table 10. The seawater system flow rates remain constant at each steady state power level.

TABLE 10: BYPASS VALVE SENSITIVITIES

POWER LEVEL	ΔPOWTG/ΔKBP (MW/%)	ΔMDTG/ΔKBP (10^4lbm/hr/%)	ΔNTG/ΔKBP (%/%)	ΔKBP
100%	-0.86	-4.75	-1.24	0
80%	-0.73	-4.66	-1.10	0.20
60%	-0.58	-4.43	-0.94	0.44
40%	-0.43	-4.01	-0.76	0.74
20%	-0.27	-3.35	-0.55	1.2
10%	-0.19	-2.91	-0.43	1.5
0%	-0.12	-2.34	-0.30	2

The bypass valve sensitivities are plotted versus the nominal steady state bypass valve opening in Figures 36, 37, and 38. All three sensitivities are clearly decreasing functions of the nominal bypass valve opening demonstrating the reduction in effectiveness of the bypass valve as it opens.

The sensitivity of the turbine-generator power output to the vapor mass flow rate through the turbine is a critical factor when the evaporator is operating in the burnout state. This sensitivity is given in Table 11 as a function of the nominal flow rate through the turbine.

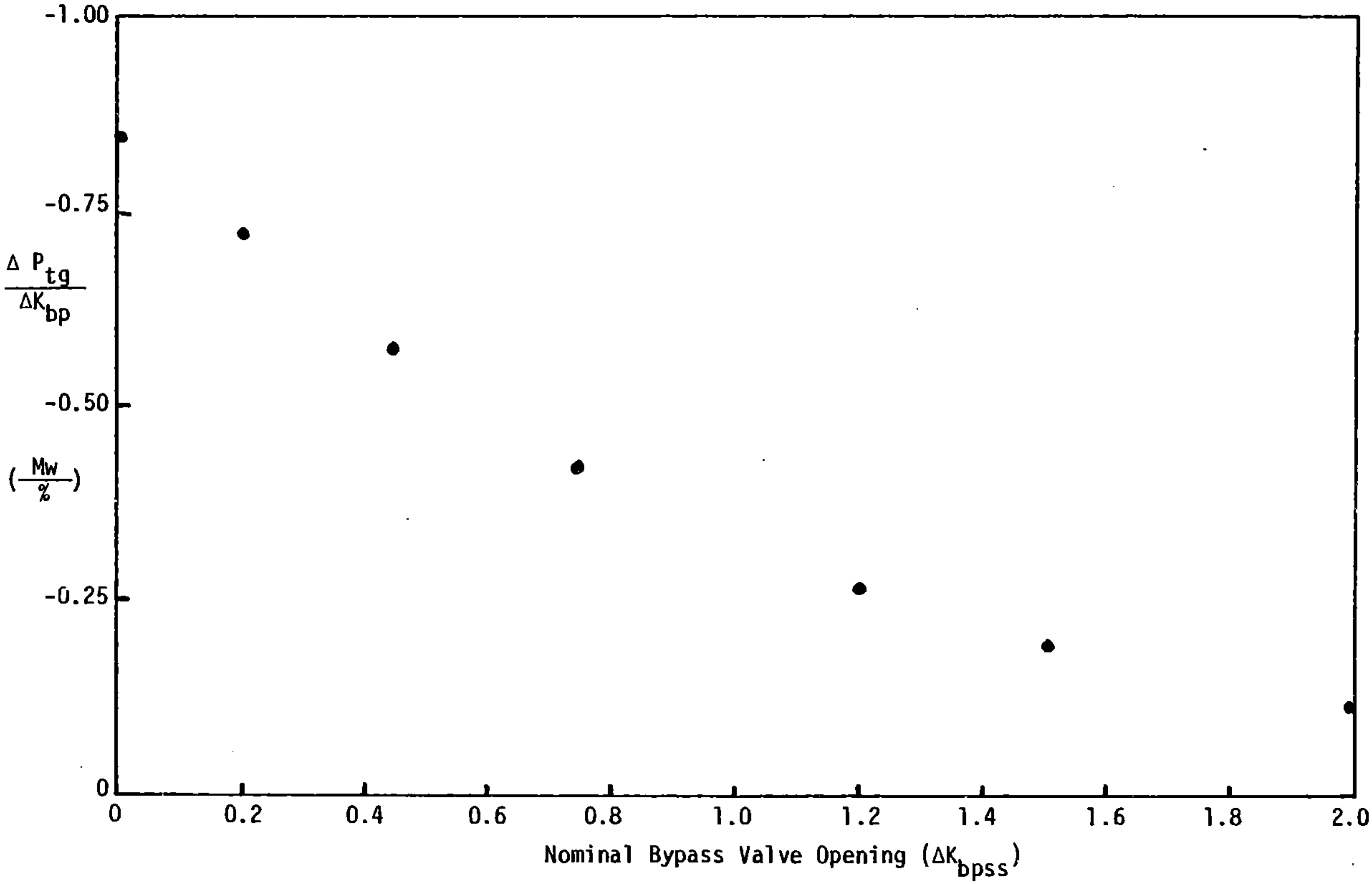

FIGURE 36: POWER OUTPUT SENSITIVITY TO THE BYPASS VALVE

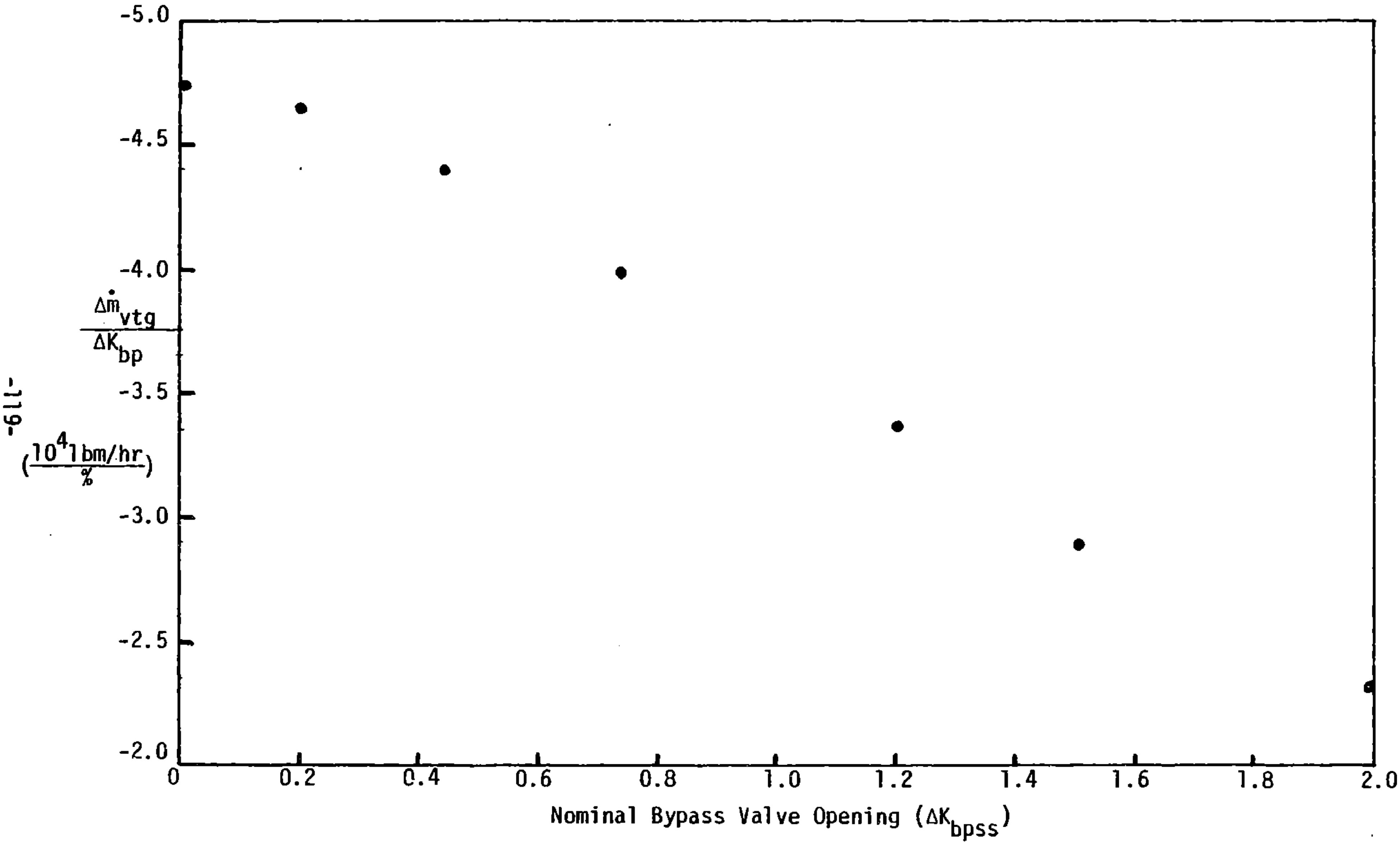

FIGURE 37: TURBINE VAPOR FLOW SENSITIVITY TO THE BYPASS VALVE

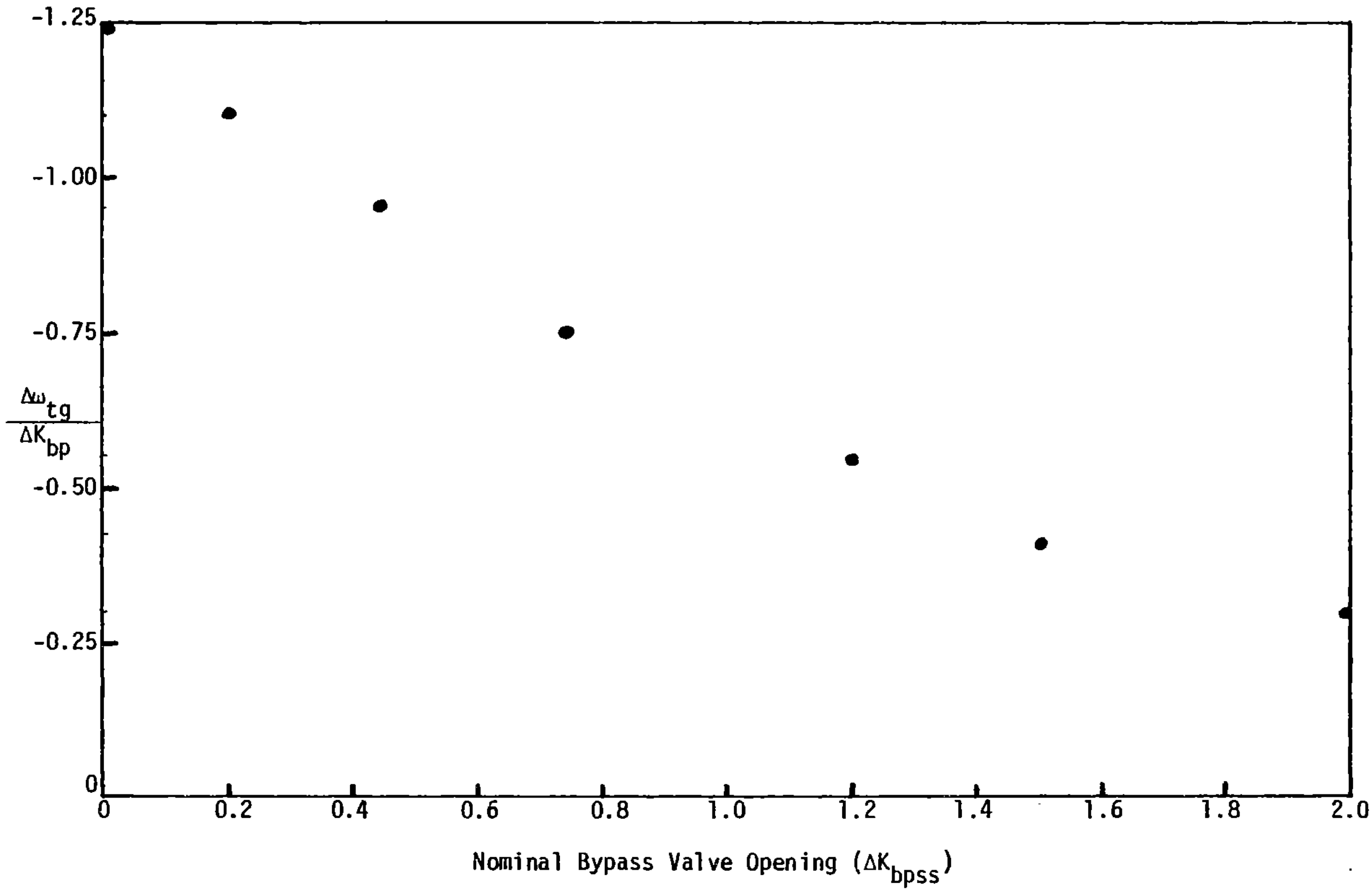

FIGURE 38: TURBINE-GENERATOR SPEED SENSITIVITY TO THE BYPASS VALVE

TABLE 11: TURBINE FLOW RATE SENSITIVITY

POWER LEVEL	MDTG(10^6 lbm/hr)	ΔPOWTG/ΔMDTG (MW/10^6 lbm/hr)
100%	15.1	18.2
80%	14.3	15.5
60%	13.3	13.1
40%	12.2	10.6
20%	10.7	7.2
10%	9.8	6.6
0%	8.6	5.0

The turbine-generator power output is clearly not a linear function of the vapor mass flow rate.

V. CONTROL SYSTEM DEVELOPMENT

The OTEC control system development is considered in four stages:

1) Examination of a proposed turbine-generator load loss overspeed protection system

2) Design of a turbine-generator speed governor which will regulate the plant when it is directly connected to the on-shore AC power grid

3) Design of a turbine-generator speed governor which will regulate the plant when it is connected to the on-shore AC power grid by a DC transmission system

4) Design of a pump motor controller which will reduce the power surges associated with wave disturbances.

The bypass valve is used as the principle turbine-generator control mechanism because of the desirable characteristics established previously. However, when the OTEC plant is at full load, the bypass valve is completely closed; in this event, other control mechanisms are suggested. The proposed sensor-actuator mechanism is a conventional electro-hydraulic governor system. This system is represented by a constant gain of the form shown in Figure 39.[8]

The governor droop, δ^*, is defined as the percent drop in turbine-generator speed resulting in a total power reduction. Graphically, this is represented in Figure 40.

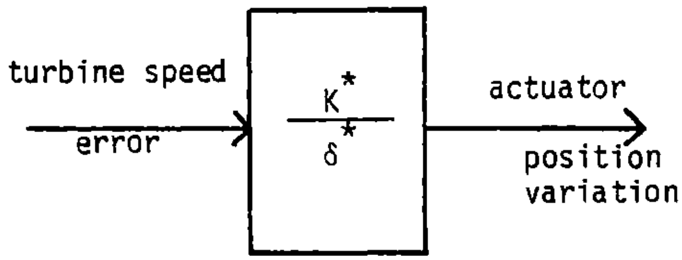

FIGURE 39: GOVERNOR MODEL SCHEMATIC

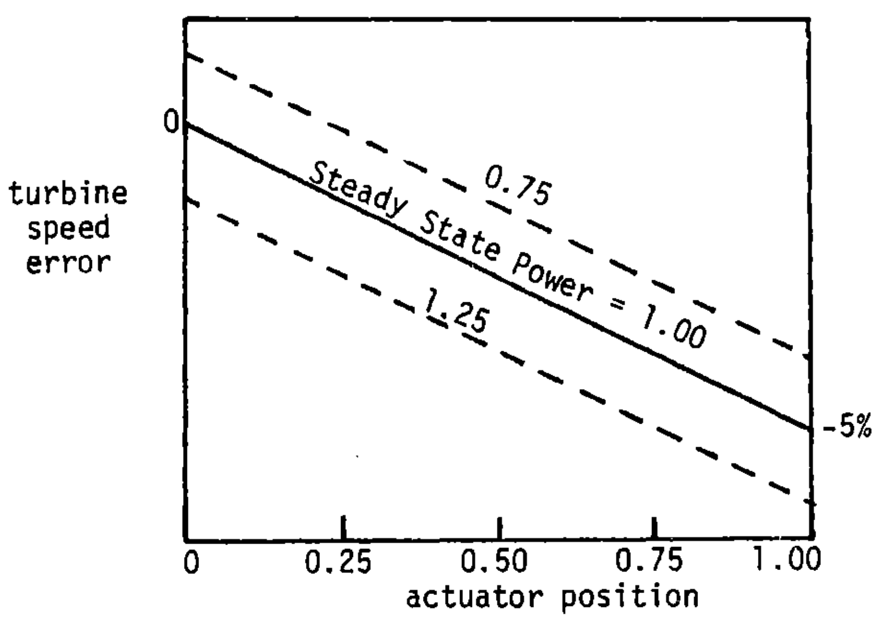

FIGURE 40: 5% GOVERNOR DROOP CHARACTERISTICS

K^* represents the open loop sensitivity of the controlled variable to the actuator signal.

$$\frac{\text{"actuator signal"}}{\text{"controlled variable"}} = K^* \tag{73}$$

Initially, actuator dynamics are ignored; however, this restriction is relaxed in the final analysis. The seawater flow rates remain constant at each load level unless otherwise stated.

5.1 Turbine-Generator Overspeed Protection

A turbine-generator requires protection from overspeed in the event of a complete load loss. The principle criteria for the protective system is to maintain the turbine-generator overspeed at less than 40% maximum. The open loop OTEC model at 100% power level was simulated for a 100% turbine-generator torque load drop to determine the uncontrolled overspeed response. The turbine-generator speed, shown in Figure 41, reaches a maximum of 100% overspeed in approximately 70 seconds. An overspeed controller is now added to the turbine-generator with the following specifications as proposed by Westinghouse[19] a) ability to sense a full load drop in 0.25 seconds and b) fully closed to fully open bypass valve in 0.25 seconds. The maximum bypass valve opening as indicated by the steady state analysis for zero power output of the OTEC plant is $\Delta K_{bpmax} = 2$. However, because of the nonlinear nature of the bypass valve, the maximum bypass valve opening for the

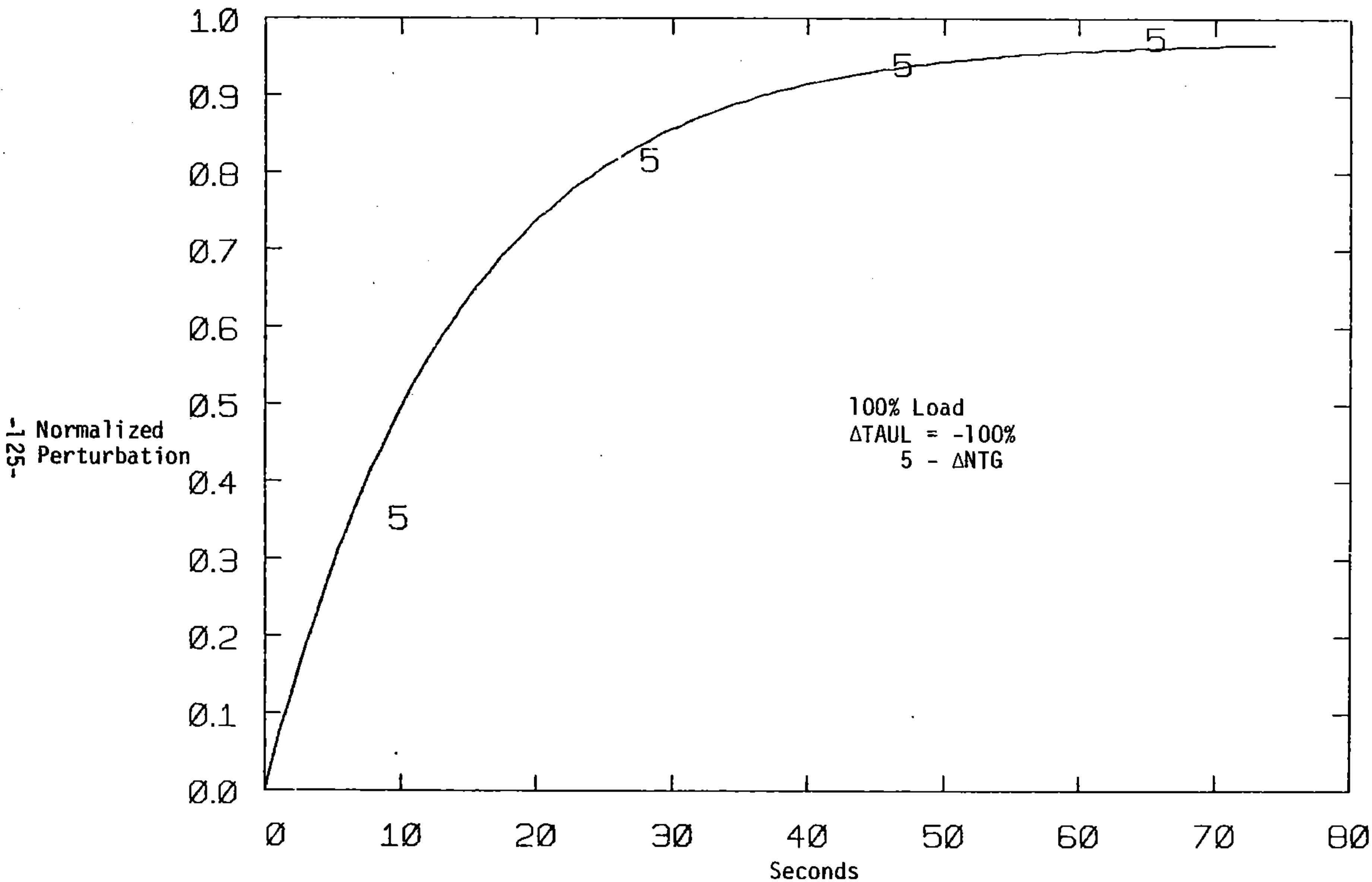

FIGURE 41: TURBINE-GENERATOR LOAD DROP-UNCONTROLLED

linear model must be adjusted to account for this nonlinearity. This is accomplished by evaluating the power sensitivity of the bypass valve opening at 100% load.

$$\frac{\Delta P_{tg}}{\Delta K_{bp}} = 1.28 \qquad (74)$$

Thus, the maximum bypass valve opening for a full load reduction of the linear model is $\Delta K_{bpmax} = 0.78$.

The 100% load OTEC model is simulated for a full load drop with the proposed overspeed controller. The result is shown in Figure 42. The maximum turbine-generator overspeed, 12%, is reached in 6 seconds and it returns to the steady state in approximately 80 seconds following load loss, well within the required safety criteria.

5.2 OTEC Plant Control - AC Power Grid

A turbine-generator connected directly to a large AC power grid becomes a synchronous machine whose frequency is controlled directly by the frequency of that power grid. Figure 43 shows the response of the open loop OTEC plant operating at 80% load as the AC bus frequency rises 1% in 5 seconds. The turbine-generator speed follows the bus frequency and is maintained at a 1% higher level. The turbine-generator power fluctuates rapidly as the power angle acts to maintain synchronization; however, the

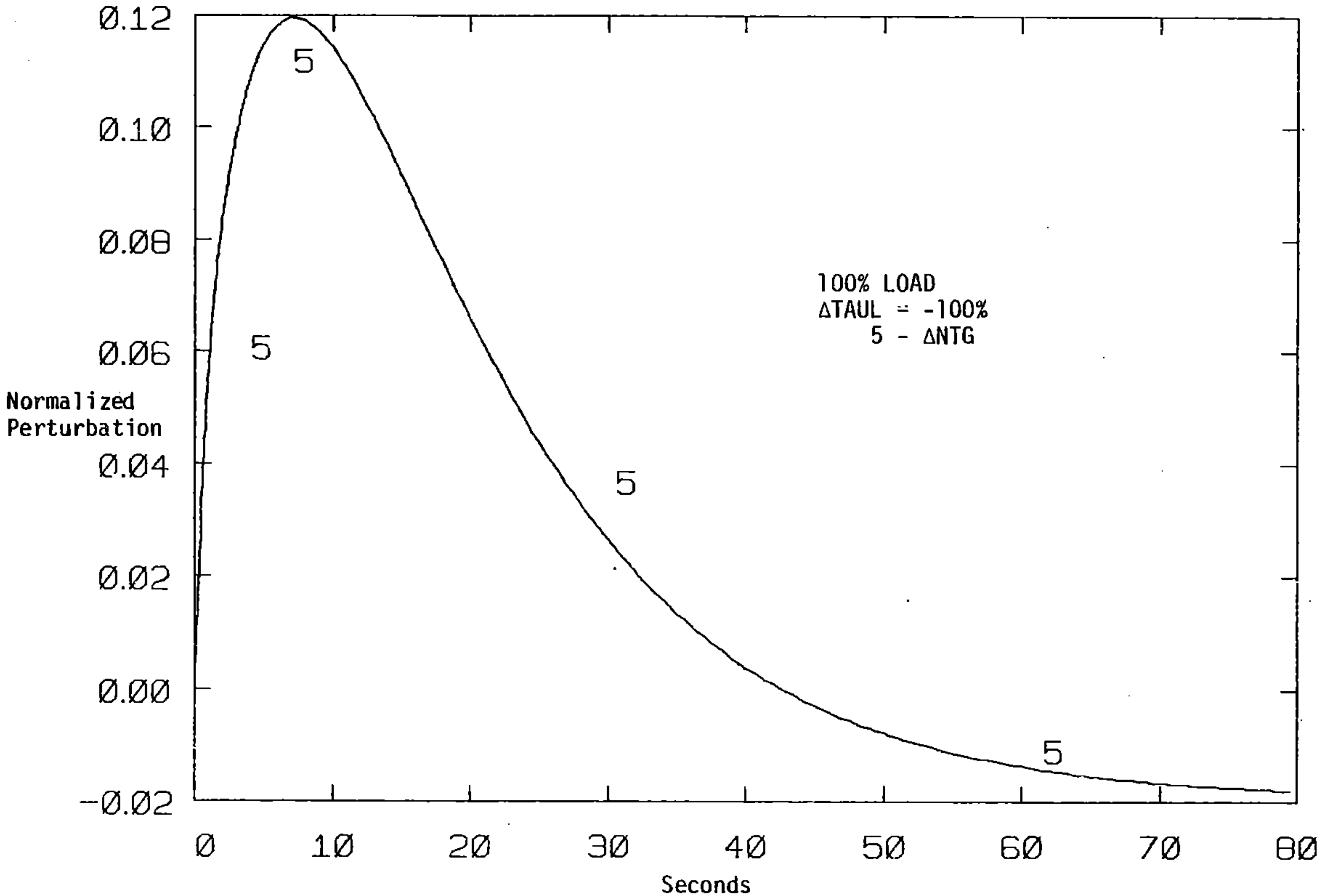

FIGURE 42: TURBINE-GENERATOR LOAD DROP-OVERSPEED CONTROLLER

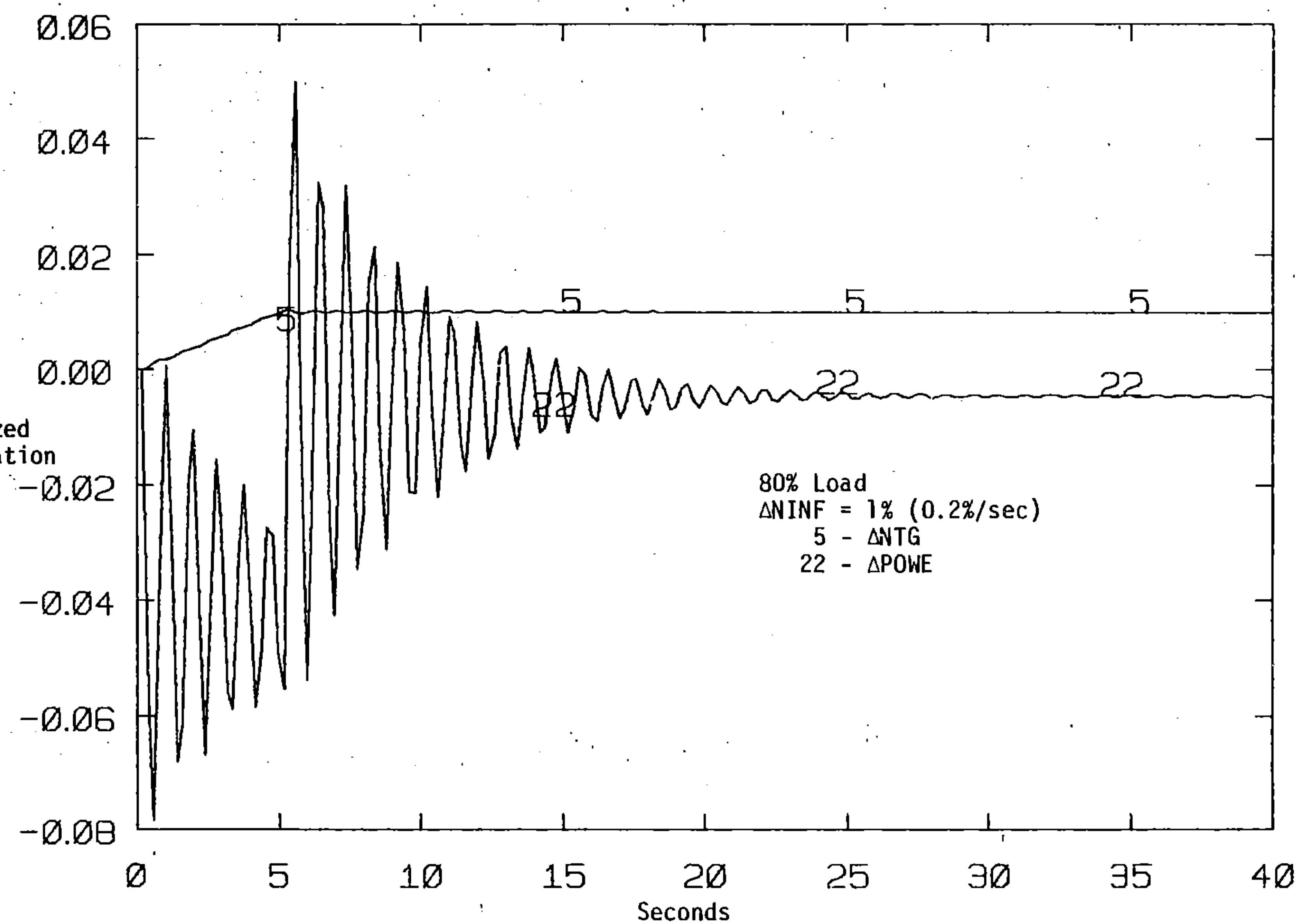

FIGURE 43: AC BUS FREQUENCY DISTURBANCE (Open Loop)

steady state power remains essentially constant. The control strategy for a power plant of this type is to use this change in the AC grid frequency to control the power produced by the turbine generator. This strategy is based on the physical reality that a drop in AC grid frequency signifies that the power supplied to the grid is lagging the power demand; the reverse is true for a rise in the grid frequency. Thus, the control methodology suggests that when the AC bus frequency falls, the OTEC plant power should increase. The inverse is also true. This power control helps to stabilize the power grid. The control is accomplished by the action of the governor droop. The typical conventional power plant is designed for a 5% droop, that is, a 5% change in AC bus frequency will produce a 100% change in the full load power output. The identical requirement is assumed for the OTEC power plant.

$$\delta^* = 0.05 \tag{75}$$

The governor gain, based on a total bypass valve opening of $\Delta K_{bpmax}=2$ is

$$\Delta K_{bp} = 40.0\ \Delta\omega_{tg} \tag{76}$$

The OTEC plant at 80% load is simulated using this governor for a 1% increase in the AC bus frequency in 5 seconds. The results are in Figures 44, 45, and 46. As the turbine-generator speed drops, the bypass valve opens, increasing the total vapor flow and decreasing the turbine vapor flow by the pressure effect, thus

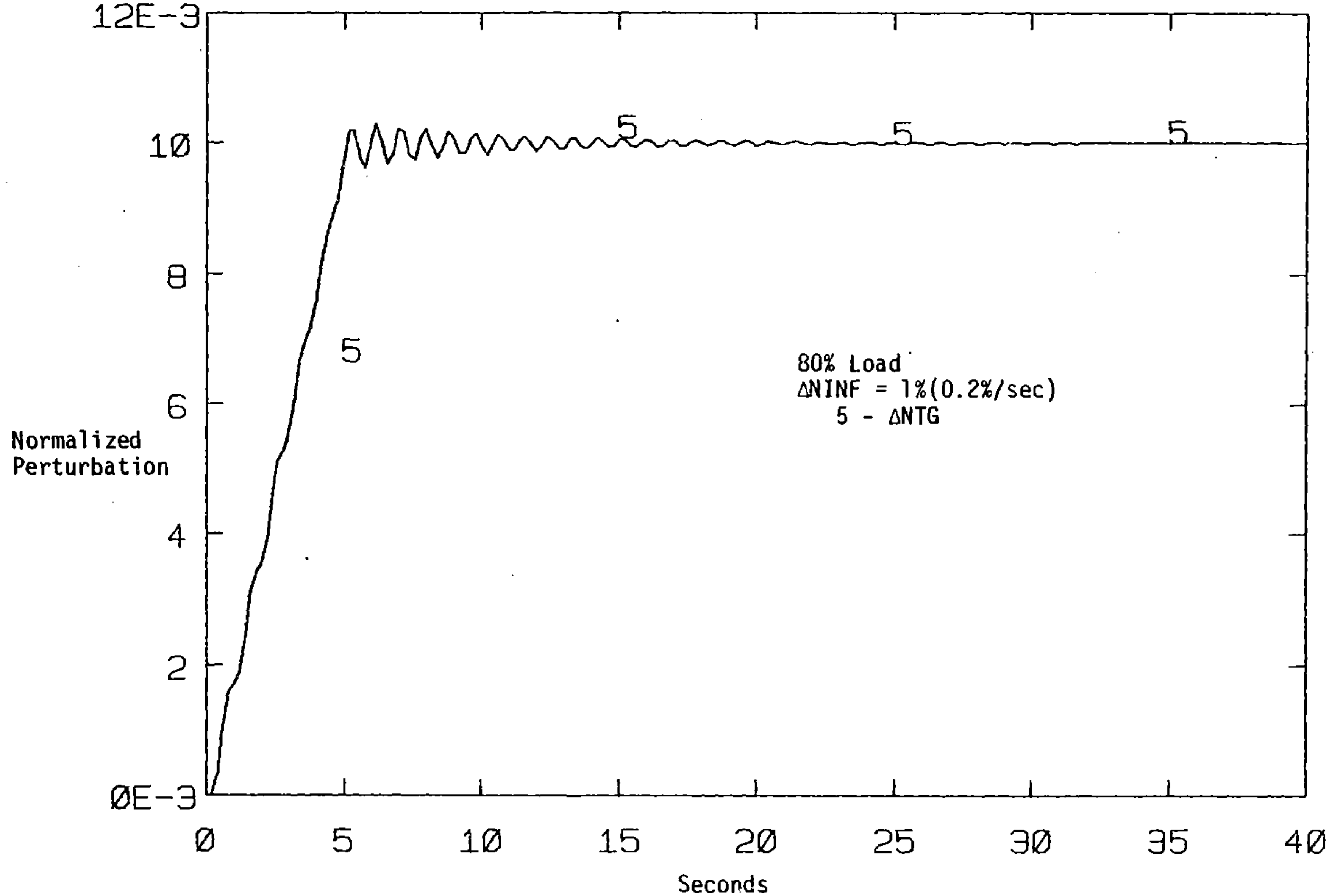

FIGURE 44: AC BUS FREQUENCY DISTURBANCE-INITIAL GOVERNOR CONTROL

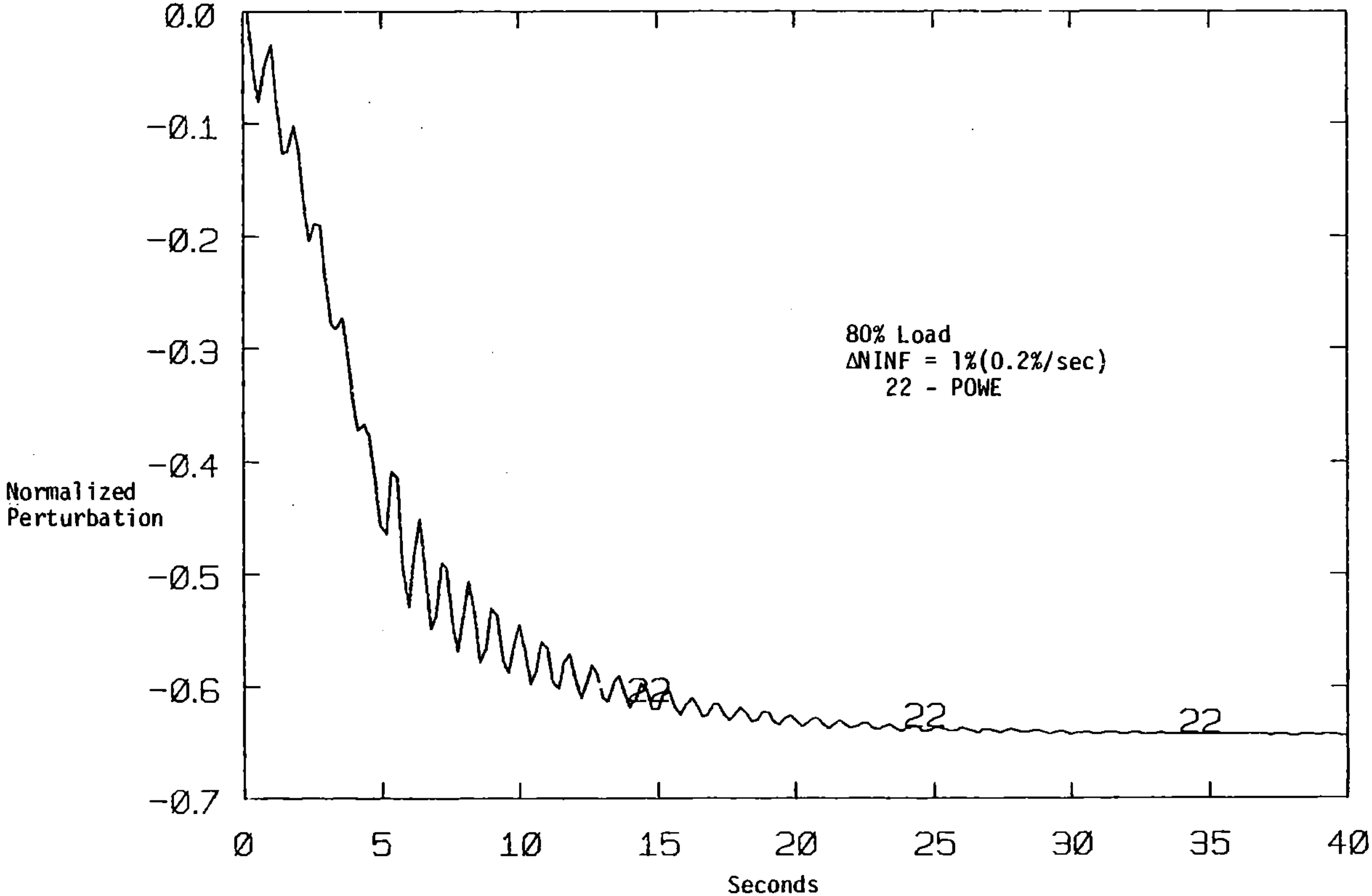

FIGURE 45: AC BUS FREQUENCY DISTURBANCE-INITIAL GOVERNOR CONTROL

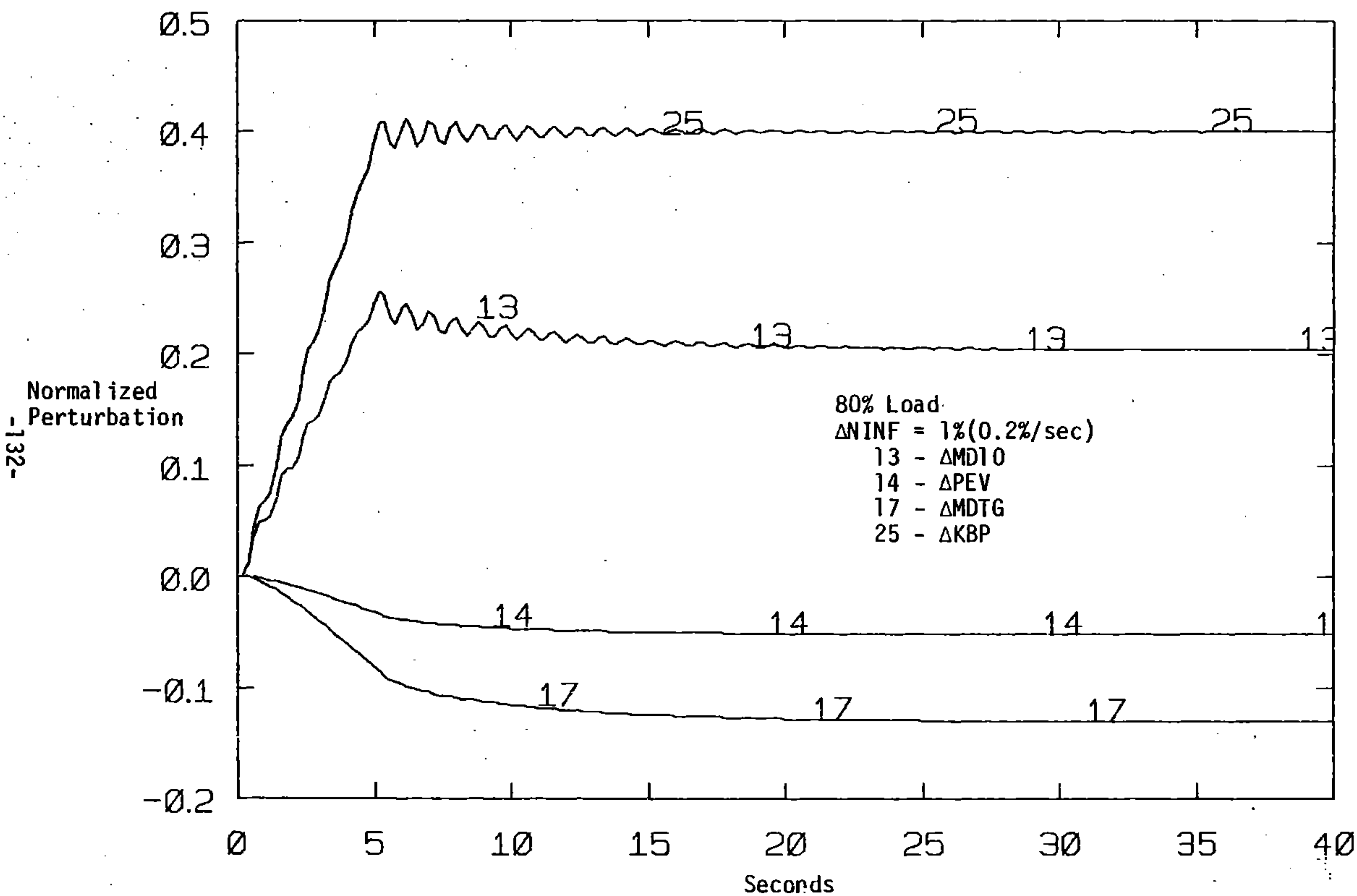

FIGURE 46: AC BUS FREQUENCY DISTURBANCE INITIAL GOVERNOR CONTROL

reducing the power output. The small variations in system variables (other than those as a result of control action) beyond 10 seconds are the result of the heat exchangers responding to a new thermal equilibrium caused by the disturbance to the system. The reduction in generated power is not 20% as desired, but approximately 50% (remembering the steady state power level is 80% load). The reason for this discrepancy is the nonlinear sensitivity of the power output to the bypass valve opening has been ignored; the greater sensitivity at smaller nominal bypass valve openings must be considered. A methodology for designing the governor gain as a function of the nominal bypass valve opening is presented in Appendix VI. The open loop sensitivity, K^*, is plotted as a function of the nominal bypass valve opening in Figure 47. The feedback gains for a 5% droop governor are plotted in Figure 48.

The OTEC plant operating at 80% load using the compensated governor is subjected to the identical AC frequency disturbance. The results are presented in Figures 49, 50, and 51. The reduction in power is now 20% of the maximum as desired. The reduction in governor gain has not noticeably affected the stability of the synchronous system. The OTEC plant operating at 100% load and at 40% load, subjected to the same AC bus disturbance, is simulated and the results are given in Figures 52, 53, 54, and Figures 55, 56, and 57 respectively. The reduction in power output in both instances is 20% of the maximum. However, the OTEC plant at 40% load is

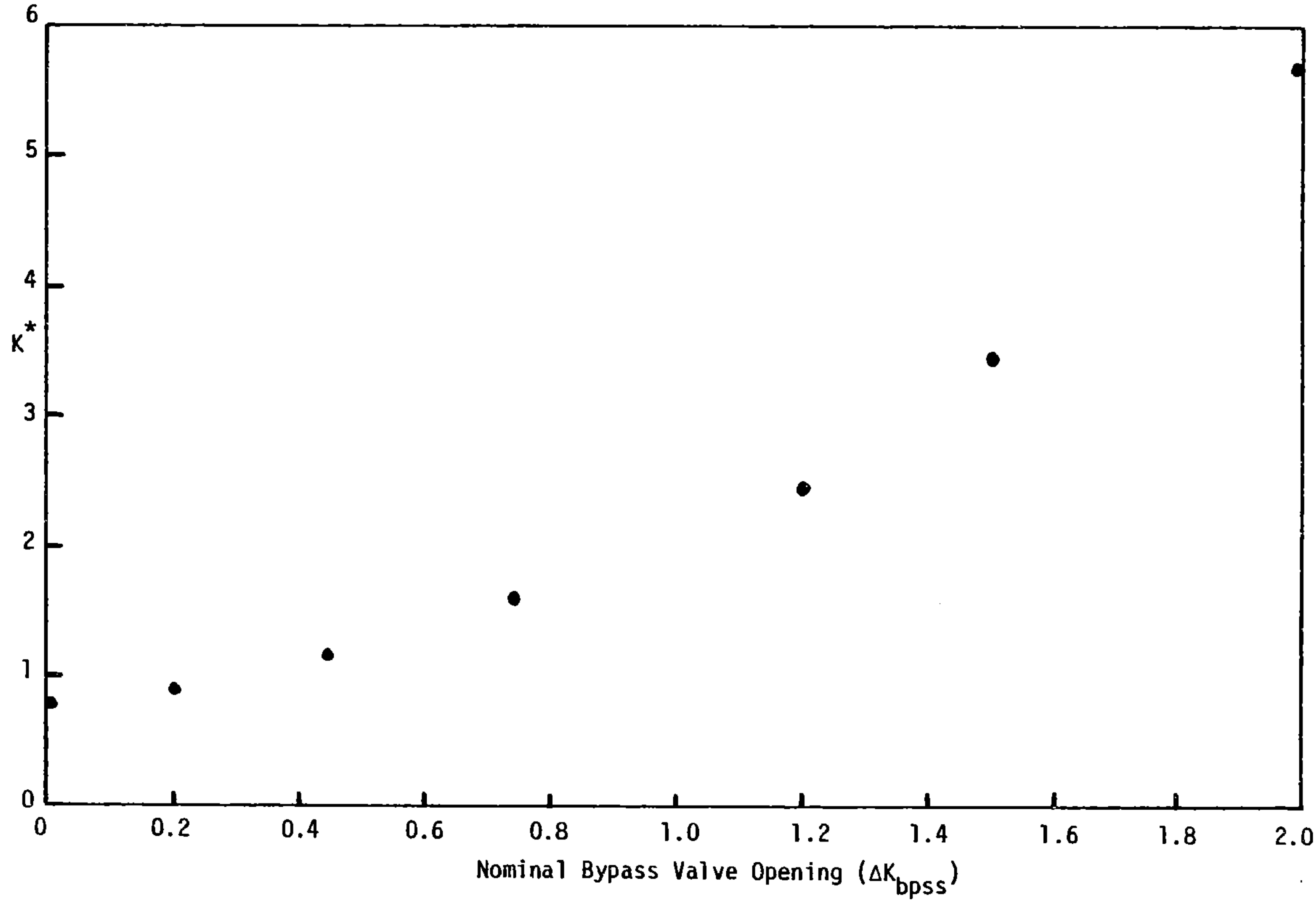

FIGURE 47: OPEN LOOP GOVERNOR SENSITIVITY (power criterion)

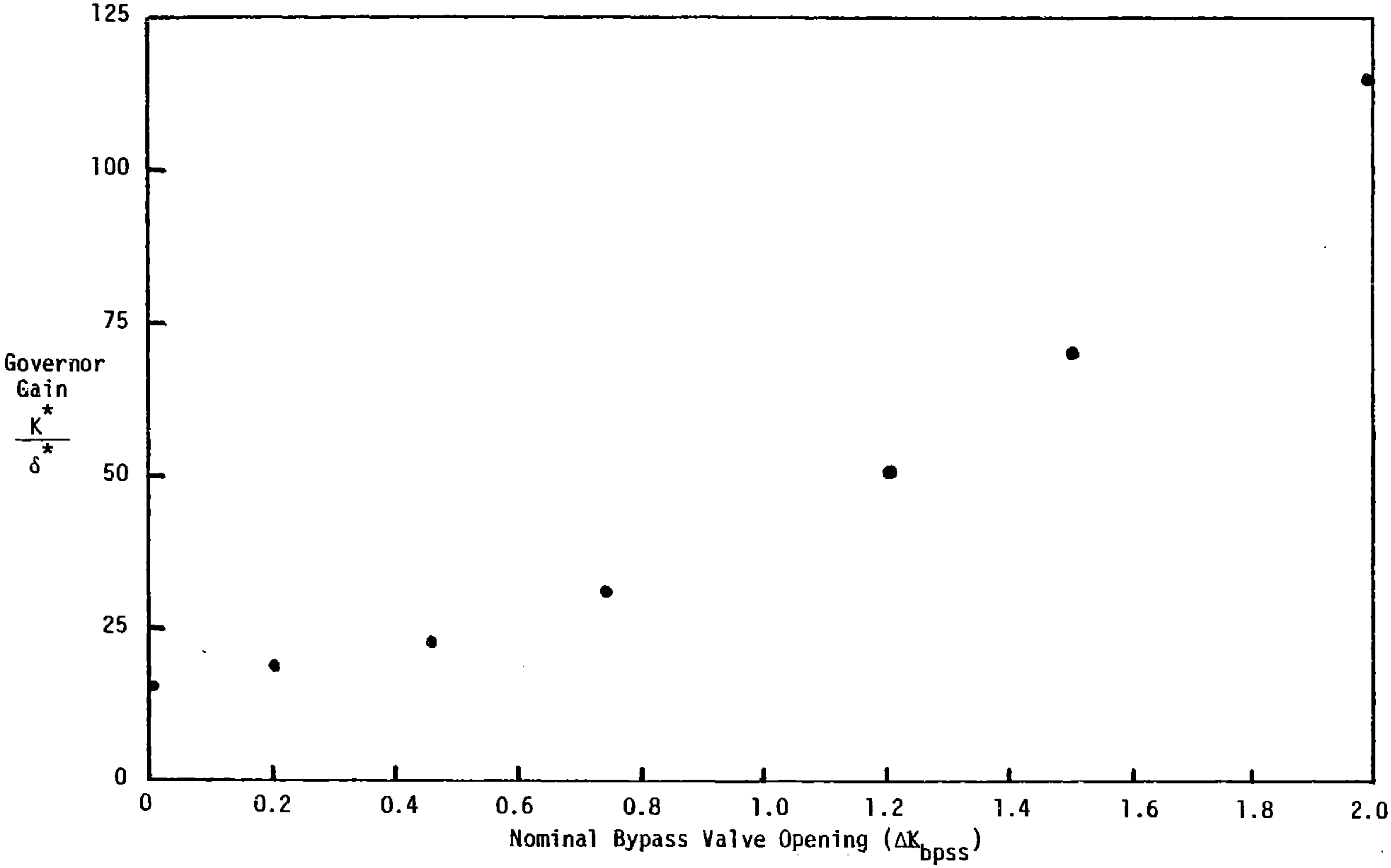

FIGURE 48: GOVERNOR GAIN FOR 5% DROOP (AC BUS)

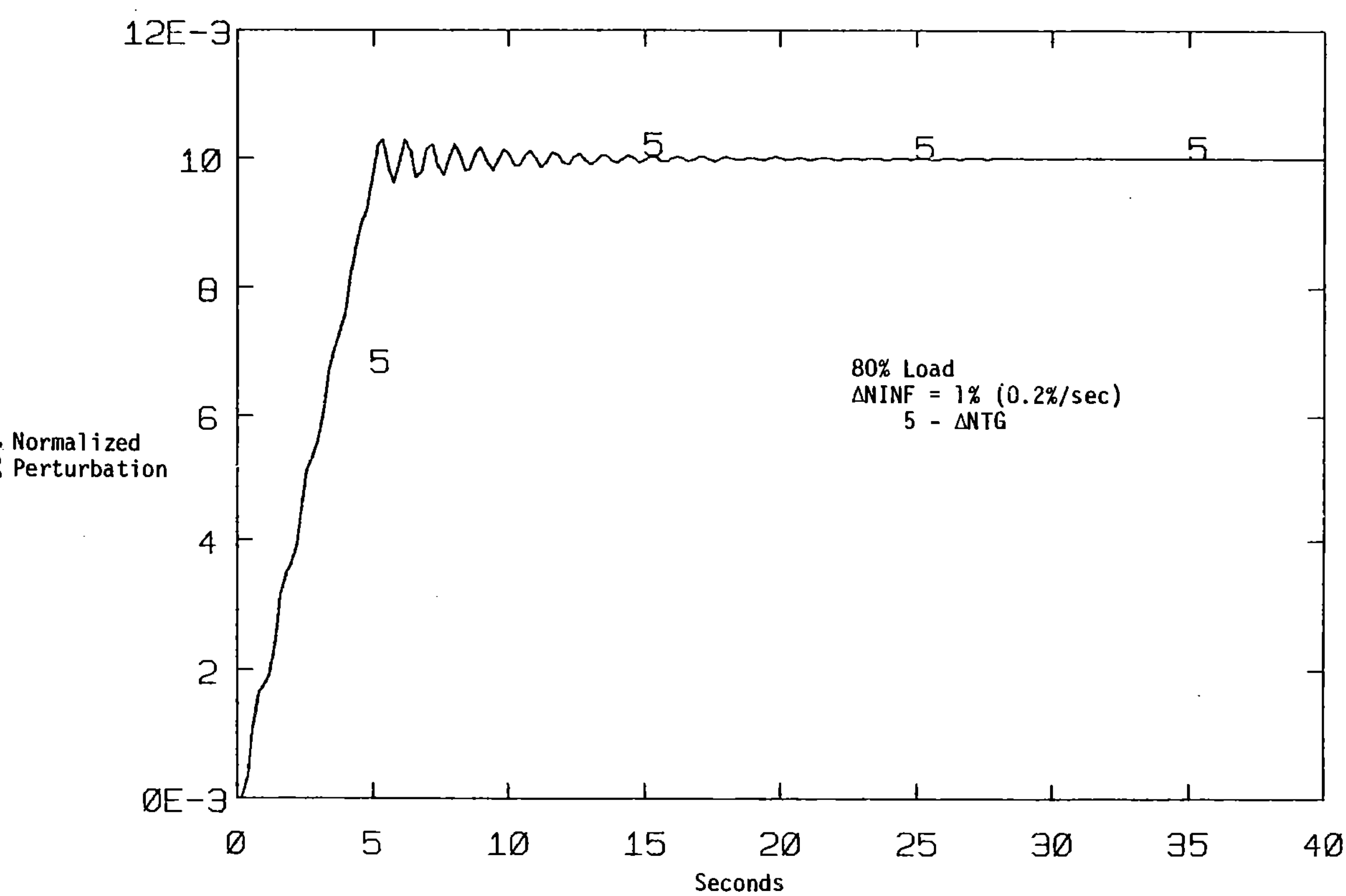

FIGURE 49: AC BUS FREQUENCY DISTURBANCE-COMPENSATED GOVERNOR CONTROL

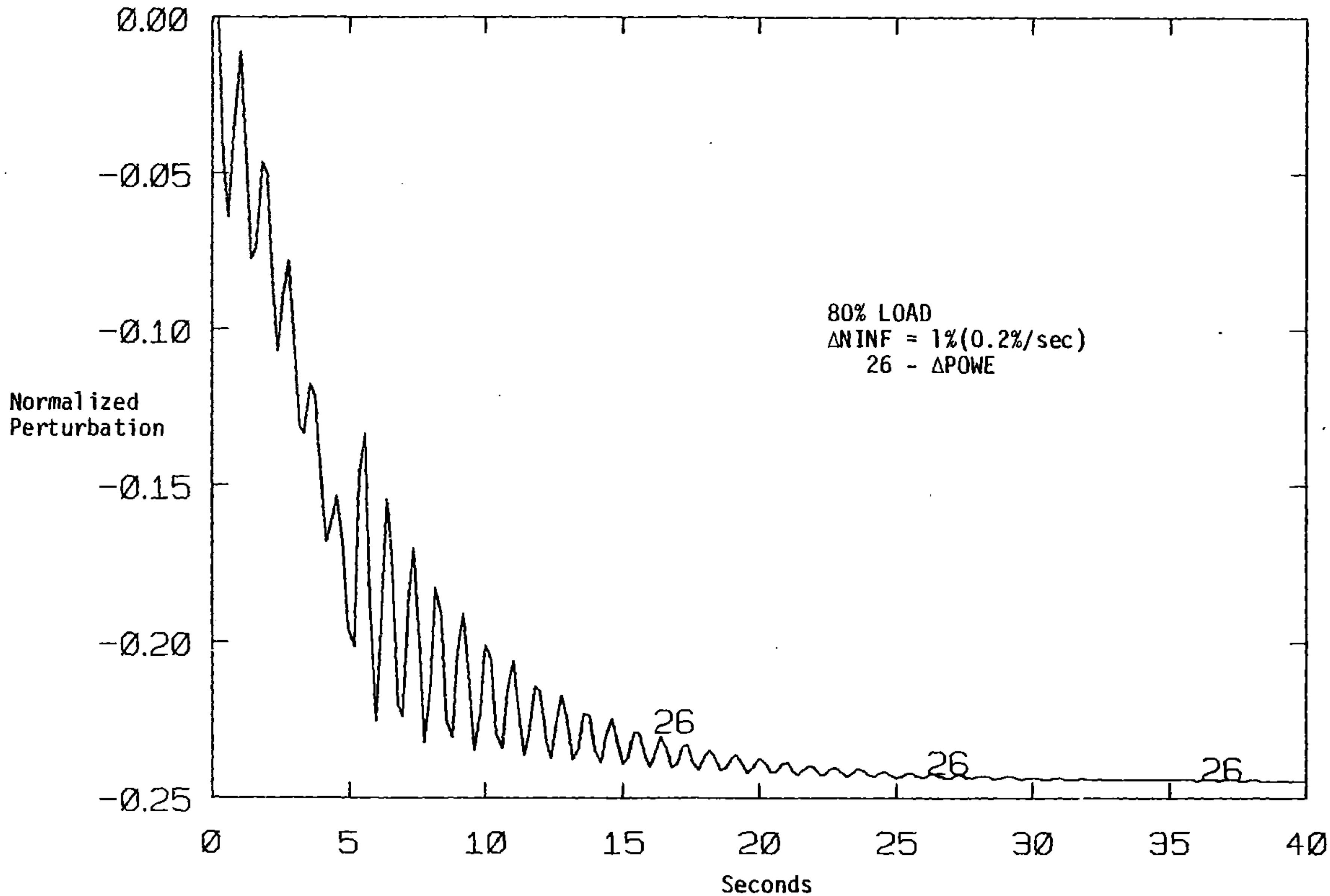

FIGURE 50: AC BUS FREQUENCY DISTURBANCE-COMPENSATED GOVERNOR CONTROL

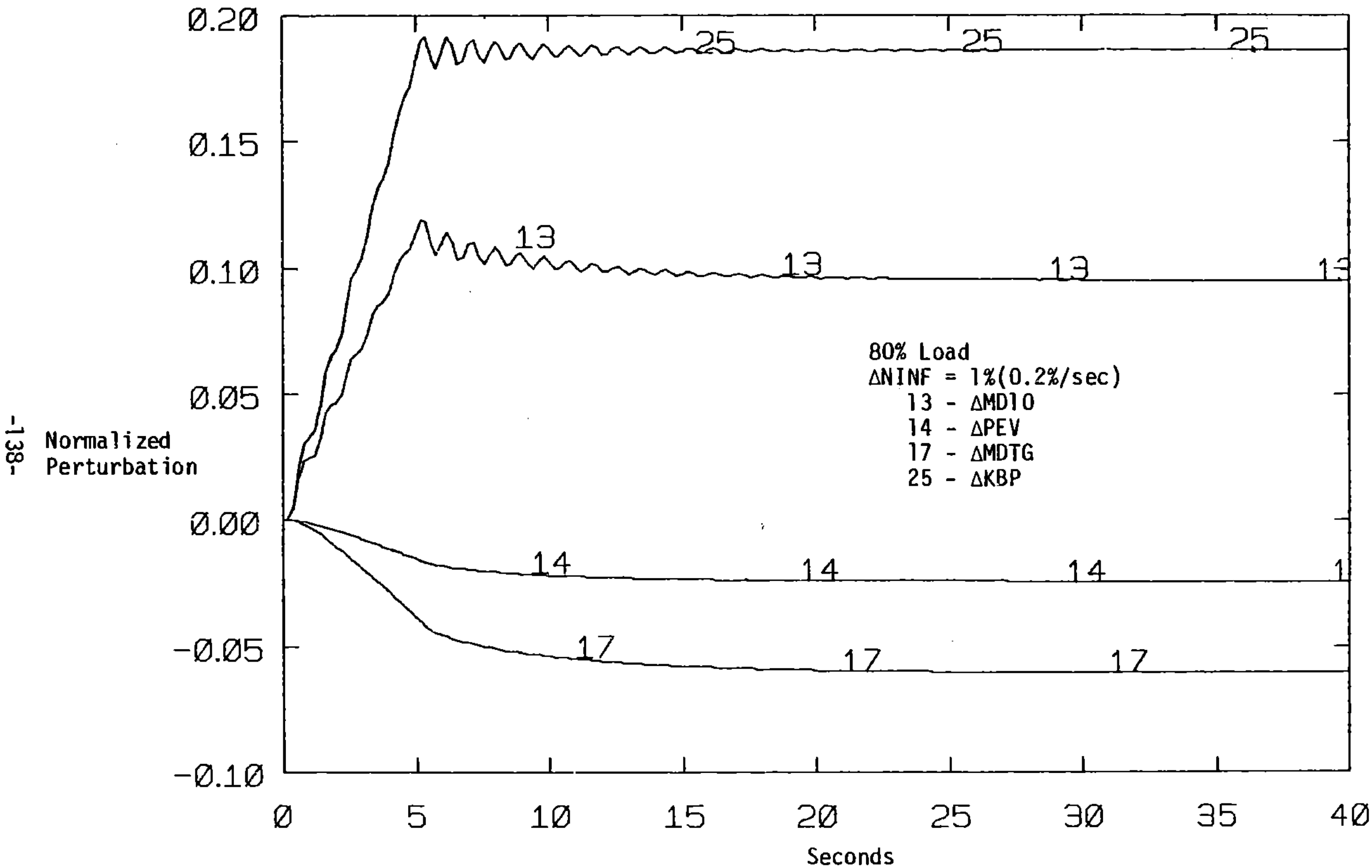

FIGURE 51: AC BUS FREQUENCY DISTURBANCE-COMPENSATED GOVERNOR CONTROL

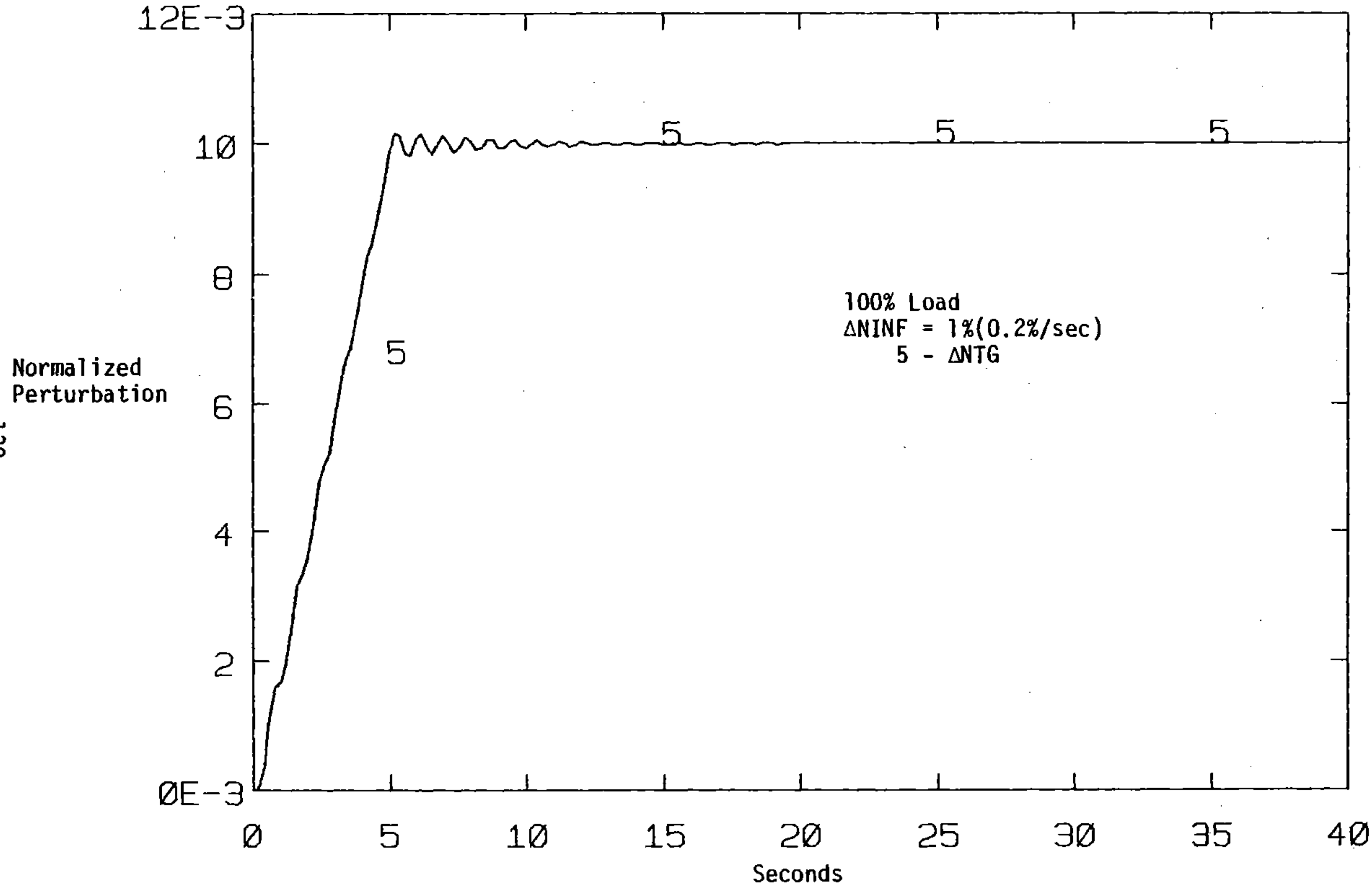

FIGURE 52: AC BUS FREQUENCY DISTURBANCE-COMPENSATED GOVERNOR CONTROL

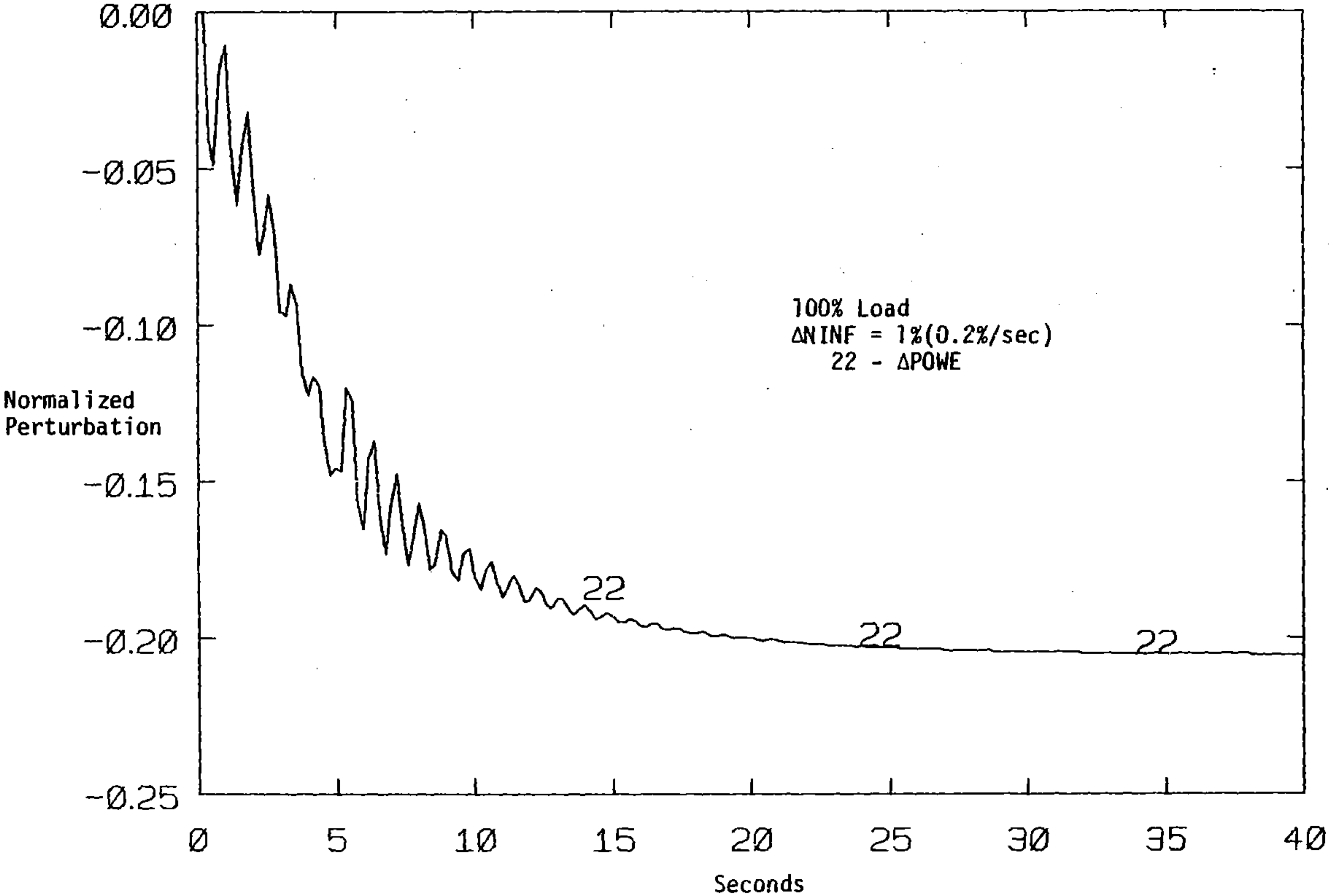

FIGURE 53: AC BUS FREQUENCY DISTURBANCE-COMPENSATED GOVERNOR CONTROL

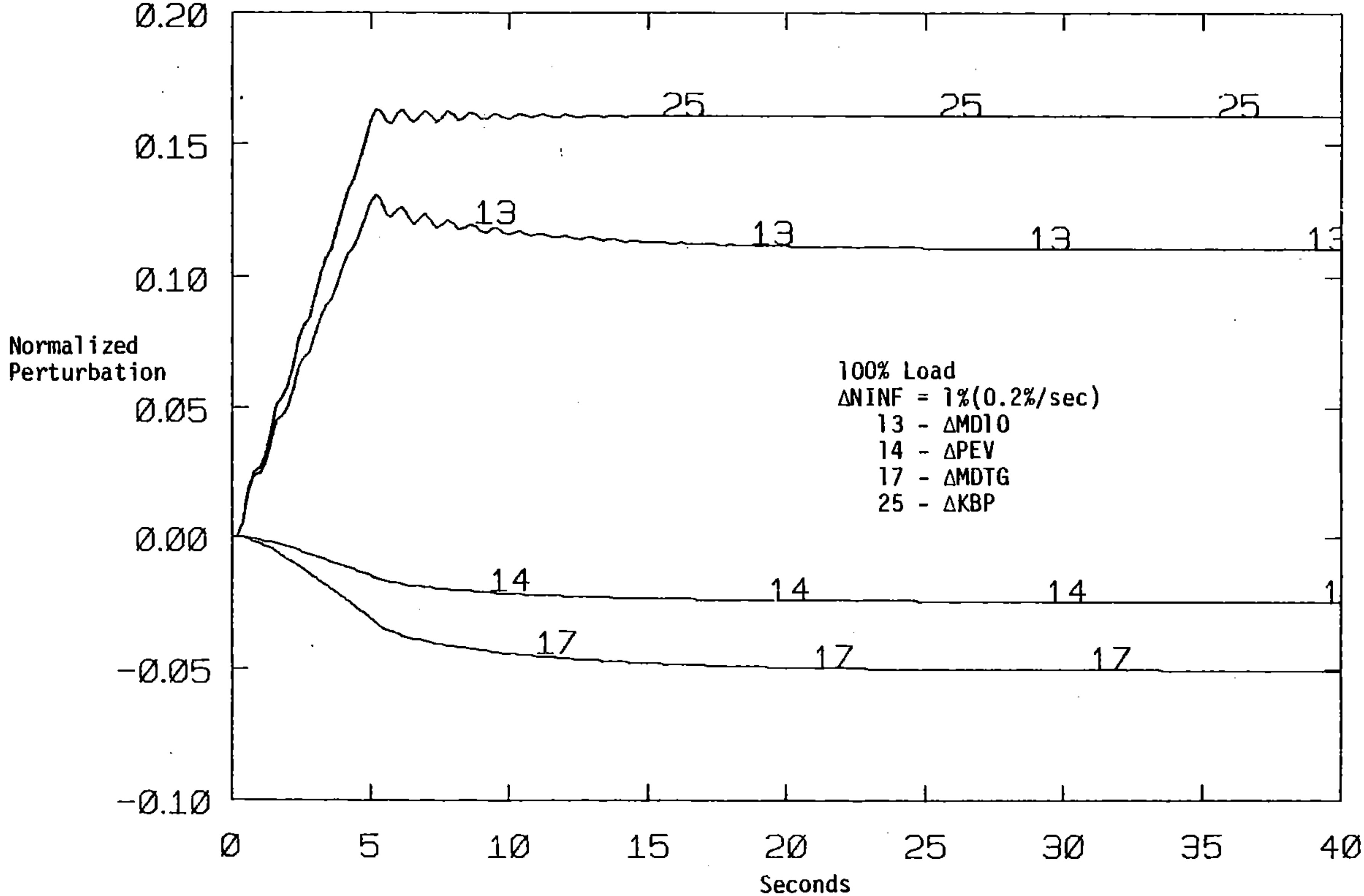

FIGURE 54: AC BUS FREQUENCY DISTURBANCE-COMPENSATED GOVERNOR CONTROL

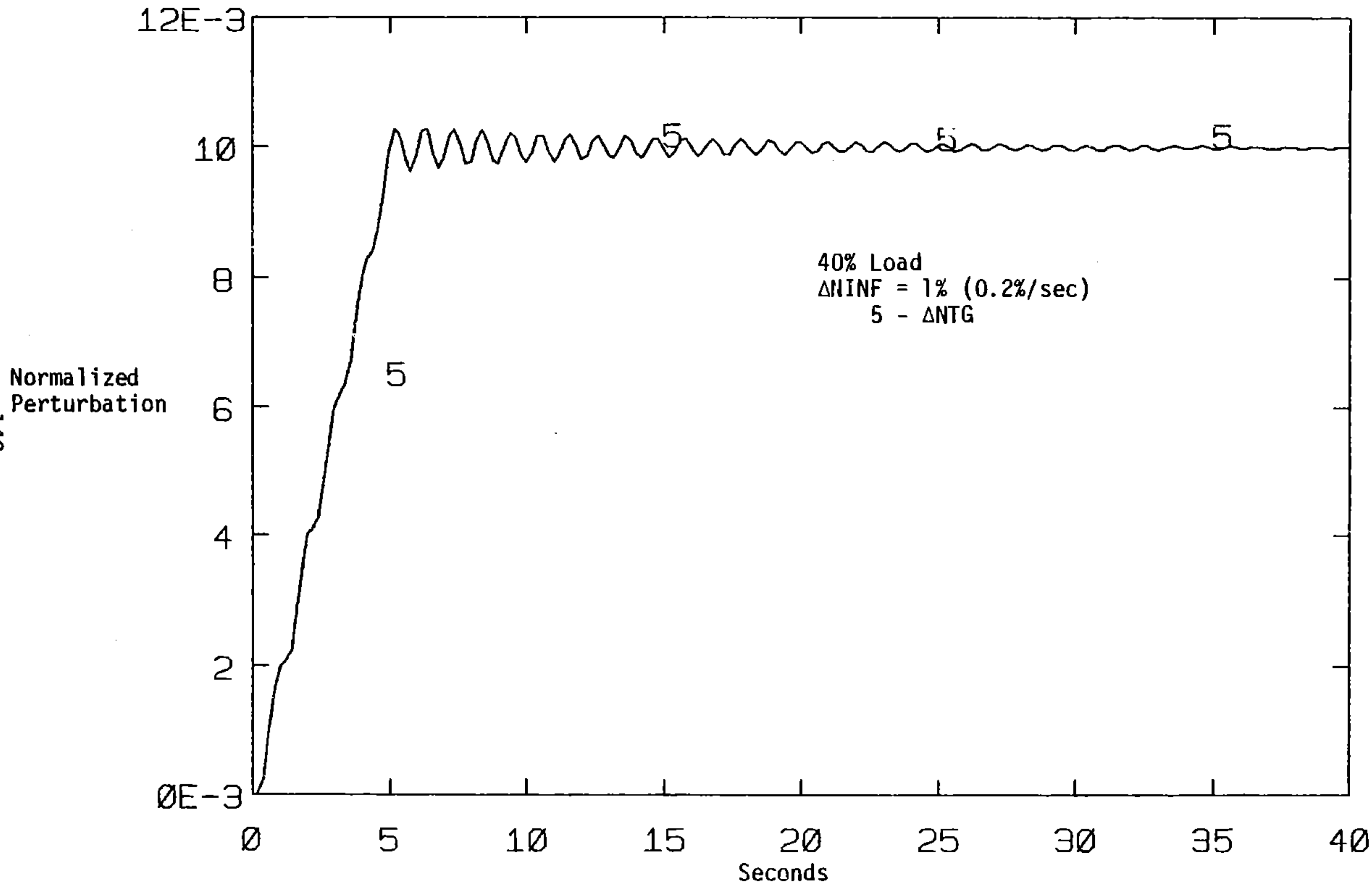

FIGURE 55: AC BUS FREQUENCY DISTURBANCE-COMPENSATED GOVERNOR CONTROL

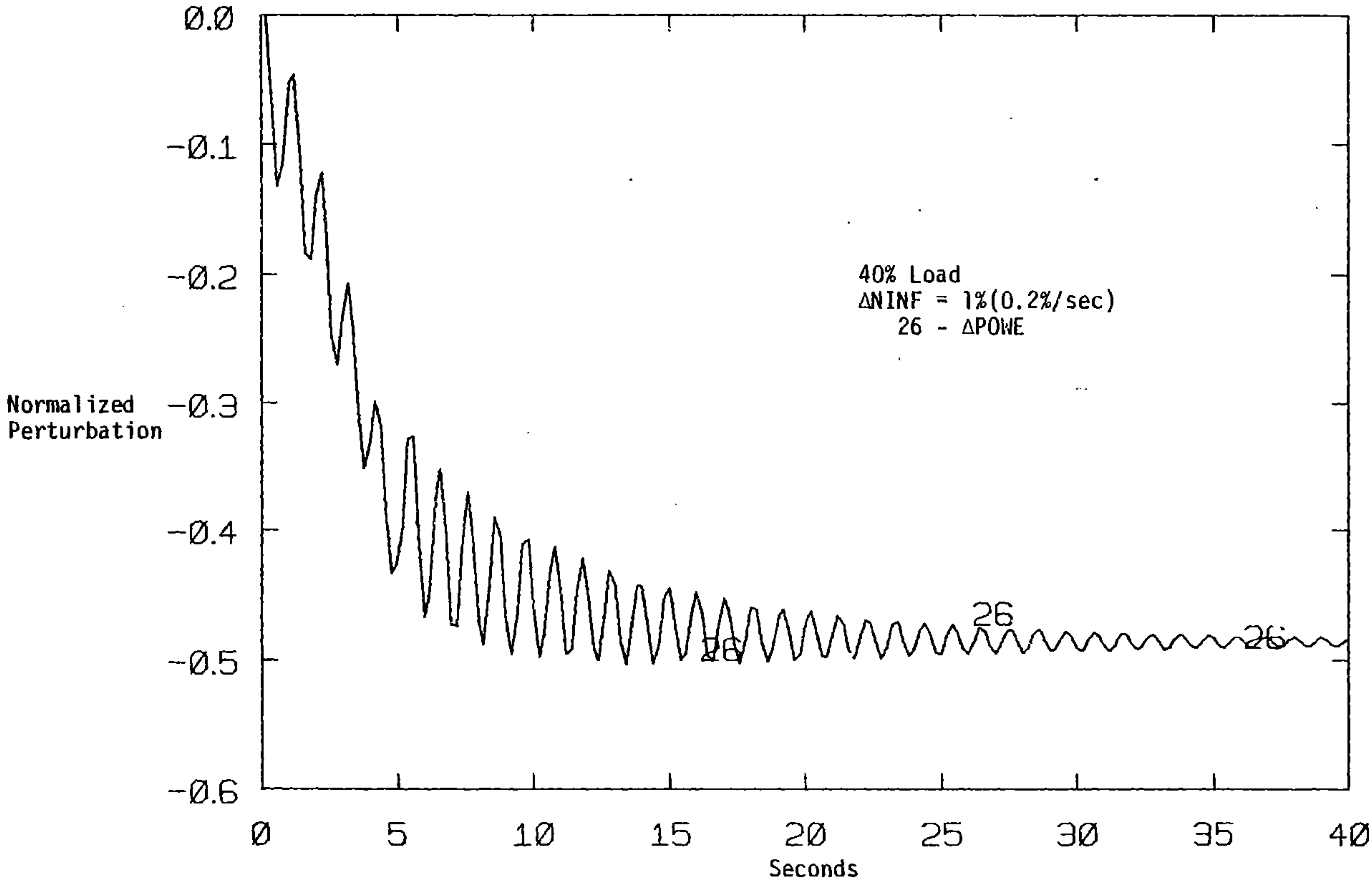

FIGURE 56: AC BUS FREQUENCY DISTURBANCE-COMPENSATED GOVERNOR CONTROL

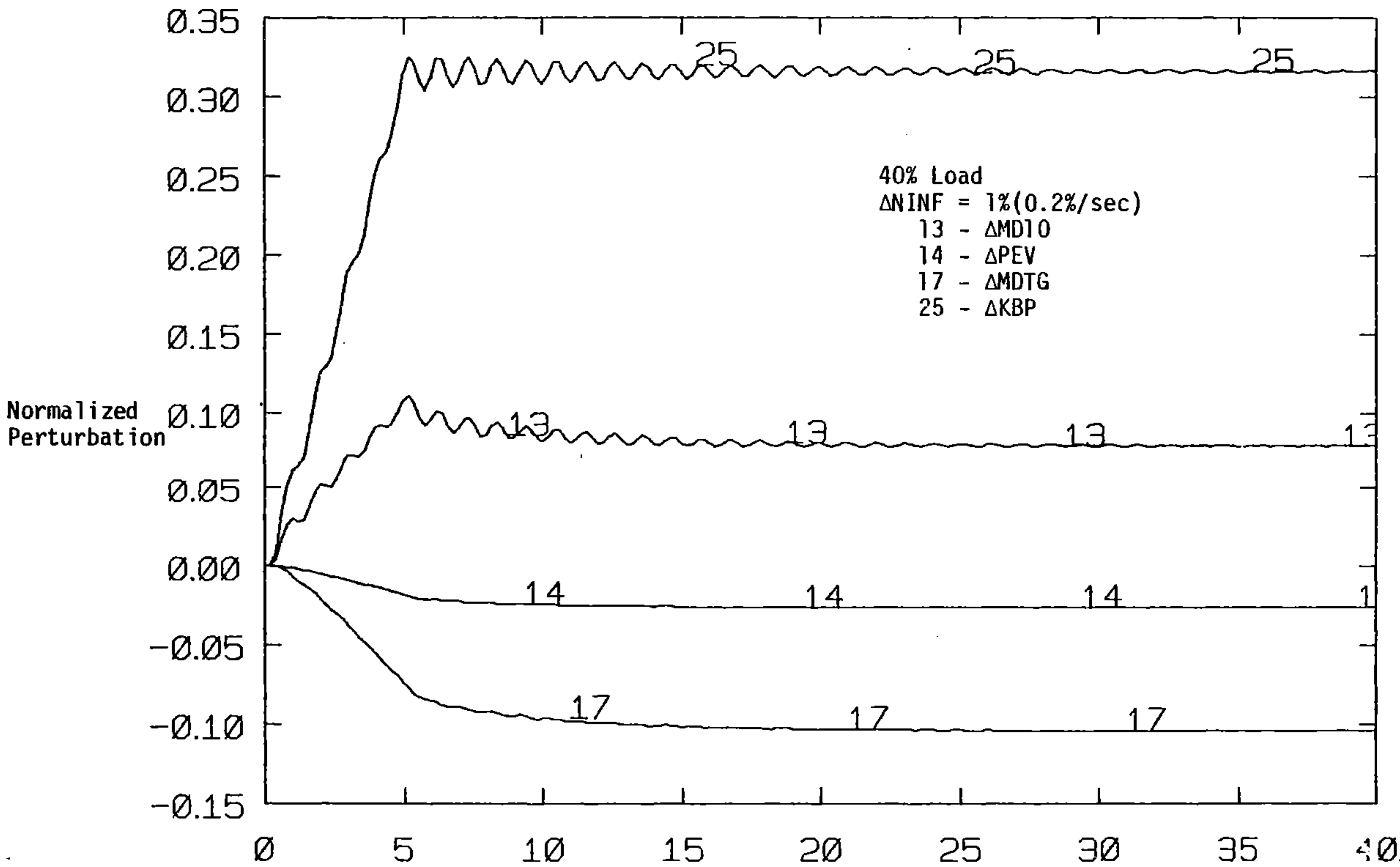

FIGURE 57: AC BUS FREQUENCY DISTURBANCE-COMPENSATED GOVERNOR CONTROL

decidedly less stable, still experiencing power angle swings at 40 seconds following the initial disturbance. In each of these cases, the remainder of the system is very well behaved.

5.3 OTEC Plant Control - DC Power Transmission

The principle aim of a controller when the OTEC plant is connected to a DC transmission system is to maintain the turbine-generator speed in response to load and environmental disturbances. Figure 58 shows the response of the uncontrolled OTEC plant at 80% load when the DC load demand is step increased by 5%. The turbine-generator speed begins to drop to an unacceptable level.

Three methods of control are investigated:

1) A basic turbine-generator speed feedback governor
2) A state variable feedback control system based on the linear-quadratic (L-Q) control design methodology
3) Turbine-generator speed control by DC power load regulation

The third method of control becomes necessary when the OTEC plant is operating at or near 100% load and the bypass valve becomes an ineffective control mechanism because of valve saturation.

The requirements for a turbine-generator speed controller are that it provide a fast, stable response to a disturbance with as little steady state error as possible. The limits to satisfying these requirements are established by the characteristics of both

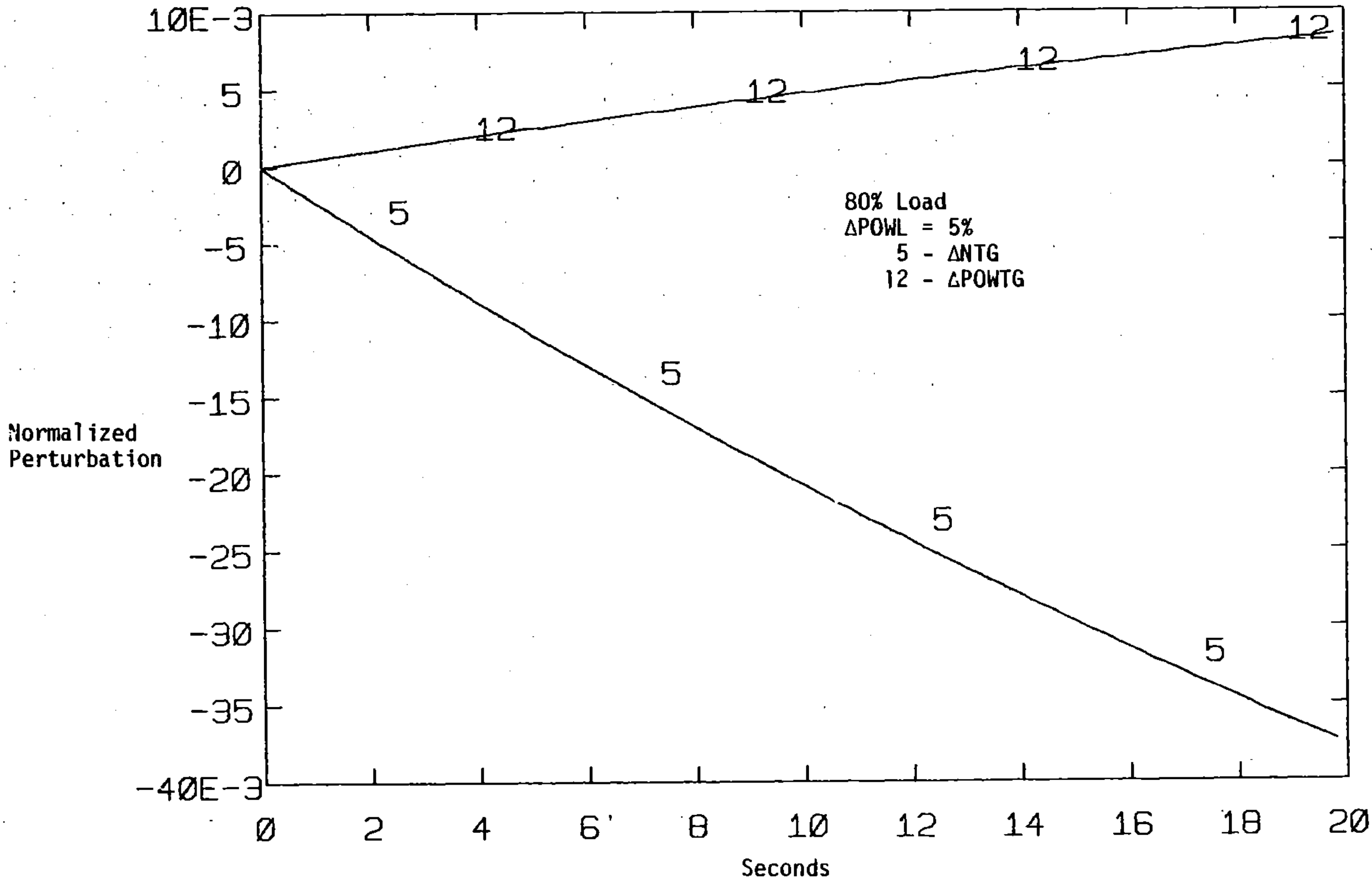

FIGURE 58: DC LOAD DEMAND DISTURBANCE (Open Loop)

the system and the control mechanism. Tradeoffs in performance are usually necessary in achieving a satisfactory response.

5.3.1 Basic Speed Governor Control

The speed governor is of the same design as that for the previous analysis, that is,

$$\text{governor gain} = \frac{K^*}{\delta^*} \tag{77}$$

However, for DC transmission, the turbine-generator speed is the controlled variable. Therefore, the governor design is based upon the turbine-generator speed sensitivity to the bypass valve. This design methodology is presented in Appendix VI. The open loop sensitivity, K^*, based on this criteria, is plotted versus the nominal bypass valve opening in Figure 59.

The design of a governor droop for a turbine-generator speed controller requires a direct trade-off between steady state error and transient stability. As the governor droop decreases, the steady state error is reduced at the expense of a more oscillatory response. Three different governor droop gains were experimented with: 1%, 3%, and 5%. The OTEC plant response to a 5% DC load step demand increase is simulated for each of the governor droops. The plant is operating at 80% load. The results for a 1% governor droop are shown in Figures 60, 61 and 62, 3% in Figures 63, 64, and 65, and 5% governor droop in Figures 66, 67 and

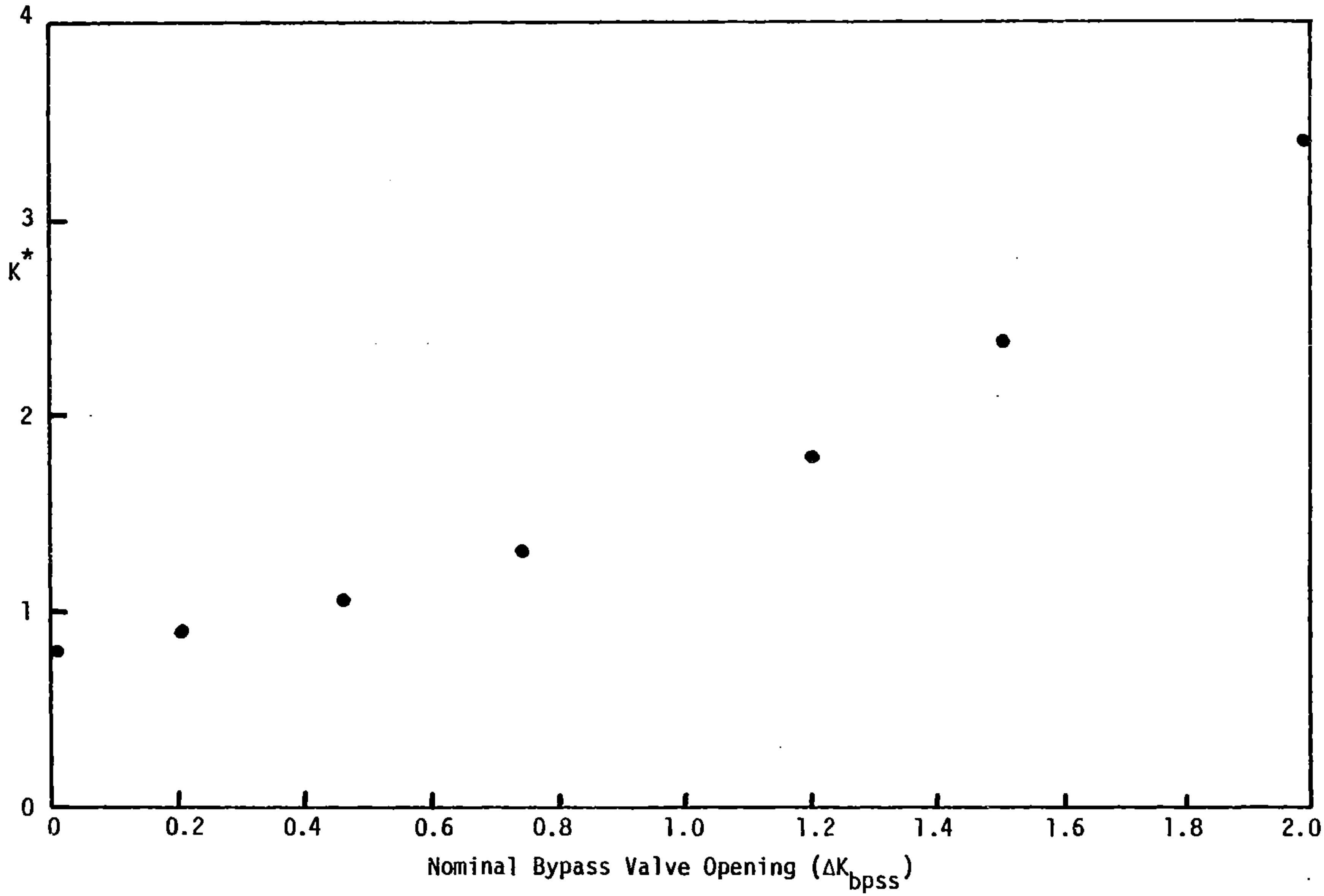

FIGURE 59: OPEN LOOP GOVERNOR SENSITIVITY (turbine speed criterion)

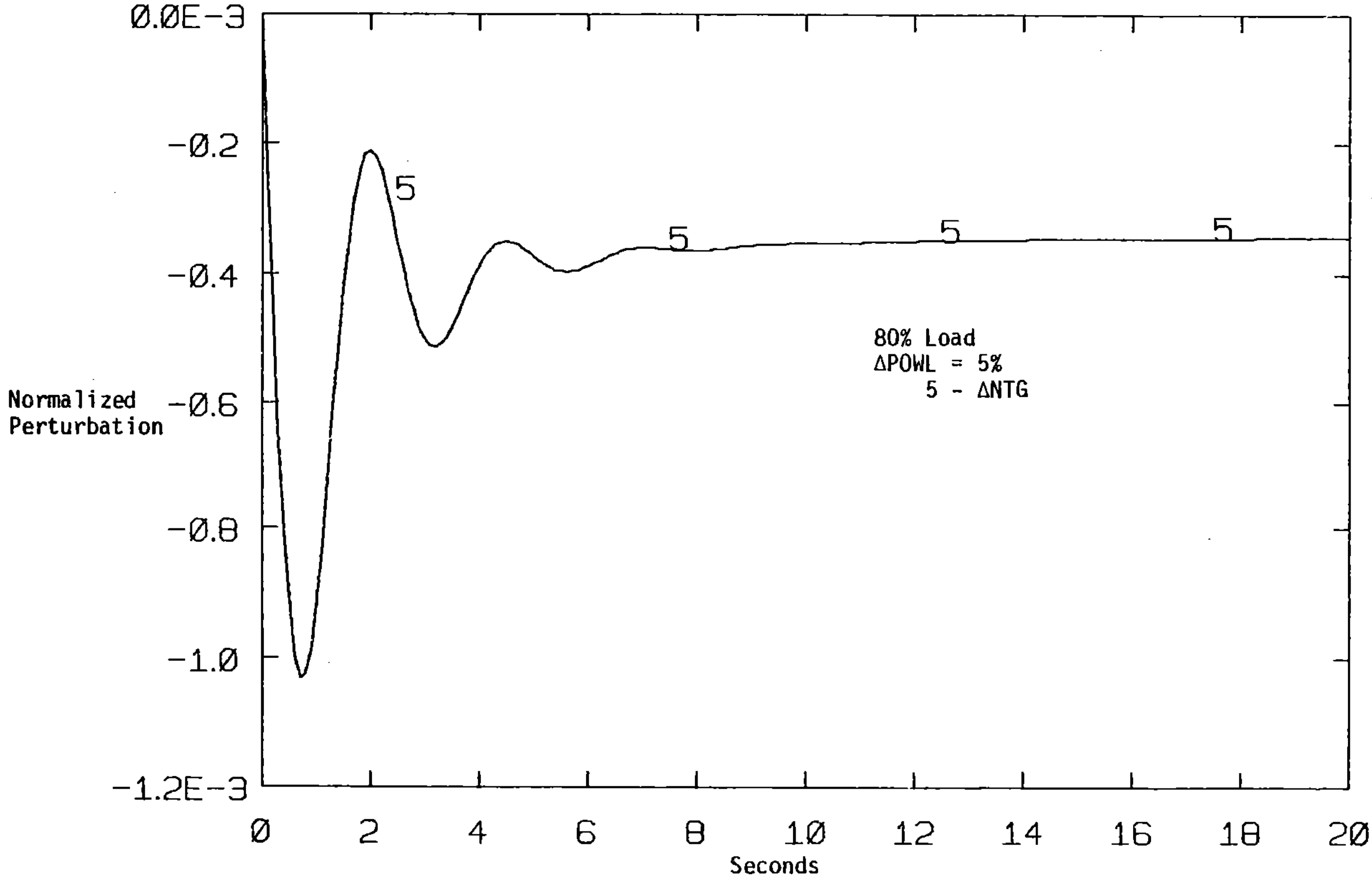

FIGURE 60: DC LOAD DEMAND DISTURBANCE-1% DROOP GOVERNOR

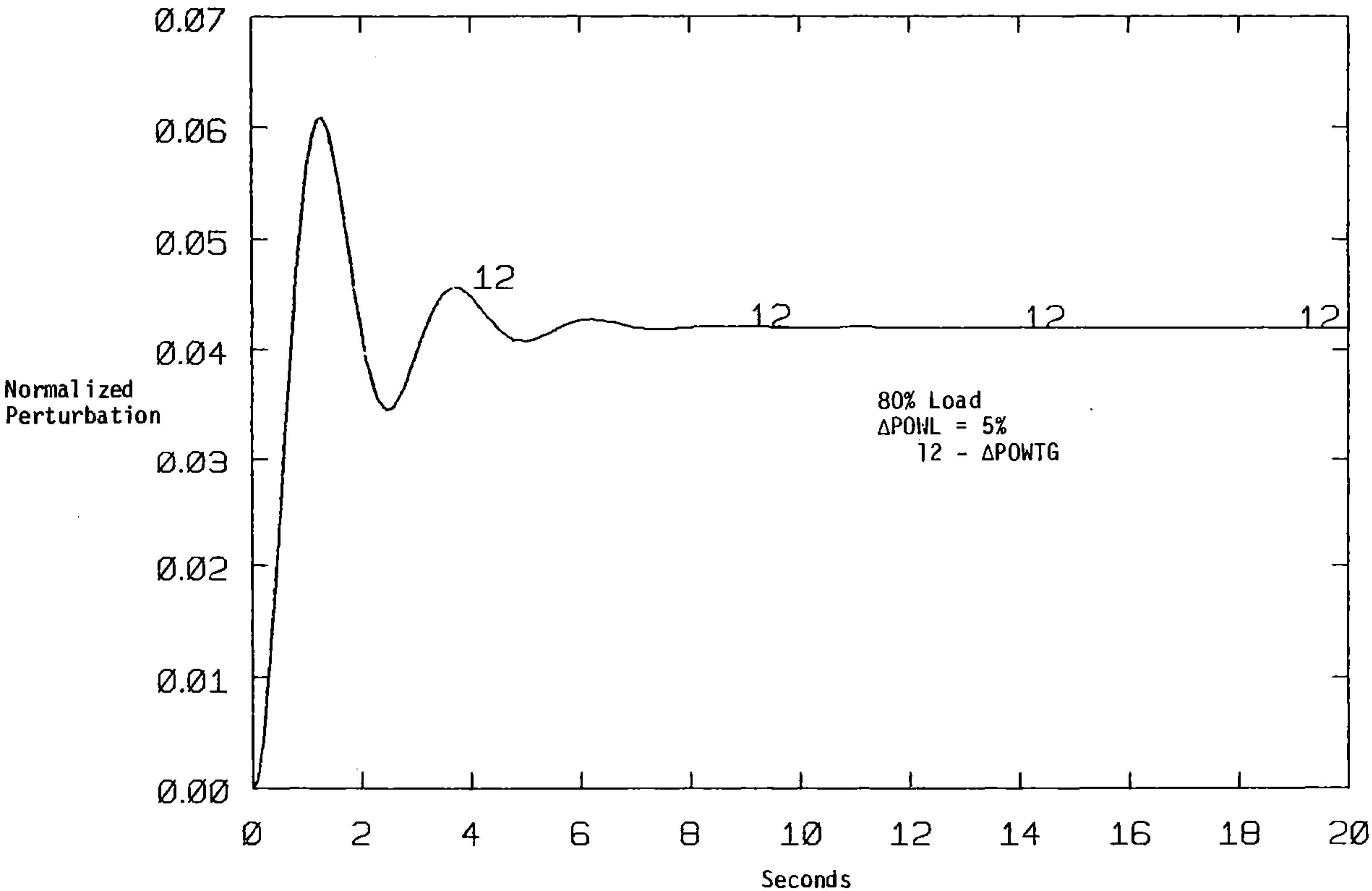

FIGURE 61: DC LOAD DEMAND DISTURBANCE-1% DROOP GOVERNOR

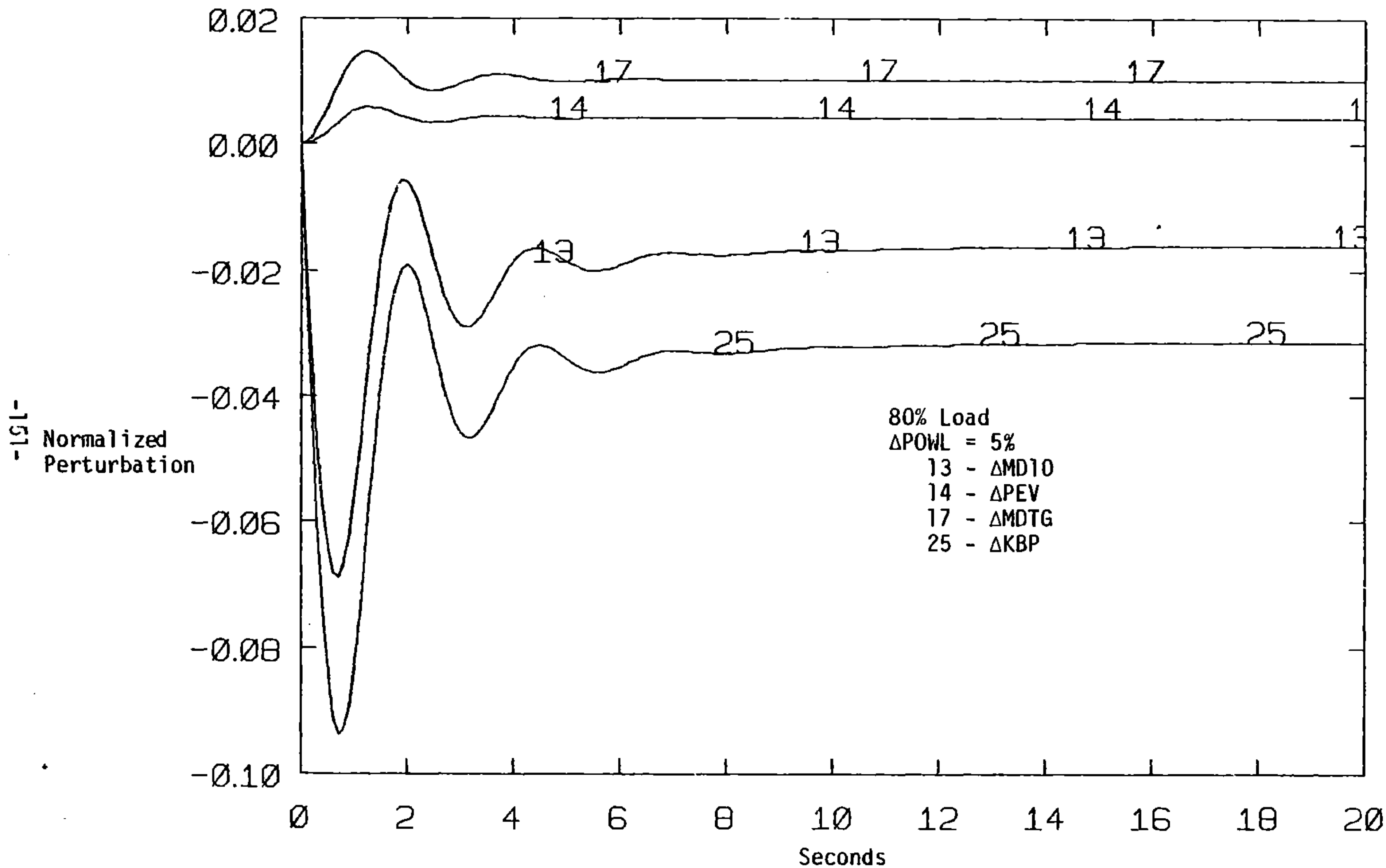

FIGURE 62: DC LOAD DEMAND DISTURBANCE-1% DROOP GOVERNOR

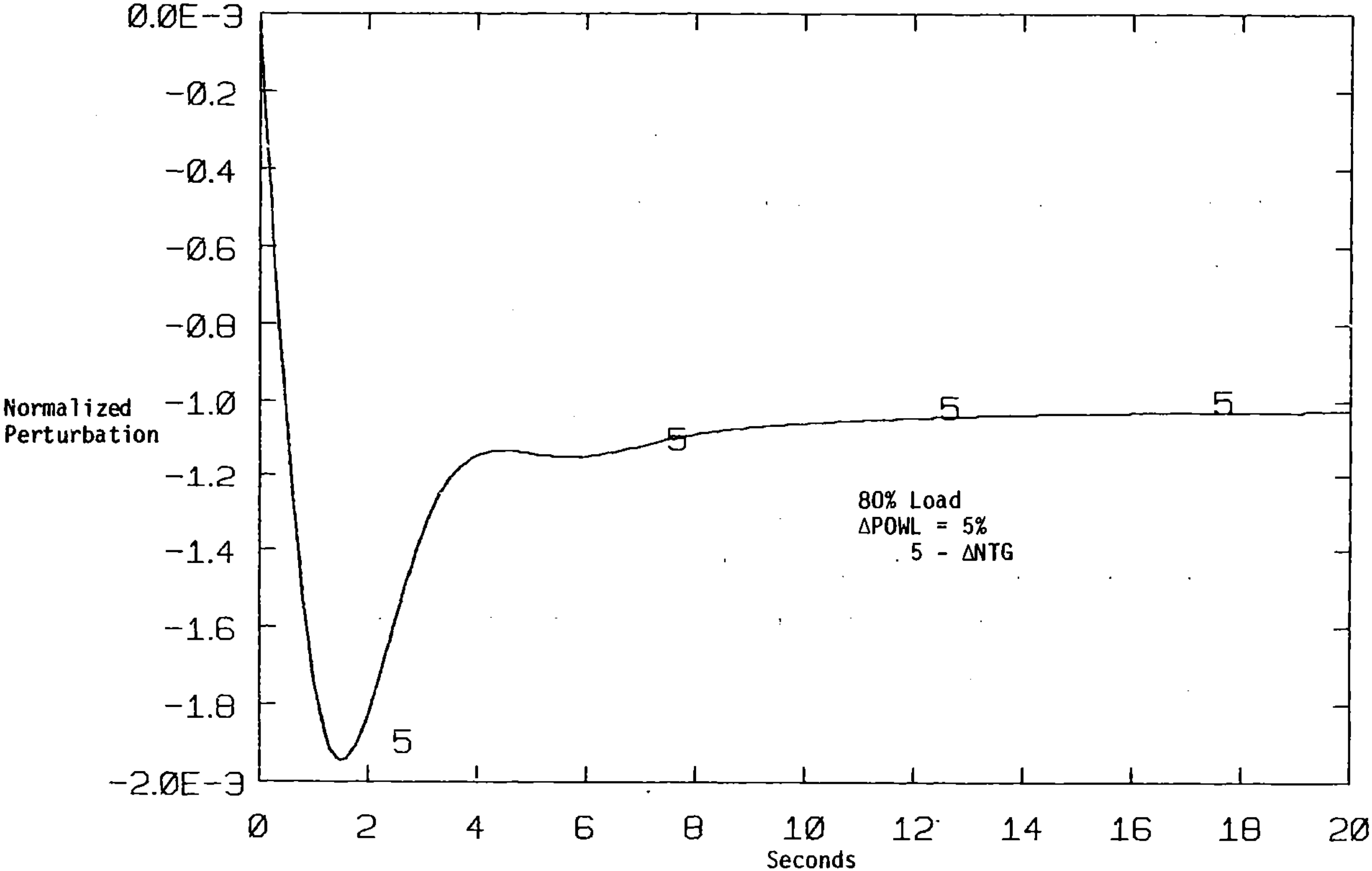

FIGURE 63: DC LOAD DEMAND DISTURBANCE-3% DROOP GOVERNOR

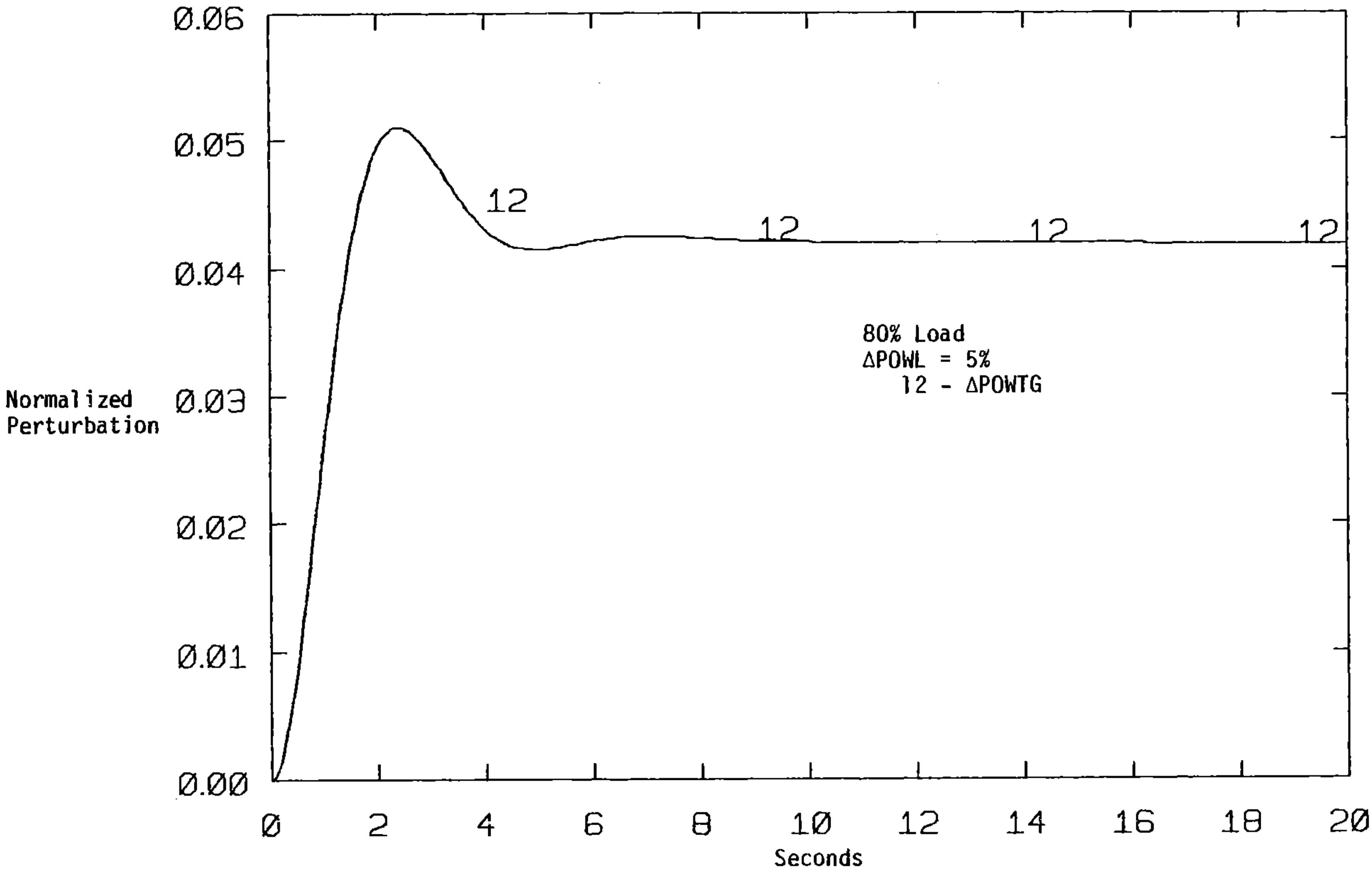

FIGURE 64: DC LOAD DEMAND DISTURBANCE-3% DROOP GOVERNOR

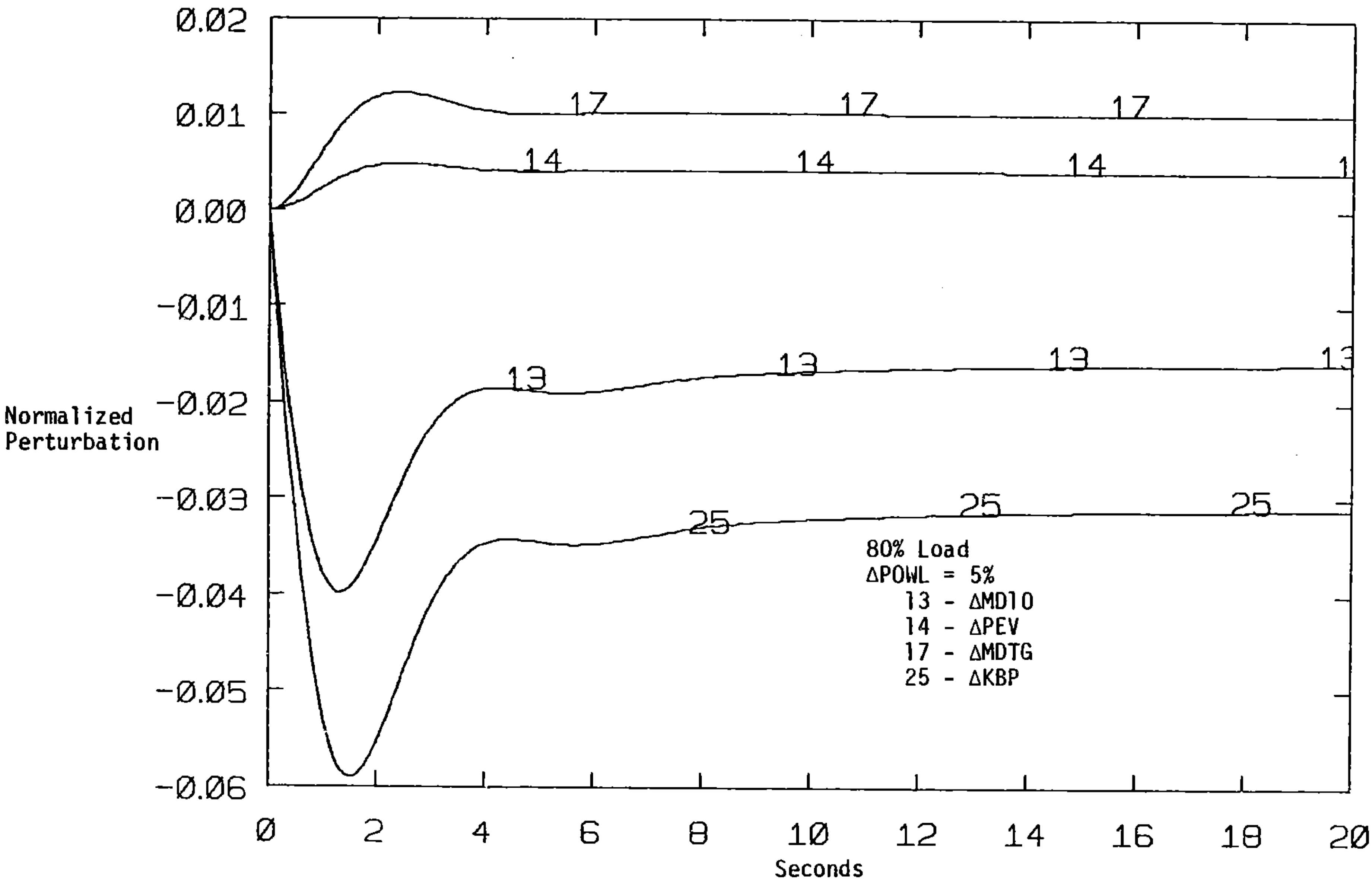

FIGURE 65: DC LOAD DEMAND DISTURBANCE-3% DROOP GOVERNOR

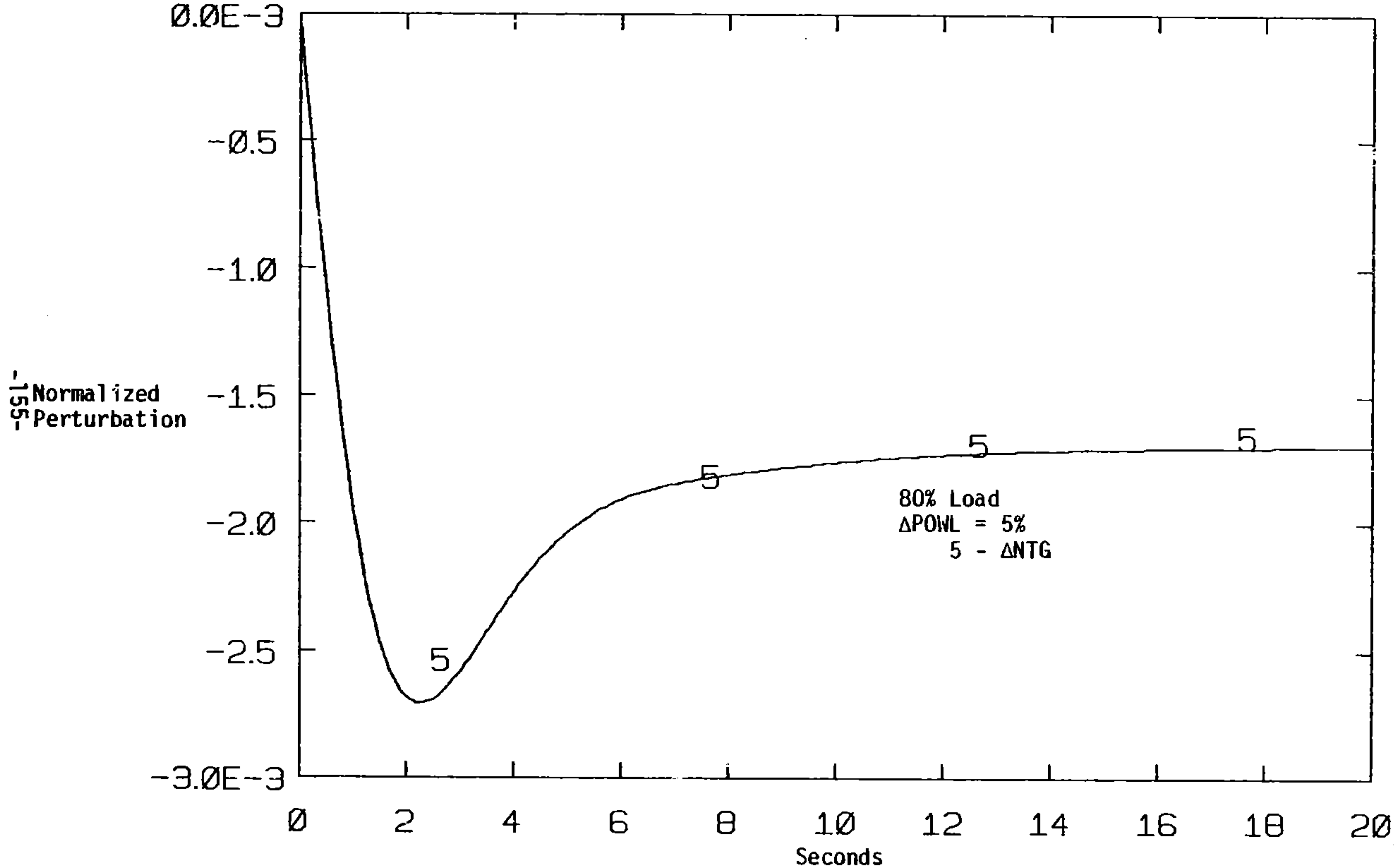

FIGURE 66: DC LOAD DEMAND DISTURBANCE-5% DROOP GOVERNOR

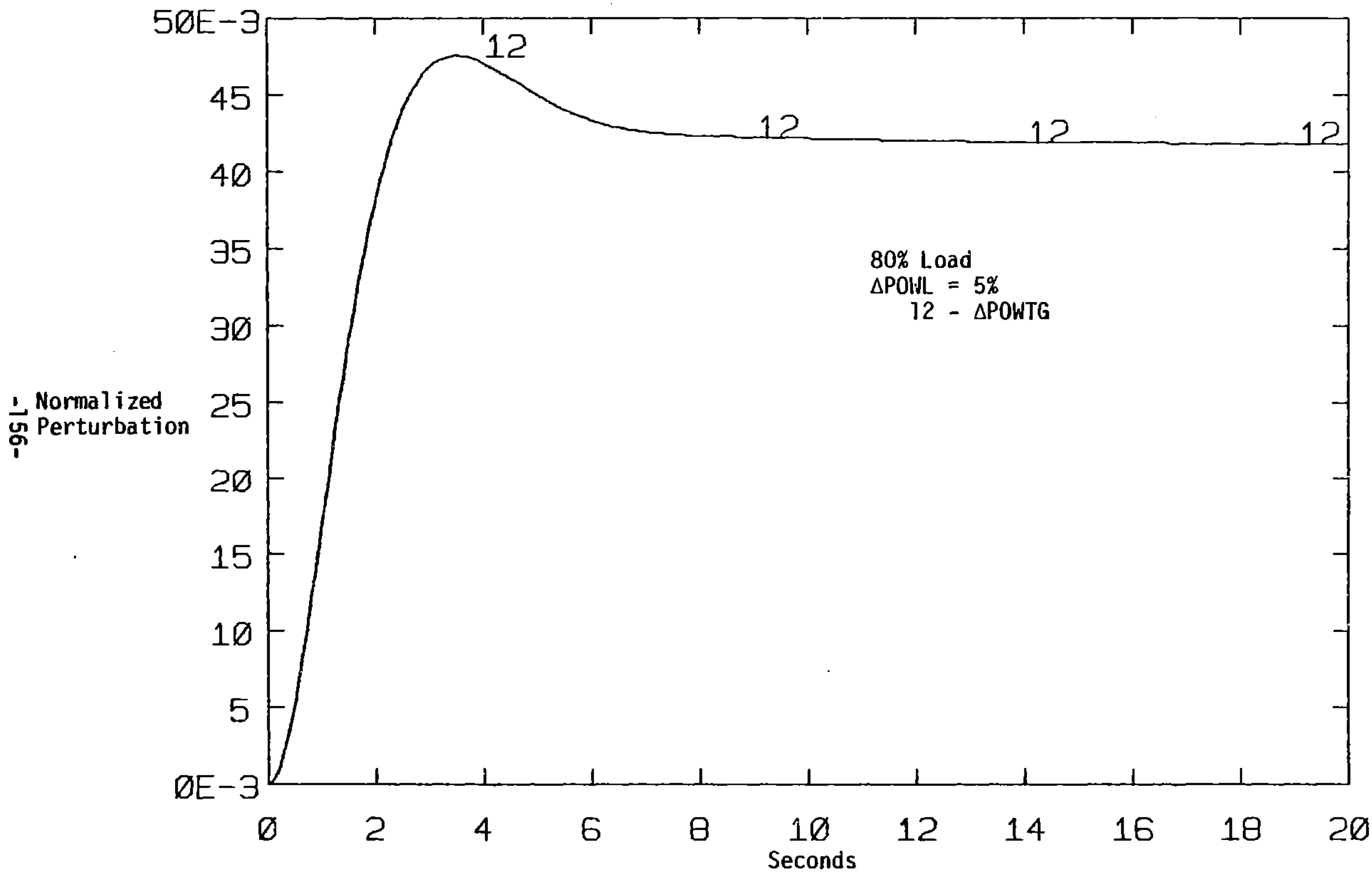

FIGURE 67: DC LOAD DEMAND DISTURBANCE-5% DROOP GOVERNOR

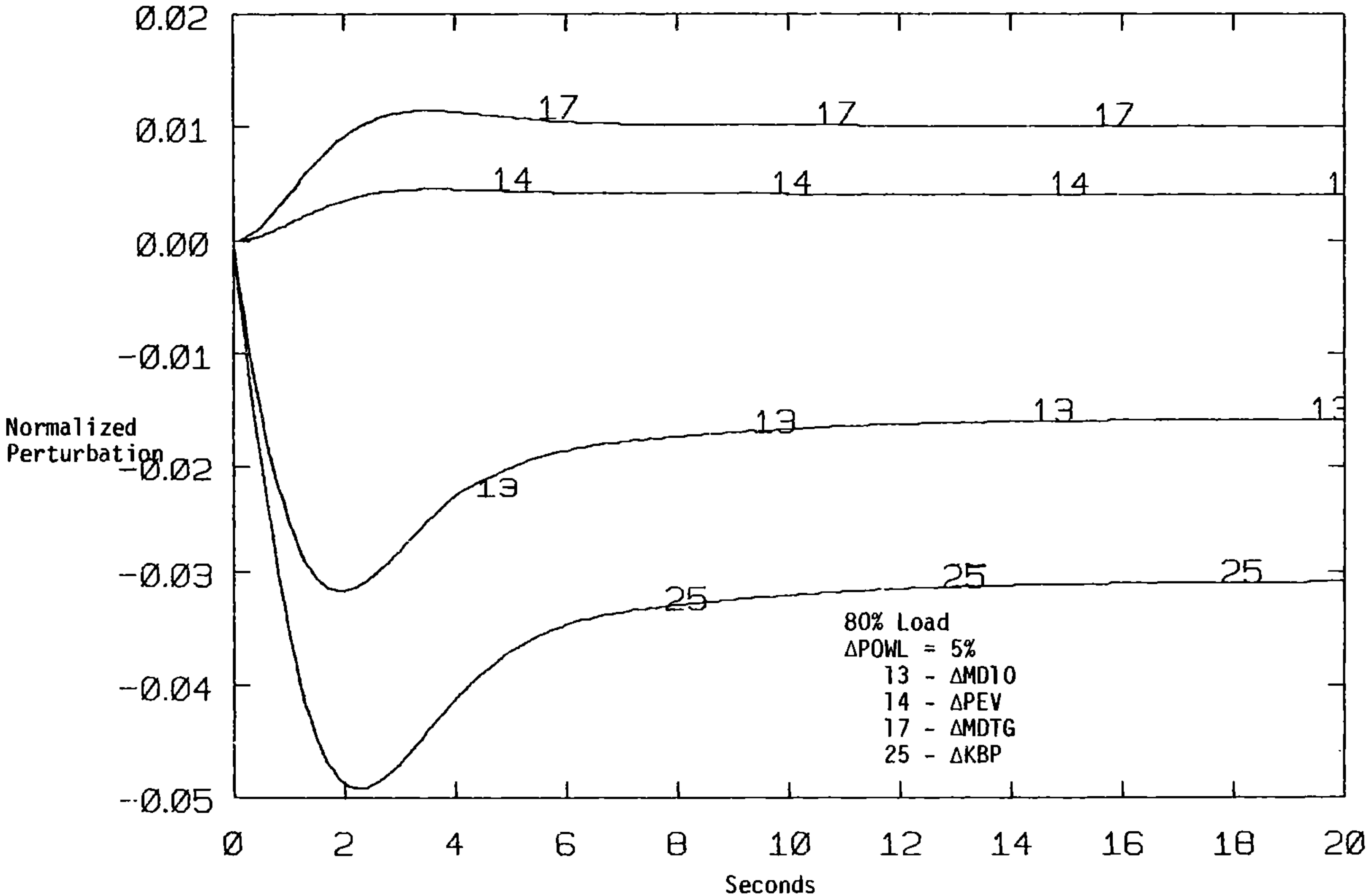

FIGURE 68: DC LOAD DEMAND DISTURBANCE-5% DROOP GOVERNOR

and 68. In each case the drop in turbine-generator speed because of the load mismatch causes the bypass valve to close, reducing the total vapor flow rate but increasing the turbine vapor flow by the pressure effect. This increases the turbine-generator power output until it again matches the load. The small variations in system variables beyond 6-8 seconds are once again the result of the heat exchangers reaching a new thermal equilibrium. The 5% governor droop responds both sluggishly and exhibits a large steady state turbine speed error. The 1% governor droop exhibits a steady state error of 0.04% but the response is highly oscillatory; the 3% governor droop response is more stable but the steady state error rises to 0.1%. Both respond in about 6 seconds. The bypass valve does not exceed its maximum fully closed valve of 20% in any of the cases. All other system variables respond acceptably. Based on these responses, a 3% governor droop is chosen as giving the most satisfactory overall response.

The governor gains for a 3% droop design are plotted as a function of nominal bypass valve opening in Figure 69. The damping ratio and natural frequency of the turbine-generator speed response at varying power levels using those gains are given in Table 12. The turbine-generator speed dynamics maintain a fairly constant level throughout the load spectrum. The increase in damping at low power levels is compensated for by an increased speed

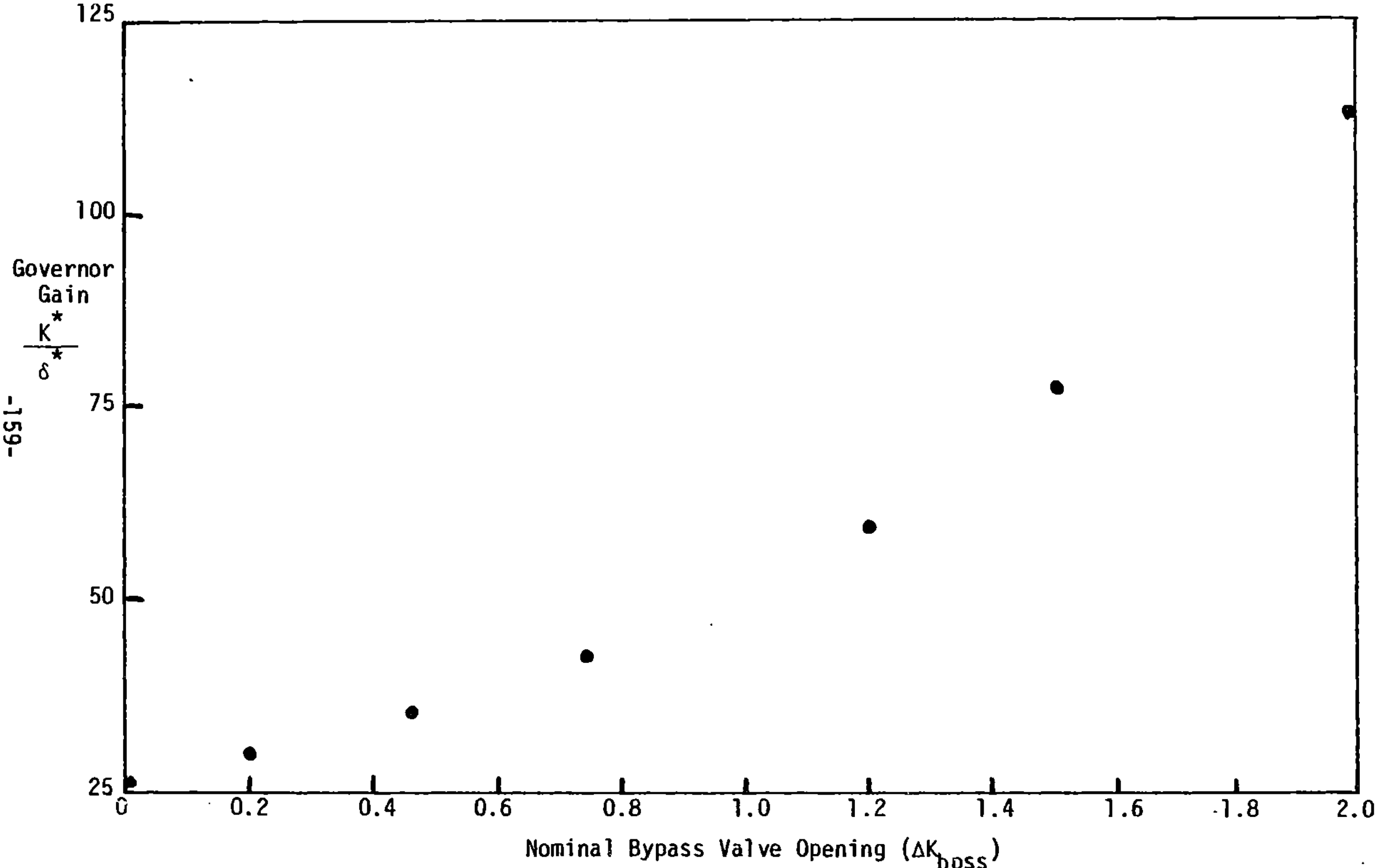

FIGURE 69: GOVERNOR GAIN FOR 3% DROOP (DC LOAD)

TABLE 12: TURBINE-GENERATOR SPEED DYNAMICS FOR 3% DROOP

LOAD LEVEL	DAMPING RATIO, ξ	NATURAL FREQUENCY ω_n (rad/sec)
100%	0.52%	1.48
80%	0.55%	1.52
60%	0.58%	1.58
40%	0.63%	1.67
20%	0.71%	1.79
10%	0.78%	1.88
0%	0.90%	2.00

of response. The controlled plant was simulated at a 40% power level using the same DC load demand increase as before. The results of the simulation are shown in Figures 70 and 71. The turbine-generator speed response is remarkably similar to the 80% load response, exhibiting only slightly less overshoot and steady state error.

Up to this point, the effects of actuator dynamics on the system response have been totally ignored. The actuator dynamics can be adequately represented by a first order lag of the form shown in Figure 72.

For modern electro-hydraulic turbine-generator control systems, the lag time constant, τ, is on the order of 0.2 seconds.

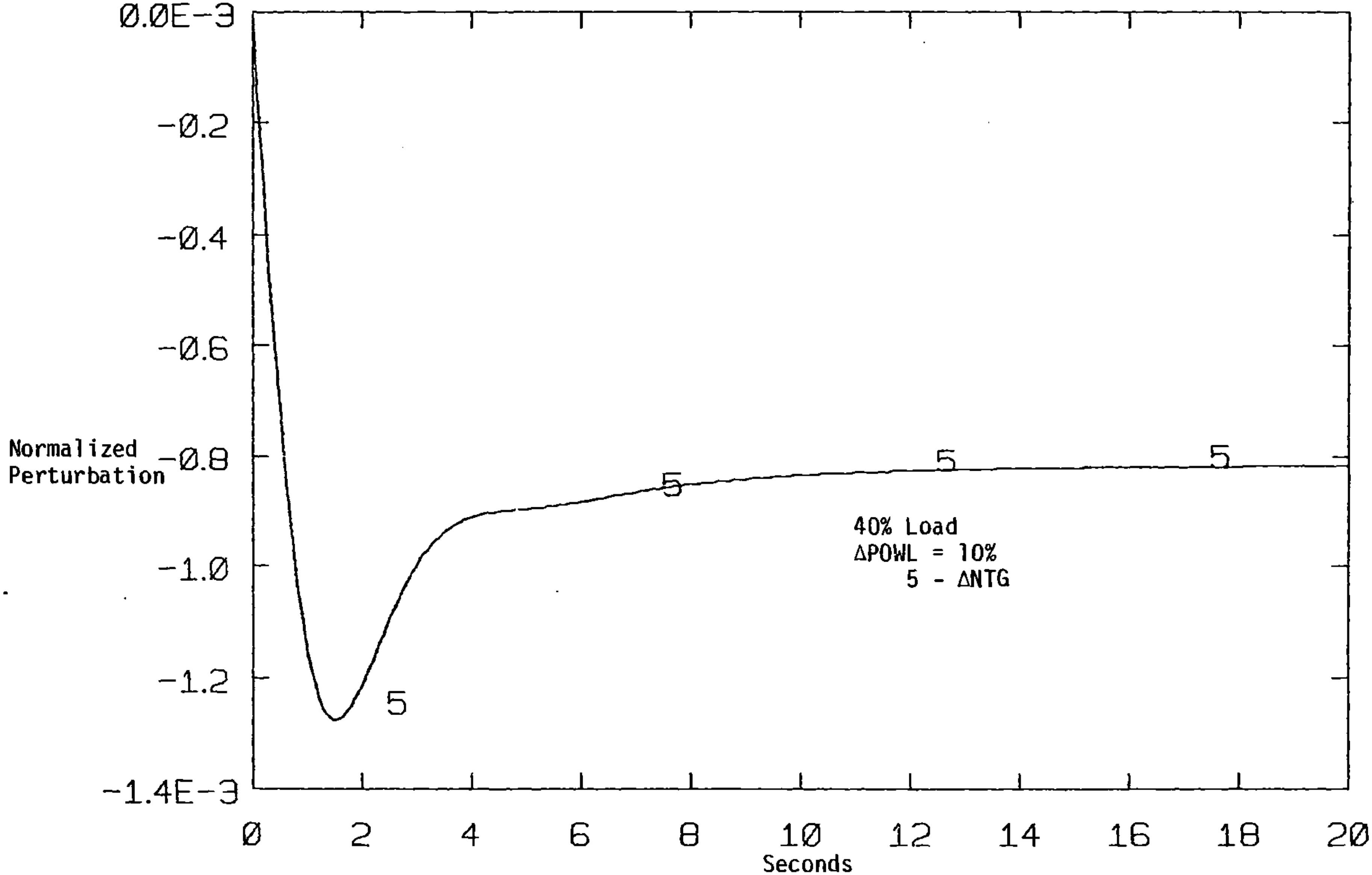

FIGURE 70: DC LOAD DEMAND DISTURBANCE-3% DROOP GOVERNOR

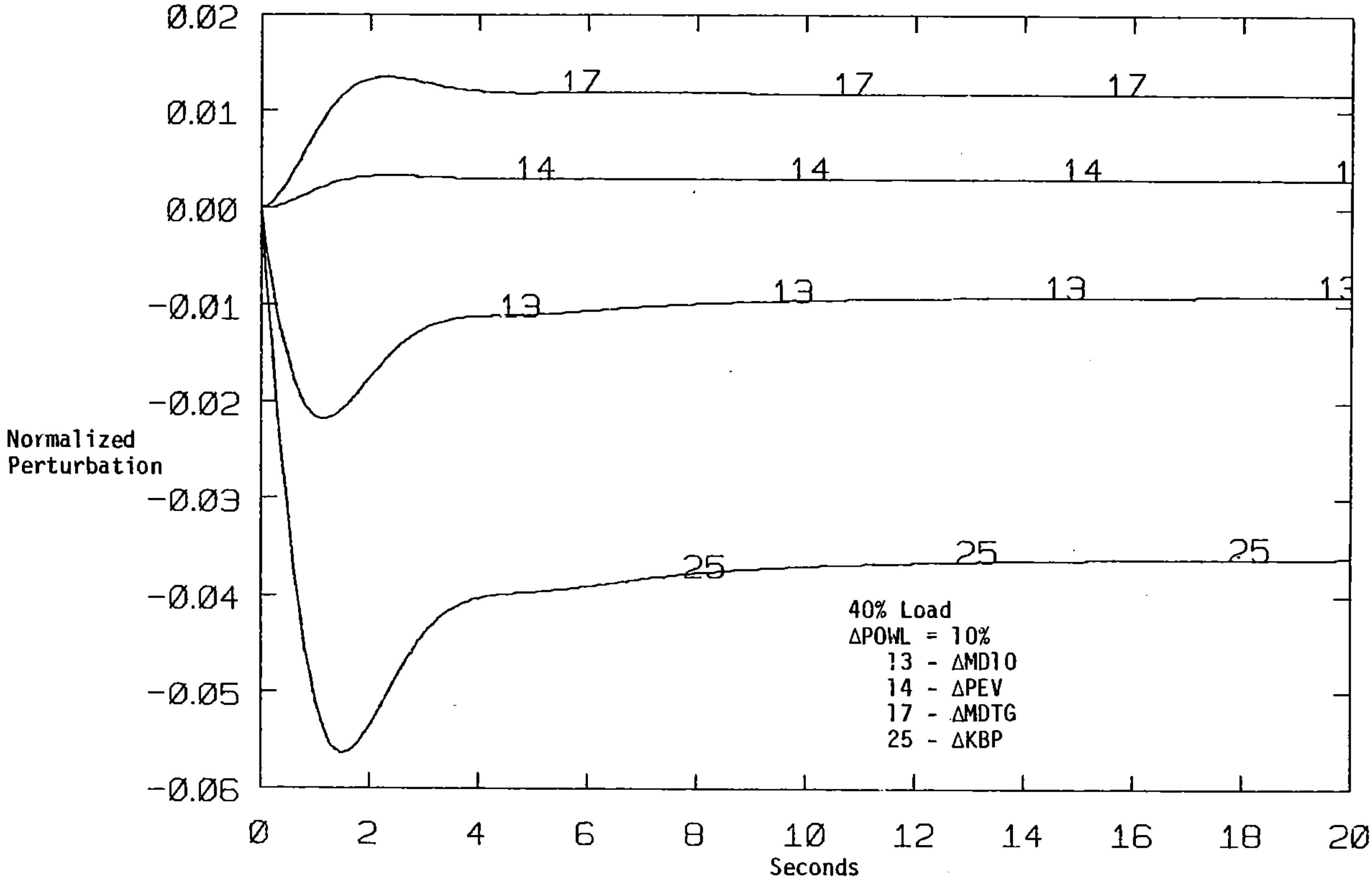

FIGURE 71: DC LOAD DEMAND DISTURBANCE-3% DROOP GOVERNOR

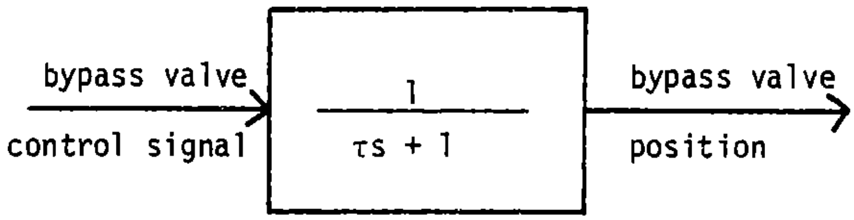

FIGURE 72: ACTUATOR DYNAMICS MODEL

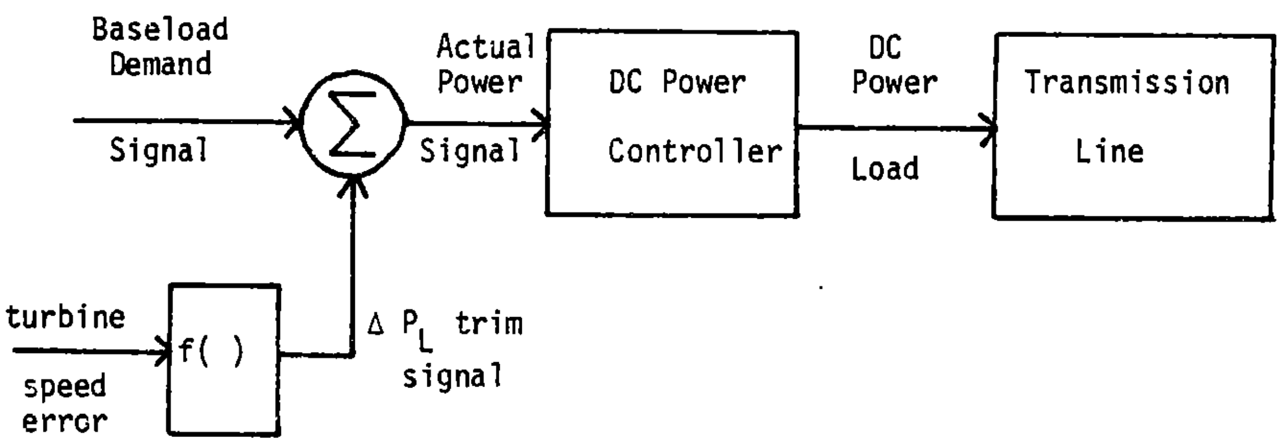

FIGURE 97: DC LOAD CONTROL SCHEMATIC

The controlled OTEC plant is simulated with the actuator lag included for a 5% DC power demand load increase. The plant is operating at 80% load. The response in Figure 73 shows a more oscillatory turbine-generator speed response than without the actuator lag. The response time is slightly slower. Figure 74 shows the effect of the actuator dynamics in this case; the bypass valve position initially lags behind the control signal by about 0.2-0.3 seconds. Figure 75 shows the response of other system variables. Although somewhat degraded by the actuator dynamics, the control system still seems to maintain an adequate system response to DC power load demand disturbances.

In order to investigate the effects of seawater environment changes on the controlled OTEC plant, the evaporator is subjected to a 0.2% step decrease in the warm seawater temperature (~1°F). The OTEC plant is operating at 80% load with a 3% droop turbine-generator speed controller; actuator dynanics are included. Figures 76, 77, 78, and 79 show the system response. As the seawater temperature in the evaporator begins to decline, the ammonia vapor flow rate begins to decrease causing the generated power to fall. As the turbine-generator speed begins to fall because of the load mismatch, the control system comes into action by closing the bypass valve, thus reducing the total vapor flow even faster; however, the turbine vapor flow rate begins to rise because of the pressure effect. The greater turbine flow rate increases the generated power

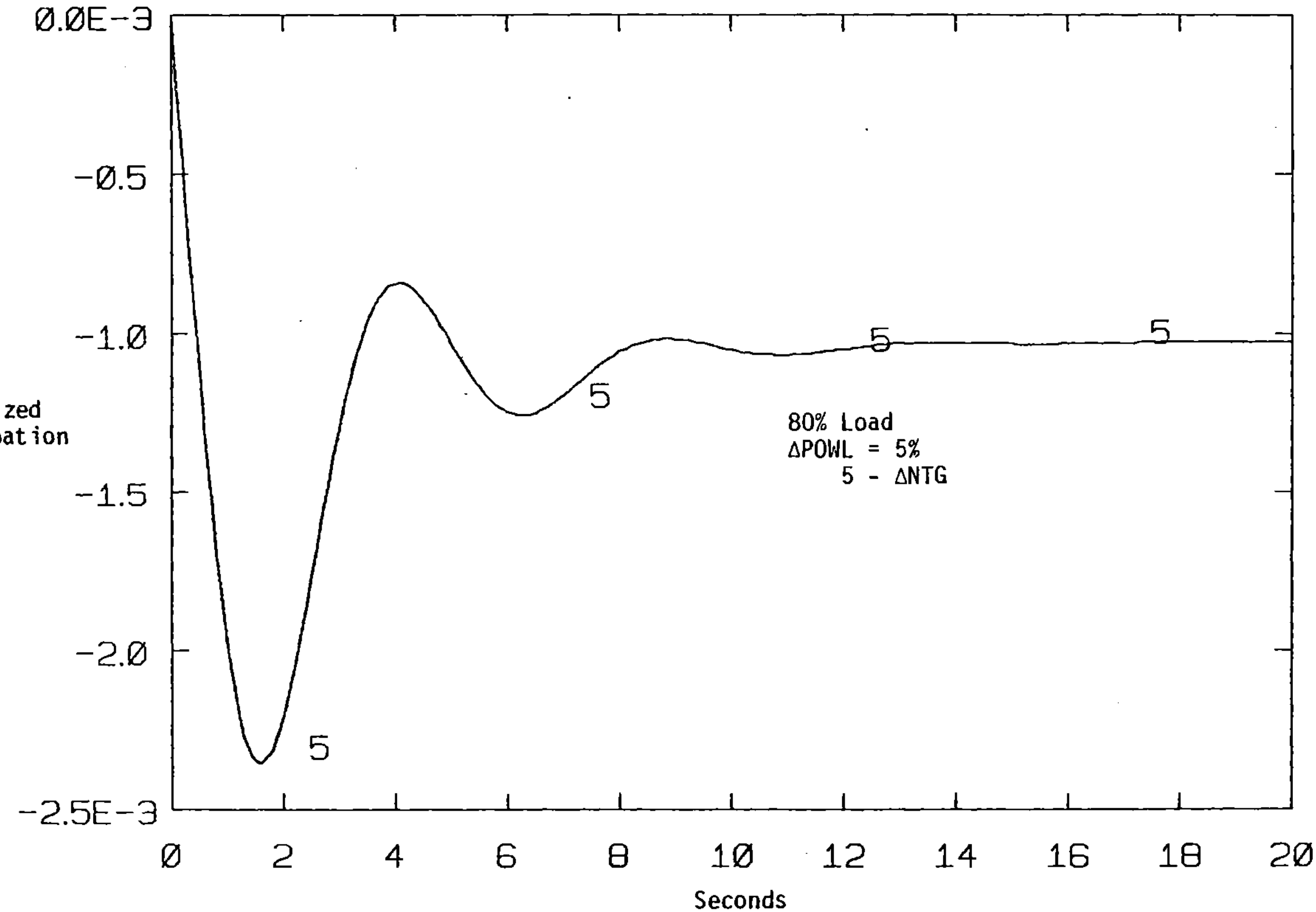

FIGURE 73: DC LOAD DEMAND DISTURBANCE-3% DROOP GOVERNOR (Lag)

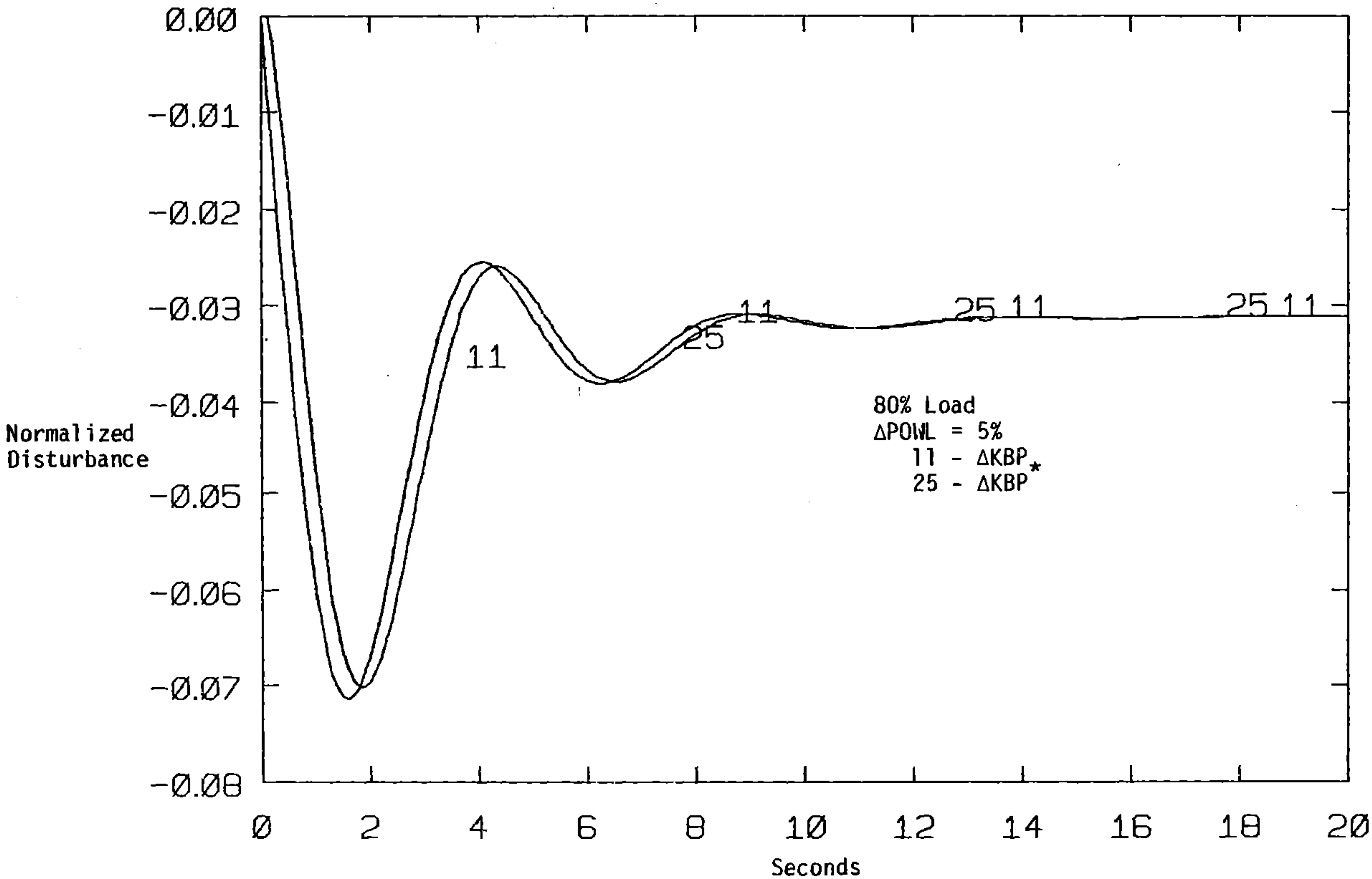

FIGURE 74: DC LOAD DEMAND DISTURBANCE-3% DROOP GOVERNOR (Lag)

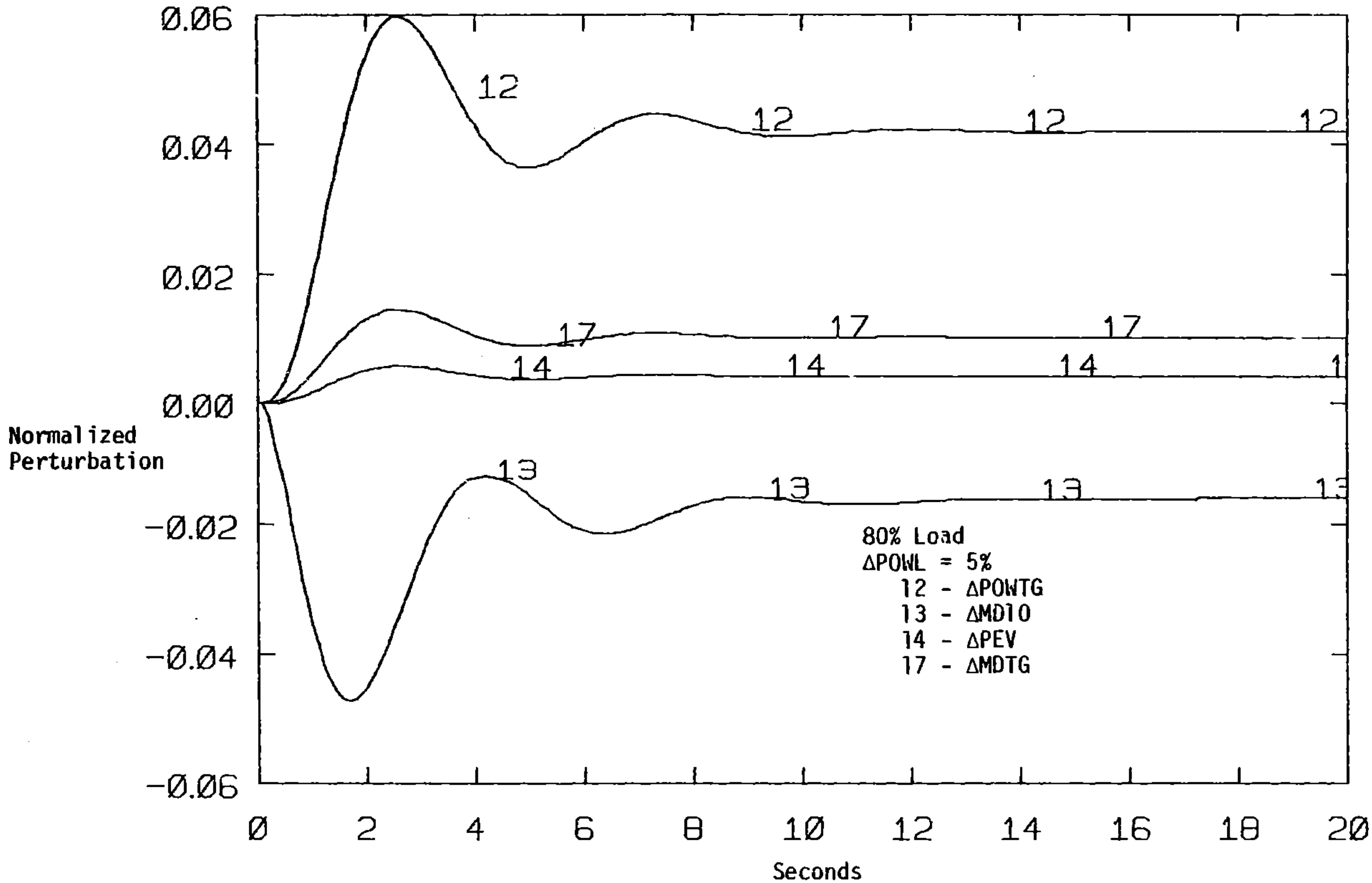

FIGURE 75: DC LOAD DEMAND DISTURBANCE-3% DROOP GOVERNOR (Lag)

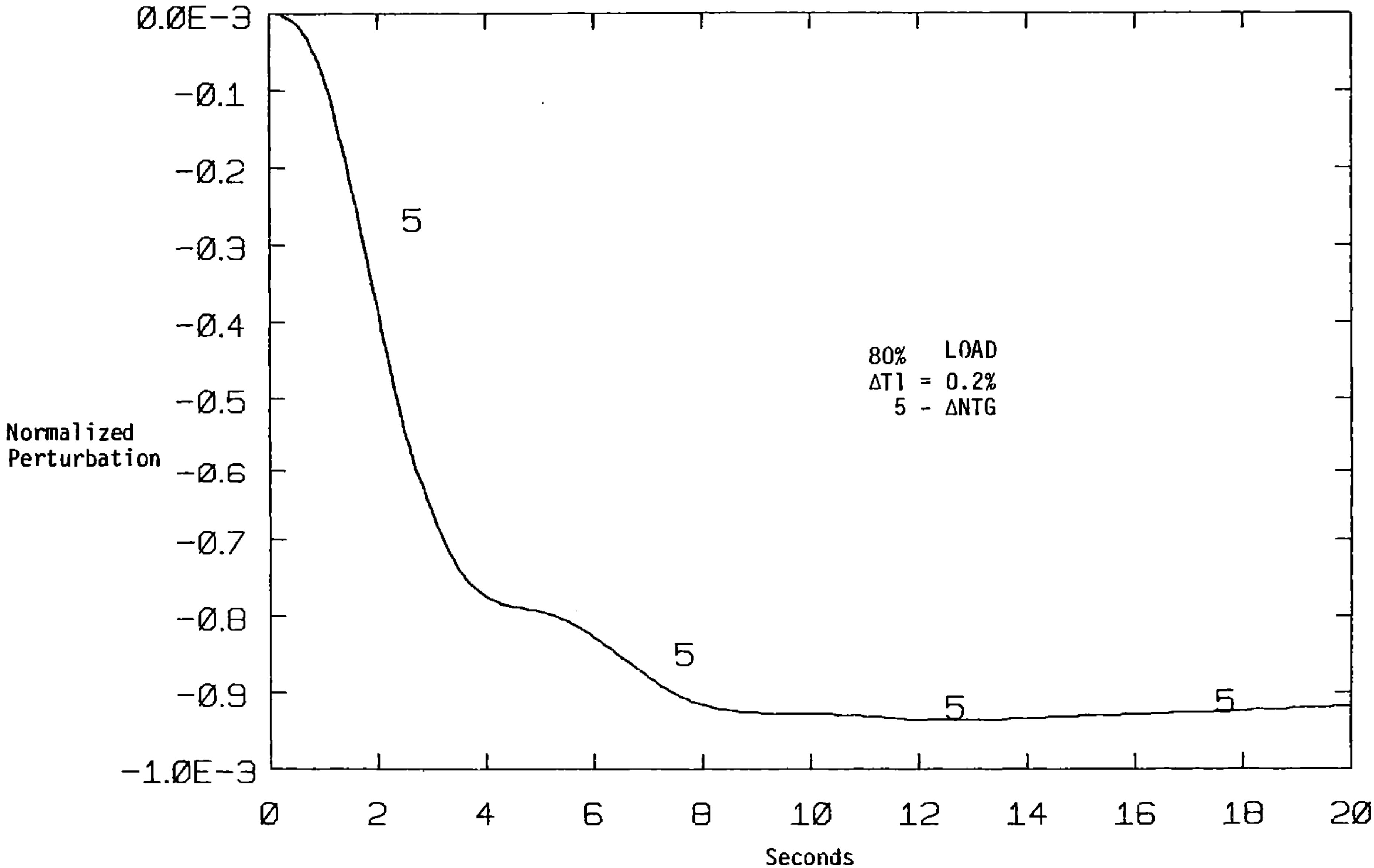

FIGURE 76: WARM SEAWATER TEMPERATURE DISTURBANCE-3% DROOP GOVERNOR (Lag)

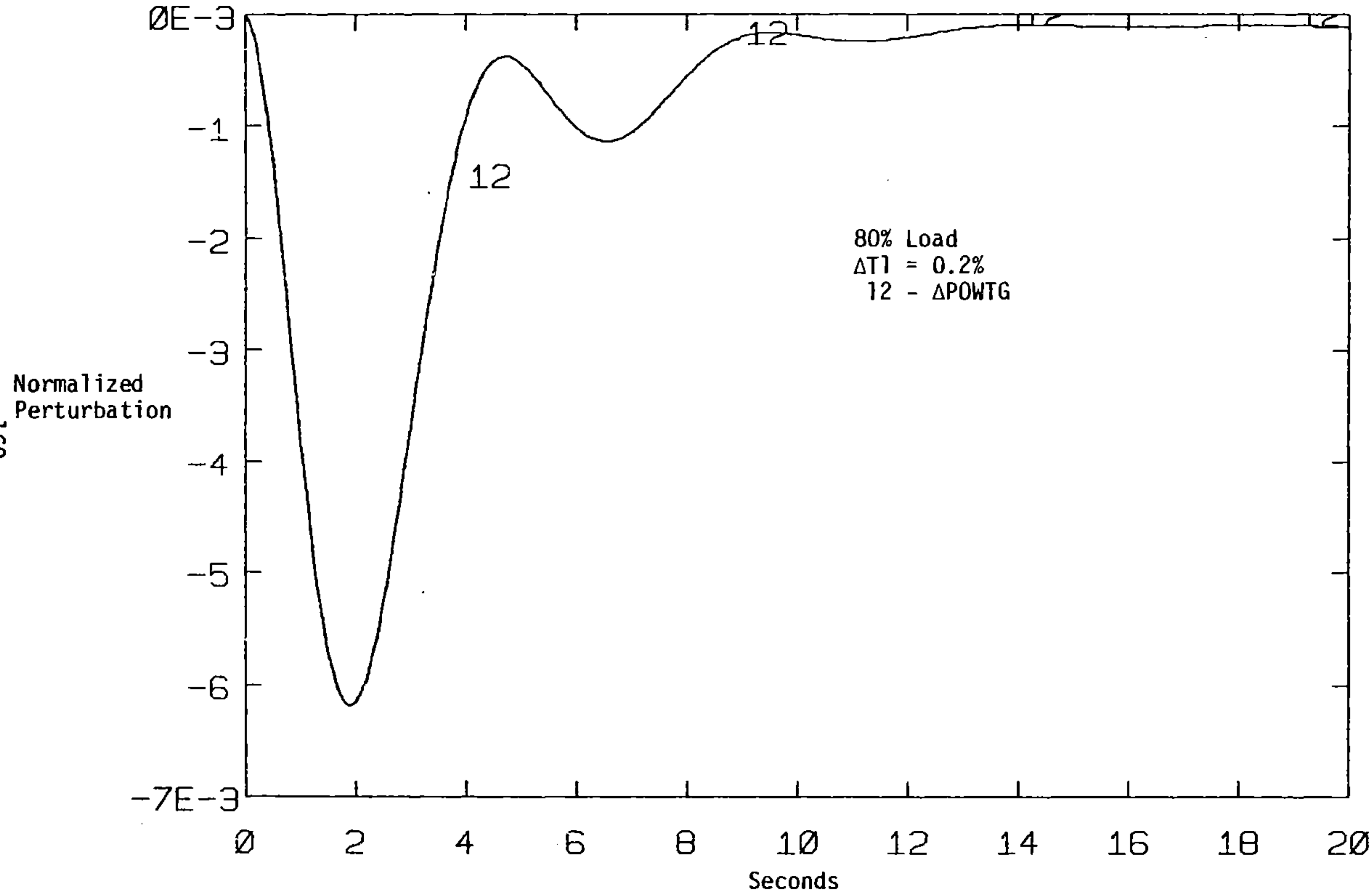

FIGURE 77: WARM SEAWATER TEMPERATURE DISTURBANCE-3% DROOP GOVERNOR (Lag)

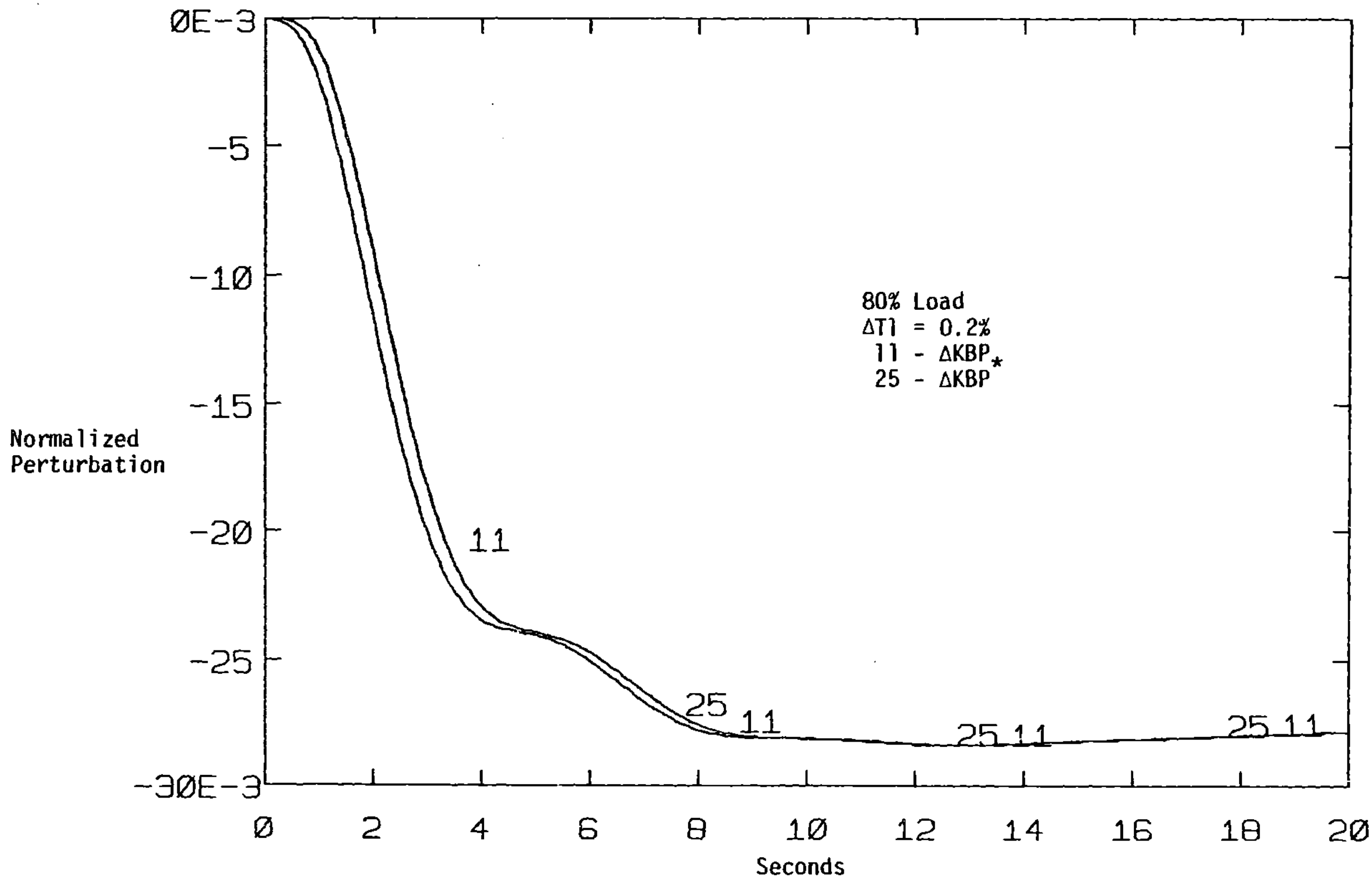

FIGURE 78: WARM SEAWATER TEMPERATURE DISTURBANCE-3% DROOP GOVERNOR (Lag)

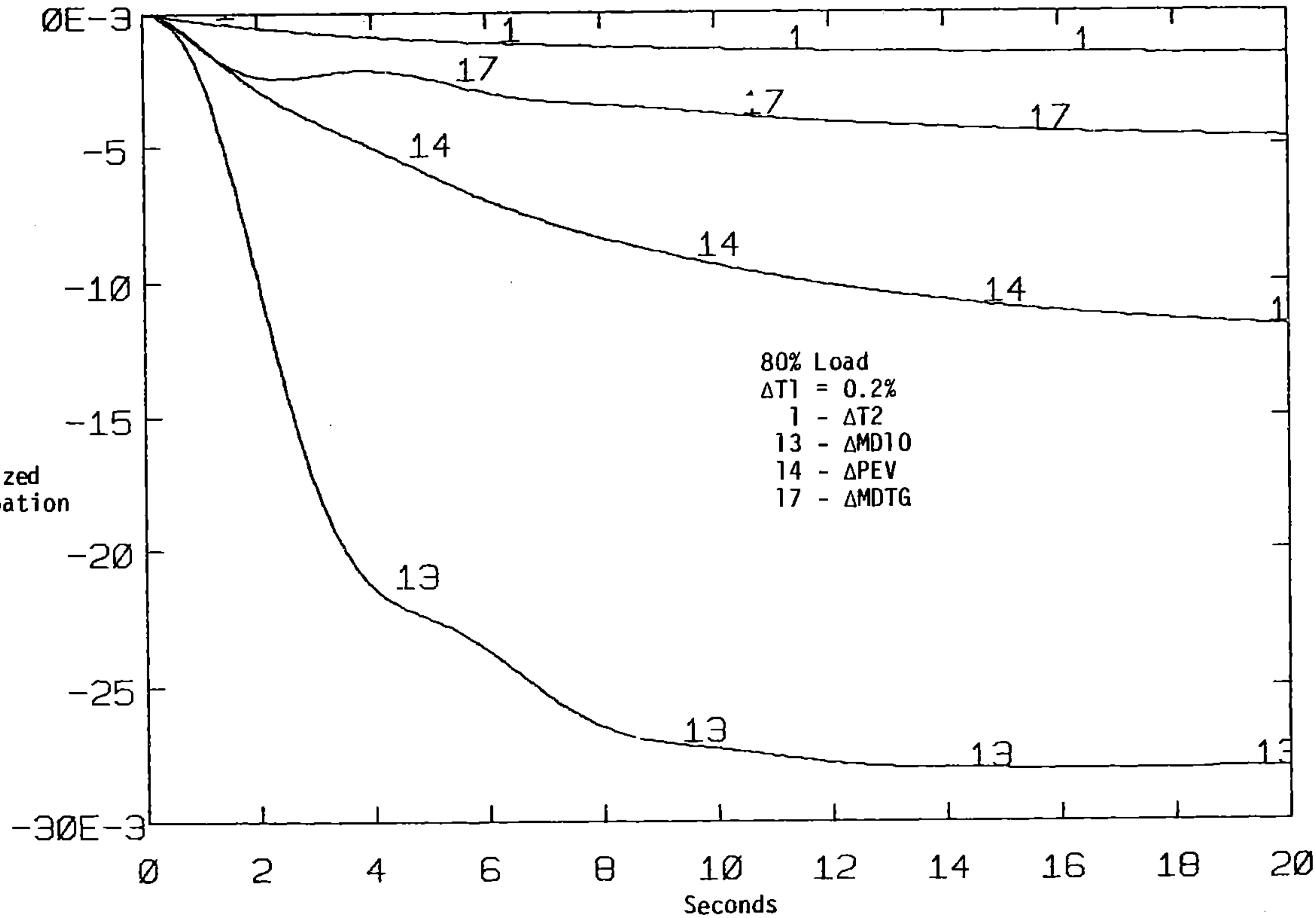

FIGURE 79: WARM SEAWATER TEMPERATURE DISTURBANCE-3% DROOP GOVERNOR (Lag)

back to the steady state level thereby matching the load. This system response is largely complete in about 10 seconds; small variations occur beyond this time as the system adjusts to a new thermal equilibrium. The turbine-generator governor works well in this case-the turbine generator speed responds well and exhibits only about 0.09% steady state error.

5.3.2 State Variable Feedback Control

It is usually possible to achieve better control of the dynamic characteristics of a system by a feedback control system based on more than one state of the system. The powerful techniques of linear-quadratic (L-Q) regulator design allow arbitrary control over the closed loop eigenvalues of a system by feedback of all the independent states of that system. The method also insures absolute stability of the system provided all controllability requirements are met. For a state-determined system of the form

$$\underline{\dot{x}} = \underline{\bar{A}}\ \underline{x} + \underline{\bar{B}}\ \underline{u} \tag{78}$$

L-Q regulator design consists of minimizing the quadratic performance index

$$J = 1/2 \int_0^{\infty} (\underline{x}^T \underline{\bar{Q}}\ \underline{x} + \underline{u}^T \underline{\bar{R}}\ \underline{u}) dt \tag{79}$$

where $\underline{\bar{Q}}$ and $\underline{\bar{R}}$ are the "weights" on the states and controls of the system. The solution to this problem results in the steady state

Ricatti equation[20].

$$\underline{\bar{Q}} - \underline{\bar{S}}\,\underline{\bar{B}}\,\underline{\bar{R}}^{-1}\,\underline{\bar{B}}^T\underline{\bar{S}} + \underline{\bar{S}}\,\underline{\bar{A}} + \underline{\bar{A}}^T\underline{\bar{S}} = 0 \qquad (80)$$

where $\underline{\bar{S}}$ is the steady state Ricatti gain matrix. The "optimal" state variable feedback control law which minimizes the performance integral is given by

$$\underline{u} = -\underline{\bar{R}}^{-1}\,\underline{\bar{B}}^T\underline{\bar{S}}\;\underline{x} \qquad (81)$$

In essence, the optimal regulator designed by the L-Q method attempts to minimize the state perturbations both dynamically and in the steady state according to the "weights" given to them in the performance index. The turbine-generator control for the OTEC power plant is an attempt to minimize the turbine-generator speed variations in response to load and environmental disturbances. The judicious application of the L-Q regulator design method to the OTEC system should result in a substantial improvement in turbine-generator speed and system control.

Before the L-Q design method is applied to the OTEC power plant, it is wise to define those states which are important to turbine-generator control. The result of applying the design method to the full order OTEC model would be to construct a complex multi-state variable feedback control system when the control of a few important states of a reduced order model would result in comparable performance and would be more physically realizable. The states of the OTEC model which are most important to the turbine-generator response are those of the vapor flow system and of the turbine-generator itself = $\Delta\rho_{ev}$, $\Delta\rho_{cd}$, and $\Delta\omega_{tg}$. The thermal states of the heat exchangers have slow transient responses and will not affect the rapid control of the turbine-generator. The water system states, if constant seawater flows are maintained, will have no effect on the system whatsoever. Because each of the states in the reduced order model must be physically measurable, the fact that $P_v = f(\rho_v)$ for the ammonia vapor allows the transformation to the physically measurable reduced order model of the OTEC power plant at 80% load given below.

$$\frac{d}{dt} \begin{bmatrix} \Delta PEV \\ \Delta PCD \\ \Delta NTG \end{bmatrix} = \underline{\bar{A}} \begin{bmatrix} \Delta PEV \\ \Delta PCD \\ \Delta NTG \end{bmatrix} + \underline{\bar{B}} \, [\Delta KBP] + \underline{\bar{\Gamma}} \, [\Delta POWL] \quad (82)$$

The L-Q control design methodology consists of choosing a performance index and evaluating the system performance using the resulting control law. It is usually an iterative process requiring trial and error until a controller is obtained which produces a satisfactory system response. Because the turbine-generator speed is the state of interest, a performance index weighting only that state and the control variable, ΔKBP, is used. By increasing the weighting on the turbine-generator speed, its transient response becomes faster and approaches 0.707 damping, a highly desirable result. The following feedback control law is obtained:

$$\Delta KBP = [13.559, -22.642, 314.45] \begin{bmatrix} \Delta PEV \\ \Delta PCD \\ \Delta NTG \end{bmatrix} \tag{83}$$

The turbine-generator speed response of the reduced order model to a 5% DC load demand increase using this controller is shown in Figure 80. A noticeable improvement over the simple speed governor is demonstrated: a response time of 1.5 seconds and a steady state error of .06% with negligible overshoot. The state variable feedback control is now applied to the full order model at 80% load subjected to the same disturbance. The system response is shown in Figures 81, 82 and 83. The turbine-generator speed response is almost identical. The major difference is the slow variation because of the thermal transients in the heat exchanges. This same effect is also present when the basic speed governor is used; however, it is more pronounced here because the state of the heat exchanger is being fed back as a controlled variable. The maximum bypass valve opening is slightly greater for this controller: 10% as compared to 7% for the basic speed governor.

The same system and disturbance are simulated with the actuator dynamics included. Figures 84, 85, and 86, show this response. The system is now decidedly less stable, still experiencing oscillations beyond 10 seconds following the disturbance. The discrepancy

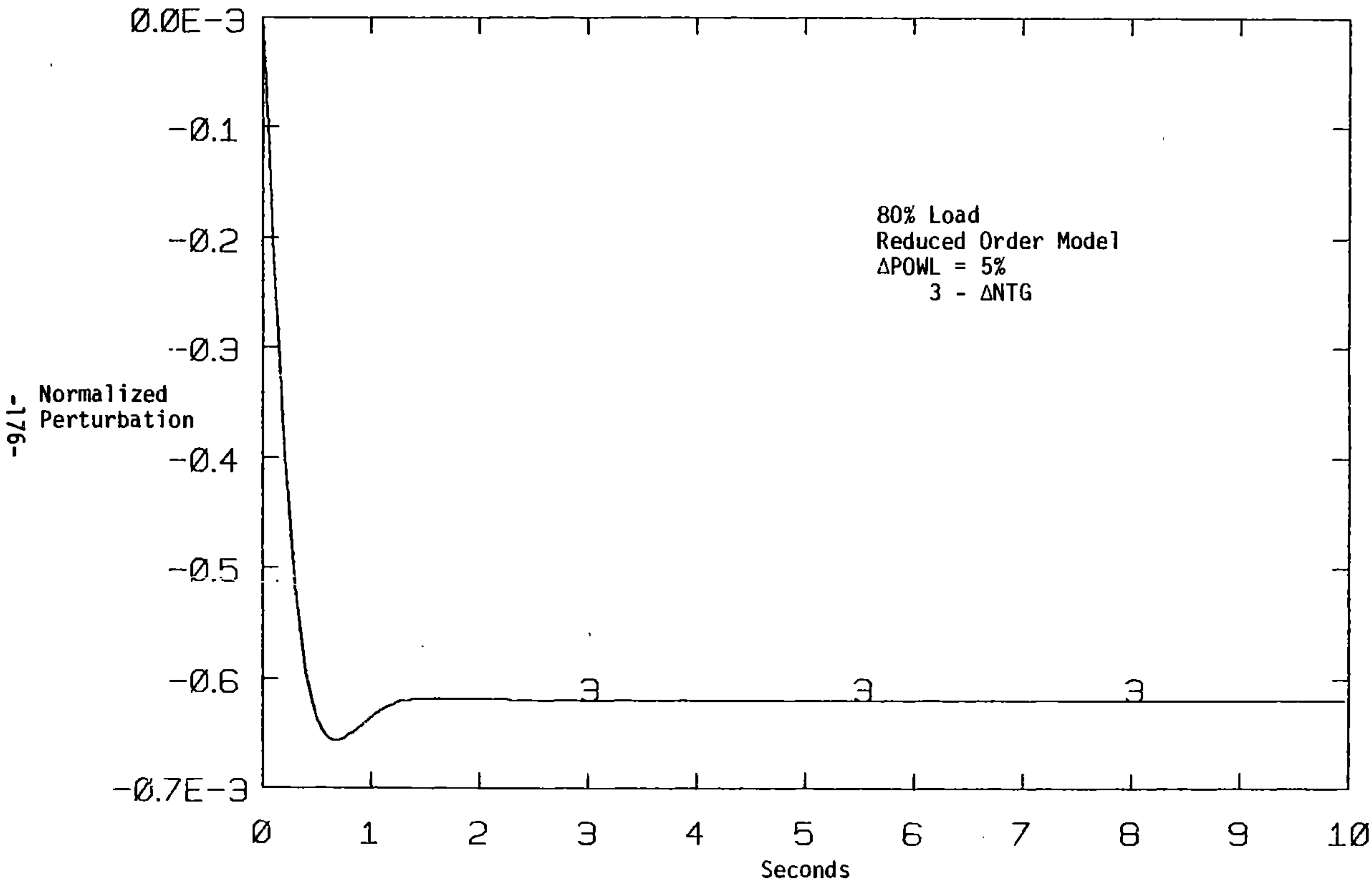

FIGURE 80: DC LOAD DEMAND DISTURBANCE-L-Q CONTROLLER

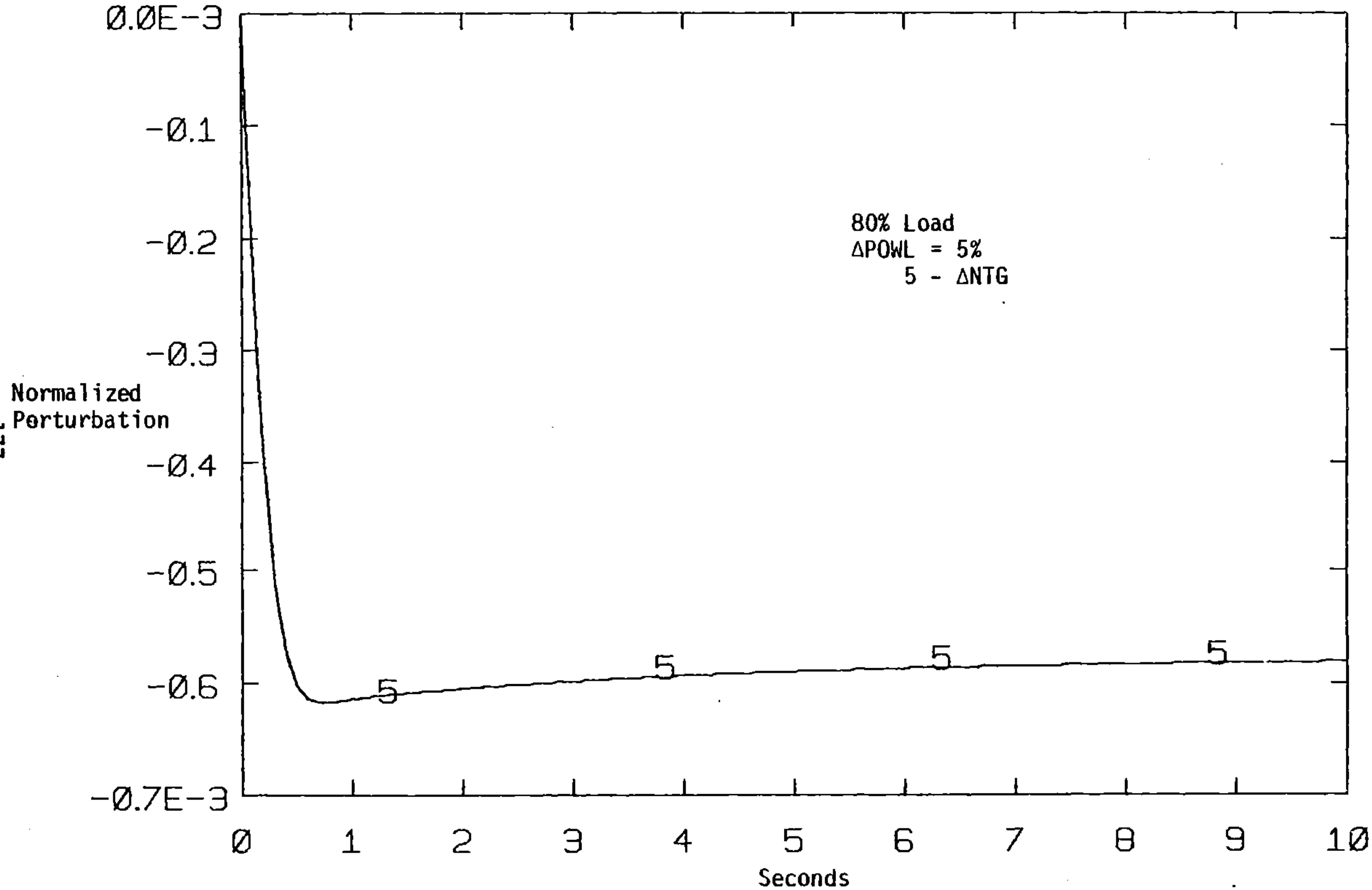

FIGURE 81: DC LOAD DEMAND DISTURBANCE-L-Q CONTROLLER

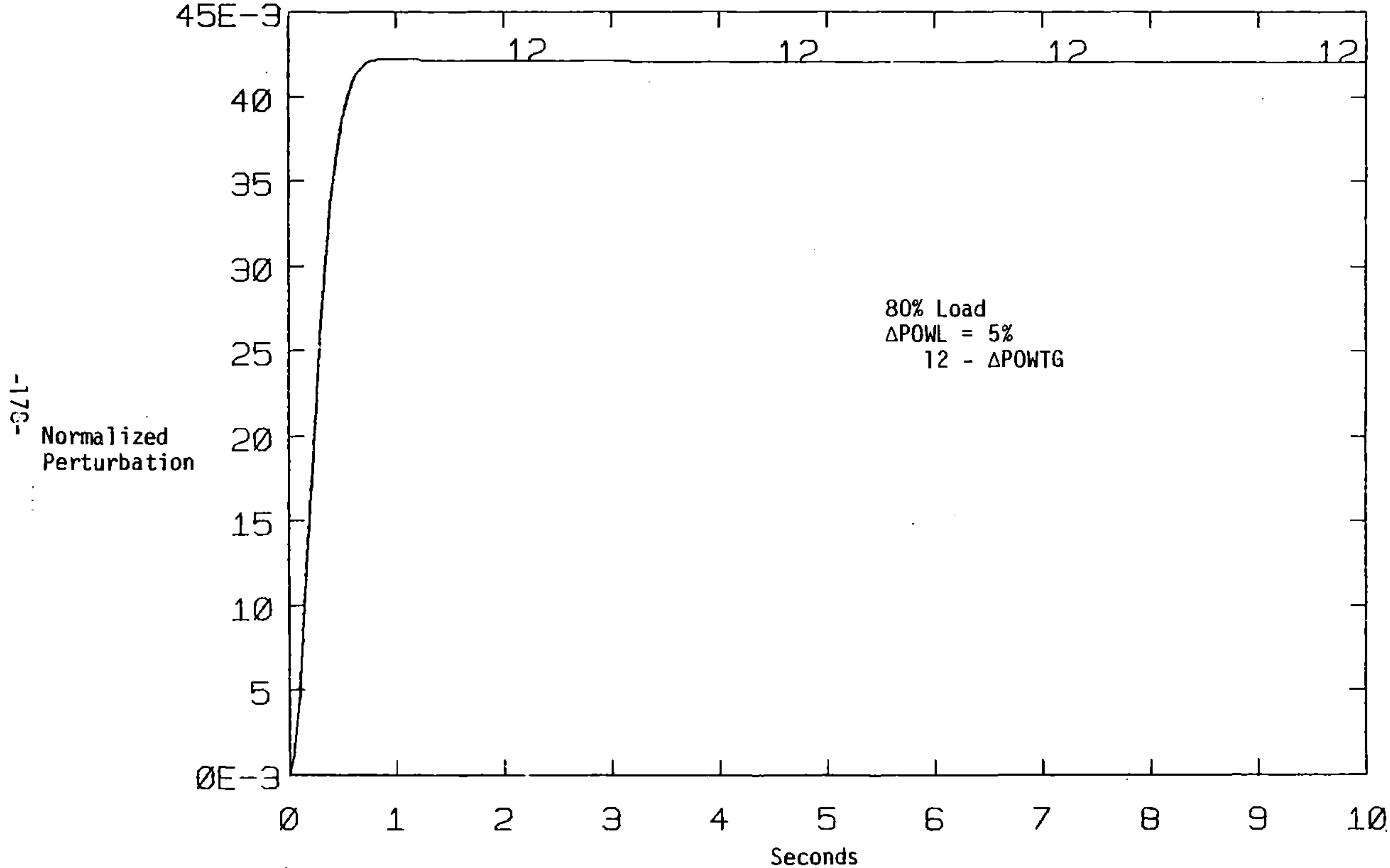

FIGURE 82: DC LOAD DEMAND DISTURBANCE-L-Q CONTROLLER

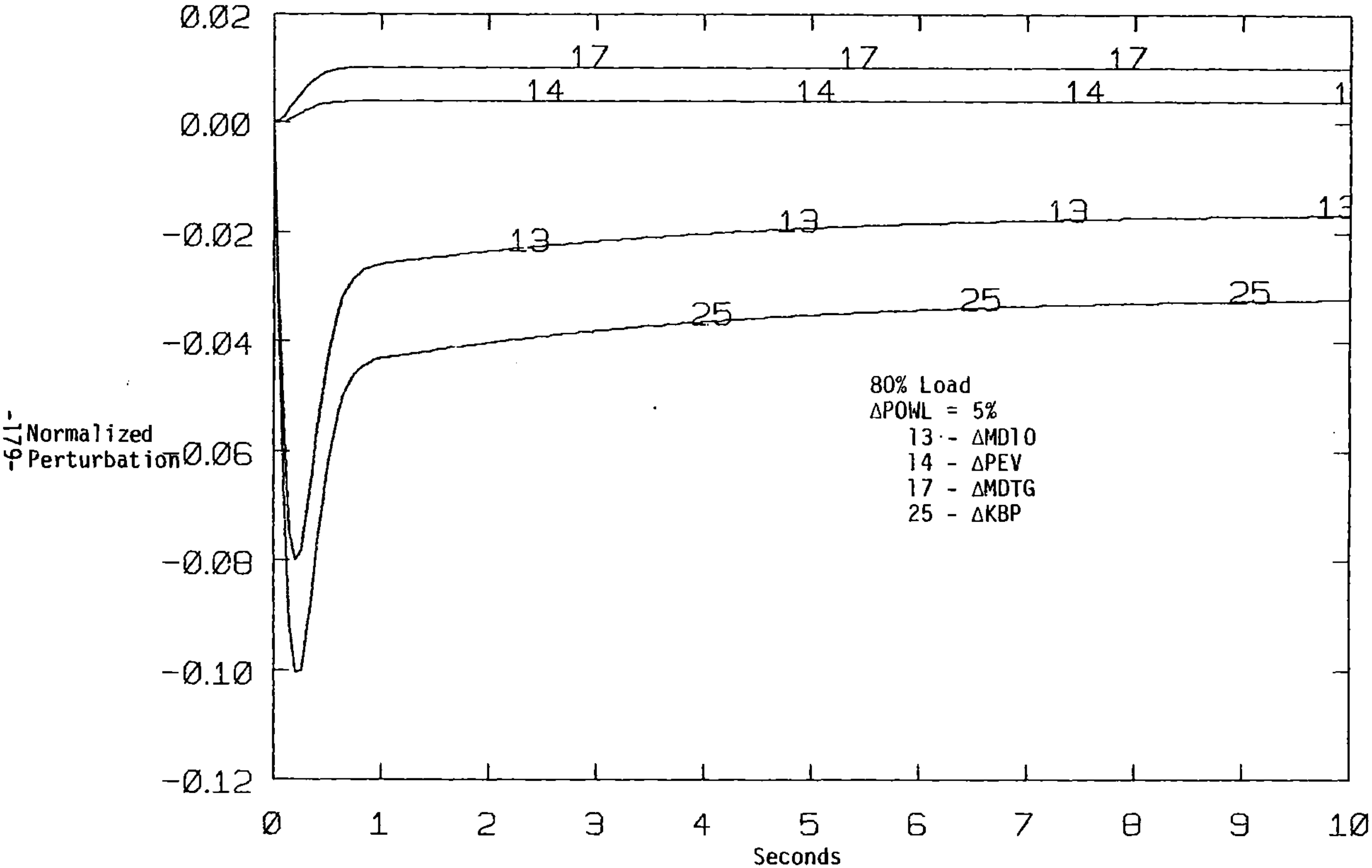

FIGURE 83: DC LOAD DEMAND DISTURBANCE-L-Q CONTROLLER

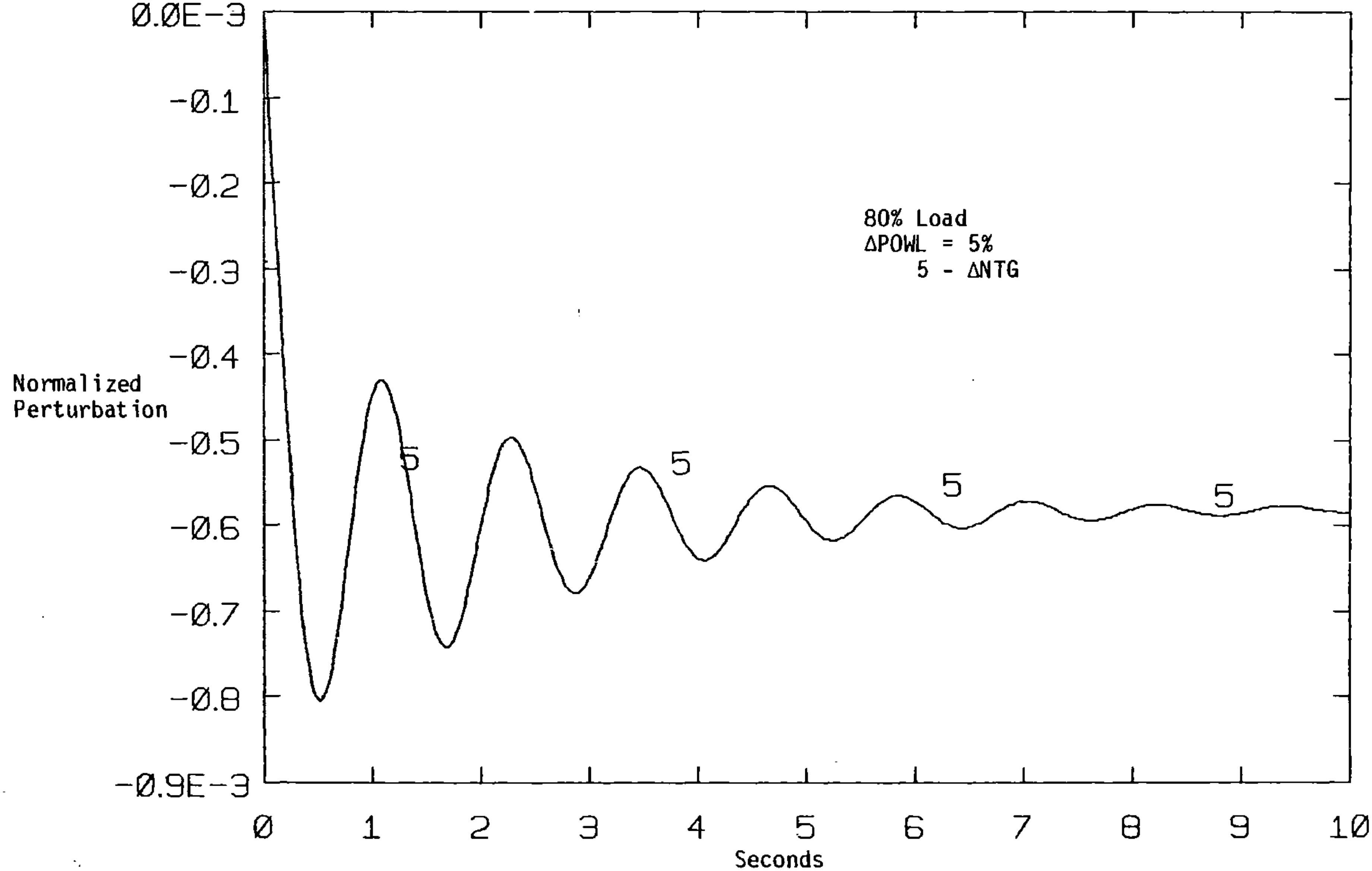

FIGURE 84: DC LOAD DEMAND DISTURBANCE-L-Q CONTROLLER (Lag)

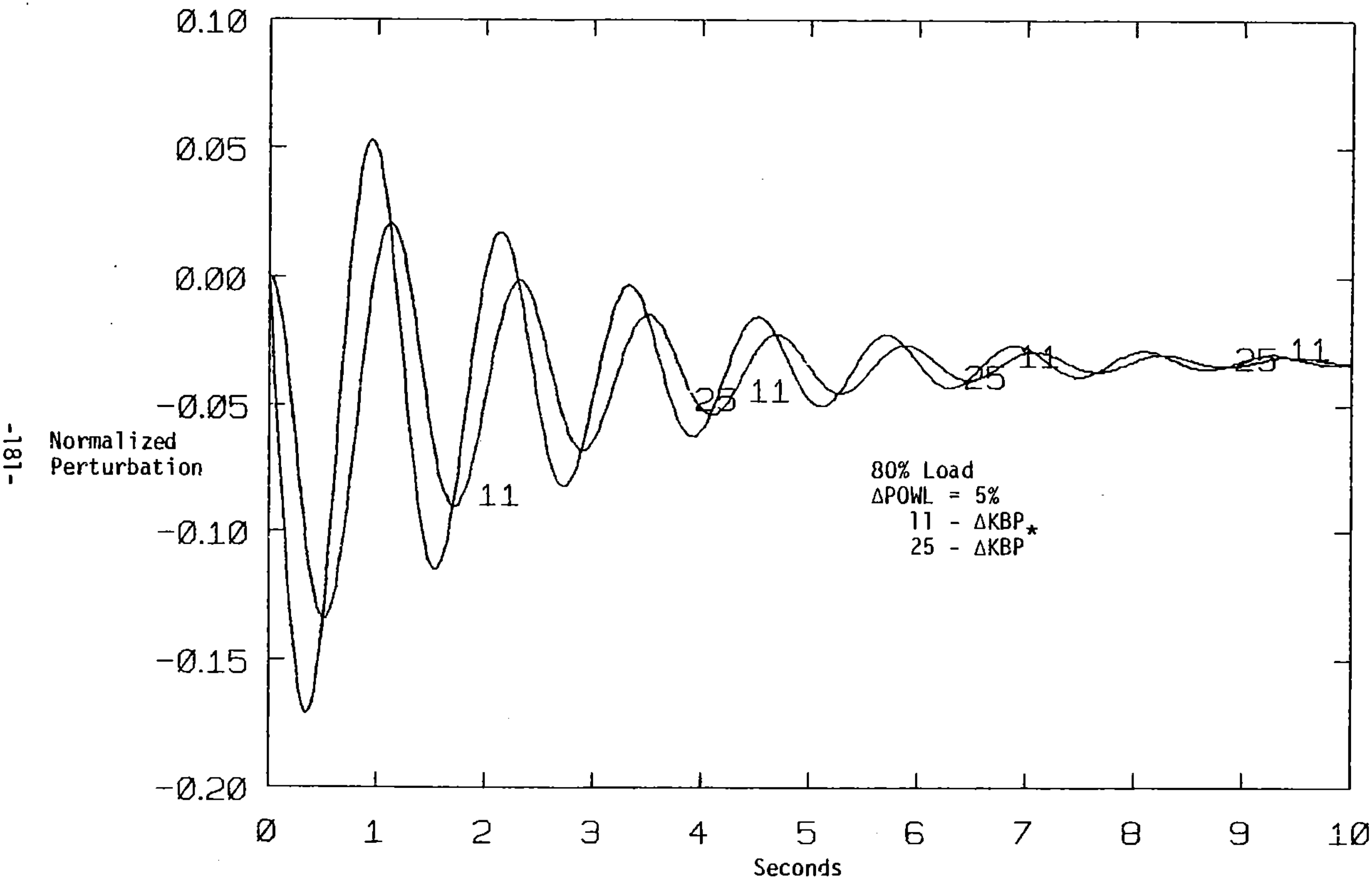

FIGURE 85: DC LOAD DEMAND DISTURBANCE-L-Q CONTROLLER (Lag)

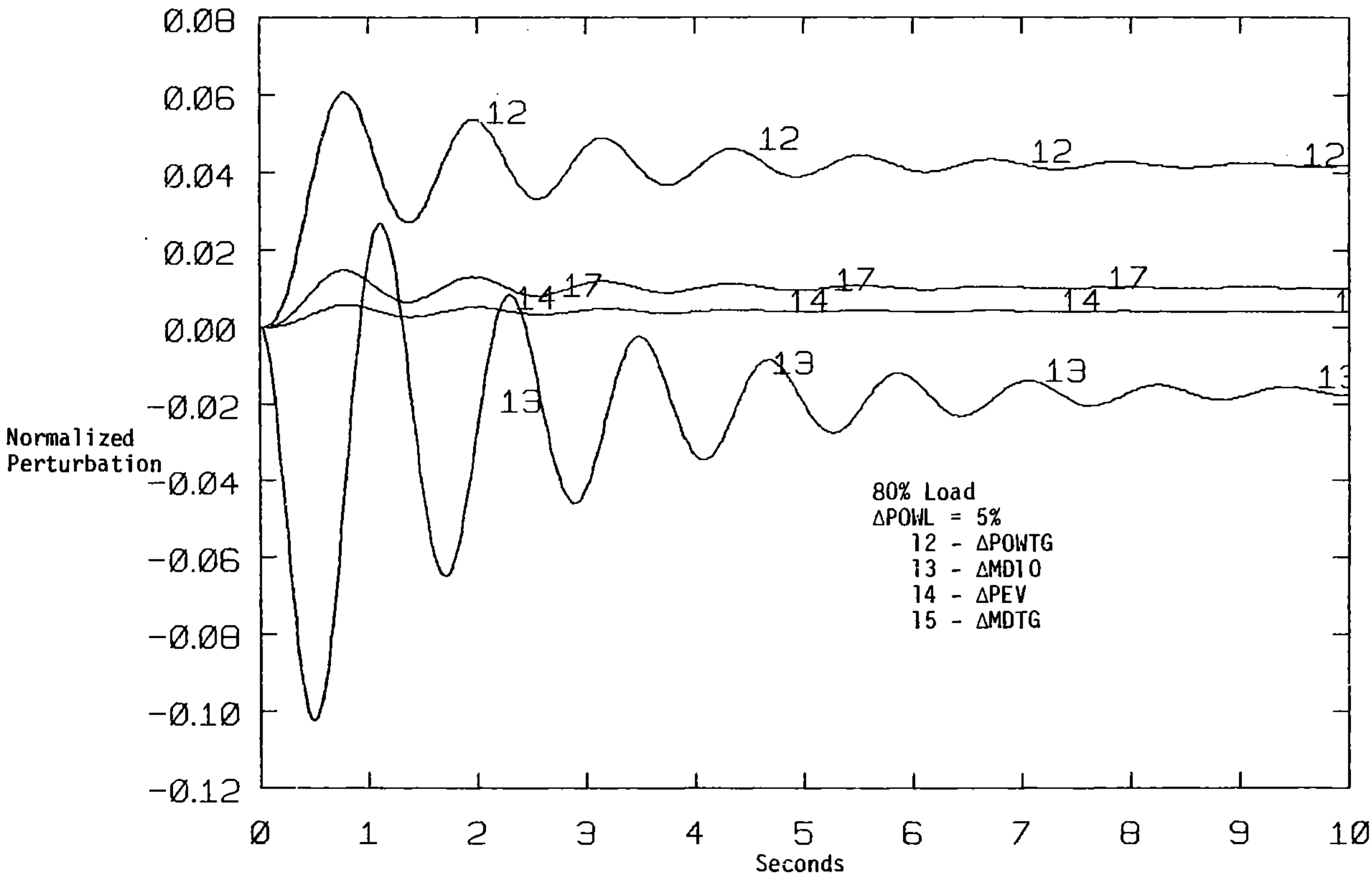

FIGURE 86: DC LOAD DEMAND DISTURBANCE-L-Q CONTROLLER (Lag)

between the actuator signal and the actual bypass valve position is large. This demonstrates the major drawback of a high performance state variable feedback regulator - any important dynamics which are not included into the design model can seriously degrade the system response. To compensate for this problem, the reduced order model was augmented to include the actuator dynamics.

$$\frac{d}{dt}\begin{bmatrix}\Delta PEV\\ \Delta PCD\\ \Delta NTG\\ \Delta KBP\end{bmatrix} = \underline{A}^{*}\begin{bmatrix}\Delta PEV\\ \Delta PCD\\ \Delta NTG\\ \Delta KBP\end{bmatrix} + \underline{B}^{*}[\Delta KBP^{*}] + \underline{\Gamma}^{*}[\Delta POWL] \quad (84)$$

The new state, the bypass valve opening, is also a physically measurable quantity and presents no new problems in this respect. The L-Q control design methodology is performed again resulting in the following controller:

$$\Delta KBP^{*} = [50.43, -84.631, 993.08, -3.3918]\begin{bmatrix}\Delta PEV\\ \Delta PCD\\ \Delta NTG\\ \Delta KBP\end{bmatrix} \quad (85)$$

The turbine-generator speed response of the augmented reduced order model for a 5% DC load demand increase using this controller is shown in Figure 87. The performance is almost identical to the initial controller. By monitoring the actual bypass valve position, the controller is compensating for the difference between the actual and desired positions caused by the actuator dynamics. The new controller is applied to the full

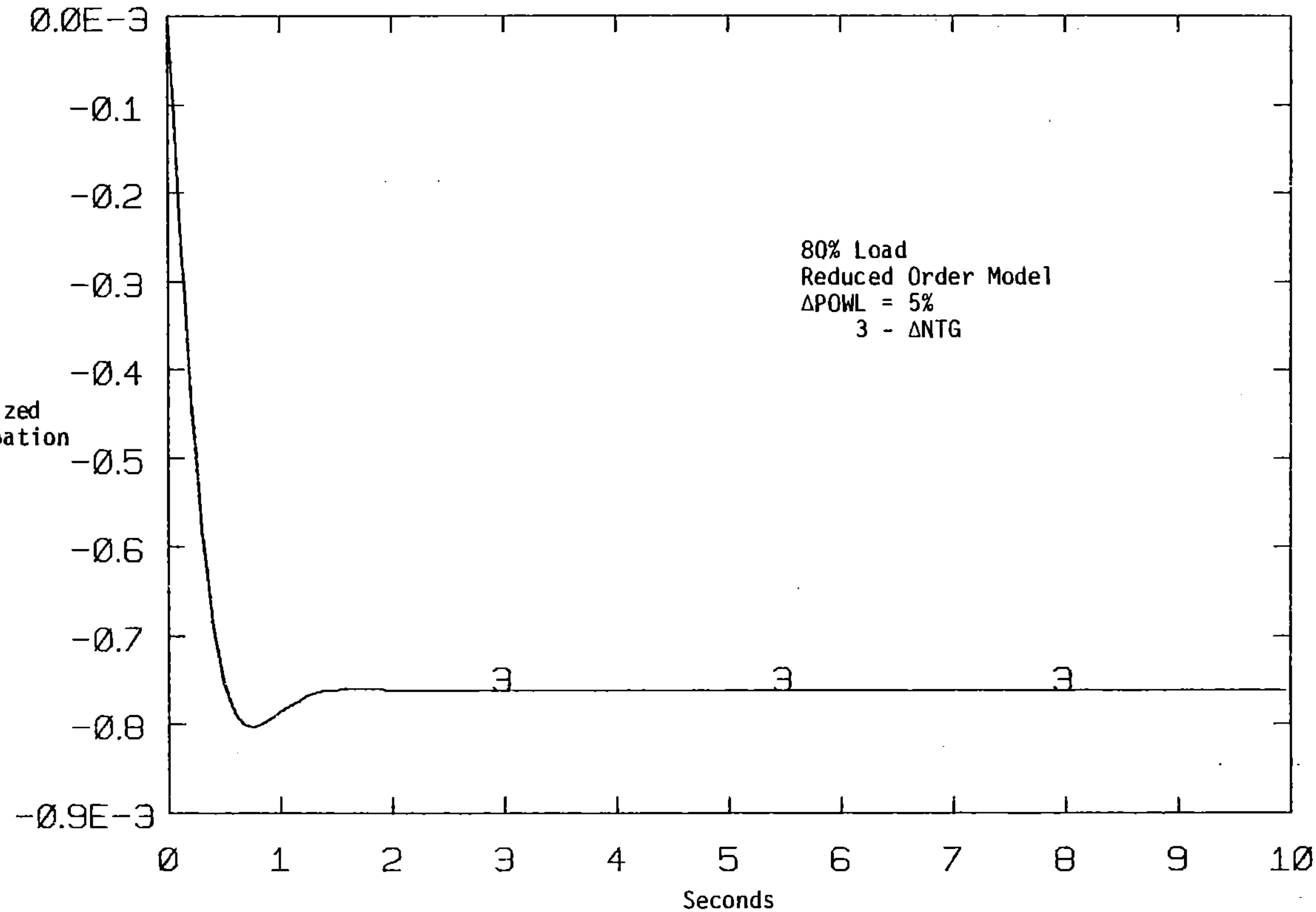

FIGURE 87: DC LOAD DEMAND DISTURBANCE-ACTUATOR COMPENSATED L-Q CONTROLLER

order OTEC model which is subjected to the same disturbance. The turbine-generator speed response, Figure 88, is almost identical to the reduced order case, except for the thermal effects. Figure 89 demonstrates quite well how the controller compensates for the actuator lag while Figure 90 shows the response of the rest of the system. The total system response is quite satisfactory.

The OTEC model at 40% and 10% load was subjected to the same 5% DC demand load disturbance to investigate the performance of the new state feedback controller at different load levels. The turbine-generator speed response at 40% load is shown in Figure 91, and for 10% in Figure 92. There is almost no difference in performance between any of the load levels, demosntrating that the L-Q state feedback controller is relatively insensitive to the operating level of the OTEC power plant.

The effect of seawater environment changes on the performance of the state feedback controlled system are studied. The OTEC plant is operating at 80% load and the warm seawater temperature experiences a 0.2% step decrease ($\approx 1°F$). The system response is given in Figures 93, 94, 95, and 96. The system responds as a whole almost identically as it did under speed governor control. The only differences are a slightly smoother response and a slightly larger turbine-generator steady-state speed error. This larger error is caused by the change in the steady state vapor pressures

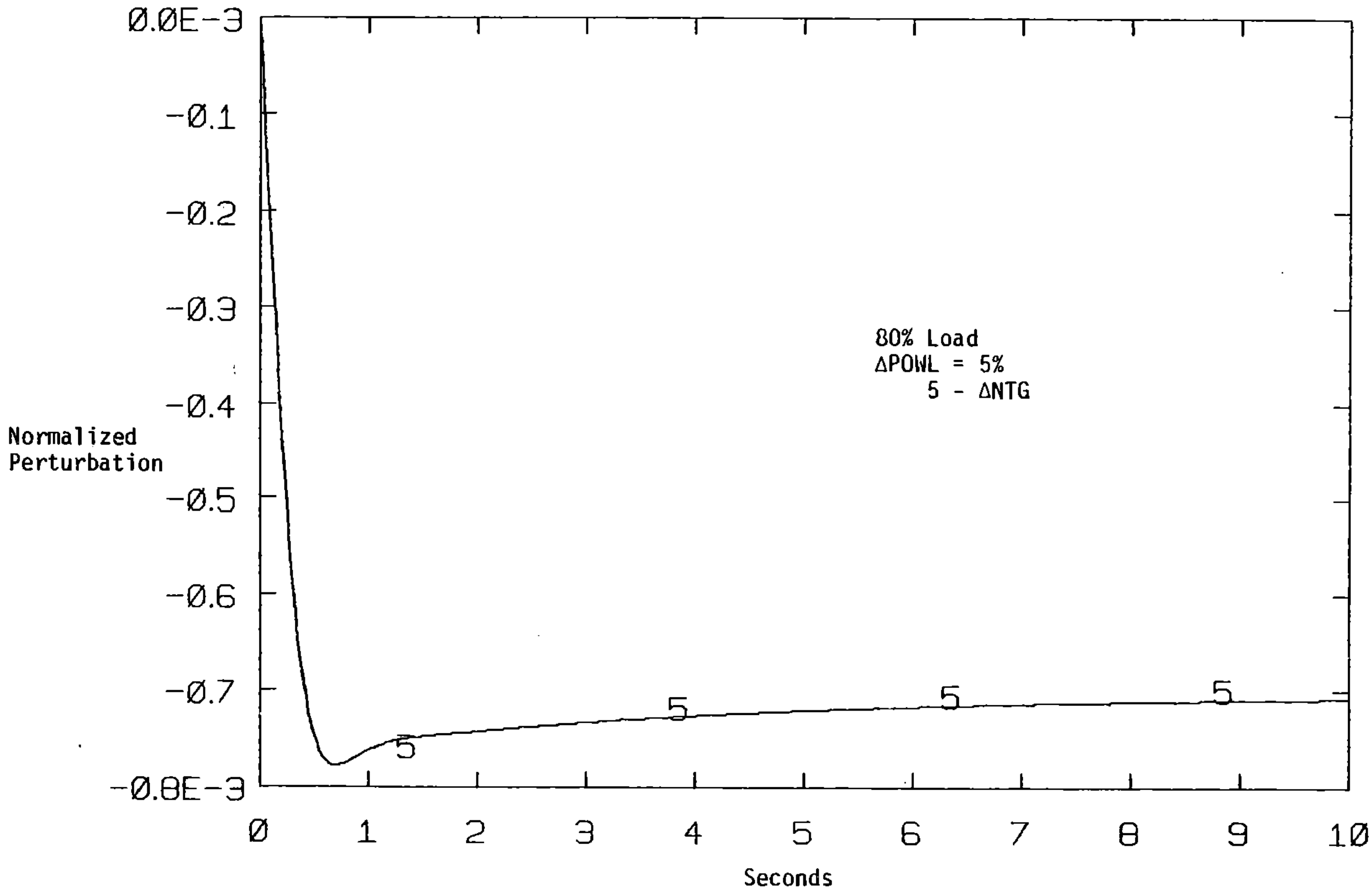

FIGURE 88: DC LOAD DEMAND DISTURBANCE-ACTUATOR COMPENSATED L-Q CONTROLLER

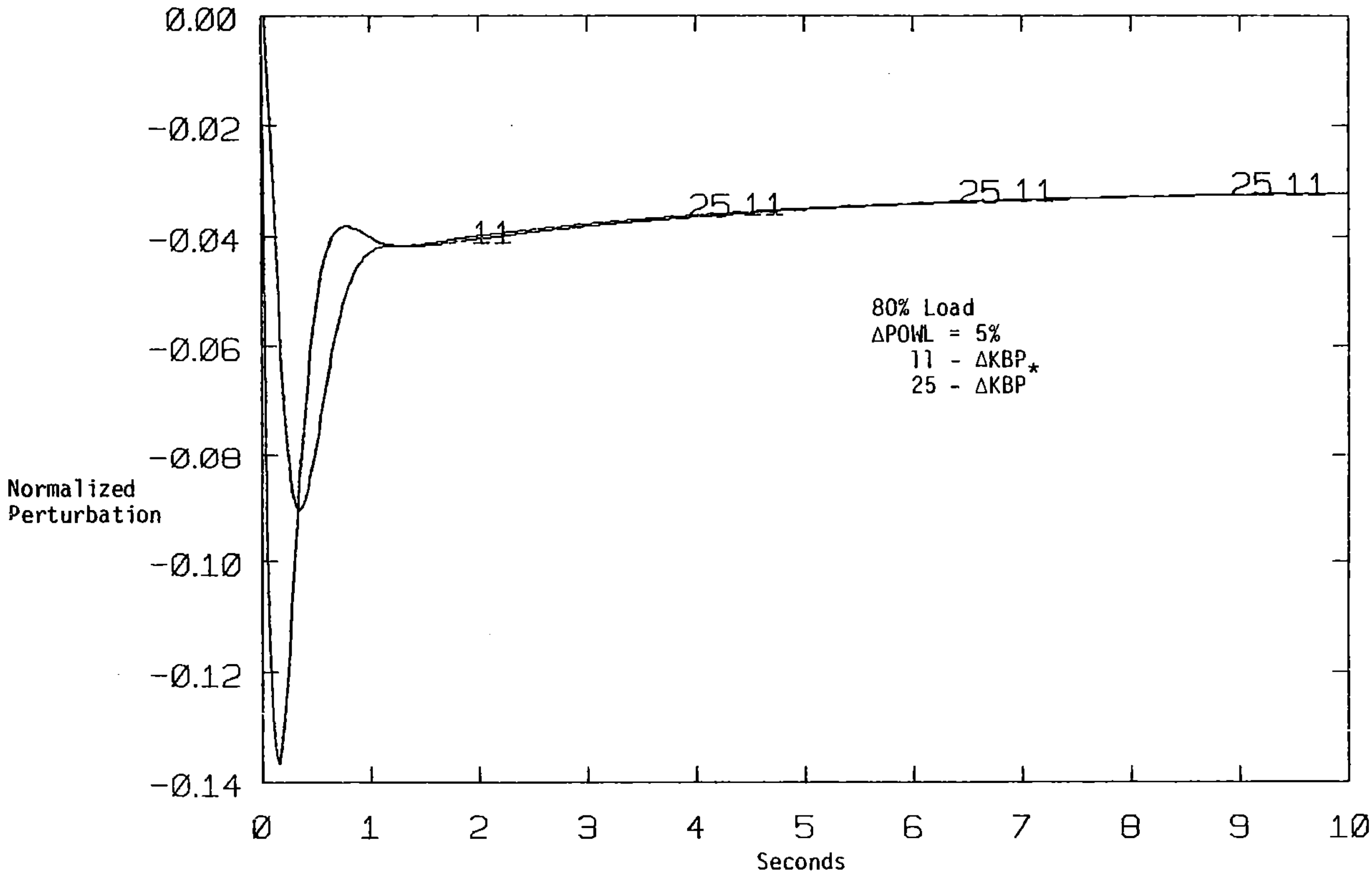

FIGURE 89: DC LOAD DEMAND DISTURBANCE-ACTUATOR COMPENSATED L-Q CONTROLLER

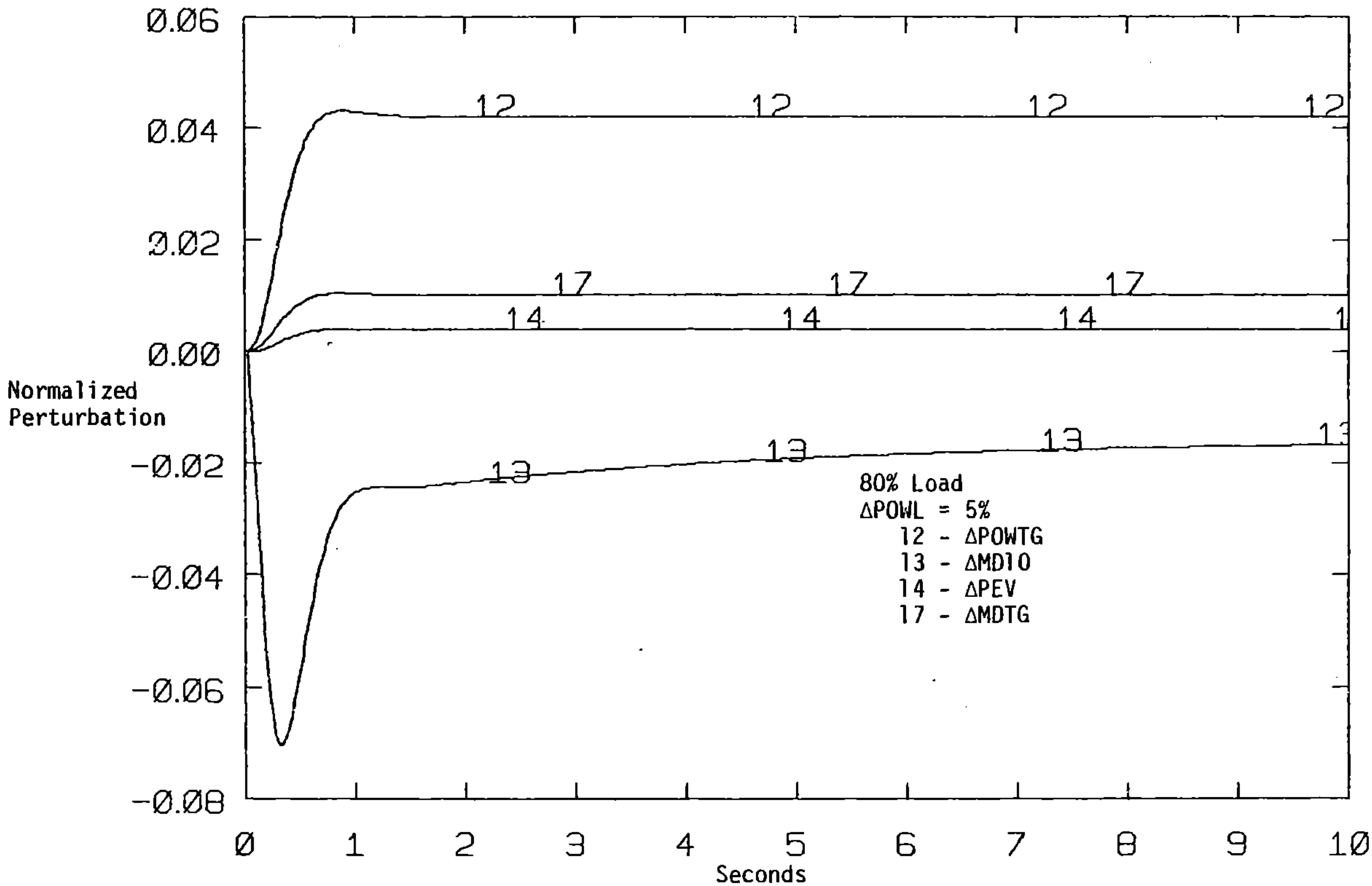

FIGURE 90: DC LOAD DEMAND DISTURBANCE-ACTUATOR COMPENSATED L-Q CONTROLLER

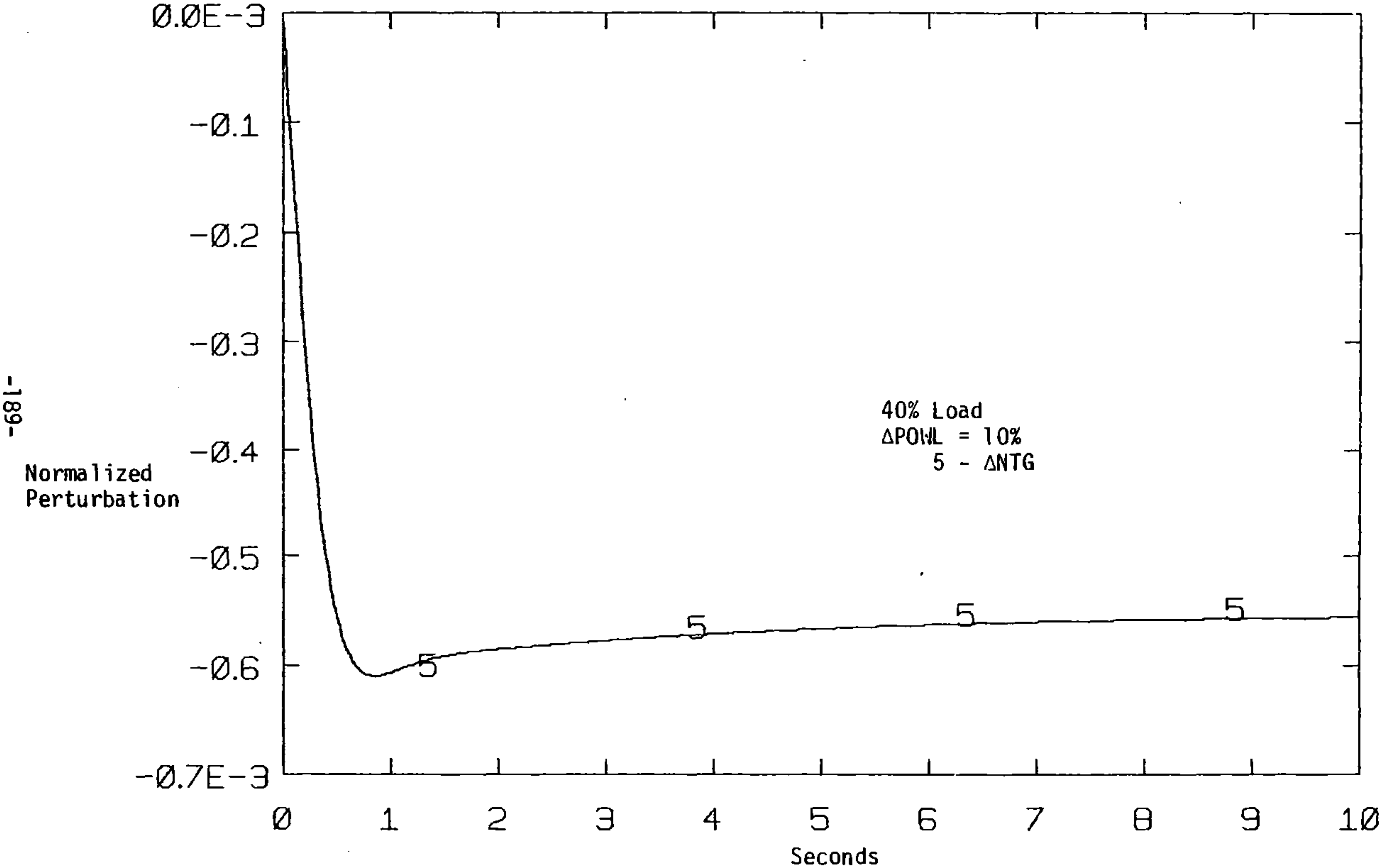

FIGURE 91: DC LOAD DEMAND DISTURBANCE-ACTUATOR COMPENSATED L-Q CONTROLLER

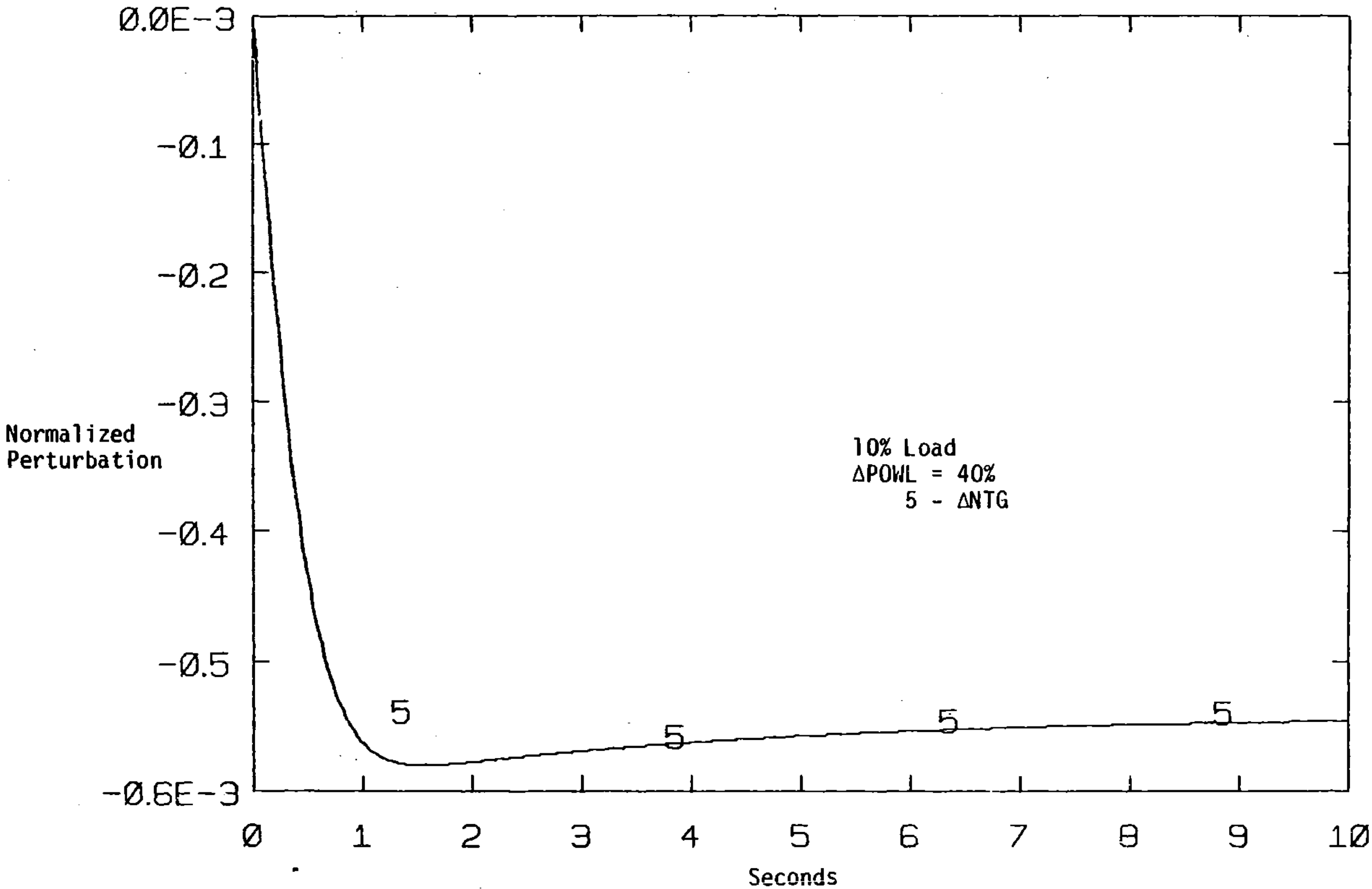

FIGURE 92: DC LOAD DEMAND DISTURBANCE-ACTUATOR COMPENSATED L-Q CONTROLLER

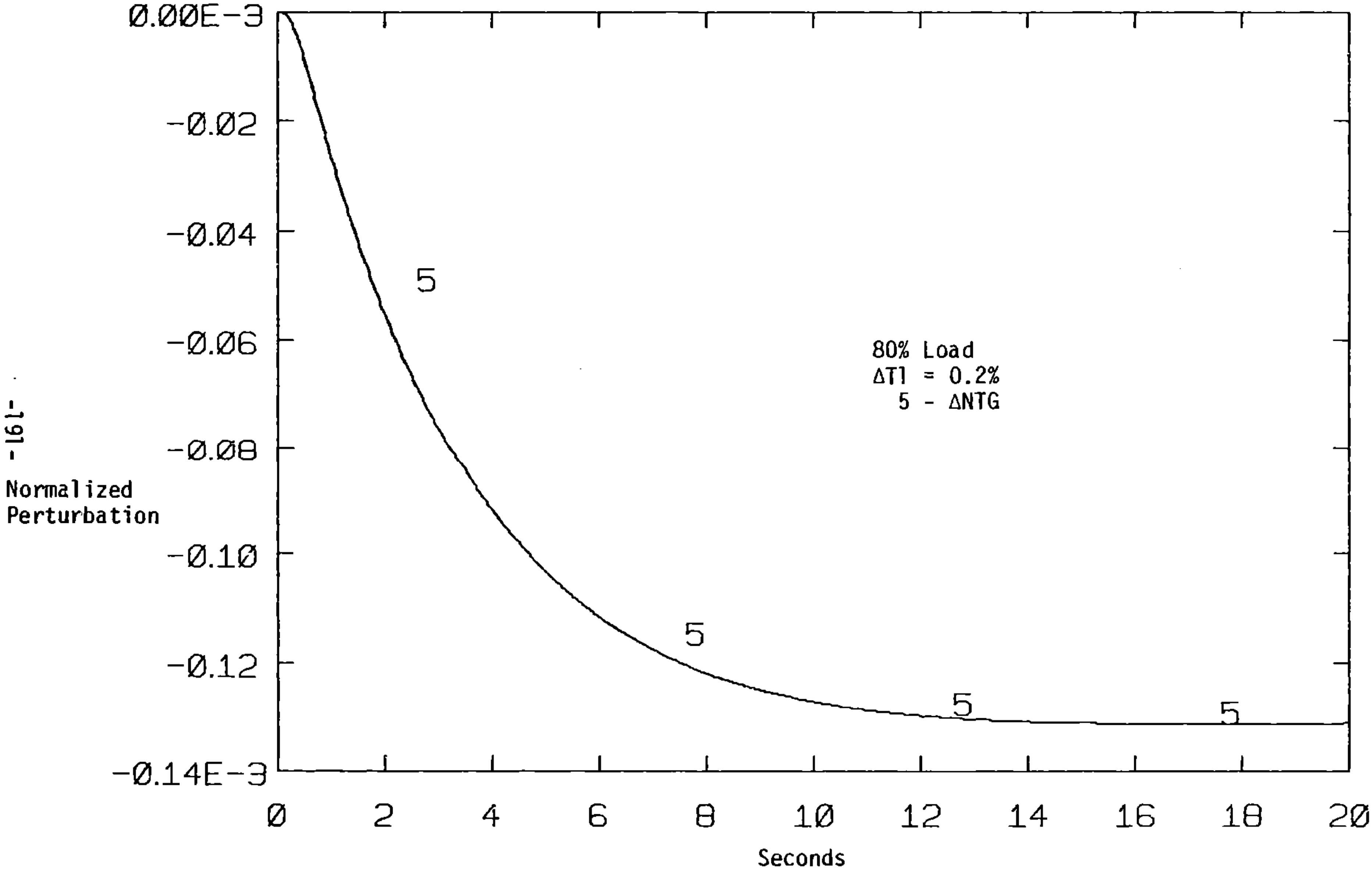

FIGURE 93: WARM SEAWATER TEMPERATURE DISTURBANCE-ACTUATOR COMPENSATED L-Q CONTROLLER

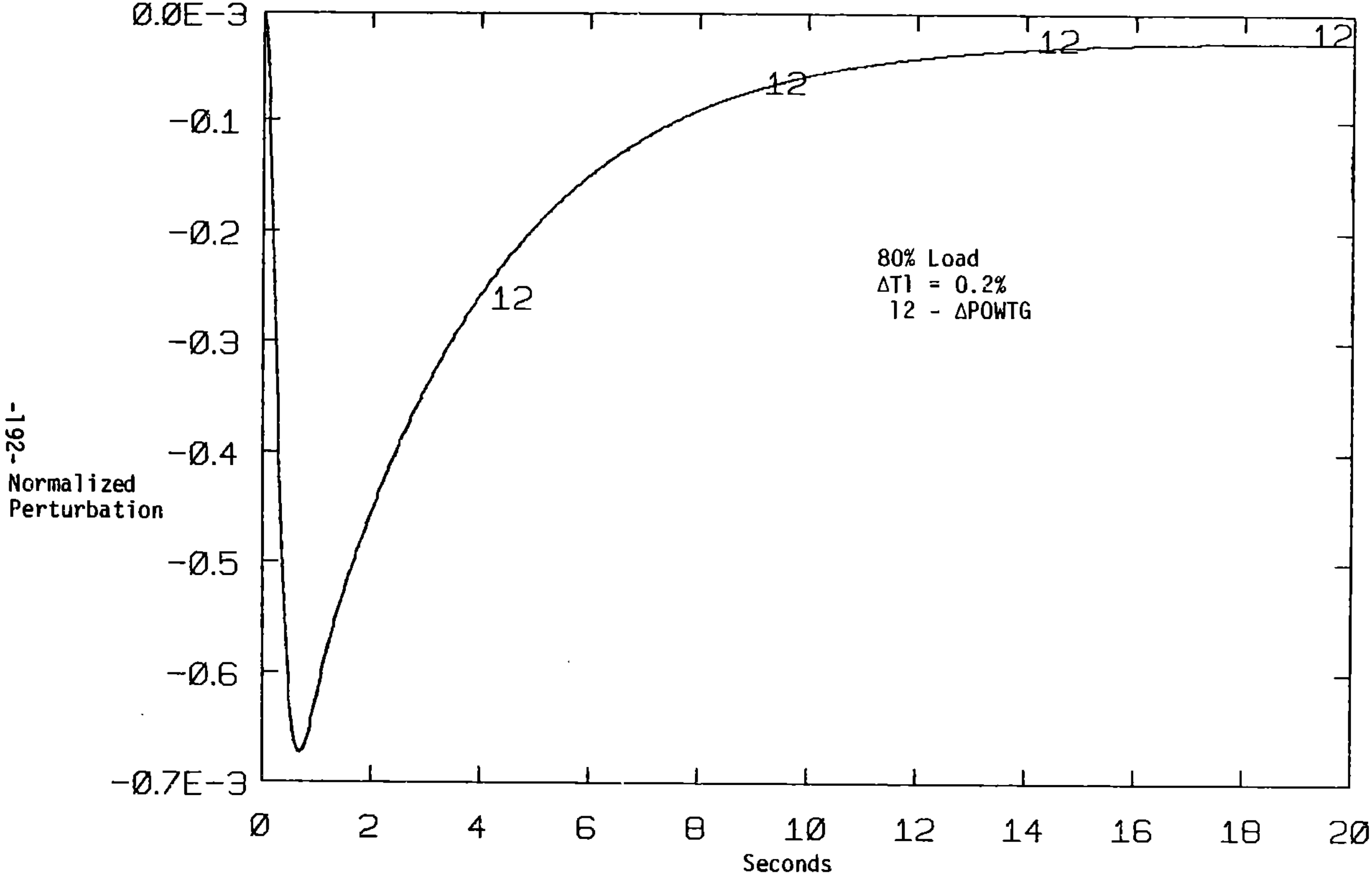

FIGURE 94: WARM SEAWATER TEMPERATURE DISTURBANCE-ACTUATOR COMPENSATED L-Q CONTROLLER

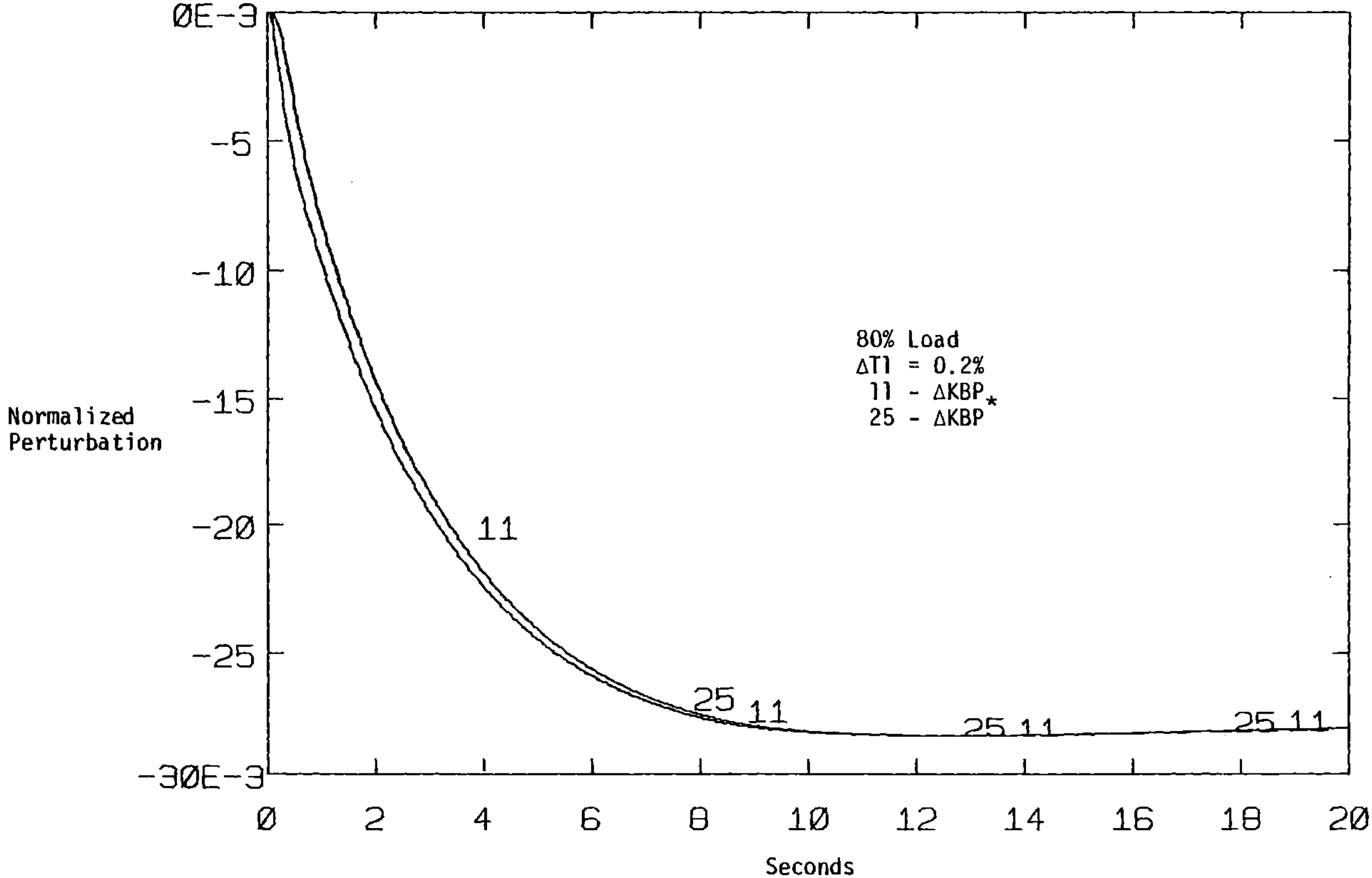

FIGURE 95: WARM SEAWATER TEMPERATURE DISTURBANCE-ACTUATOR COMPENSATED L-Q CONTROLLER

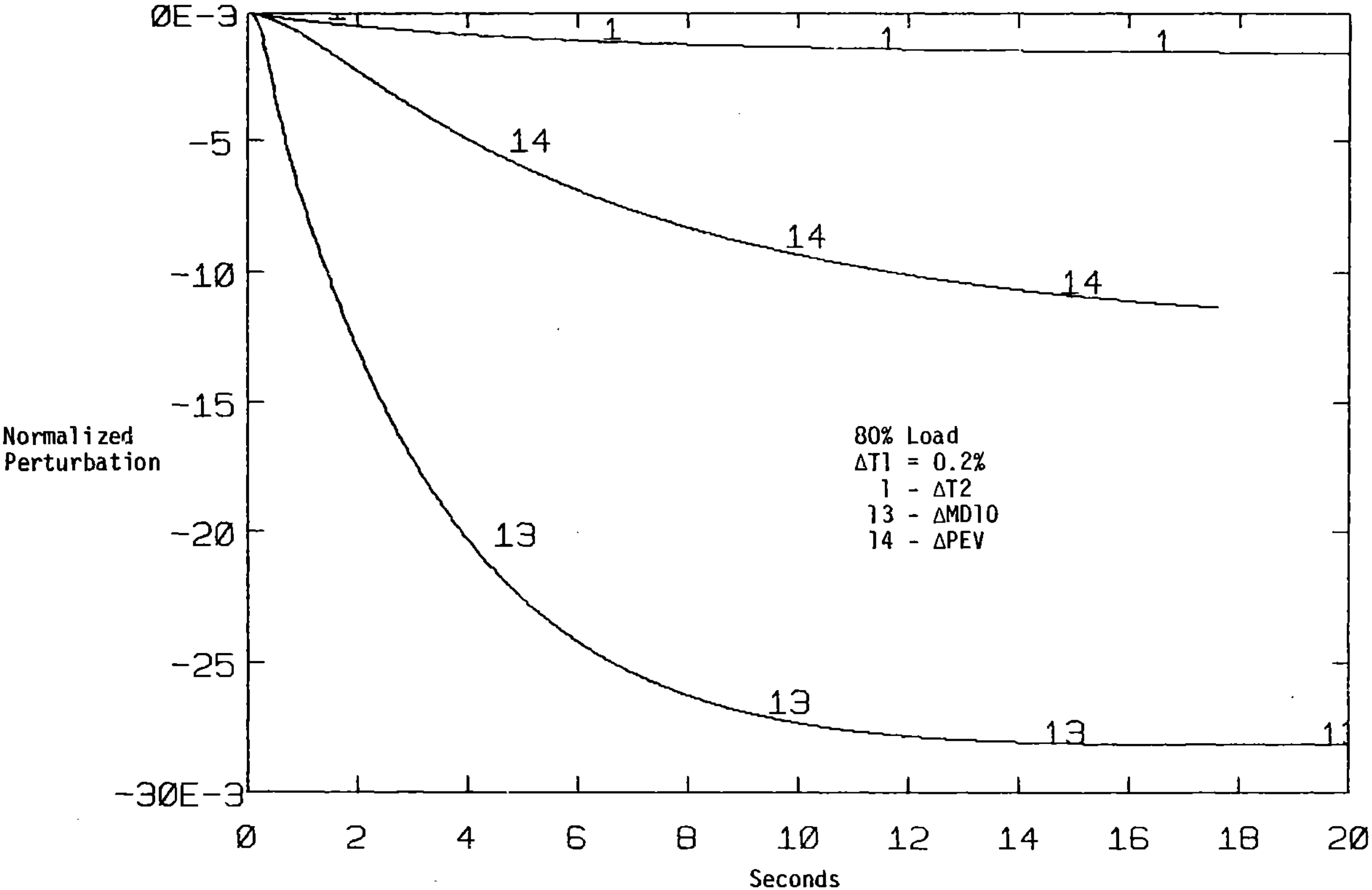

FIGURE 96: WARM SEAWATER TEMPERATURE DISTURBANCE-ACTUATOR COMPENSATED L-Q CONTROLLER

brought about by the seawater temperature changes; the error can be reduced by adjusting the pressure set points on the pressure state error feedback.

Although the state-variable feedback regulator tremendously improves the performance of the OTEC power plant, there are a few important points to consider before the controller can be implemented. As was previously demonstrated, the effect of unmodeled dynamics in the actual plant can severely degrade the system performance. Thus, any significant sensor dynamics can be a serious problem. Also, since the sensors (especially those measuring the vapor pressure) must be extremely sensitive, they become susceptible to "process noice", that is, random pressure waves occurring in the heat exchangers. This type of noise would cause undesirable reactions in the control system. This problem might be alleviated by the implementation of a state observer, or Kalman filter. Lastly, the state feedback controller requires evaluation of the steady state vapor pressures in the heat exchangers at various load levels in order that the pressure set points can be implemented for the state perturbation feedback.

The state-variable feedback control system can actually be implemented through a simple speed governor electro-hydraulic control system by using the feedback signals from the other states as trimming signals for the hydraulic actuator system. The steady state vapor pressure levels can be evaluated at the time of initial start up.

5.3.3 DC Load Control

When the OTEC power plant is operating at 100% load, it does not enjoy the same excess capacity capabilities as a conventional land based power plant. A conventional power plant operating at 100% load is able to meet load demand increases for short periods of time by increasing by the steam flow rate; however, the OTEC power plant operating at maximum load with bypass valve fully closed cannot meet any demands for increased power. If the OTEC plant is connected directly to a large AC power grid, the plant will essentially be self-regulating; the power grid will maintain the turbine-generator speed while accepting any and all power the OTEC system is able to generate. However, if the OTEC plant has DC power transmission to the shoreline, the DC power demand must be regulated to match the OTEC plant output; that is, DC load control of the OTEC power plant. This type of control is also necessary when the OTEC plant is operating near full load, since the bypass valve is only marginally open and will "saturate" at an increased load demand.

There are many examples of DC load control of the turbine-generator of a conventional power system in the literature.[21] The control signal which is based on the turbine-generator speed error acts as a trimming signal to the DC transmission system base-load power demand signal. A schematic diagram of the control system is shown in Figure 97. The control system acts to match the

DC power load to the generated power by sensing changes in the turbine-generator speed. The power trim signal function is designed identically to a turbine-generator governor, that is, there is a certain "droop" to the signal. This is represented as

$$\frac{\Delta P_{DC}}{\Delta w_{tg}} = - \frac{1}{\delta^*} \tag{86}$$

which is the feedback gain, or the change in DC power load for a given turbine-generator speed variation from the steady state level. The smaller the droop, the smaller the turbine-generator steady state error will be for a given load variation. Since the dynamic response of the DC power transmission system is extremely fast in comparison with the turbine-generator speed response, the droop can be designed for a very small steady state error without causing a reduction in stability.

The OTEC power plant operating at full load is subjected to a 0-10% step change in the bypass valve opening. The plant is under DC load control with a 5% droop. The system response is shown in Figures 98, 99, and 100. The response of all the system variables except the turbine-generator speed are identical to the open loop system with an identical disturbance (See Section 3.2.4). However, as the turbine-generator speed begins to drop because of the load mismatch, the DC load trim signal begins to reduce the DC

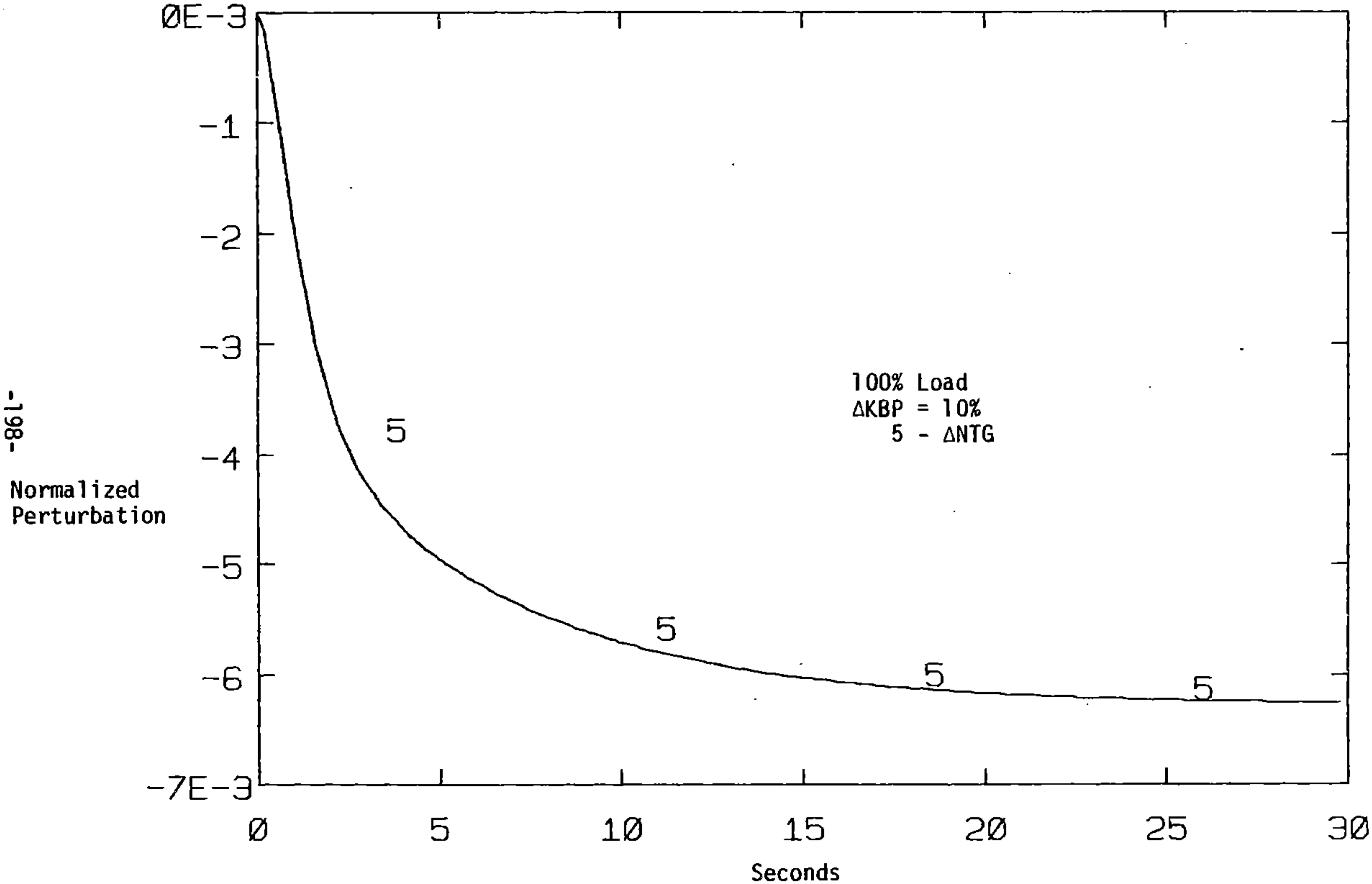

FIGURE 98: BYPASS VALVE OPENING DISTURBANCE-DC LOAD CONTROLLER

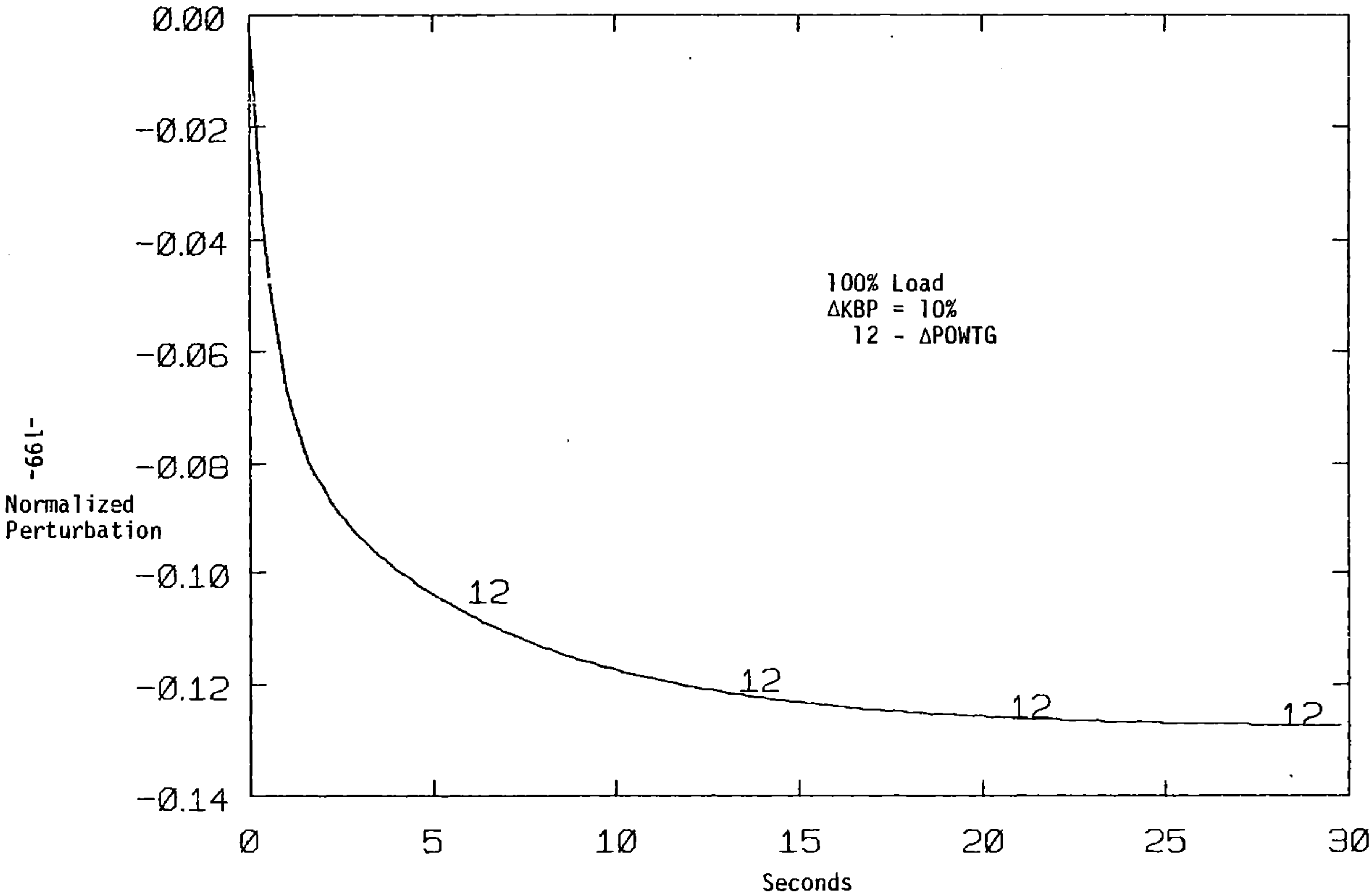

FIGURE 99: BYPASS VALVE OPENING DISTURBANCE-DC LOAD CONTROLLER

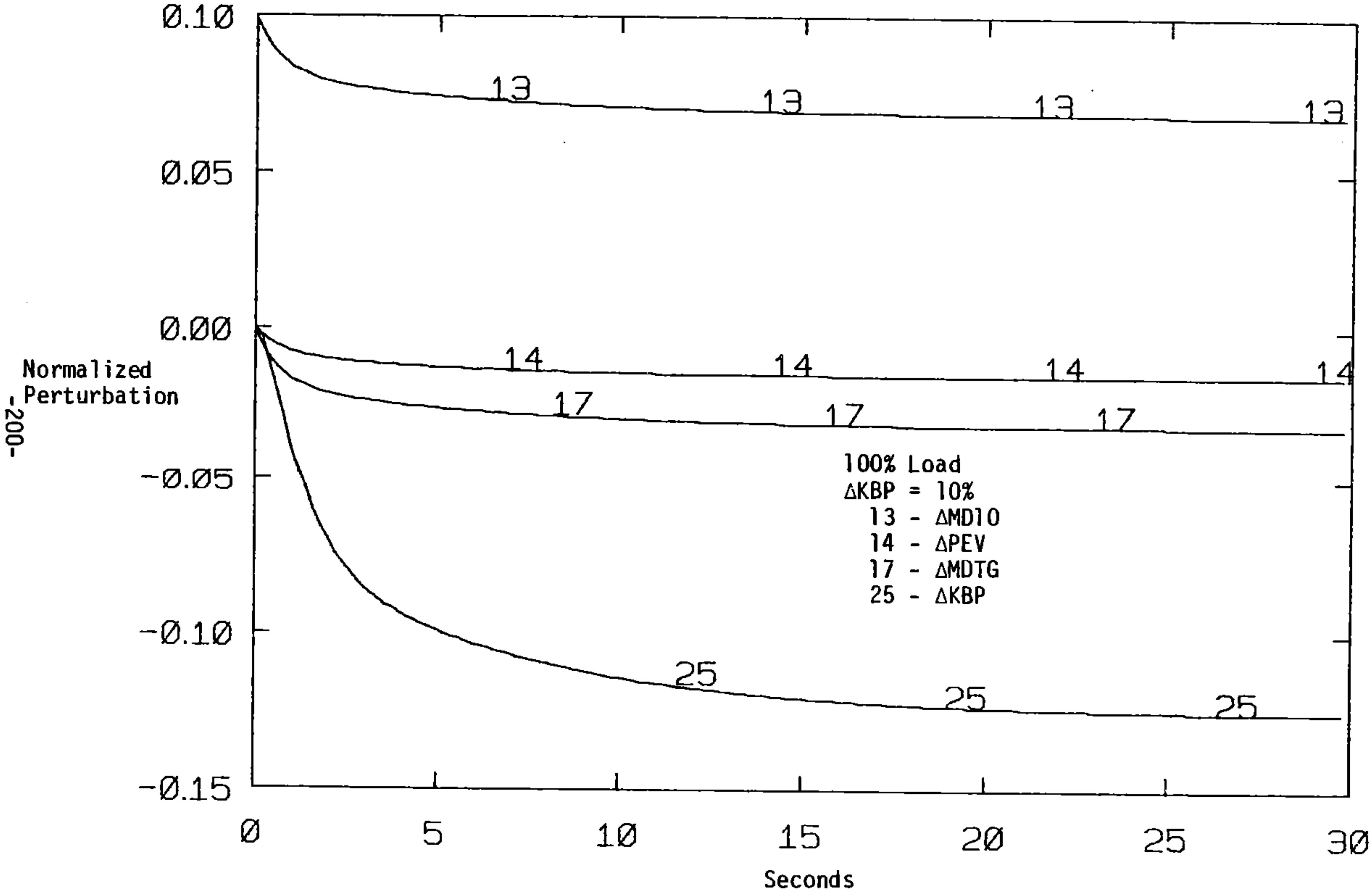

FIGURE 100: BYPASS VALVE OPENING DISTURBANCE-DC LOAD CONTROLLER

load in order to stabilize the turbine-generator speed. The turbine-generator speed stabilizes after about 10 seconds; the entire system requires about 30 seconds to reach a new equilibrium at a power level of -13%. The turbine-generator speed error is 0.65% or a 5% droop as designed. Thus, the DC load control does an effective job of regulating the OTEC plant at or near full load when the bypass valve is no longer an effective control mechanism.

5.4 Pump Motor Controls

The open loop dynamic analysis of the OTEC system demonstrated a need for some form of pump motor control to attenuate the power surges inherent in the warm water pumping system synchronous motors during large wave disturbances. The cold water pumping system, subjected to the same conditions, does not experience this surge problem and is therefore exempt from this study. The reason for this disparity is demonstrated more dramatically by the amplitude versus frequency plots in Figure 101 and 102 of the pumping power to wave height ratio for both the warm and cold water systems. This information is obtained from a transfer function analysis of the linear OTEC model. The cold water pipe fluid inertance has a large attenuating effect on the wave disturbances over the entire wave frequency range of interest. The warm water system does not contain any such fluid inertances and the wave disturbance effect is only attenuated at the high frequencies, where the wave heights are negligible to begin with.

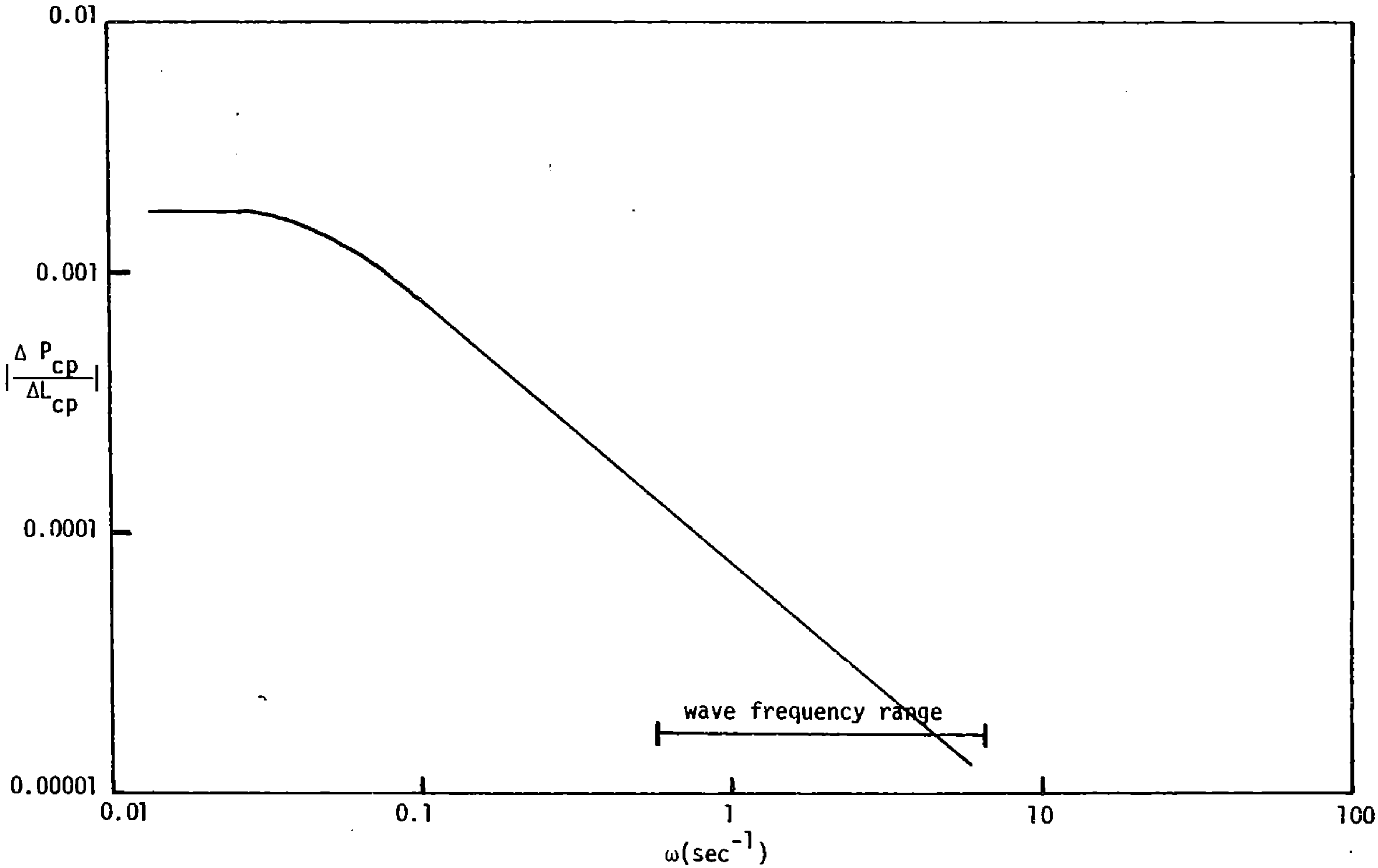

FIGURE 101: WAVE DISTURBANCE ATTENUATION OF COLD WATER SYSTEM

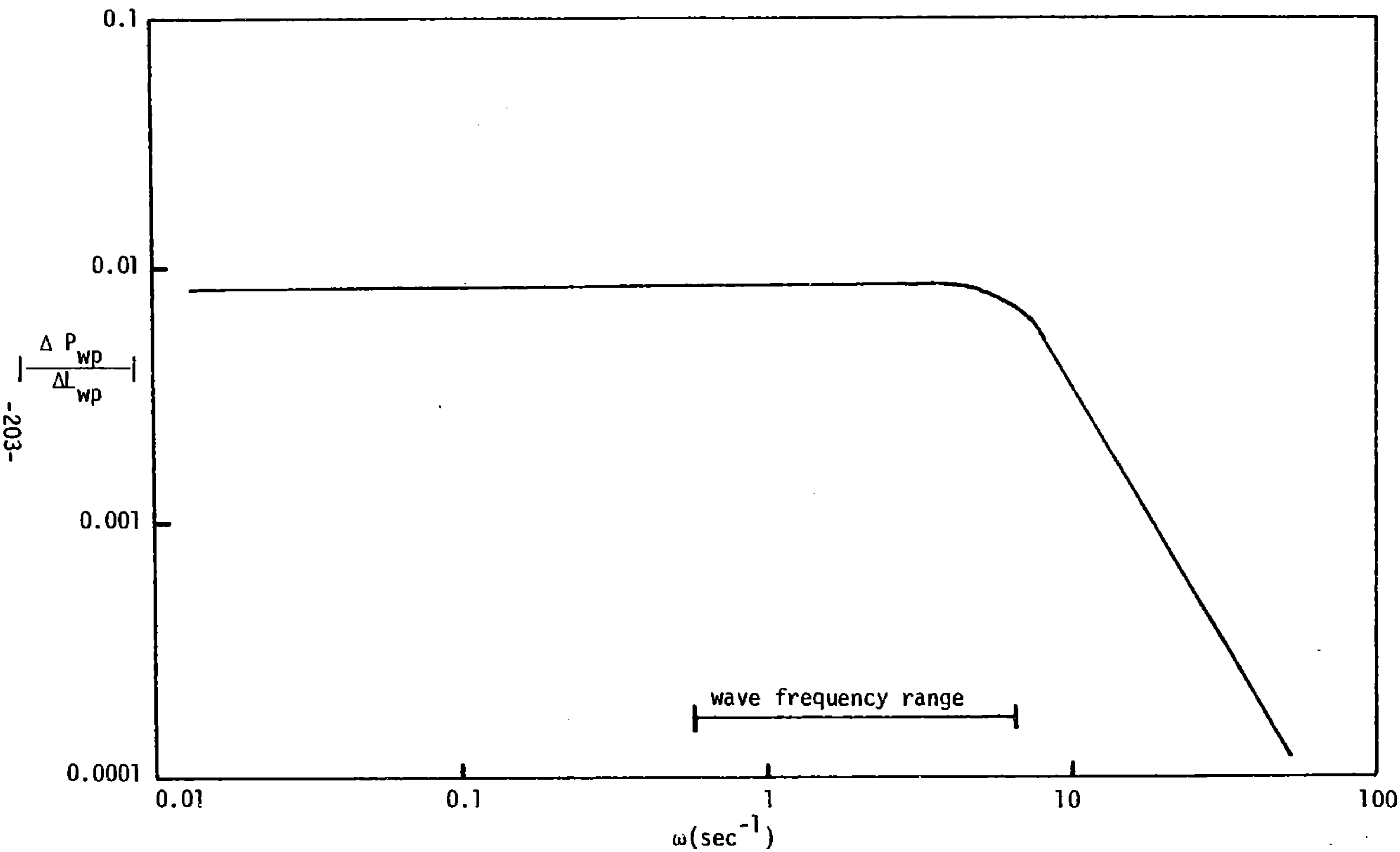

FIGURE 102: WAVE DISTURBANCE ATTENUATION OF WARM WATER SYSTEM

An open loop block diagram for the warm water pumping system is given in Figure 103.

The total variation in pumping power is composed of two components: a) the variation because of a wave disturbance, ΔP_{wp2}, and b) the variation as a result of a change in the pump motor set speed, ΔP_{wp1}. One method of controlling the total power fluctuations is to construct a feedback control system like the one shown in Figure 104. $H_1(s)$, obtained from the linear model of the OTEC plant, is

$$H_1(s) = \frac{K(\tau s + 1)}{\left(\frac{s^2}{\omega_n^2} + \frac{2\xi}{\omega_n} + 1\right)} \tag{87}$$

where

$$\tau = .1335 \text{ sec}$$
$$\omega_n = 6.32 \text{ sec}^{-1}$$
$$\xi = 0.42$$
$$K = 3.343$$

Since ΔP_{wp2} is already known as a function of the wave height and frequency, it is treated as a known disturbance. Letting the controller be a constant gain, K_c, a disturbance transfer function is obtained for the controlled system relating ΔP_{wp2} to ΔP_{wp}.

$$D(s) = \frac{\Delta P_{wp}}{\Delta P_{wp2}} = \frac{1}{1 + K_c H_1(s)} \tag{88}$$

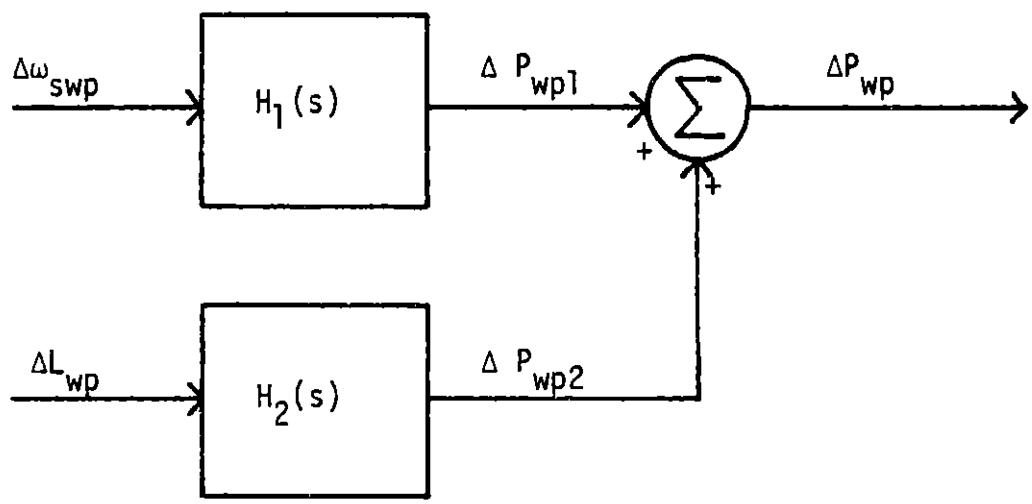

FIGURE 103: OPEN LOOP BLOCK DIAGRAM OF WARM WATER SYSTEM

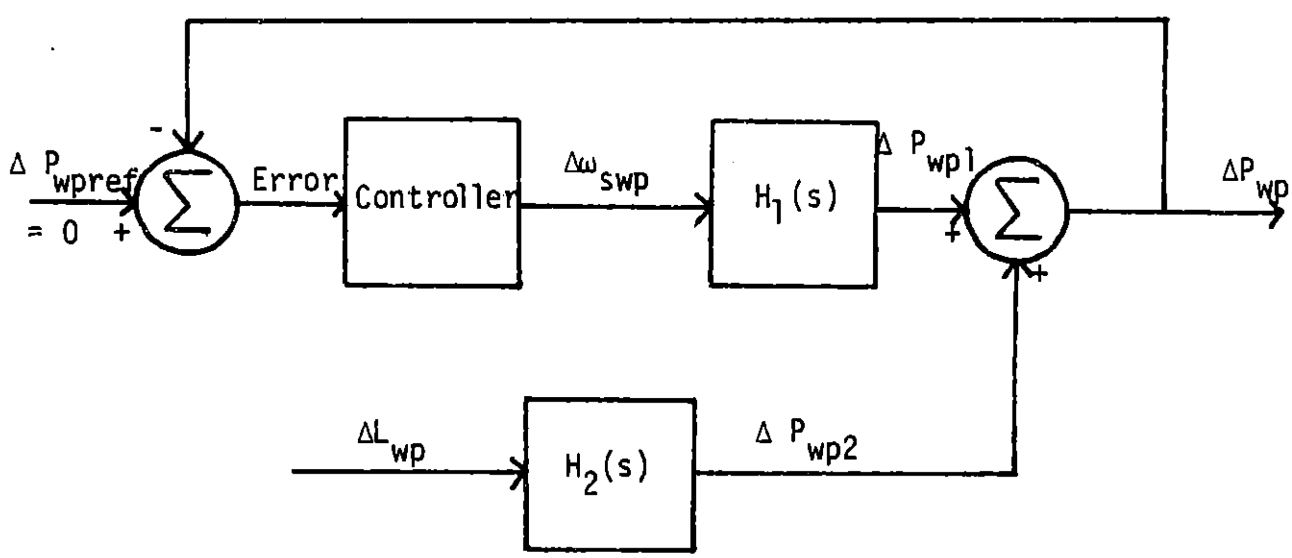

FIGURE 104: POWER FLUCTUATION FEEDBACK CONTROL SYSTEM

The magnitude of D(s) as a function of wave frequency (since the wave power disturbance fluctuates at the same frequency as the wave disturbance itself) is

$$D(s) = \left| \frac{\Delta P_{wp}}{\Delta P_{wp2}} \right| = \frac{\frac{1}{(1+K_c K)} \sqrt{\left(1 - \frac{\omega^2}{\omega_n^2}\right) + \left(2\xi \frac{\omega}{\omega_n}\right)^2}}{\sqrt{\left(1 - \frac{\omega^2}{(1+K_c K)\omega_n^2}\right) + \left[\left(\frac{2\xi}{\omega_n} + K_c K \tau\right) \frac{\omega}{(1+K_c K)}\right]^2}} \qquad (89)$$

The open loop analysis demonstrated that the largest pumping power surges occur for low frequency, high amplitude waves (Sea State 6). In this region, the disturbance transfer function can be approximated by ($\omega \to 0$)

$$|D(s)| = \left| \frac{\Delta P_{wp}}{\Delta P_{wp2}} \right| = \frac{1}{(1+K_c K)} \qquad (90)$$

The power surges caused by low frequency, high amplitude waves can be reduced by careful choice of the controller gain, K_c.

The pump motor control system is designed for an 80% reduction in the power variation during Sea State 6. This requires a controller gain of $K_c = 1.2$. The controlled warm water system is simulated during Sea State 6; the system response is shown in Figure 105. The total pumping power surge is reduced to 20% from

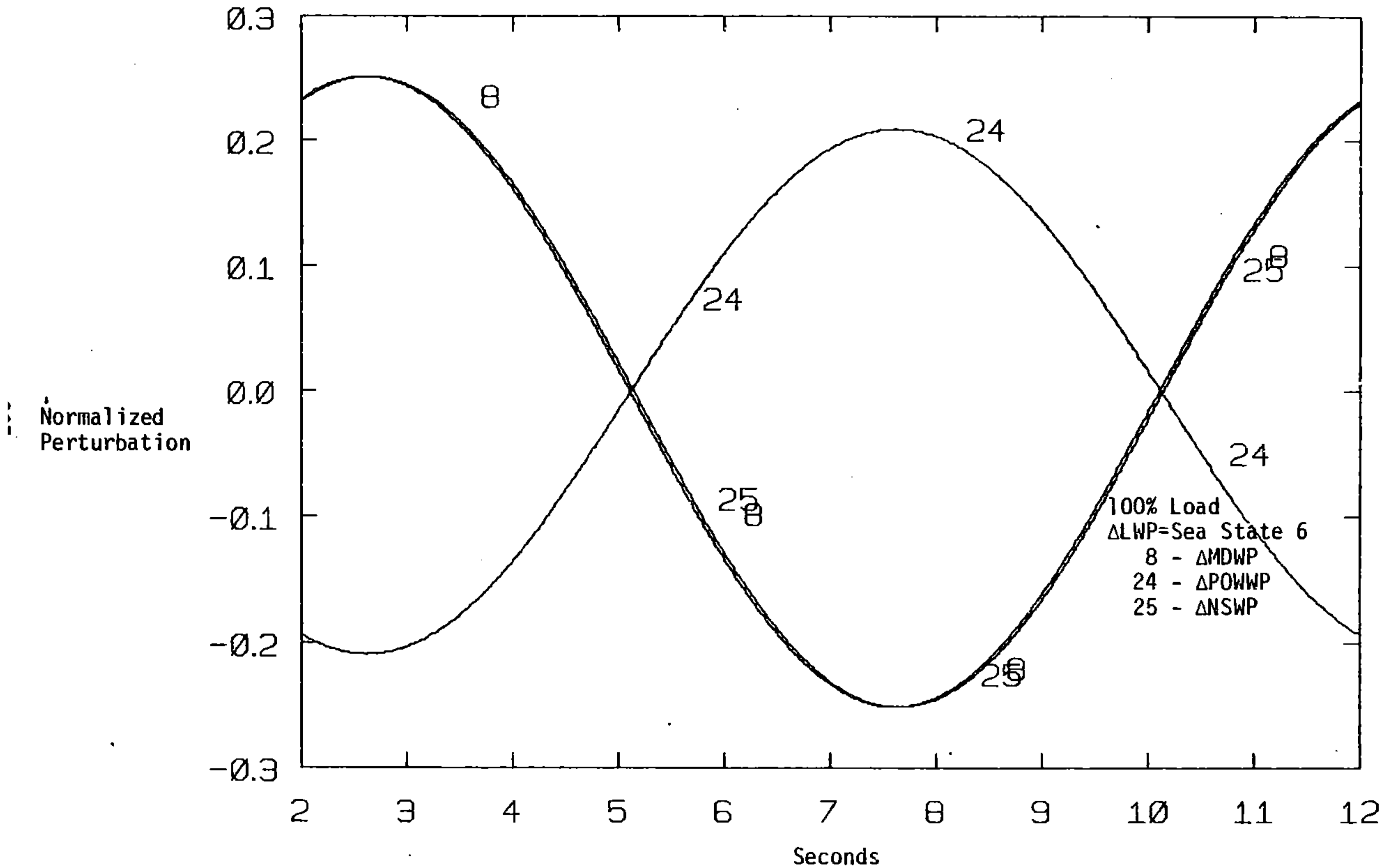

FIGURE 105: WARM WATER SYSTEM WAVE DISTURBANCE-POWER CONTROLLER

the 100% level of the uncontrolled system, or 2% of the total OTEC power output. The seawater flow variation has risen from 5% to 25%, which results in a 1.3% turbine-generator power fluctuation.

It is not known whether the pump motor frequency controller will have the capability to vary the pump speed by as much as the 20% required for this power controller design. The actual power controller gain will result from a design compromise between the pump motor frequency controller capabilities and the power surge limits of the OTEC power plant.

VI. DISCUSSION

Three major topics are addressed in this section. They are:

1) Start-up considerations for the OTEC power plant-consisting of start up of the plant subsystems and bringing the plant "on-line"

2) Set point control of the OTEC power plant-maximizing the power output for given environmental conditions

3) Special synchronization problems associated with the OTEC baseload power system consisting of 8 50 MW modules.

In each case the discussion centers on a qualitative analysis of each topic based on this research and prior research efforts. Quantitative analysis is used wherever applicable and whenever data exists for a particular topic.

6.1 OTEC Plant Start Up Considerations

The start up of the OTEC plant consists of sequentially activating each of the OTEC sub-systems in order to activate the vapor power loop, bringing the turbine-generate up to speed, subsequently linking the plant to the on-shore power grid and stabilizing it at the desired power level. Two on-board diesel generators are provided to supply the initial power to the principle sub-systems such as the water pumps and liquid ammonia pumps and also the various auxilliary systems necessary to plant start up. Once the cold and warm water systems are stabilized at the desired levels, liquid ammonia is admitted to the evaporator to initiate the vapor cycle. At this point there are two methods of controlling the unloaded turbine-generator speed: the liquid ammonia influx rate and the bypass valve. By opening the bypass valve completely, the liquid ammonia influx rate can be raised to the full load level and the turbine-generator is brought up to speed. However, this results in about 80% excess vapor production and severely restricts the movement of the bypass valve for speed control. By opening the bypass valve by 20-30%, the liquid ammonia influx rate is increased until the turbine-generator is brought up to speed. Under this situation, the evaporator is operating at burn-out conditions and the vapor mass flow rate is equal to the liquid influx mass flow rate. The bypass valve now has freedom of movement to control the turbine-generator speed.

Linking the OTEC plant to the on-shore AC power grid by direct AC transmission requires that the turbine-generator speed be synchronized with the AC bus frequency. This is accomplished by the turbine-generator speed control system. Once the two frequencies are synchronized, the main breaker is opened and the power plant is brought up to the required load by increasing the liquid ammonia influx rate and then closing the bypass valve. The AC bus acts to maintain the turbine-generator frequency. Based on the prior grid frequency analysis, the power rate limit should be 1 MW/sec to maintain a conservative stable response. Thus the plant can be brought from no load to full load in a minimum of 67 seconds, with an additional 20-30 seconds required for heat exchanger thermal stabilization.

A DC power transmission link to shore removes the need to synchronize the turbine-generator speed. The power plant can be brought to power in either the DC load or turbine-generator speed controlled mode. In the DC load controlled mode, the liquid ammonia influx rate is increased to the maximum level and the bypass valve closed to increase the power while the DC load is regulated to match the generator power. In the turbine-generator speed controlled mode, the liquid ammonia influx rate is increased to the maximum level resulting in the bypass valve increasing to the maximum opening to maintain a zero turbine-generator power output. The DC power load is then increased to the desired level while the speed controller maintains the generated power equal to the demand. The DC transmission system adds stability to the OTEC plant based on the step responses of the OTEC system to DC load demand changes. Thus, the power rate limit can be increased to about 2 MW/sec.

In conclusion, there do not seem to be any specific problems related to start-up of the OTEC power plant. However, since the liquid influx rate to the evaporator is used to control the power output while under "burn-out" conditions, it is necessary to know the response of the system to this type of process. This requires that both the steady state sensitivity and dynamic properties of the process be known. The steady state sensitivity of the turbine-generator power output to the turbine vapor flow rate is analyzed using the linear model and is given in Section 4.2; these can be used as a reasonable guideline assuming that the liquid ammonia mass influx always equals the vapor mass flow rate in the system. While this is true in the steady state for evaporator burn-out, it is not true during a transient. These dynamic features should be explored before full confidence in this method of start-up power control is obtained.

6.2 Set Point Control Considerations

The OTEC power plant will be operated as a baseload power station operating at the maximum power whenever possible since the "fuel" for the plant is supplied at zero cost. Thus, it is necessary to operate the OTEC power plant in a way as to maximize the power output under given environmental conditions. Conversely, when the plant is operating at less than full capacity, no consideration need be given to operating the power plant in an optimum fashion.

The optimization of the OTEC power plant in order to maximize the power output requires the seawater flow rates in the heat exchangers be adjusted according to such environmental variables as the seawater temperatures and the heat transfer loss resulting from biofouling of the heat exchanger tubes. This optimization process requires a detailed knowledge of the various sensitivities of the system obtained from a complex steady state analysis. This type of analysis is beyond the scope of this work. However, certain operational guidelines can be noted here. When the OTEC power system is directly connected to an on-shore AC power grid, the plant is essentially self-regulating. That is, the power grid will accept the entire output of the OTEC plant while maintaining the turbine-generator frequency essentially constant. Therefore, the optimization control system need only to maintain the plant at its maximum power through pump speed control. This brings up another important point. The turbine-generator speed governor for the OTEC plant directly linked to the on-shore AC grid can conceivably be omitted from the system. The principle aim of the speed governor on conventional power systems is to help match the power load of the grid with the power supply by indirectly monitoring the AC grid frequency. However, since the OTEC power plant is supplying the least expensive electricity available to the power grid, it would be more cost efficient to maintain the OTEC plant at full capacity while reducing the output of the other conventional power plants supplying the grid in response to a frequency increase. This could be accomplished by removing the turbine-generator speed governor from the OTEC plant and allowing it to be regulated by the AC power grid, always producing the maximum possible power. This would not be feasible for stability reasons if the OTEC power system were supplying a large fraction of the total load on the AC grid.

For the case of a DC transmission link to the on-shore AC power grid, the OTEC power plant would be under DC load control at maximum power output. The power optimization control system would maintain the plant output at the maximum possible level as environmental conditions vary while the load controller would regulate the DC load to match the OTEC plant output. Under this arrangement, the OTEC power supplied to the on-shore grid would always be maximized. If the OTEC system supplied a significant portion of the grid load, however, the DC load demand signal would need to be a function of the grid power demand to help maintain grid stability, and the OTEC plant would require operation under a turbine-generator speed governing system using the bypass valve as a control mechanism. As a result, the OTEC plant would require continuous operation at less than full load.

6.3 OTEC Baseload Power System Considerations

The OTEC baseload power system consisting of 8 50 MW modules requires some special operating considerations. When direct AC transmission to shore is used for the baseload plant, no significant problems are encountered. Each module can be synchronized and operated independently as 8 separate power plants. However, when DC ship-to-shore power transmission is used, some synchronization problems may be encountered. Because each of the power plants is tied to a common bus prior to DC conversion (removing the need for 8 separate DC links), the whole system must be synchronized and remain in synchronization during operation. The actual dynamics of this synchronized system are beyond the scope of this work; it is the opinion of the author that the following topics should be investigated before satisfactory operation of this system can be assumed:

1) the dynamics and stability of this type of synchronous system

2) the effect on synchronization of independent governor control of the turbine-generator speed for each module

3) the effect of wave induced pump and turbine generator power surges on the synchronous system

4) the effect on synchronization of each power module operating at different power levels

5) the effect of a frequency controlled DC link used to control the baseload power system at full load when bypass valve control is no longer possible

VII. CONCLUSIONS

The principle conclusion of this work is that the OTEC power system can be efficiently and satisfactorily controlled when interfaced with a large on-shore power grid, regardless of whether the connection is direct or via a solid state AC/DC rectifier/inverter transmission system. This work has also shown that the dynamics of the power plant are the most important factor in designing an effective control system - that while a steady state analysis is important in optimizing individual components and the system as a whole, it is the transient dynamic characteristics which ultimately determine the stability and feasibility of operation of the OTEC plant as a whole. In an environment void of outside disturbances, a steady state analysis would be all that is required for successful operation of the OTEC plant; in the environment that actually encompasses the OTEC plant, actual steady state operation is rarely if ever realized.

The OTEC plant has two principle modes of control: relatively rapid control in response to sudden, unexpected disturbances and slow, deliberate control in order to maximize power output in response to long term environmental changes. The rapid control is shown to be handled adequately by the turbine bypass valve under part load conditions and by the DC transmission system while the plant is operating at full load. The seawater system pumps are the principle means of maintaining the OTEC plant at the maximum possible power output in response to changing long term environmental conditions.

For the OTEC plant directly interfaced with the on-shore AC power grid, a simple turbine-generator governor is able to control the power output of the plant in response to bus frequency disturbances. While operating at full load, the OTEC plant no longer has an overload capability; however, if the AC power grid is composed of several conventional land-based power plants which have this capability, this should not affect the stability of the AC system. It must be noted that the stability of the synchronous system of an individual turbine-generator is usually maintained by regulation of the generator field current, which is not included specifically in the model used for this analysis. However, the analysis did show a decreasing stability margin of the synchronous system at reduced loads which should be vital in the design of the synchronous controller.

The OTEC power plant which is interfaced with the AC power grid through a DC transmission link can also be efficiently controlled by a simple turbine-generator speed governor at part load capacity. The major portion of a transient initiated by a load disturbance is stabilized in 6-8 seconds by the speed governor. A considerable improvement over this performance is achieved by using a multi-state variable feedback control system designed by linear-quadratic methods. This type of controller is capable of stabilizing the system in approximately 2 seconds following a load disturbance. Both types of control systems perform equally as well in response to sudden environmental changes, stabilizing about 5-8 seconds following the disturbance. DC load control is a satisfactory means of controlling the OTEC plant when it is operating at maximum capacity. Plant stability is achieved in approximately 10 seconds following a disturbance for this type of control.

The dynamic response of the controlled OTEC power plant is characterized by two distinct transients: a) the initial response in which the controller acts to maintain system stability in the event of a rapid disturbance and b) the long term system response which is the result of the OTEC system adjusting to a new thermal equilibrium. The initial response is that previously mentioned-lasting from 2 to 8 seconds following the disturbance, depending upon the type of controller used. The long term system response is characterized by the slow variations of the temperatures and pressures in the heat exchanges as they reach a new thermal equilibrium following the disturbance and the subsequent control action. This adjustment usually requires 20-30 seconds. Thus, the controlled OTEC plant reaches a new steady state in a maximum of 30-40 seconds following the initial environmental or load disturbance.

Because the OTEC power plant has no overload capabilities, the bypass valve becomes an increasingly ineffective means of controlling the plant at near maximum loads. For disturbances of sufficient magnitude, the bypass valve will "saturate" or become fully closed even though the control signal is demanding more control action. This will not present a problem for the direct AC interfaced OTEC plant since the fully closed bypass valve will only result in the plant reaching its maximum power limit. The DC interfaced power plant will experience a degradation in the controlled system response because of this saturation effect and could possibly destabilize the system if the disturbance were large enough that the power plant could not match the load even with a fully closed bypass valve. Therefore, care must be taken when operating in this range under bypass valve control. The analysis also shows that the state-variable control is more susceptible to saturation than ordinary speed governor control-the maximum bypass valve position variation for a given load change is about 30% greater under state-variable control. As a result, it would probably be wise to operate under DC load control when the plant capacity exceeds 90% load in order to avoid bypass valve saturation problems.

The seawater system pumps will not be affected by disturbances in the AC system supplying them with power because the variable frequency AC/DC link essentially decouples the two systems. Thus, degradation in the AC bus frequency or voltage will not affect the DC plant power output in this manner. The ammonia liquid feedpump, powered directly from the AC bus through an induction motor, will be affected by AC bus frequency or voltage degradation. However, the plant output will not be affected unless the liquid ammonia influx into the evaporator is reduced sufficiently to cause burn-out of the evaporator tubes.

The pumping power surges resulting from wave disturbances will have no effect on the OTEC power plant when the system is directly linked to the large on-shore AC power grid which can absorb these power fluctuations unnoticed. However, the DC interfaced OTEC system will experience these power surges directly since the power can only be transmitted in one direction through the DC link to shore. If the power surges are controlled, they will not cause a serious problem with system control because the maximum power variations occur at the lowest wave frequencies. To avoid this problem altogether, two solutions are possible:

1) Running a separate AC power line from the on-shore power grid specifically to power the seawater system pumps. Since this addition will remove the need for the auxilliary start-up diesel generators, it would be very close to being cost effective also.

2) Operating the pumps under constant power. The open loop analysis shows that the turbine-generator power fluctuations resulting from pump operation in this mode would be small and of low frequency, thereby causing no system control problems. This mode of operation could be made feasible by the AC/DC pump motor control system.

A separate AC power transmission link from shore for the seawater pumps and other auxilliaries would also preclude the necessity of a complete system shutdown in the event of a loss of load accident. If the entire OTEC plant including auxilliaries were operating from a common bus, the loss of the on-shore load requires that all systems tied to the common bus be shut down to avoid overload of the electrical circuits because of the sudden increase in power. A separate AC link would reduce tremendously the time required for bringing the OTEC system back "on-line" following a loss of load by maintaining the operation of the sea-water pumps and other auxilliary systems.

The direct continuation of this present work has been undertaken concurrently with this project: development of a large multi-state variable nonlinear model of the OTEC power plant to verify and extend the results of both the open and closed loop analysis covered in this work. This will become an important factor when control of the system requires rapid and large variations in the bypass valve opening in response to large disturbances. The linearized perturbation analysis may become totally inadequate for substantial variations from the steady state. A related and also important consideration not covered in this work which should be analyzed closely is the effect of burnout and flooding of the evaporator during transients, another consequence of large and rapid changes in the system. These conditions, should they exist in the evaporator during a transient, would tremendously alter the dynamic performance of the plant and could result in sluggish or unstable controlled response of the entire OTEC system.

Some aspects of the seawater pumping systems should be investigated further. A more detailed model of the warm water system should be developed to investigate in greater scope the effects of surface waves on the system. Because the entire system is totally submerged, there may be some further attenuating effects on this disturbance. Also, fluid inertia effects should be included into the model. A more detailed model of the cold water system should be developed to include the effects of each of the eight condenser systems operating independently. A preliminary study revealed sudden flow surges in the system as a result of independent pumping action.

REFERENCES

1. Ocean Thermal Energy Conversion: Power System Development, Phase 3, Westinghouse Electric Corporation, prepared for D.O.E., 1978.

2. Ocean Thermal Energy Conversion: A State of the Art Study, M.I.T., principal investigator: A. Douglas Carmichael, prepared for EPRI, 1979.

3. Owens, W.L., "OTEC System Response and Control Analysis", 6th OTEC Conference, Washington, D.C., 19-22 June 1979.

4. Richards, D., P.J. McEvaddy, and L.L. Perini, "Off-Design Performance and Control Considerations for an OTEC Plant-ship", 6th OTEC Conference, Washington, D.C., 19-22 June 1979.

5. Westinghouse, p. 6-6.

6. Sotelo, José, Ph.D. Thesis Research, M.I.T., 1980.

7. Rego, Macedo, Reynaldo Browndo, A Reduced Order Model for An Ocean Thermal Energy Conversion Plant, M.S. Thesis, M.I.T., 1980.

8. Profos, Paul, Die Regelung von Dampfanlagen, Berlin, Springer, 1962.

9. Masada, Glenn Y., Modeling and Control of Power Plant Boiler-Turbine-Generator Systems, Ph.D. Thesis, M.I.T., 1979.

10. Masada, Chapter 3.

11. Rohsenow, Warren M., and Harry Choi, Heat, Mass, and Momentum Transfer, New Jersey, Prentice-Hall, Inc., 1961.

12. Gould, Leonard Abraham, The Dynamic Behavior and Control of Heat Transfer Processes, Ph.D. Thesis, M.I.T., 1953.

13. Stodola, A., Steam and Gas Turbines, Vol. 1, New York, Peter Smith, 1945.

14. Westinghouse, p. 6-30.

15. Fitzgerald, A.E., Charles Kingsley, Jr., and Alexander Kusko, Electric Machinery, New York, McGraw Hill, 1971.

16. Kimbark, Edward Wilson, Direct Current Transmission, Volume I, New York, Wiley-Interscience, 1971.

17. Connor, Jerome, D., and S. Shyam Sunder, Wave Theories, Wave Statistics, and Hydrodynamic Loads, Dept. of Civil Eng., M.I.T., 1980.

18. Hetyei, Steven Alexander, Dynamic Modeling, Simulation, and Control of Ocean Thermal Energy Conversion Power Plants, Ph.D Thesis, Carnegie-Mellon University, 1979.

19. Westerberg, Arthur W., Shichune Yao, Stephen J. Jennings, and William H. Coleman, "Dynamic and Off-Design Analysis of OTEC Conference, Washington, D.C., 19-22, June 1979.

20. Kwakernaak, Huibert, and Raphael Sivan, Linear Optimal Control Systems, New York, Wiley-Interscience, 1972.

21. Thal-Larsen, H., Dynamics of Heat Exchangers and Their Models, Journal of Basic Eng., June 1960.

APPENDIX I

I. EVAPORATOR ANALYSIS - AMMONIA VAPOR SIDE[21]

Liquid Mass Balance

$$\frac{d}{dt}\left(\overset{1}{\cancel{m_{\ell tr}}} + \overset{2}{\cancel{m_{\ell f}}} + \overset{3}{\cancel{m_{\ell sh}}}\right) = \dot{m}_{\ell in} - \dot{m}_{\ell out} - \dot{m}_{\ell v} - \overset{4}{\cancel{\dot{m}_{\ell vsh}}} \qquad (1)$$

Assumptions

1) no liquid storage tray
2) neglect liquid film mass
3) constant liquid level
4) no flashing of liquid in storage

therefore,

$$\dot{m}_{\ell out} = \dot{m}_{\ell in} - \dot{m}_{\ell v} \qquad (2)$$

Vapor Mass Balance

$$\frac{dm_v}{dt} = \dot{m}_{\ell v} + \overset{4}{\cancel{\dot{m}_{\ell vsh}}} - \dot{m}_{vout} \qquad (3)$$

therefore,

$$\frac{dm_v}{dt} = \dot{m}_{\ell v} - \dot{m}_{vout} \qquad (4)$$

Energy Balance

$$\frac{d}{dt}\left(m_v h_v + \cancelto{2}{m_{\ell f}} h_{\ell f} + \cancelto{1}{m_{\ell tr}} h_{\ell tr} + \cancelto{5}{m_{\ell sh}} h_{\ell sh}\right) = \dot{Q}_{net} \tag{5}$$

$$-\dot{m}_{vout} h_{vout} - (\dot{m}_{\ell out} h_{\ell out} - \dot{m}_{\ell in} h_{\ell in}) \tag{5}$$

5) neglect heat capacity of liquid storage

$$\frac{d}{dt}(m_v h_v) = \dot{Q}_{net} - \dot{m}_{vout} h_{vout} - \dot{m}_{\ell out} h_{\ell out} + \dot{m}_{\ell in} h_{\ell in} \tag{6}$$

using Equation (2)

$$\frac{d}{dt}(m_v h_v) = \dot{Q}_{net} - \dot{m}_{vout} h_v + \dot{m}_{\ell v} h_{\ell out} + \dot{m}_{\ell in}(h_{\ell in} \cancelto{6}{-} h_{\ell out}) \tag{7}$$

6) neglect enthalpy flux of liquid film

Rewriting Equation (7)

$$m_v \frac{dh_v}{dt} + h_v \frac{dm_v}{dt} = \dot{Q}_{net} - \dot{m}_{vout} h_v + \dot{m}_{\ell v} h_{\ell out} \tag{8}$$

using Equation (4)

$$m_v \frac{dh_v}{dt} = \dot{Q}_{net} - \dot{m}_{vout} h_v + \dot{m}_{\ell v} h_{\ell out} + \dot{m}_{vout} h_v + \dot{m}_{\ell v} h_v \tag{9}$$

or

$$m \frac{dh_v}{dt} = \dot{Q}_{net} + \dot{m}_{\ell v}(h_{\ell out} - h_v) \tag{10}$$

but since

$$h_v - h_{\ell out} = h_{fg} \qquad 7 \tag{11}$$

7) vapor and liquid ammonia are in saturated equilibrium

$$m_v \frac{dh_v}{dt} = Q_{net} - \dot{m}_{\ell v} h_{fg} \tag{12}$$

using Equation (4) once again

$$m_v \frac{dh_v}{dt} = \dot{Q}_{net} - \dot{m}_{vout} h_{fg} - \frac{dm_v}{dt} h_{fg} \tag{13}$$

or

$$\frac{dm_v}{dt} + \frac{m_v}{h_{fg}} \frac{dh_v}{dt} = \frac{\dot{Q}_{net}}{h_{fg}} - \dot{m}_{vout} \tag{14}$$

but since $h_v = f(T_v) = f(\rho_v)$

and $m_v = \rho_v V_{ev}$

$$V_{ev}[1 + \frac{\rho_v}{h_{fg}} (\frac{\partial h_v}{\partial \rho_v})] \frac{\partial \rho_v}{\partial t} = \frac{\dot{Q}_{net}}{h_{fg}} - \dot{m}_{vout} \tag{15}$$

The quantity

$$\frac{\rho_v}{h_{fg}} \left(\frac{\partial h_v}{\partial \rho_v}\right)$$

evaluated at steady state values is ≈ 0.02 therefore

$$V_{ev} \frac{\partial \rho_v}{\partial t} = \frac{\dot{Q}_{net}}{h_{fg}} - \dot{m}_{vout} \tag{16}$$

But we know that $\dot{Q}_{net} = UAS_o(T_{wout} - T_v)$ 8

8) no heat transfer to the environment

Therefore

$$V_{ev} \frac{\partial \rho_v}{dt} = \frac{UAS_o(T_{wout} - T_v)}{h_{fg}} - \dot{m}_{vout} \tag{17}$$

II. SATURATED VAPOR STATE EQUATIONS

Since the vapor is assumed to always be in the saturated state, the temperature and pressure are both functions of the vapor density, that is

$$T = f(\rho_v), \; p_v = f(\rho_v) \tag{18}$$

These correlations are determined by a curve fit of the saturation data for ammonia. The extrapolated state relationships for the evaporator are

$$T_v = -58.000(1 - \rho_v/\rho_c) + T_c \tag{19}$$

$$P_v = -131.946(1 - \rho_v/\rho_c) + P_c \tag{20}$$

where $\rho_c = .4298 \text{ lbm/ft}^3$

$T_c = 529.23°R$

$P_c = 127.645 \text{ psi}$

Likewise, the saturated vapor state relationships valid for the condenser are

$$T_v = -55.124(1 - \rho_v/\rho_c) + T_c \tag{21}$$

$$P_v = -93.787(1 - \rho_v/\rho_c) + T_c \tag{22}$$

where $\rho_c = .3055$

$T_c = 509.94$

$P_c = 89.77$

III. HEAT TRANSFER AREA

The heat transfer are of the tubes is lumped into one equivalent heat transfer area.

$$AS_o = N_t \, \pi \quad OD_t \, L_{eff} \tag{23}$$

where

N_t - no. of heat exchanger tubes

OD_t - outside diameter of HX tubes

L_{eff}- effective tube heat transfer length

APPENDIX II

I. TURBINE FLOW ANALYSIS[6]

The turbine flow velocity vector analysis is shown in Figure 106.

Assuming mid-radius conditions and inlet velocity = outlet velocity

$$V_{x1} = V_{x2} = V_x$$

Euler's Equation for a turbine

$$P_{tg} = \dot{m}_v(h_{vin} - h_{vout}) \tag{1}$$

but since

$$h_{vin} - h_{vout} = u_{tg}(V_{\theta 1} - V_{\theta 2}) \tag{2}$$

$$u_{tg} = \omega_{tg} r_{tg} \tag{3}$$

and

$$P_{tg} = \tau\omega_{tg} \tag{4}$$

we have

$$\frac{\tau}{\dot{m}_v} = r_{tg}(V_{\theta 1} - V_{\theta 2}) \tag{5}$$

$$V_{\theta 1} = V_x \tan\alpha_1 \qquad V_{\theta 2} = V_x \tan\beta_2 - u_{tg} \tag{6}$$

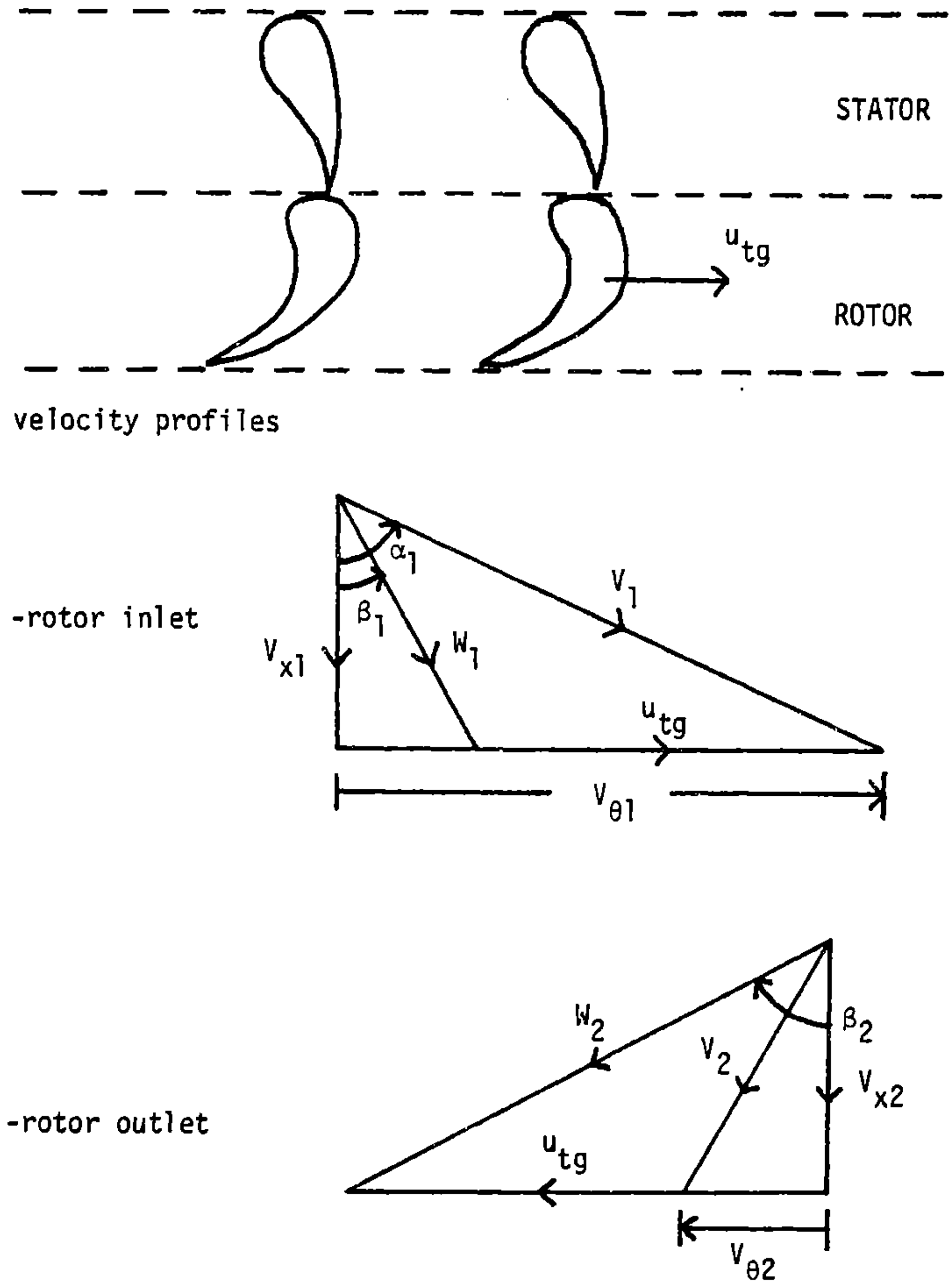

FIGURE 106: TURBINE FLOW VELOCITY VECTOR ANALYSIS

therefore

$$\frac{\tau}{\dot{m}_v} = r_{tg}V_x(\tan\alpha_1 + \tan\beta_2) - \omega_{tg}r_{tg}^{\,2} \qquad (7)$$

since $$\dot{m}_v = \rho_v A_{tg} V_x$$

$$\tau = \frac{r_{tg}}{\rho_v A_{tg}}\,\dot{m}_v^{\,2}(\tan\alpha_1 + \tan\beta_2) - \dot{m}_v\omega_{tg}r_{tg}^{\,2} \qquad (8)$$

This analysis is for a single flow turbine. However, we have a double flow turbine.

Therefore,

$$\dot{m}_v = \dot{m}_{vtg}/2 \qquad (9)$$

and $$\tau_{tg} = 2\tau \qquad (10)$$

which gives

$$\tau_{tg} = \frac{r_{tg}}{2\rho_v A_{tg}}\,\dot{m}_{vtg}^{\,2}(\tan\alpha_1 + \tan\beta_2) - \dot{m}_{vtg}\omega_{tg}r_{tg}^{\,2} \qquad (11)$$

$\alpha_1 + \beta_2$ are shown to be approximately constant even with large variations of the incidence angle.

APPENDIX III

I. COLD WATER SYSTEM ANALYSIS[7]

Momentum Balance on Fluid in Cold Pipe

$$H_1 - H_2 - \Delta H_{fpi} = y\, I_{pi} \frac{dF_{wcp}}{dt} \quad (1)$$

$$H_1 = \rho_{av} L_{pi}$$

where ρ_{av} is the average water density of the surrounding ocean

$$\rho_{av} = \frac{\int_0^{L_{pi}} \rho_w dx}{L_{pi}} \quad (2)$$

$$H_2 = P_2 + \rho_{wcp} L_{pi} + \left(\frac{yF_{wcp}}{\pi \; ID_{pi}^2/4}\right)^2 \left(\frac{\rho_{wcp}}{2 g_c}\right) \quad (3)$$

where

L_{pi} - length of cold water pipe

ID_{pi} - inside diameter of cold water pipe

$$\Delta H_{fpi} = 4f \left(\frac{L_{eq}}{ID_{pi}}\right) \frac{\rho_{wcp}}{2g_c} \left(\frac{yF_{wcp}}{\pi \; ID_{pi}^2/4}\right)^2 \quad (4)$$

$$f = .046/Re^{0.2} \quad (5)$$

and

$$Re = \frac{\rho_{wcp}\left(\frac{y\ F_{wcp}}{\pi\ ID_{pi}^{2}/4}\right) ID_{pi}}{\mu_{wcp}} \qquad (6)$$

We will let f be a constant which is evaluated at the steady state conditions

Now

$$L_{eq} = L_{pi} + 3ID_{pi} + 26ID_{pi} \qquad (7)$$

where the second term accounts for the screen and the third term approximates the 90° bend in the manifoled.

Also,

$$I_{pi} = \frac{\rho_{wcp} L_{pi}}{g_c\ \pi\ ID_{pi}^{2}/4} \qquad (8)$$

Combining

$$y I_{pi} \frac{dF_{wcp}}{dt} = L_{pi}(\rho_{av} - \rho_{wcp}) - \left[\left(\frac{y}{\pi\ ID_{pi}^{2}/4}\right)^{2} \left(\frac{\rho_{wcp}}{2g_c}\right)\left(1 + 4f\left(\frac{L_{eq}}{ID_{pi}}\right)\right)\right] \times F_{wcp}^{2} - P_2 \qquad (9)$$

Now, solving for P_2

$$H_5 = \rho_{av} L_d + \rho_{wwp} \Delta L_{cp}$$

where $$\rho_{av} = \frac{\int_0^{L_d} \rho_w \, dx}{L_d}$$

and ΔL_{cp} = the wave height above normal sealevel

Neglecting losses in the diffuser and assuming that the velocity is the same everywhere as it is in the condenser

$$H_5 = P_4 + \frac{\rho_{wcp}}{2g_c} \left[\frac{F_{wcp}}{N_{tcp} \pi \ ID_{cd}^2/4}\right]^2 + \rho_{wcp} L_d \tag{11}$$

$$H_4 - H_3 = \Delta H_{cp} \tag{12}$$

$$\Delta H_{cp} = A\left(\frac{\omega_{cp}}{\omega_d}\right)^2 + B\left(\frac{\omega_{cp}}{\omega_d}\right) \frac{F_{wcp}}{2} + C \frac{F_{wcp}^2}{4} \tag{13}$$

assuming the velocity and the height remains constant through the pump, i.e., $Z_4 = Z_3$ and $V_4 = V_3$,

$$P_4 - P_3 = \Delta H_{cp} \tag{14}$$

Now

$$\Delta H_2 - H_3 = H_{fcd} \tag{15}$$

where ΔH_{fcd} = the friction head loss in the condenser

$$\Delta H_{fcd} = 4f(\frac{L_{tcd}}{ID_{tcd}}) \frac{\rho_{wcp}}{2g_c}(\frac{F_{wcp}}{N_{tcd}\ \pi\ ID_{tcd}^2/4})^2 \qquad (16)$$

where ID_{tcd} - inside diameter of condenser tubes. Once atain evaluating Re + f at the steady state conditions.

But $Z_2 = Z_3$ and $v_2 = v_3$

Therefore $$P_2 - P_3 = \Delta H_{fcd} \qquad (17)$$

or $$P_2 = \Delta H_{fcd} + P_3 \qquad (18)$$

II. WARM WATER SYSTEM ANALYSIS

We will assume that the inlet velocity equals the exit velocity $V_1 = V_3$. Therefore, the only losses in the system are the frictional losses in the evaporator tubes. These are

$$\Delta H_{fev} = 4f(\frac{L_{tev}}{ID_{tev}}) \frac{\rho_{wwp}}{2g_c}(\frac{F_{wwp}}{N_{tev}\ \pi\ ID_{tev}^2/4}) \qquad (19)$$

where Re and f are evaluated as before.

The pump head is

$$\Delta H_{wp} = A(\frac{\omega_{wp}}{\omega_d})^2 + B(\frac{\omega_{wp}}{\omega_d}) \frac{F_{wwp}}{2} + C\ \frac{F_{wwp}^2}{4} \qquad (20)$$

Equating

$$\Delta H_{fev} = \Delta H_{wp} \tag{21}$$

we can solve for F_{wwp} as a function of ω_{wp}, or

$$F_{wwp} = C_{wp}\omega_{wp} \tag{22}$$

APPENDIX IV

I. NONLINEAR SYSTEM EQUATIONS

A. Evaporator

$$\frac{d(T2)}{dt} = Z_1*(T1 - T2) - Z_2*(T2 - TEV) \tag{1}$$

$$\frac{d(RHOEV)}{dt} = Z_3*(T2 - TEV) - Z_4*MD10 \tag{2}$$

B. Condenser

$$\frac{d(T5)}{dt} = Z_5*(T4 - T5) + Z_6*(TCD - T5) \tag{3}$$

$$\frac{d(RHOCD)}{dt} = Z_7*MD13 - Z_8*(TCD - T5) \tag{4}$$

C. Turbine-Generator

$$\frac{d(NTG)}{dt} = \frac{1}{J_{tg}} * (B_1 * \frac{MDTG^2}{RHO13} + B_2*MDTG*NTG-(1+a)*TAUL) \tag{5}$$

D. Cold Water System Model

$$\frac{d(VDCP)}{dt} = \frac{1}{yI_{pi}} *(Z_9+Z_{10}*\Delta LCP+Z_{11}*NCP^2+Z_{12}*NCP*VDCP-Z_{13}*VDCP^2) \tag{6}$$

$$\frac{d(NCP)}{dt} = \frac{1}{J_{cp}} *(TAUCP - \frac{\Delta H_{cp}}{2\,\eta_{cp}} * \frac{VDCP}{NCP}) \tag{7}$$

$$Z_9 = L_{pi}(\rho_{av} - \rho_{wcp}) - L_d(\rho_{av} - \rho_{wwp})$$

$$Z_{10} = \rho_{wwp} \qquad Z_{11} = A/\omega_d^2 \qquad Z_{12} = B/2\omega_d$$

$$Z_{13} = [(\frac{y}{\pi\, ID_{pi}^2/4})^2(\frac{\rho_{wcp}}{2g_c})(1 + 4f*(\frac{L_{eq}}{ID_{pi}}))]+4f(\frac{L_{tcd}}{ID_{tcd}})(\frac{\rho_{wcd}}{2_{gc}})$$

$$(\frac{1}{N_{tcd}\,\pi\, ID_{tcd}^2/4})^2 - (\frac{\rho_{wcp}}{2g_c})(\frac{1}{N_{tcd}\,\pi\, ID_{tcd}^2/4})^2 - \frac{C}{4}$$

$$\Delta H_{cp} = A*(\frac{NCP}{\omega_d})^2 + B*(\frac{NCP}{\omega_d})* \frac{VDCP}{2} + C* \frac{VDCP^2}{4}$$

$$\eta_{cp} \doteq D + E*\frac{VDCP}{2} + F* \frac{FDCP^2}{4}$$

E. Warm Water System

$$\frac{d(NWP)}{dt} = \frac{1}{J_{wp}} *(TAUWP - \frac{\Delta H_{wp}}{2\,\eta_{wp}} * C_{wp} + Z_{14} * LWP) \qquad (8)$$

$$Z_{14} = \frac{\rho_{wwp} * C_{wp}}{2}$$

$$\Delta H_{wp} = A*(\frac{NWP}{\omega_d})^2 + B*C_{wp}* \frac{NWP^2}{2} + C*(\frac{C_{wp}*NWP}{2})^2$$

$$\eta_{wp} = D+E*C_{wp}* \frac{NWP}{2} + F*(\frac{C_{wp}*NWP}{2})^2$$

F. Vapor Transport System

$$MD10 = a + b*(\frac{P_{11}}{PEV}) \qquad (9)$$

$$MDTG = K_{tg}\sqrt{1 - (\frac{P_{13}}{P_{11}})^2} \qquad (10)$$

$$MDBP = K_{bp}\sqrt{1 - (\frac{P_{13}}{P_{11}})^2} \qquad (11)$$

$$MDTG = MD10/(1 + \frac{K_{bp}}{K_{tg}}) \qquad (12)$$

APPENDIX V

PHYSICAL TIME CONSTANT ESTIMATION

The time constants of a physical system, whether linear or nonlinear, can be estimated by evaluating the ratio of the "holdup" of the system (i.e., mass, energy capacity) to the "thruput" of the system (i.e., mass, energy transport through the system)

$$\tau = \frac{\text{"Holdup"}}{\text{"Thruput"}} \qquad (1)$$

This type of analysis is especially useful for nonlinear systems where the actual time constants cannot be evaluated directly. The time constants of the OTEC plant are evaluated in this manner at the 100% load steady state conditions.

I. Heat Exchanger Thermal Time Constants

The "holdup" of the heat exchanger is the heat capacity of that system. Neglecting the vapor side of the heat exchanger, this is the product of the water-tube effective mass and the specific heat.

$$\text{"Holdup"} = (\rho AX)_{eff}\, C_{pw} L_{ev} \qquad (2)$$

The "thruput" of the heat exchanger is composed of two parts: a) the convective heat flow and b) the conductive heat flow.

The convective "heat flow" is given by

$$\bar{Q}_{cv} = \rho_w A X_w v_w c_{pw} \tag{3}$$

and the conductive "heat flow" is given by

$$\bar{Q}_{cd} = UAS_o \tag{4}$$

The total thruput is the sum of $\bar{Q}_{cv} + \bar{Q}_{cd}$

$$\text{"Thruput"} = UAS_o + \rho_w A X_w v_w c_{pw} \tag{5}$$

Evaluated at the steady state conditions for the evaporator and condenser

$$\tau_{ev} = 3.3 \text{ sec}$$
$$\tau_{cd} = 3.9 \text{ sec}$$

II. Vapor Flow System Time Constants

The vapor flow system is represented by the schematic in Figure 107.

The holdup for this system is the mass capacity

$$\text{"Holdup"} = \rho_v V_{eff} \tag{6}$$

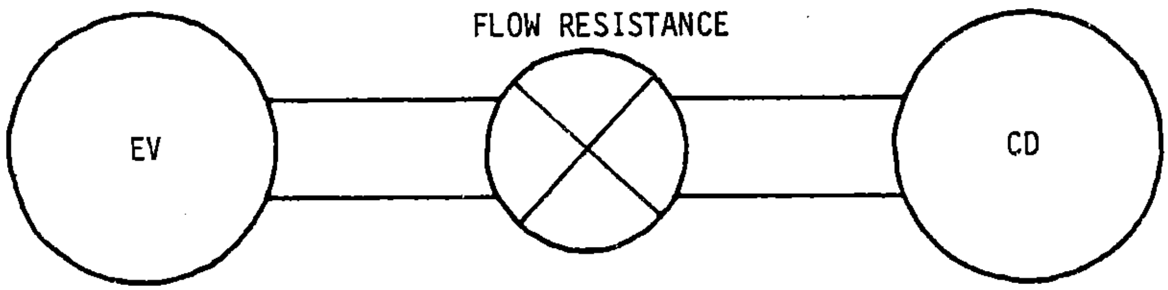

FIGURE 107: VAPOR FLOW SYSTEM SCHEMATIC

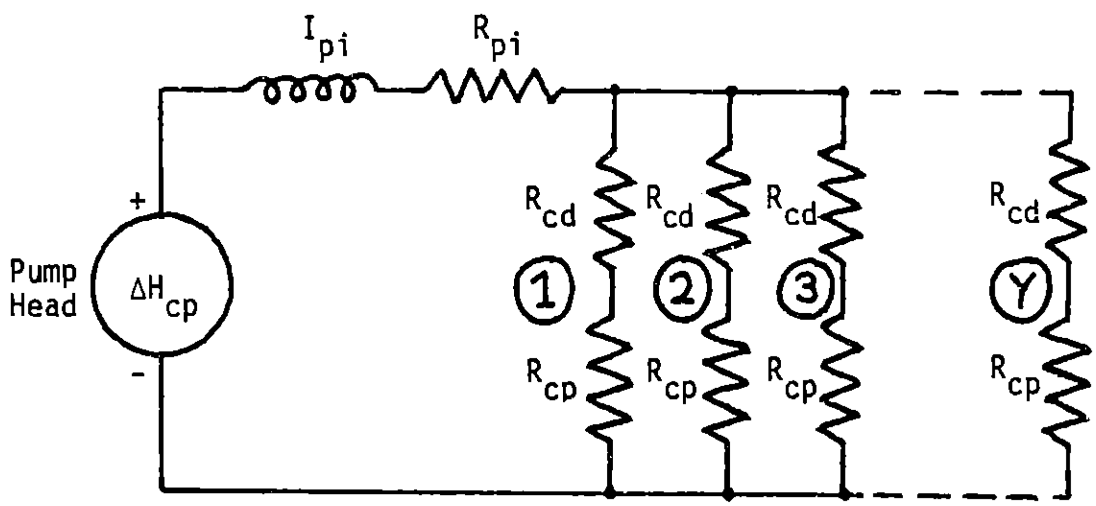

FIGURE 108: COLDWATER FLOW SYSTEM CIRCUIT ANALOGY

The effective volume is determined by idealizing the system as two mass capacitances in parallel, where

$$V_{eff} = \frac{V_{ev}}{2} \quad (7)$$

since $V_{ev} \simeq V_{cd}$

The thruput for the system is the total vapor mass flow rate

$$\text{"Thruput"} = \dot{m}_v$$

Evaluated at the steady state conditions, the vapor flow time constant is 3.3 seconds.

III. Turbine Time Constant

The turbine time constant is a function of the turbine-generator rotational inertia, J_{tg}, and the turbine "damping", B_{tg}, i.e., the energy dissipation associated with the velocity droop across the turbine because of its angular rotation. The time constant is then

$$\tau = J_{tg}/B_{tg} \quad (8)$$

The "damping" associated with the turbine droop is evaluated as

$$B_{tg} = \frac{d}{d(\omega_{tg})} (\tau_{tg}) = \frac{1}{\dot{m}_{vtg} r_{tg}^2} \tag{9}$$

Evaluated at the steady state conditions, the turbine time constant is 14.1 seconds.

IV. Seawater Pump Time Constant

The seawater pump time constants are evaluated in the same manner as the turbine time constant, which is the ratio of the pump effective rotational inertia to the effective "damping", given by

$$B_p = \frac{d}{d(\omega_p)} (\tau_p) \tag{10}$$

where

$$\tau_p = \frac{H_p}{\eta_p} \frac{F_{wp}}{\omega_p} \tag{11}$$

The seawater pump time constants evaluated at steady state are 0.14 seconds for the cold pump and 0.23 seconds for the warm pump.

V. Coldwater Flow Time Constant

A schematic circuit analogy of the cold water flow system is given in Figure 108.

The pump resistances and condenser resistances in each loop are considered identical.

The time constant for this circuit analogy is given by

$$\tau_{pi} = \frac{I}{R_{pi} + (R_{cd}+R_{cp})/y} \tag{12}$$

The fluid inertia in the cold pipe is given by

$$I = \frac{\rho_w L_{pi}}{AX_{pi}} \tag{13}$$

The fluid resistance in the cold pipe is given by

$$R_{pi} = \frac{\partial}{\partial(F_{wcp})} (\Delta H_{fpi}) \tag{14}$$

The fluid resistance in the condenser is given by

$$R_{cd} = \frac{\partial}{\partial(F_{wcp})} (\Delta H_{fcd}) \tag{15}$$

Finally, the fluid resistance in the cold water pump is given by

$$R_{cp} = \frac{\partial}{\partial(F_{wcp})} (\Delta H_{fcp}) \tag{16}$$

Evaluated at the steady state, the time constant for the cold sea-water flow is 17.9 seconds.

APPENDIX VI

GOVERNOR FEEDBACK GAIN DESIGN

The governor gain is given by

$$\text{governor gain} = \frac{K^*}{\delta^*} \qquad (1)$$

The droop is chosen by the designer.

K^* is the open loop relationship between the actuator and the controlled variable

$$\frac{\text{"actuator position"}}{\text{"controlled variable"}} = K^* \qquad (2)$$

For the bypass valve, the actuator position varies from $\Delta K_{bp} = 0$ to $\Delta K_{bp} = 2$. However, the sensitivity of the bypass valve changes as it varies from fully closed to fully open; that is, K^* is not a constant. Therfore, the governor gain must be varied as the nominal bypass valve opening changes.

There are two cases that we wish to control: a) the power generated when directly connected to an AC grid and, b) the turbine speed when linked by a DC transmission line. The governor design methcdology for each case is presented below.

Case a) Power sensitivity to the bypass valve at a given nominal bypass valve opening is:

$$\left(\frac{\Delta P_{tg}}{\Delta K_{bp}}\right)_{ss} = (A)MW/\Delta K_{bp} \qquad (2)$$

The steady state full load power generated by the OTEC plant is:

$$P_{tgmax} = 67.4 \text{ MW} \qquad (3)$$

Therefore, at this sensitivity, the bypass valve need be opened

$$\Delta K_{bpmax} = \frac{67.4}{A} \qquad (4)$$

for a 100% reduction in full load power output. Since in the linear case in normalized variables

$$K^* = \frac{\Delta K_{bpmax}}{\Delta P_{tgmax}} \qquad (5)$$

and $\Delta P_{tgmax} = 1.0$, therefore

$$K^* = \Delta K_{bpmax} \qquad (6)$$

Case b) Since in this instance we are directly controlling the turbine-generator speed, this sensitivity is used (normalized)

$$\frac{\omega_{tg}}{\Delta K_{bp}} = B \qquad (7)$$

Since we require that $\Delta\omega_{tg} = 1.0$ for $\Delta K_{bp} = \Delta K_{bpmax}$

$$\Delta K_{bpmax} = 1/B \qquad (8)$$

Once again for the linear case

$$K^* = \frac{\Delta K_{pbmax}}{\Delta\omega_{tgmax}} \qquad (9)$$

or

$$K^* = \Delta K_{bpmax} \qquad (10)$$

Thus, K^* is a function of the bypass valve sensitivity which in turn is a function of the nominal bypass valve opening.

$$K^* = f(K_{bp}) \qquad (11)$$

In normalized variables, the governor is implemented as follows.

$$\Delta K_{bp} = \frac{K^*}{\delta^*} \Delta\omega_{tg} \qquad (12)$$

APPENDIX VII

I. Description and Units for OTEC Parameters

1) Heat Exchangers (HX)

NETV(CD) - number of HX tubes
ODEV(CD) - outside diameter of HX tubes (ft)
LEFFEV(CD)- effective heat transfer length of HX tubes (ft)
CWEV(CD) - specific heat of seawater in HX (Btu/lbm°R)
HFGEV(CD) - heat of vaporization-working fluid (Btu/lbm)
UEV(CD) - overall heat transfer coefficient in HX (Btu/ft^2/hr°R)
DIAMEV(CD)- diameter of HX shell (ft)
LENGEV(CD)- length of HX shell (ft)
VOIDEV(CD)- void fraction in HX
X13SS - steady state vapor quality at turbine exit
WTEV(CD) - wall thickness of heat exchanger tubes (ft)
RHOALUM - density of HX tube material (lb/ft^3)
CALUM - specific heat of HX tube material (BTU/lbm°R)
APEV - linearized evaporator flow coefficient (lbm/hr)
BPEV - linearized evaporator flow coefficient (lbm/hr)

2) Turbine-Generator (TG)

MRTG - TG blade mid-radius (ft)
XAREATG - TG blade exit area (ft^2)
JTG - TG rotational inertia (lbm ft^2)
ALPHATG - TG blade mid-radius exit angle (deg)
BETATG - TG blade mid-radius exit angle (deg)
ATG - TG load friction factor
NTGSS - TG steady state angular velocity (rpm)
KTG - TG vapor flow coefficient (lbm/hr)

3) Seawater Flow System

B1WP(CP) - pump head speed coefficient (lb/ft^2)
B2WP(CP) - pump head cross term coefficient (lb sec/ft^5)
B3WP(CP) - pump head flow coefficient (lb sec^2/ft^8)
B4WP(CP) - pump efficiency 1st coefficient
B5WP(CP) - pump efficiency 2nd coefficient (sec/ft^3)
B6WP(CP) - pump efficiency 3rd coefficient (sec^2/ft^6)
NDWP(CP) - design speed of pump (rpm)
JWP(CP) - pump effective rotational inertia (lbm ft^2)
MUWP(CP) - seawater viscosity (lbm/ft sec)
LACTEV(CP)- actual length of HX tubes (ft)
DIAMPI - cold water pipe diameter (ft)
Y - number of OTEC 50 MW modules operating

RHOAVG - average seawater density-surface to LENGPI (lbm/ft^3)
DEPTH - cold seawater discharge depth (ft)
LENGPI - length of cold water pipe (ft)

4) Working Fluid Vapor State Coefficients
AEV(CD) - $T_v = f(\rho_v)$ slope (°R)
BEV(CD) - $T_v = f(\rho_v)$ ρ_c(lbm/ft^3)
CEV(CD) - $T_v = f(\rho_v)$ T_c(°R)
DEV(CD) - $p_v = f(\rho_v)$ slope (psi)
EEV(CD) - $p_v = f(\rho_v)$ ρ_c(lbm/ft^3)
FEV(CD) - $p_v = f(\rho_v)$ p_c(psi)

5) Synchronous machines
PFTG(WP,CP) - power factor of generator (motor)
HPWP(CP) - horsepower of pump motor (HP)
KVATG - generator KVA rating (KVA)
VBVSP - pump motor bus voltage (KV)
EFFMWP(CP) - pump motor power supply efficiency
NBUSSS - shoreline power grid frequency (rpm)
XTG(WP,CP) - synchronous reactance of generator (motor)

II. Important parameters

A. Heat Exchangers

$$\text{ALPHAEV(CD)} = \left(\frac{UAS_o * T_{wout}}{\dot{m}_v * h_{fg}}\right)_{ss}$$

$$\text{RTIMEEV(CD)} = \left(\frac{\rho_v * V_{HX}}{\dot{m}_v}\right)_{ss}$$

$$\text{NTUEV(CD)} = \left(\frac{UAS_o}{\dot{m}_w * c_{pw}}\right)_{ss}$$

$$\text{TTIMEEV(CD)} = \left(\frac{(\rho AX)eff}{\dot{m}_w}\right)_{ss}$$

B. Turbine-Generator

$$GAMMA = \left(\frac{B_1}{J_{tg} * \dot{m}_{vtg}}\right)_{ss}$$

$$TIMETG = \left(- \frac{J_{tg}}{B_2 * \dot{m}_{vtg}}\right)_{ss}$$

C. Warm Water System

$$TIMEWP = \left(\frac{\eta_{wp} * \omega_{wp} * J_{wp}}{\Delta H_{wp} * C_{wp}}\right)_{ss}$$

D. Cold Water System

$$MTIMECP = \left(\frac{y * I_{pi}}{Z_{13} * F_{wcp}}\right)_{ss}$$

$$NTIMECP = \left(\frac{\eta_{wp} * \omega_{wp}^{2} * J_{cp}}{\Delta H_{cp} * F_{wcp}}\right)_{ss}$$

$$ZETA = \left(\frac{B * \omega_{cp}}{\omega_d * Z_{13} * F_{wcp}}\right)_{ss}$$

E. Synchronous machines

$$STIMECP = \left(\frac{\delta_{cp}}{\omega_{cp}}\right)_{ss}$$

$$STIMEWP = \left(\frac{\delta_{wp}}{\omega_{wp}}\right)_{ss}$$

$$STIMETG = \left(\frac{\delta_{G}}{\omega_{\infty}}\right)_{ss}$$

III. Parameter Values

1) Turbogenerator
   MRTG = 3.333
   XAREATG = 30.2815
   JTG = 6.5627E05
   ALPHATG = 75.
   BETATG = 60.
   ATG = .005
   NTGSS = 1800.
   KTG = 2.1335E07
2) Evaporator
   LEFFEV = 35.18
   CWEV = .956
   HFGEV = 508.6
   APEV = 16.916E08
   BPEV = -16.84E08
   UEV = 650.9
   LENGEV = 35.2
   VOIDEV = .658
   DIAMEV = 62.9
3) Condenser
   LEFFCD = 42.55
   CWCD = .93714
   HFGCD = 527.3
   UCD = 506.9
   DIAMCD = 64.4

LENGCD = 42.6
VOIDCD = .657
X13SS = 1.0

4) Warm Water System
B1WP = 231.11
B2WP = .8056
B3WP = -187.36E-06
NDWP = 55.
B4WP = -136.
B5WP = .145
B6WP = -24.E-06
JWP = 1.8041E6
MUWP = 1.4305E-03
LACTEV = 35.51

5) Cold Water System
B1CP = 231.11
B2CP = .8056
B3CP = -187.36E-06
NDCP = 55.
B4CP = -136.
B5CP = .145
B6CP = -24.E-06
DIAMPI = 100.
Y = 8.
JCP = 1.8041E6
MUCP = 8.055E-04
DEPTH = 200.
LENGPI = 3280.
LACTCD = 42.88
RHOAVG = 64.13

6) Cross Parameters
NTEV = 192229.
ODEV = .08333
RHOWP = 63.87
WTEV = 2.3333E-03
PI = 3.14159
NTCD = 201955.
ODCD = .08333
RHOCP = 64.21
WTCD = 2.3333E-03
GC = 32.19
RHOALUM = 302.8
CALUM = .13

7) State Parameters
ACD = -55.127
BCD = .30551
CCD = 509.938

DCD = -93.787
ECD = .3055
FCD = 89.77
AEV = -58.000
BEV = .4298
CEV = 529.23
DEV = -131.946
EEV = .4298
FEV = 127.645

8) Synchronous Machine Parameters

PFCP = .9
PFWP = .9
PFTG = .9
HPCP = 5500
HPWP = 4000
KVATG = 75000
VBUSP = 4.16
VBUSTG = 13.8
EFFMCP = .912
EFFMWP = .912
NBUSSS = 3600
XCP = 2.67
XWP = 2.67
XTG = 1.72

APPENDIX VIII

I. STEADY STATE MODEL COMPUTER OUTPUT

SYSTEM DESCRIPTION NUMBER 4.

STATES	**INPUTS**	**OUTPUTS**
T2	T1	POWTG
RHOEV	POWL	MD10
T5	NSCP	TEV
RHOCD	NSWP	PEV
NTG	T4	TCD
NCP	KBP	PCD
MDCP	MD7	MDWP
NWP	LCP	MDTG
ANGCP	LWP	MD21
ANGWP	EPM	MD14
		POWCP
		POWWP

POWLSS =   67.410 MW
KBPSS = 0.0000E+00 LBM/HR
T28SS = 499.600 DEG R
T1SS = 539.600 DEG R
TCDSS = 509.938 DEG R

STEADY STATE VALUES

TURBOGENERATOR
TAULSS = 0.2638E+06 FT-LBS
MDBPSS = 0.0000E+00 LBM/HR
MDTGSS = 0.1510E+08 LBM/HR
P11SS = 127.074 PSIA
EVAPORATOR
PEVSS = 127.643 PSIA
RHOEVSS = 0.42979 LBM/FT**3
TEVSS = 529.229 DEG R
T2SS = 533.612 DEG R
CONDENSER
T5SS = 505.493 DEG R
RHOCDSS = 0.30551 LBM/FT**3
PCDSS =   89.773 PSIA
WARM WATER SYSTEM
NWPSS =   45.851 RPM
EFFWPSS = 0.82999
HDWPSS =   3.261 PSI
TAUWPSS = 0.3585E+06 FT-LBS
MDWPSS = 0.1399E+10 LBM/HR
CWP = 132.714 FT**3/SEC/RPM
COLD WATER SYSTEM
NCPSS =   50.788 RPM
EFFCPSS = 0.82780
HDCPSS =   4.825 PSI
TAUCPSS = 0.4922E+06 FT-LBS
MDCPSS = 0.1442E+10 LBM/HR
SYNCHRONOUS MACHINES
ANGCPSS = 16.443 DEG
ANGWPSS = 11.909 DEG
ANGTGSS = 25.169 DEG
POWCPMX = 13.753 MW
POWWPMX = 12.405 MW
POWTGMX = 158.504 MW
POWCPSS = 3.893 MW
POWWPSS = 2.560 MW

NON-DIMENSIONAL PARAMETERS

TURBOGENERATOR
GAMMA = -.1972E+01
GAMMAP = -.2917E+01
TIMETG = 14.084
EVAPORATOR
ALPHAEV = 80.067
BETA = -111.524
RTIMEEV = 7.375
NTUEV = 0.862
TTIMEEV = 5.827
TRANSIT TIME = 5.401 SEC
LUMPING COEFF. = 1.000
CONDENSER
NTUCD = 0.844
TTIMECD = 7.231
ALPHACD = 72.395
RTIMECD = 6.640
TRANSIT TIME = 6.695 SEC
LUMPING COEFF. = 1.000
WARM WATER SYSTEM
TIMEWP = 0.75066
COLD WATER SYSTEM
ZETA = 0.99954
MTIMECP = 17.9086
NTIMECP = 0.6057
TRANSIT TIME = 516.256 SEC
SYNCHRNOUS MACHINES
STIMECP = 0.05396
STIMEWP = 0.04329
STIMETG = 0.001

AMATRIX

-.3195E+00	0.1607E-01	0.0000E+00	0.0000E+00	0.0000E+00	0.0000E+00	0.0000E+00	0.1926E-02	0.0000E+00	0.0000E+00
0.1086E+02	-.1312E+01	0.0000E+00	0.1399E+00	0.0000E+00	0.0000E+00	0.0000E+00	0.0000E+00	0.0000E+00	0.0000E+00
0.0000E+00	0.0000E+00	-.2550E+00	0.1273E-01	0.0000E+00	0.0000E+00	-.1612E-02	0.0000E+00	0.0000E+00	0.0000E+00
0.0000E+00	0.1466E+00	0.1090E+02	-.1344E+01	0.0000E+00	0.0000E+00	0.0000E+00	0.0000E+00	0.0000E+00	0.0000E+00
0.0000E+00	0.2034E+00	0.0000E+00	-.3556E+00	-.2016E-02	0.0000E+00	0.0000E+00	0.0000E+00	-.7748E-02	-.5164E-02
0.0000E+00	0.0000E+00	0.0000E+00	0.0000E+00	0.0000E+00	-.4331E+01	0.1205E+01	0.0000E+00	0.1606E+01	0.0000E+00
0.0000E+00	0.0000E+00	0.0000E+00	0.0000E+00	0.0000E+00	0.6529E-01	-.5586E-01	0.0000E+00	0.0000E+00	0.0000E+00
0.0000E+00	0.0000E+00	0.0000E+00	0.0000E+00	0.0000E+00	0.0000E+00	0.0000E+00	-.2715E+01	0.0000E+00	0.1313E+01
0.0000E+00	0.0000E+00	0.0000E+00	0.0000E+00	0.0000E+00	-.1853E+02	0.0000E+00	0.0000E+00	0.0000E+00	0.0000E+00
0.0000E+00	0.0000E+00	0.0000E+00	0.0000E+00	0.0000E+00	0.0000E+00	0.0000E+00	-.2310E+02	0.0000E+00	0.0000E+00

BMATRIX

0.1716E+00	0.0000E+00	0.0000E+00	0.0000E+00	0.0000E+00	0.0000E+00	0.0000E+00	0.0000E+00	0.0000E+00	0.0000E+00
0.0000E+00	0.0000E+00	0.0000E+00	0.0000E+00	0.0000E+00	-.1344E+00	0.0000E+00	0.0000E+00	0.0000E+00	0.0000E+00
0.0000E+00	0.0000E+00	0.0000E+00	0.0000E+00	0.1383E+00	0.0000E+00	0.0000E+00	0.0000E+00	0.0000E+00	0.0000E+00
0.0000E+00	0.0000E+00	0.0000E+00	0.0000E+00	0.0000E+00	0.1493E+00	0.0000E+00	0.0000E+00	0.0000E+00	0.0000E+00
0.0000E+00	-.6898E-01	0.0000E+00	0.0000E+00	0.0000E+00	-.1859E-02	0.0000E+00	0.0000E+00	0.0000E+00	0.0000E+00
0.0000E+00	0.0000E+00	-.1651E+01	0.0000E+00	0.0000E+00	0.0000E+00	0.0000E+00	0.0000E+00	0.0000E+00	0.1651E+01
0.0000E+00	0.0000E+00	0.0000E+00	0.0000E+00	0.0000E+00	0.0000E+00	0.0000E+00	0.1536E-02	0.0000E+00	0.0000E+00
0.0000E+00	0.0000E+00	0.0000E+00	-.1332E+01	0.0000E+00	0.0000E+00	0.0000E+00	0.0000E+00	0.1248E+00	0.1332E+01
0.0000E+00	0.0000E+00	0.1853E+02	0.0000E+00	0.0000E+00	0.0000E+00	0.0000E+00	0.0000E+00	0.0000E+00	0.0000E+00
0.0000E+00	0.0000E+00	0.0000E+00	0.2310E+02	0.0000E+00	0.0000E+00	0.0000E+00	0.0000E+00	0.0000E+00	0.0000E+00

CMATRIX

0.0000E+00	0.2963E+01	0.0000E+00	-.5180E+01	-.3437E-01	0.0000E+00	0.0000E+00	0.0000E+00	0.0000E+00	0.0000E+00
0.0000E+00	0.9732E+00	0.0000E+00	-.1032E+01	0.0000E+00	0.0000E+00	0.0000E+00	0.0000E+00	0.0000E+00	0.0000E+00
0.0000E+00	0.1087E+00	0.0000E+00	0.0000E+00	0.0000E+00	0.0000E+00	0.0000E+00	0.0000E+00	0.0000E+00	0.0000E+00
0.0000E+00	0.1034E+01	0.0000E+00	0.0000E+00	0.0000E+00	0.0000E+00	0.0000E+00	0.0000E+00	0.0000E+00	0.0000E+00
0.0000E+00	0.0000E+00	0.0000E+00	0.1090E+00	0.0000E+00	0.0000E+00	0.0000E+00	0.0000E+00	0.0000E+00	0.0000E+00
0.0000E+00	0.0000E+00	0.0000E+00	0.1045E+01	0.0000E+00	0.0000E+00	0.0000E+00	0.0000E+00	0.0000E+00	0.0000E+00
0.0000E+00	0.0000E+00	0.0000E+00	0.0000E+00	0.0000E+00	0.0000E+00	0.0000E+00	0.1000E+01	0.0000E+00	0.0000E+00
0.0000E+00	0.9732E+00	0.0000E+00	-.1032E+01	0.0000E+00	0.0000E+00	0.0000E+00	0.0000E+00	0.0000E+00	0.0000E+00
-.8007E+02	0.8703E+01	0.0000E+00	0.0000E+00	0.0000E+00	0.0000E+00	0.0000E+00	0.0000E+00	0.0000E+00	0.0000E+00
0.0000E+00	0.0000E+00	-.7240E+02	0.7895E+01	0.0000E+00	0.0000E+00	0.0000E+00	0.0000E+00	0.0000E+00	0.0000E+00
0.0000E+00	0.0000E+00	0.0000E+00	0.0000E+00	0.0000E+00	0.0000E+00	0.0000E+00	0.0000E+00	0.9724E+00	0.0000E+00
0.0000E+00	0.0000E+00	0.0000E+00	0.0000E+00	0.0000E+00	0.0000E+00	0.0000E+00	0.0000E+00	0.0000E+00	0.9856E+00

DMATRIX

0.0000E+00	0.0000E+00	0.0000E+00	0.0000E+00	0.0000E+00	-.2708E-01	0.0000E+00	0.0000E+00	0.0000E+00	0.0000E+00
0.0000E+00	0.0000E+00	0.0000E+00	0.0000E+00	0.0000E+00	0.9911E+00	0.0000E+00	0.0000E+00	0.0000E+00	0.0000E+00
0.0000E+00	0.0000E+00	0.0000E+00	0.0000E+00	0.0000E+00	0.0000E+00	0.0000E+00	0.0000E+00	0.0000E+00	0.0000E+00
0.0000E+00	0.0000E+00	0.0000E+00	0.0000E+00	0.0000E+00	0.0000E+00	0.0000E+00	0.0000E+00	0.0000E+00	0.0000E+00
0.0000E+00	0.0000E+00	0.0000E+00	0.0000E+00	0.0000E+00	0.0000E+00	0.0000E+00	0.0000E+00	0.0000E+00	0.0000E+00
0.0000E+00	0.0000E+00	0.0000E+00	0.0000E+00	0.0000E+00	0.0000E+00	0.0000E+00	0.0000E+00	0.0000E+00	0.0000E+00
0.0000E+00	0.0000E+00	0.0000E+00	0.0000E+00	0.0000E+00	0.0000E+00	0.0000E+00	0.0000E+00	0.0000E+00	0.0000E+00
0.0000E+00	0.0000E+00	0.0000E+00	0.0000E+00	0.0000E+00	-.8894E-02	0.0000E+00	0.0000E+00	0.0000E+00	0.0000E+00
0.0000E+00	0.0000E+00	0.0000E+00	0.0000E+00	0.0000E+00	0.0000E+00	0.1000E+01	0.0000E+00	0.0000E+00	0.0000E+00
0.0000E+00	0.0000E+00	0.0000E+00	0.0000E+00	0.0000E+00	0.0000E+00	0.0000E+00	0.0000E+00	0.0000E+00	0.0000E+00
0.0000E+00	0.0000E+00	0.0000E+00	0.0000E+00	0.0000E+00	0.0000E+00	0.0000E+00	0.0000E+00	0.0000E+00	0.1000E+01
0.0000E+00	0.0000E+00	0.0000E+00	0.0000E+00	0.0000E+00	0.0000E+00	0.0000E+00	0.0000E+00	0.0000E+00	0.1000E+01